The Role of the ELAVL Family of RNA-binding Proteins in LRRK2-dependent Models of Parkinson's Disease

Olanta Negeri

Thesis submitted in partial fulfillment of the requirements for the
Doctorate in Philosophy Cellular and Molecular Medicine

Department of Cellular and Molecular Medicine
Faculty of Medicine
University of Ottawa

Abstract

Parkinson's disease (PD) is the second most common neurodegenerative disease, yet it has no cure. It is characterized by the loss of dopaminergic neurons and accumulation of dense aggregates, primarily composed of α-synuclein protein. Many causative genes have been identified including *SNCA,* encoding α-synuclein, and *Leucine-rich-repeat kinase 2 (LRRK2)*. The *LRRK2 G2019S* mutation is known to cause hyperactive kinase activity, but its cellular functions, including its kinase substrates, remain poorly understood. PD has many risk factors including environmental and genetic modifiers. Polymorphisms in the *Embryonic lethal-abnormal vision-like 4* (*ELAVL4*) gene modify PD age-of-onset or susceptibility. Incidentally, a genetic screen in *Drosophila* identified an ELAVL homologue as required for LRRK2-induced pathology. Therefore, we hypothesized that LRRK2 phosphorylates ELAVL4 to control phenotypes relevant to PD. We discovered that three neuronal ELAVLs including ELAVL4 (also known as HuD) bind to, and post-transcriptionally regulate mRNA encoding α-synuclein and LRRK2. We also show that LRRK2 phosphorylates HuD and its homologues HuB and HuC. This controls binding of nELAVLs (i.e., HuB, HuC, and HuD) to mRNA and post-transcriptionally regulates mRNA abundance and splicing in the mouse midbrain. In mice, the complex interaction between *HuD* and *Lrrk2 G2019S* is associated with motor deficits, dopaminergic neuron loss, and accumulated α-synuclein protein levels. Targets of nELAVLs are also selectively misregulated in iPSC-derived neurons and tissues from PD patients. In a model of PD-relevant inflammation, we also show that the ubiquitously expressed ELAVL homologue, HuR, controls LRRK2 protein levels. We show that mice lacking *Lrrk2* are more susceptible to an acute model of dextran sodium sulfate (DSS) chemical-induced colitis. *Lrrk2*-deficient mice treated with DSS also show accumulated α-synuclein in brain tissue. Using *in vitro* models and mouse tissue we show that LRRK2 controls

HuR binding to RNA probes and to the proinflammatory cytokine *Tnfa* in colon tissue, and this has implications for intestinal pathology relevant to PD. Together, this suggests that misregulation of ELAVLs may be implicated in neurodegeneration and inflammation observed in Parkinson's disease.

Acknowledgements

I'd like to express my deepest gratitude to my supervisor, Dr. Derrick Gibbings for the opportunity to join the lab. It has been an absolute privilege to begin my career under your mentorship. You inspired me to think critically and creatively and allowed me to grow independently while providing invaluable guidance that shaped my research experience. Your patience and willingness to answer my questions on a moment's notice helped me more than you know. I would like to especially thank you for providing me with the flexibility to pursue meaningful opportunities outside of my research.

My sincere thank you to the members of my TAC committee, Drs. Diane Lagace, Tommy Alain, and Subash Sad for your contributions to my research and for the words of encouragement. I would also like to thank the Parkinson's Research Consortium for the graduate fellowships that helped fund my research.

Thank you to all the many past and present members of the Gibbings lab for all the debates about science, life, and world-issues and of course for all the cringe jokes. It was never a dull moment in the lab. I owe a special shout out to the ladies of the lab who I started this journey with, Maneka Chitiprolu and Danielle McCulloch. Maneka, I can't thank you enough for being my unofficial grad school guide. Danielle, for the positive energy and humour you carried with you every day. My sincere gratitude to my coffee buddy, Yunping Xue for adhering to our after-hours "no abandonment" policy for those long days.

To my friends, my cheerleaders, and my part-time therapists who each have a unique approach to life that inspire me every day. India Walker, for teaching me balance. Candice Lee, for reminding me that there's nuance in everything. Tanya Foley, for always showing me the humour in *every* situation. Abdo Elnakouri for your positive yet realistic advice. Thanks team, you all held me together the days I couldn't do it myself.

Finally, to my parents, Tesfaye Negeri and Lelisie Theophilos. Thank you for being my examples of resilience and adaptability as you restarted on three continents, and nonetheless thrived in

unfamiliar and challenging environments. If you could do that, then I could do this. Dad, thank you for all the lab tours when I was little that inspired me to explore a career in research and for always reminding me to stay curious. Mom, for all your wisdom. The lessons you taught me that didn't really make sense back then became very clear (and necessary) throughout this journey.

Table of Contents

List of Figures

List of Tables

List of Abbreviations

ARE: Adenylate-uridylate (AU)-rich element
ATP: adenosine triphosphate
BDNF: brain-derived neurotrophic factor
CD: Crohn's disease
Cdkn1 (p21): cyclin dependent kinase inhibitor 1
Co-IP: co-immunoprecipitation
DJ1: protein deglycase DJ-1
DNA: deoxyribonucleic acid
DSS: dextran sodium sulfate
EDTA: ethylenediaminetetraacetic acid (EDTA)
EGTA: ethylene glycol tetraacetic acid
ELAVL: embryonic vision abnormal protein- like
GD: Gaucher's disease
GBA: glucocerebrosidase
GWAS: genome-wide association studies
HCl: hydrochloric acid
HuB-C-D-R: Human antigen B-C-D-R
IBD: inflammatory bowel disease
IFNg:interferon gamma
IgG: immunoglobulin G
Il-1b : interleukin 1 beta
Il-6 : interleukin 6
iPD: idiopathic Parkinson's disease
iPSC: induced pluripotent stem cells
Kd: kidney
kDa: kilodalton
LB: Lewy body
LC-MS: mass-spectrometry
L-DOPA: levodopa

LPS: lipopolysaccharide

LRRK2: Leucine rich repeat kinase 2

MB: midbrain

MEF: mouse embryonic fibroblast

MFF: mitochondrial fission factor

MFN1 /2: mitofusin1/2

miRNA: microRNA

MgCl2: magnesium chloride

MPP+: 1-methyl-4-phenylpyridinium ion

MPTP: 1-methyl-4-phenyl-1,2,3,6-tetrahydropyridine

mRNA: messenger RNA

NaCl: sodium chloride

OGTT: oral glucose tolerance test

OPA1: optic atrophy 1

OPA3: outer mitochondrial membrane lipid metabolism regulator

PAGE: polyacrylamide gel electrophoresis

PBS: phosphate buffered saline

PCR: polymerase chain reaction

PD: Parkinson's disease

PINK1: PTEN-induced kinase 1

PKC: protein kinase C

PVDF: poly(vinylidene fluoride)

R-IP: RNA immunoprecipitation

RBP: RNA-binding protein

RNA: ribonucleic acid

ROS: reactive oxygen species

SDS: sodium dodecyl sulfate

Ser: serine

siRNA: silencing RNA

SNCA: alpha-synuclein

SNP: single nucleotide polymorphism

SNc: substantia nigra pars compacta

Seq: sequencing

TBS: tris-buffered saline

TH+: Tyrosine Hydroxylase

Thr: Threonine

TLR: Toll-like receptor

Tgfb1: transforming growth factor beta 1

Tnfa: tumour necrosis factor alpha

Tris: tris(hydroxymethyl)aminomethane

UTR: untranslated region

VPS35: Vacuolar protein sorting ortholog 35

WT: wild-type

Chapter 1

Introduction

1.1 Parkinson's Disease

Parkinson's disease (PD) is a currently incurable neurodegenerative disorder characterized by motor impairment caused by the selective loss of dopaminergic neurons of the substantia nigra (Schmidt et al., 2022). PD affects over 6 million people globally, making it the second most common neurodegenerative disease after Alzheimer's disease (Armstrong & Okun, 2020). Recent estimates suggest that Parkinson's incidence is increasing more than any other neurological disorder (Armstrong & Okun, 2020).

1.1.1 History of PD

Records describing a Parkinson's-like disorder in Chinese and Indian text date back millennia (Goetz, 2011; Manyam, 1990; Z.-X. Zhang et al., 2006). The traditional medicines used to treat the Parkinson's-like symptoms in these civilizations share properties with the medicine used to treat PD today (Section 1.5). Traditional Chinese medicine included an anti-tremor pill made of a mixture of plants with anticholinergic compounds, antioxidants, and Monoamine oxidase B inhibiting compounds (Goetz, 2011; Z.-X. Zhang et al., 2006). In India, the Masabaldi pacana medicine contained seeds of the *Mucana pruriens* plant- a source of Levodopa (Goetz, 2011; Manyam, 1990). These texts indicate that Parkinson's like movement disorders predates many of the hypothesized causative agents that exist today (Goetz, 2011).

The first medical description of PD is attributed to the English physician Dr. James Parkinson who described the affliction as "The Shaking Palsy" in an essay he published in 1817 (Goetz, 2011). Jean-Martin Charcot, a French neurologist who coined the term "Parkinson's disease" is credited

for his meticulous characterization of PD symptoms and distinguishing it from other movement disorders like multiple sclerosis (Goetz, 2011).

1.2 PD epidemiology

Parkinson's risk increases with age and is present in an estimated 1-2% of the population over 65 and up to 4-5% over 85 years of age (Váradi, 2020). Risk factors for Parkinson's disease include genetic and environmental factors (Dorsey et al., 2018). PD prevalence correlates with the increased presence of toxins like pesticides and solvents in industrialized countries (Dorsey et al., 2018). PD shows a sex-bias towards males, likely caused by the lower levels of estrogen which is thought to be protective (Váradi, 2020). Other potentially protective factors include smoking and coffee consumption (Váradi, 2020). In addition to the environmental risk factors, PD is also associated with several genetic risk factors (Section 1.6). Mutations in the *Leucine-rich repeat kinase 2* (*LRRK2*), α-synuclein (*SNCA*), and glucocerebrosidase (*GBA)* genes are autosomal dominant while recessive and early onset PD risk alleles include PTEN-induced kinase 1 (*PINK1*), Parkin (*PRKN*) and Parkinsonism associated deglycase, DJ-1 (*PARK7*) (Bonifati et al., 2003; Gasser, 2004; Kitada et al., 1998; Valente et al., 2004). An estimated 5-10% of PD cases are caused by mutations in one of these genes; however, most cases are sporadic (Gialluisi et al., 2021).

1.3 Clinical features of PD

1.3.1 Primary symptoms

The cardinal symptoms of PD are the primary motor deficits including postural instability, tremor, rigidity, and bradykinesia (Váradi, 2020). Bradykinesia, which describes a slowness in movement, is the main motor symptom in PD. The lack of energy manifests as slower movements affecting actions from delayed reaction times to decreased blinking. The rest tremor describes a muscular contraction in the 4-6 Hz frequency range that can be controlled with dopamine therapies. Rigidity is characterized by a decreased range of motion and can be managed with some therapies. Finally, postural instability is associated with more advanced PD and is a risk factor for injuries. It is poorly managed by dopamine therapies (Váradi, 2020) .

1.3.2 Other symptoms

PD patients are also burdened with a variety of other symptoms like speech impairment and difficulty swallowing (Pfeiffer, 2016; Polychronis et al., 2019). One of the most common prodromal symptoms includes constipation, which is experienced by roughly 60% of patients and can precede the onset of motor symptoms by decades (Roos et al., 2022; Váradi, 2020). Hyposmia, or a reduced sense of smell, occurs in over 80% of PD patients coinciding with α-synuclein accumulation in the olfactory neurons prior to dopaminergic neuron degeneration (Váradi, 2020.) Sleep disturbances are also commonly reported in PD and severely decrease quality of patient life (Albers et al., 2017). In addition to these symptoms, patients may present with cognitive impairment and mood dysregulation (Rektorova, 2019).

1.4 PD pathology

Degeneration of dopaminergic neurons

PD is characterized by the progressive loss of dopaminergic (DA) neurons in the substantia nigra pars compacta, a region of the midbrain (Grosch et al., 2016). These DA neurons project to the dorsal striatum to form the nigrostriatal pathway where they control motor movement (Grosch et al., 2016). In Parkinson's disease, these neurons begin to degenerate and manifest as motor impairment which can be observed as early as after ~30% of DA neurons are lost (Grosch et al., 2016). A hallmark feature of PD is the presence of Lewy bodies (LB) that refers to dense structures found in remaining dopaminergic neurons (Stefanis, 2012). Most literature on Lewy bodies suggest that they are protein aggregates mostly composed of α-synuclein (Shahmoradian et al., 2019). Recent ultrastructure analyses of LBs confirm the presence of α-synuclein, including the toxic phosphorylated S129 species; however, LBs were found to be mostly composed of fragmented lipids including membranes and organelles (Shahmoradian et al., 2019).

1.5 Current treatments

Levodopa

There are currently no true disease modifying treatments for Parkinson's disease (de Bie et al., 2020). The most widely used and most effective treatment is Levodopa which is the precursor to dopamine and therefore addresses the decrease in dopamine levels associated with motor impairment (de Bie et al., 2020). Levodopa, or L-DOPA, was first used in PD treatment in the 1960s (Abbott, 2010). Ironically, L-DOPA use may also lead to dyskinesias, and its use may be

avoided or delayed. Clinical trial data, however, supports its use early in disease onset as it was shown to minimize PD disability, and debunked the notion that levodopa therapy should be delayed for the sake of avoiding levodopa-induced toxicity (de Bie et al., 2020; PD MED Collaborative Group, 2014; Verschuur et al., 2019).

Deep Brain Stimulation (DBS)

Deep brain stimulation describes the delivery of electrical pulses to selected brain regions via surgically implanted devices (Pycroft et al., 2018). DBS may be employed for movement disorders and was specifically approved for Parkinson's by the FDA in 2003 (Bucur & Papagno, 2023). In the case of PD, DBS targets the subthalamic nucleus (STN) or globus pallidus internus (GPi) (Bucur & Papagno, 2023). Candidate patients may be selected if drug therapy is insufficient (Geraedts et al., 2019).

Dopamine Agonists

Dopamine agonists were first used in the 1970s to treat PD (Antonini et al., 2009). Dopamine agonists differ in their pharmacological profile from Levodopa showing a longer half-life and are associated with fewer complications but are overall less effective than Levodopa at managing PD symptoms (Antonini et al., 2009). Dopamine agonists are commonly used both as an early monotherapy and as an adjunct therapy to levodopa and are associated with numerous negative side effects including leg and peripheral edema, decreased impulse control, psychosis, depression, confusion, and excessive sleepiness (Antonini et al., 2009).

Other drugs

Anticholinergic drugs were the first class of drugs used to treat PD. They are antagonists of muscarinic receptors that were used to treat motor symptoms associated with PD (Barrett et al., 2021). They were prescribed in early-stage PD to spare Levodopa for later stages, as prolonged L-DOPA use is associated with dyskinesias (Barrett et al., 2021). They were also used as an adjunctive therapy with L-DOPA in advanced cases (Brocks, 1999).

Monoamine oxidase inhibitors are another class of drug used to treat PD. Monoamine oxidases (MAO) are a group of enzymes that degrade amine-based neurotransmitters, which include dopamine (Cho et al., 2021). Monoamine oxidase B (MAOB) inhibitors are mostly believed to simply increase extracellular dopamine levels; however, there is some evidence that they might be effective via a different mechanism (Cho et al., 2021). MAOB inhibitors in the use of PD are effective at slowing down the progression of motor symptoms and may be used as an adjuvant therapy in PD to mitigate levodopa-related complications (Tan et al., 2022).

1.6 Genetics of Parkinson's Disease

1.6.1 Autosomal recessive

DJ1 (PARK7)

Mutations in the deglycase-1 (DJ-1/*PARK7*) gene are associated with early-onset familial PD (Bonifati et al., 2003). Patients with DJ-1 mutations present with an earlier onset of classic PD motor symptoms that are manageable with L-DOPA, and eventually may develop cognitive and mood symptoms (Repici & Giorgini, 2019). DJ-1 has been associated with many cellular processes including mitochondrial homeostasis, oxidative stress, transcription, and glucose homeostasis (Ariga et al., 2013). DJ-1 plays a neuroprotective role in cells and its loss of function results in increased sensitivity to toxins like MPTP in dopaminergic neurons of DJ-1 deficient mice (Aleyasin et al., 2010).

PINK1 (PARK6)

The PTEN-induced kinase 1 (*PINK1*) gene encodes a mitochondrial serine/threonine kinase involved in mitochondrial homeostasis and the selective degradation of damaged mitochondria (i.e., mitophagy)(Quinn et al., 2020). Mutations in *PINK1* are among the most common form of autosomal recessive PD and are associated with an age at onset of around 30 years (Gonçalves & Morais, 2021). Clinically, patients with *PINK1* mutations present with a slower, and less severe progression of symptoms principally characterized by motor dysfunction, with little cognitive impairment (Gonçalves & Morais, 2021).

In cells, damaged mitochondria cause the loss of mitochondrial membrane potential which signals the recruitment and accumulation of PINK1 to the mitochondrial outer membrane. This recruits its protein partner, Parkin and together they initiate mitophagy (Vizziello et al., 2021). PINK1 is also related to the mitochondrial respiratory chain, where loss of function results in impaired Complex 1 function and subsequent mitochondrial dysfunction (Vizziello et al., 2021). Despite the obvious detrimental effects of mutant *PINK1* in humans, and accumulation of *in vitro* evidence, *Pink1*-deficient rodent models do not exhibit significant impairment in mitophagy or neuronal cell survival (Han et al., 2023).

Parkin (PARK2/PRKN)

The *PRKN* gene encodes the protein Parkin, which is an E3 ubiquitin ligase best known for its roles in mitophagy. PRKN-PD is associated with an early onset, but slowly progressing form of PD, with minimal non-motor symptoms (X. Liu & Le, 2020), and is caused by mutant or truncated forms of the protein, resulting in its loss of function (van der Vlag et al., 2020).

In cells, Parkin is recruited to damaged mitochondrial through its phosphorylation by PINK1 where it ubiquitinates its substrates, marking the mitochondria for degradation (van der Vlag et al., 2020). Aside from its function in mitophagy, evidence suggests that Parkin plays a protective role in oxidative stress through redox control (El Kodsi et al., 2023; Tokarew et al., 2021).

Like PINK1, animal models of Parkin deficiency do not recapitulate hallmark PD symptoms but do show evidence of mitochondrial dysfunction and impaired oxidative stress responses (Paul & Pickrell, 2021). The rodent models show minor or no behavioural and motor deficits and no

dopaminergic neuron loss, except for one model that exhibited both in *Prkn*$^{-/-}$ mice aged over 2 years (Noda et al., 2020; Paul & Pickrell, 2021).

1.6.2 Autosomal dominant

GBA

The glucocerebrosidase gene encodes the lysosomal hydrolase enzyme, glucocerebrosidase (GCase), that is best known as the causative gene for Gaucher disease (GD), an autosomal recessive lysosomal storage disorder (Riboldi & Di Fonzo, 2019). Mutations in GBA are now known to be the most common genetic cause of PD with up to 15% of the global PD patient population expressing a GBA variant (Smith & Schapira, 2022). The clinical presentation of GBA-PD is nearly indistinguishable from sporadic cases and display hallmark characteristics like motor symptoms, nigrostriatal degeneration, and Lewy Body formation (Smith & Schapira, 2022). Furthermore, mutations in GBA are associated with a more rapid progression of motor symptoms and an earlier onset compared to idiopathic cases (Behl et al., 2021).

VPS35 (PARK17)

The vacuolar protein sorting 35 (*VPS35*) gene encodes an endosome associated protein that makes up a component of the retromer complex that regulates retrograde transport from the endosome to the Golgi (Seaman et al., 1998). VPS35 is expressed in most cell types and is associated with lysosomal and mitochondrial function, and autophagy (Sassone et al., 2021). VPS35 mutations are linked to late-onset autosomal dominant PD and are a relatively rare cause (Sassone et al., 2021). Both motor and non-motor symptoms observed in PD patients with VPS35 mutations closely resemble idiopathic cases (Sassone et al. 2021).

Alpha-synuclein (SNCA/PARK4)

Mutations and duplications of the *SNCA* gene are associated with autosomal dominant PD (Gasser, 2004) It was first linked to PD through the discovery of the A53T substitution that segregated with early onset familial PD in Italian and Greek families (Polymeropoulos et al., 1997). In the same year, α-synuclein was identified as the principal component of LBs post-mortem brain tissue of PD and dementia with LB (Spillantini et al., 1997). In subsequent years, gene duplications and triplications were reported in families with late onset, and early onset PD, respectively (Chartier-Harlin et al., 2004; Singleton et al., 2003).

Though the focus has been on mutations in the coding region of *SNCA*, genome-wide association studies (*GWAS*) provide evidence for the 3' untranslated region (UTR) in regulation of *SNCA* (Fuchs et al., 2008; Simón-Sánchez et al., 2009). It was later discovered that an α-synuclein transcript bearing a long 3'UTR is associated with increased protein accumulation and mitochondrial localization (Rhinn et al., 2012). The RNA-binding protein (RBP) HuR, has been linked to the regulation of specifically, the long 3'untranslated region (UTR) of *SNCA*. These data suggest that variants in the 3'UTR may contribute to the regulation of mRNA stability or translation of *SNCA* in the PD brain (Marchese et al., 2017).

The *SNCA* gene encodes a small 14 kDa natively unfolded protein homologous to β and γ-synuclein (Stefanis, 2012). α -synuclein is highly expressed in neurons and is localized to both the nucleus and the presynaptic terminals. Elevated expression of α -synuclein in contexts of neuronal activity and its presynaptic localization led to investigating its potential role in neurotransmission (Stefanis, 2012). In agreement, α -synuclein was shown to associate with and facilitate SNARE

complex assembly, a process that is required to dock synaptic vesicles and has implications in neurotransmitter release (Burré et al., 2010; Miraglia et al., 2018).

α -synuclein typically exists in its unfolded, monomeric state but under pathological conditions can oligomerize and this aggregation contributes to the formation of Lewy Bodies (Du et al., 2020). Oligomeric α -synuclein is associated with mitochondrial dysfunction, ER stress and inflammation among other impairments (Du et al., 2020). Interestingly, α -synuclein is capable of neuron-to-neuron transmission akin to prion proteins (Danzer et al., 2009). α -synuclein seeding was observed in healthy cells from neuronal grafts in patients, suggesting a cell-to-cell transmission mechanism (Danzer et al., 2009).

Several animal models of α -synuclein pathology have been developed including the use of pre-formed fibrils (PFFs) (Gómez-Benito et al., 2020). Recombinant α -synuclein is processed such that it generates fibrils, and they are injected into the brains of animal models (Gómez-Benito et al., 2020). This model recapitulates the aggregation of α -synuclein and contributes to hallmark characteristics of PD including DA neuron loss and motor deficits (Gómez-Benito et al., 2020; Paumier et al., 2015; Shimozawa et al., 2017).

LRRK2 (PARK8)

LRRK2 in Parkinson's disease

The *Leucine-rich repeat kinase 2* (*LRRK2*) gene was first genetically linked to Parkinson's disease in 2002 through a genome-wide linkage analysis of a Japanese family with autosomal dominant PD (Funayama et al., 2002). The association of this risk locus was independently confirmed by two studies in 2004 (Paisán-Ruíz et al., 2004; Zimprich et al., 2004). Mutations in *LRRK2* account for an estimated 1-5% of sporadic cases and 5-13% of familial PD, where the gain-of-function G2019S mutation is the most common (Kalogeropulou et al., 2022). Interestingly, in Ashkenazi Jewish and North African Berber populations, the prevalence of the G2019S mutation is increased to nearly 20% and 40%, respectively (Gasser, 2011). The G2019S mutation is associated with incomplete penetrance that is known to increase with age; however, the estimated penetrance varies widely between studies and populations (Gasser, 2011; Healy et al., 2008a; A. J. Lee et al., 2017). The molecular mechanisms contributing to penetrance is unclear, but risk factors like age, lifestyle, inflammation, and exposure to toxins are all contributing factors (Trinh et al., 2022).

LRRK2 mutation carriers with PD present with the cardinal symptoms including postural instability, rigidity, and tremor such that the clinical manifestation of LRRK2-PD is often said to be indistinguishable from sporadic cases; however, some differences have been observed. For example, a slightly earlier age-at-onset, slower progression of motor symptoms, and a lack of sex differences in LRRK2-G2019S carriers has been reported (Gan-Or et al., 2015; Healy et al., 2008b; Tolosa et al., 2020). LRRK2 mutation carriers present with the same non-motor and cognitive changes observed in typical PD cases, but the prevalence and severity are less than in idiopathic patients (Tolosa et al., 2020).

LRRK2 in Crohn's disease

Genome-wide association studies (GWAS) have also linked *LRRK2* mutations to the inflammatory bowel disease (IBD), Crohn's, which causes chronic inflammation of the gastrointestinal tract (Herrick & Tansey, 2021). This is perhaps initially surprising, but the development of IBD symptoms in Parkinson's patients highlights the commonality between PD and CD, and it is therefore conceivable that LRRK2 is a causative gene of two seemingly unrelated disorders. In support of the shared etiology of PD and CD, it has been reported that IBD patients have a ~30% increased chance of developing Parkinson's disease (Peter et al., 2018). A recently identified gain of function risk variant, *LRRK2 N2081D*, has been defined as a shared risk locus for PD and CD(Hui et al., 2018). In Crohn's patients, the *LRRK2 G2019S* mutation was associated with CD, but not significant, and the N2081D substitution was the dominant risk allele associated with CD in the studied cohort (Hui et al., 2018; Levine et al., 2016).

LRRK2 in Leprosy

Leprosy is an ancient human disease caused by infection with *Mycobacterium leprae* (Santacroce et al., 2021). Infection with *M. leprae* is dependent on the genetic susceptibility of the host and the severity of the disease is dependent on the environment and host-specific factors (F.-R. Zhang et al., 2009). Leprosy is classified as paucibacillary if the patient has fewer than 5 lesions or multibacillary if the patient has more than 5 lesions (Parkash, 2009). Interestingly, a 2009 GWAS indicated a trend in SNPs found at the *LRRK2* locus, and the association of *LRRK2* with leprosy was increased in multibacillary cases (F.-R. Zhang et al., 2009). In some Leprosy cases, patients may experience type-1 reactions (T1R) that are described as episodes of exacerbated inflammation that may lead to irreversible nerve damage. A study of families affected by T1R indicated a strong

association with SNPs at the *LRRK2* locus with T1R (Fava et al., 2016). Some of these SNPs were also associated with Crohn's and Ulcerative colitis (Fava et al., 2016). In contrast with PD and CD which are associated with LRRK2 gain-of-function mutations, the SNP with the strongest association with T1R, was the LRRK2 M2397T which decreases LRRK2 protein half-life (Fava et al., 2016; Z. Liu et al., 2011). This decrease in LRRK2 protein stability was linked to an exacerbated inflammatory phenotype in a mouse model of colitis, suggesting that LRRK2 loss of function can also cause inflammation (Z. Liu et al., 2011).

LRRK2 protein structure and function

The Leucine-rich repeat kinase 2 (*LRRK2*) gene is located on chromosome 12 in humans and spans 51 exons (Di Fonzo et al., 2006). LRRK2 is most highly expressed in immune cells, lungs, kidney, intestine, and is comparatively low in the brain (Taylor & Alessi, 2020). *LRRK2* encodes a large, 286 kDa protein consisting of 7 core domains: the N-terminal Leucine-rich repeats, Armadillo repeats, ankyrin repeats, the C-terminal WD40, Ras of complex (Roc), C-terminal of Roc (COR) and a kinase domain (Kumari & Tan, 2010). Much of the understanding of LRRK2 activity surrounds the two enzymatic domains, the GTPase and kinase, due to the density of PD-linked mutations in these domains (Fig.1.6.1).

LRRK2 GTPase activity

LRRK2 possesses the characteristic domains of the ROCO family of proteins consisting of a Ras-like GTPase (i.e., Roc) and the tandem, and essential domain, COR (Gilsbach & Kortholt, 2014) . Several pathogenic mutations have been mapped to this region of the LRRK2 protein including the N1437H, R1441C, R1441G, R1441H and Y1699C, mutations which reduce LRRK2 GTPase activity, but increase LRRK2 kinase activity to some degree (Greggio & Cookson, 2009; A. P. T. Nguyen & Moore, 2017; West et al., 2005a, 2007). PD-like symptoms have been observed in animal models of LRRK2 GTPase mutants. In *Drosophila*, the R1441C and Y1699C mutants were associated with impaired axonal transport and motor deficits (Godena et al., 2014). Mouse models of the R1441G mutant were reported to exhibit age-dependent motor deficits, altered morphology of dopaminergic neurons, tau pathology, and axonopathy (Y. Li et al., 2009; Tagliaferro et al., 2015). Models of the R144C mutant have also shown altered morphology of dopaminergic neurons, in addition to impaired dopamine transmission (Tong et al., 2009; Tsika et al., 2014).

LRRK2 kinase activity

The most well characterized function in LRRK2 is its kinase activity. The focus on this region is largely attributed to the fact that the most common pathogenic mutation in *LRRK2* is the Glycine to Serine substitution at residue 2019 within the kinase domain (Rocha et al., 2022). The DFGψ motif is a canonical catalytic motif found in all kinases, but in LRRK2 it is a DYGI motif (aa 2017-2020) (Rocha et al., 2022). The G2019S mutation which typically confers a 2-3-fold increase in activity (Greggio & Cookson, 2009; West et al., 2005a), and the I2020T hyperactive kinase mutants lie within this region (Rocha et al., 2022). More recently the LRRK2 N2081D mutation was identified, and it was also found to exhibit hyperactive kinase activity (Hui et al., 2018).

Animal models of LRRK2 kinase mutants show some PD-relevant phenotypes. In *Drosophila* expression of human LRRK2-I2020T was associated with dopaminergic neuron loss and motor deficits (Marcogliese et al., 2017). In contrast, LRRK2-I2020T transgenic mice showed motor deficits on the beam test and rotarod test as well as significantly lower striatal dopamine but no dopaminergic neuron loss(Maekawa et al., 2012). Most LRRK2 rodent models fail to exhibit dopaminergic neuron loss or α-synuclein pathology with a few exceptions (Seegobin et al., 2020). A model expressing human LRRK2 G2019S-TAP showed loss of DA neurons at 15 months of age and gait deficits (Xiong et al., 2018). An earlier transgenic model expressing LRRK2-G2019S showed an age-dependent decrease in dopaminergic neuron loss along with mitochondrial and autophagic abnormalities (Ramonet et al., 2011).

LRRK2 protein-protein interaction domains

The protein-protein interaction domains of LRRK2 are essential for its signaling functions. The namesake LRR domain is important for LRRK2 interaction with the 14-3-3 family of signaling proteins (J. Chen et al., 2018). In the presence of many of the common LRRK2 mutations, phosphorylation of LRRK2 at Ser910 and Ser935 is significantly reduced and impairs LRRK2 binding to 14-3-3, altering its subcellular localization (Nichols et al., 2010). 14-3-3 proteins impact LRRK2 function, since their inhibition results in LRRK2-mediated neurite shortening (Lavalley et al., 2016). The WD40 domain was shown to be important for LRRK2 dimerization (P. Zhang et al., 2019). Some mutations in this domain, including the G2385R, increased LRRK2 kinase activity and phosphorylate threonine (Thr73) of its substrate RAB10, while the deletion of this domain impairs kinase activity (Jaleel et al., 2007; P. Zhang et al., 2019). The function of the N-terminal armadillo domain is less well characterized, but evidence suggests that it is involved in

LRRK2 protein-protein interactions with Rab proteins (McGrath et al., 2021) The adjacent ankyrin domain appears to be required for the intramolecular control of LRRK2 kinase function (Guaitoli et al., 2016).

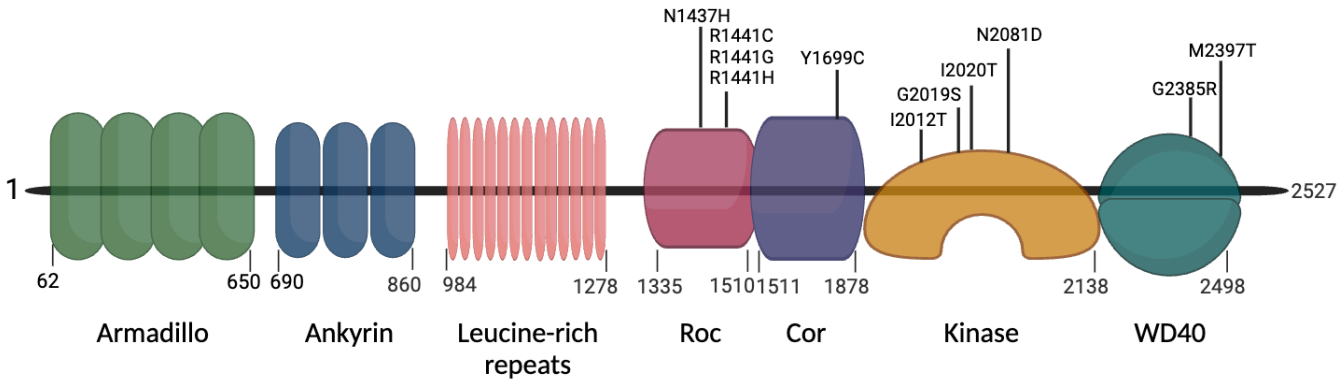

Figure 1.6.1. LRRK2 protein structure

Mutations with evidence for pathogenesis in Crohn's Disease or Parkinson's Disease are included in the figure. Adapted from (Fava et al., 2016; Greggio & Cookson, 2009; Thakur et al., 2022). Image was generated with BioRender.

LRRK2 Cellular Functions

Post-transcriptional and translational Control

Many studies have reported an effect on the transcriptome of immune and neuronal cells from LRRK2-deficient or mutant models, and patient-derived samples compared to healthy controls; however, it is unclear if these are intermediary effects or directly controlled by LRRK2 (Connor-Robson et al., 2019; Häbig et al., 2008; Levy et al., 2020; Nikonova et al., 2012; Russo et al., 2019; Schulz et al., 2011).

A 2008 study suggested that the *Drosophila* LRRK and human LRRK2 phosphorylate the eukaryotic initiation factor 4E (eIF4E)-binding protein (4E-BP). In *Drosophila*, the chronic phosphorylation of 4E-BP by LRRK inhibits 4E-BP function promoting the release of eIF4E and subsequent translation initiation. This results in aberrant translational control and loss of dopaminergic neurons (Imai et al., 2008). A later study found that LRRK2 also promotes translation by phosphorylating the small ribosomal subunit s15 in human dopaminergic neurons and *Drosophila* (Martin et al., 2014). Flies expressing the G2019S hyperactive kinase mutant exhibited motor impairment and dopaminergic neuron loss that was rescued by inhibition of global protein synthesis. Furthermore, phospho-dead mutants of s15 also inhibited phosphorylation by LRRK2 thereby rescuing LRRK2 mediated neurotoxicity (Martin et al., 2014), but this has yet to be confirmed as a physiological substrate. Follow-up studies suggested that *in vitro* phosphorylation of 4E-BP was lower than LRRK2 autophosphorylation and no observable changes were detected in 4E-BP phosphorylation in *Lrrk2*-deficient or mutant mice, nor in brain samples

from idiopathic or *LRRK2-G2019S* mutation-carriers, calling into question the clinical relevance of these targets (Kumar et al., 2010; Trancikova et al., 2012).

Cytoskeleton and morphology

Early work investigating LRRK2 function in cells indicated that it regulates neurite outgrowth (MacLeod et al., 2006). In LRRK2-deficient neuronal cells, neurite length is significantly increased. The inverse is true in the presence of pathogenic mutations in both the GTPase and kinase domains (MacLeod et al., 2006). Among the proposed LRRK2 phosphorylation substrates are proteins that control cytoskeletal organization and cell motility. The ERM (i.e., moesin, ezrin and radixin) proteins that anchor the plasma membrane are phosphorylated by LRRK2 and contribute to neurite shortening in neuronal cells derived from *Lrrk2-G2019S* expressing mice, suggesting that LRRK2 controls neuronal cell morphology homeostasis (Jaleel et al., 2007; Parisiadou et al., 2009).

Mitochondrial function

Familial PD is associated with mutations in several mitochondrial quality control proteins. Mitochondrial homeostasis is largely dependent on the dynamic fission and fusion events (Singh et al., 2019). LRRK2 was shown to directly interact with the mitochondrial fission protein, DRP1 and this interaction was impaired by a mutation within the armadillo domain (Perez Carrion et al., 2018). This led to impaired mitochondrial fission and susceptibility to MPP+ induced neurotoxicity (Perez Carrion et al., 2018). In the human neuroblastoma cell line, SH-SY5Y, LRRK2 mutations R1441C and G2019S were associated with fragmented mitochondria via a direct LRRK2 interaction with DRP1(X. Wang et al., 2012). Furthermore, the levels of Optic

Atrophy 1 (OPA1), a mitochondrial fusion protein were significantly decreased in the brains of *LRRK2-G2019S* patients (Stafa et al., 2014).

Oxidative stress

Mitochondrial respiration generates reactive oxygen species (ROS) as a by-product that may lead to cell death if inadequately controlled (Turrens, 2003). LRRK2 mutations have also been linked to impaired resilience to oxidative stress (J.-Q. Li et al., 2014). This was demonstrated in *Drosophila* expressing mutant human *LRRK2* that showed increased sensitivity to rotenone and a shortened lifespan (Ng et al., 2009). In iPSC-derived dopaminergic neurons expressing the *LRRK2-G2019S* mutation, it was observed that the cells had increased sensitivity to hydrogen peroxide induced oxidative stress (H. N. Nguyen et al., 2011).

Endolysomal Function

Evidence for LRRK2 control of lysosomal homeostasis was observed in peripheral tissues. Knockout of *Lrrk2* in rodents results in an increased number of or enlarged lysosomes in lung and kidney tissue (Baptista et al., 2013; Herzig et al., 2011). In non-human primates treated with novel LRRK2 kinase inhibitors, this phenotype was noted in the lung (Baptista et al., 2020). Primary neurons derived from mice expressing *Lrrk2 G2019S* also show lysosomal abnormalities such as decreased size and number (Kuwahara & Iwatsubo, 2020). Furthermore, LRRK2 phosphorylates many of the Rab GTPases like RAB8 and RAB10 that have roles in vesicular trafficking (Kuwahara & Iwatsubo, 2020; Steger et al., 2016). The relevance of Rab phosphorylation in PD remains elusive. Nevertheless, the Rab GTPases are currently the only widely accepted LRRK2 substrates.

Autophagy

Loss of LRRK2 or expression of mutant LRRK2 has also been linked with abnormalities in the macroautophagy pathway, a lysosome-dependent degradation system, though it is unclear if LRRK2 promotes autophagy or suppresses it as there is evidence supporting both (Kuwahara & Iwatsubo, 2020). In aged *Lrrk2*$^{-/-}$ mice, an accumulation of α-synuclein was increased in kidney tissue (Tong et al., 2010). It was accompanied by decreased levels of the autophagy marker LC3-II. Autophagic flux was also found to be decreased in *Lrrk2*-deficient macrophages and microglia (Schapansky et al., 2014), whereas G2019S expression in neuroblastoma cells promoted an increase in LC3+ autophagic vacuoles (Kuwahara & Iwatsubo, 2020).

LRRK2 in neuroinflammation

LRRK2 also appears to control various responses relevant to neuroinflammation. For example, in mice administered an intracranial injection of LPS, expression of LRRK2 and its autophosphorylation, a marker of its kinase activity, were significantly increased (Moehle et al., 2012). Silencing of LRRK2 by siRNA in rat primary microglia indicated a significant decrease in TNF-α release, chemotaxis, and microglial process outgrowth, suggesting that LRRK2 drives a proinflammatory response (Moehle et al., 2012). In *Lrrk2*-deficient primary microglia, the levels of the proinflammatory cytokine *Il1b* mRNA and protein were significantly decreased compared to wild-type cells in response to LPS (Russo et al., 2015). These same cells exhibited an attenuated inflammatory response to α-synuclein fibrils (Russo et al., 2015). In co-cultures of primary macrophages and mesencephalic neurons derived from *Lrrk2-G2019S* mice and *in vivo*, LRRK2-G2019S promoted loss of TH+ neurons in a WAVE-2 dependent manner (K. S. Kim et al., 2018a).

This was attributed to LRRK2-mediated phosphorylation and stabilization of WAVE2, which enables cytoskeletal remodeling and enhanced phagocytosis.

In another model of neuroinflammation, mice were primed with LPS injections into the SNc promoting activation of microglia and increased levels of WAVE2 in wild-type mice (Dwyer et al., 2020). This response was ablated in *Lrrk2*$^{-/-}$ mice. The data suggest that LRRK2 and WAVE2 mediate microglial activation (Dwyer et al., 2020), supporting earlier findings that LRRK2 and WAVE2 are important in microglial responses.

Finally, it was found that LRRK2 promotes the microglial proinflammatory response and neuronal impairment initiated by α-synuclein activation of Toll-like receptor 2 (TLR2) (Ho et al., 2022). In another study in the same year, it was observed that an increase in pro-inflammatory monocyte-derived macrophages were recruited to the brain in response to intracranial injection of α-synuclein fibrils (Xu et al., 2022). This was mediated through increased LRRK2 expression and phosphorylation of Rab10. This phenotype was further increased in the presence of mutant LRRK2 R1441C and LRRK2 G2019S. These findings support Moehle et al., 2012 that LRRK2 regulates chemotaxis (Xu et al., 2022).

LRRK2 in peripheral and systemic inflammation

LRRK2 is expressed in tissues with functions in the immune system including the spleen, thymus, and lymph nodes (Biskup et al., 2007; Westerlund et al., 2008). Early studies investigating the role of LRRK2 in inflammation found that it is highly expressed in cells with roles in innate immunity including monocytes, macrophages, B-lymphocytes, and dendritic cells (Gardet et al., 2010;

Hakimi et al., 2011). LRRK2 expression is significantly increased by IFN-γ stimulation in the human monocytic cell line THP-1 and the promoter region of LRRK2 harbours conserved binding sites for IFN response factors (Gardet et al., 2010). Furthermore, intestinal biopsies from Crohn's patients revealed high expression of LRRK2 (Gardet et al., 2010). It was also shown that *Lrrk2* expression significantly increased in response to proinflammatory stimuli like the bacterial lipopolysaccharide (LPS) and lentiviral particles in mouse primary macrophages (Hakimi et al., 2011).

While cytokine release is detected in a LRRK2 dependent manner in microglia cells (B. Kim et al., 2012; C. Kim et al., 2020; Moehle et al., 2012; Russo et al., 2015), the data are inconsistent for peripheral cells. In response to toll like receptor agonists, LRRK2 G2019S expressing human monocytes and macrophages secreted increased levels of cytokines and chemokines, but LRRK2 knockout or inhibition had no effect (Ahmadi Rastegar et al., 2022), suggesting that LRRK2 is dispensable in cytokine/chemokine production. Other studies however, found no effect of LPS, IFN-γ or *Salmonella typhimurium* treatment on cytokine levels in LRRK2-G2019S cells or mice (Litteljohn et al., 2018; Moehle et al., 2015; Shutinoski et al., 2019). This could be due to different cell types, contexts, or triggers.

In Paneth cells, which are intestinal epithelial cells required for host defence through secretion of antimicrobial peptides, LRRK2 was shown to associate with the bacterial sensor protein NOD2, which is also genetically linked to Crohn's disease (Q. Zhang et al., 2015). NOD2 was required for the recruitment of LRRK2 and RAB2a to initiate lysosomal sorting to the secretory granules of Paneth cells. Loss of *Lrrk2* compromised host mucosal defence and resulted in increased

susceptibility to intestinal *Listeria monocytogenes* infection compared to wild-type mice(Q. Zhang et al., 2015). A later study investigating the LRRK2 response to intraperitoneal *S.typhimurium*, found that LRRK2 interacts with the NLRC4 inflammasome, which is triggered by exposure to microbial proteins. *Lrrk2*-deficient mice showed impaired clearance of the *S. typhimurium*, suggesting that LRRK2 is protective (W. Liu et al., 2017). A subsequent study in *Lrrk2*$^{-/-}$ and *Lrrk2 G2019S* mice infected with *S.typhimurium*, showed that spleens of *Lrrk2*$^{-/-}$ mice had a higher bacterial load. In contrast, *Lrrk2 G2019S* mice showed greater clearance than wild-type mice. This was accompanied by an increase in myeloid cell recruitment to the spleen by the mutant mice, suggesting a mechanism for LRRK2-dependent pathogen clearance (Shutinoski et al., 2019).

In a mouse model of colitis, LRRK2 was found to be protective against excessive inflammatory phenotypes. It was suggested that LRRK2 sequesters NFAT in the cytoplasm and loss of *Lrrk2*$^{-/-}$ or expression of the M2397T polymorphism that decreases LRRK2 protein half-life results in NFAT translocation to the nucleus, where it promoted transcription of proinflammatory cytokines (Z. Liu et al., 2011). A subsequent study found that *LRRK2* expression is elevated in dendritic cells from Crohn's patients (Takagawa et al., 2018). In murine dendritic cells stimulated with the Dectin-1 ligand, Zymosan D, LRRK2 inhibitors suppressed TNF-α release (Takagawa et al., 2018). *Lrrk2*-transgenic mice treated with DSS showed exacerbated colitis phenotypes that was rescued by LRRK2 inhibitors (Takagawa et al., 2018). These differences could be attributed to several factors including differences in the animal model selected, the source of mice (vendor vs. experimental animal facility), and the study paradigm. In either case, it shows a role for LRRK2 in modulating immune responses relevant to intestinal pathology.

LRRK2 in the clinic

Given the extensive body of literature implicating LRRK2 in PD pathogenesis, it is unsurprising that large scale efforts have been made to develop LRRK2 inhibitors for clinical use. Investigations of LRRK2 kinase inhibitors in preclinical models initially caused concern due to the unexpected but reversible effects on lysosomal structures in the kidneys and Type II pneumocytes in the lungs of animal models, including non-human primates (Andersen et al., 2018; Baptista et al., 2020; Herzig et al., 2011), but since these side effects were deemed benign the development of inhibitors was continued (Baptista et al., 2020). In 2022, Denali Therapeutics completed a Phase 1 and Phase 1b clinical trial for the aminopyrazole kinase inhibitor DNL201, formerly GNE-0877. The study indicated that DNL201 significantly inhibits LRRK2 and altered levels of lysosomal biomarkers. The study concluded that the drug is well tolerated and LRRK2 inhibitors should be pursued as treatments for PD patients (Jennings et al., 2022).

1.7 Embryonic Lethal Abnormal Vision-like (ELAVL) family of RNA binding proteins

RNA-binding proteins (RBPs) are a class of proteins involved in regulating RNA metabolism (Hentze et al., 2018). RBPs may harbor canonical RNA-binding domains like the RNA recognition motif (RRM), KH domain, or tandem zinc finger domains (Hentze et al., 2018). RBPs bind *cis*-regulatory elements within their target transcripts to exert their functions and are tightly controlled by post-translational modifications (PTMs) (Velázquez-Cruz et al., 2021).

The Hu/ELAVL family of RBPs were discovered as antigens in paraneoplastic encephalomyelitis/neuropathy, a neurological syndrome associated with small-cell lung cancer (Dalmau et al., 1990). Patients with this syndrome produce antibodies against the Hu proteins causing an autoimmune reaction targeting the nervous system (Dalmau et al., 1990). The Hu/ELAVL genes are homologous to the *Drosophila* sex lethal (*sxl*), RNA-binding protein 9 (*Rbp9*), found in neurons (*fne*) and embryonic lethal abnormal vision (*elav*) genes (Bell et al., 1988; Y. Kim & Baker, 1993; Robinow et al., 1988).

The Hu/ELAVL protein family consists of four members: Human antigen R (HuR/ELAVL1), HuB (ELAVL2), HuC (ELAVL3) and HuD (ELAVL4). HuB-D are largely restricted to neurons whereas HuR is ubiquitously expressed (Good, 1995; Ma et al., 1996; Okano & Darnell, 1997.) HuB, HuC, and HuD are collectively referred to as the neuronal ELAVLs (nELAVLs). The expression of nELAVLs is restricted to the neuronal cell lineage in the embryonic and adult nervous system since their expression is absent from astrocytes and oligodendrocytes (Akamatsu et al., 2005).

Structurally, they are composed of three RNA-recognition motifs (RRMs) and a linker region between RRM2 and RRM3 (Bronicki & Jasmin, 2013) (Fig. 1.7.1). The nELAVLs are mostly cytoplasmic whereas HuR is predominantly nuclear and all the ELAVLs are capable of nucleocytoplasmic shuttling (Bronicki & Jasmin, 2013; Srikantan & Gorospe, 2012). The shuttling of these proteins allows them to regulate RNA metabolism from splicing of pre-mRNA, to transport and mRNA stability, and translation (Bronicki & Jasmin, 2013).

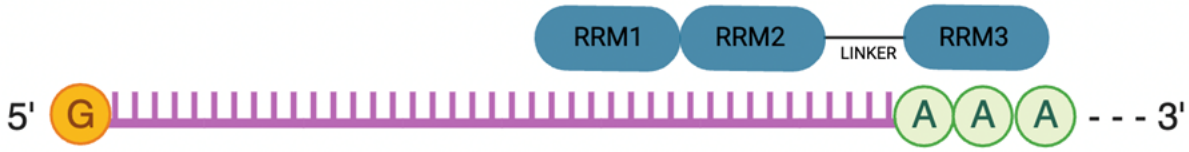

Figure 1.7.1 ELAVL protein structure.

Representation of the ELAVL family of RBP protein structure bound to an mRNA transcript. RRM=RNA Recognition Motif (RRM). Adapted from text in Bronicki & Jasmin, 2013. Image generated using BioRender.

1.8 ELAVL in RNA metabolism

ELAVL in splicing

Alternative splicing is an important step in pre-mRNA processing and contributes to the diversity of the transcriptome (C. Zhang et al., 2007). Splicing is orchestrated by the spliceosome, a complex of small nuclear ribonucleoproteins that removes the introns demarcated by a 5' and 3' splice site (C. Zhang et al., 2007). Splicing is further regulated by other RNA-binding proteins that bind cis-regulatory elements to promote or inhibit recruitment of the spliceosome to a splice site (Horn et al., 2023). The presence of RBPs can also promote exon skipping, or inclusion (Horn et al., 2023).

The ELAVL mammalian RBPs closely resemble the *Drosophila* splicing factors *sxl* and ELAVL and this provided early evidence for a role in alternative splicing (Szabo et al., 1991). *In vitro* and CLIP-seq experiments have shown that ELAVL proteins participate as splicing factors through binding of regulatory motifs in introns of target mRNAs (Bronicki & Jasmin, 2013). Furthermore, they have been shown to physically interact with RNA polymerase II and histone deacetylase 2 (HDAC2) in cells (Zhou et al., 2011). Investigation of the protein domains involved in splicing using nELAVL recombinant proteins, revealed that the linker region and RNA-recognition motif (RRM3) are required for splicing control (Bronicki & Jasmin, 2013). Evidence from various experiments showed that the ELAVL proteins function as splicing factors that enhance or repress exon inclusion of targets (Bronicki & Jasmin, 2013).

In neuronal cells exposed to stress and Alzheimer's disease samples, the nELAVL proteins were found to significantly bind Y-RNAs, a class of non-coding RNAs (Scheckel et al., 2016).

Interestingly, the redistribution of nELAVL from associations with their usual target mRNAs was shifted to increased association with Y-RNAs, suggesting a novel regulatory mechanism of nELAVL function. This shift resulted in differentially spliced targets (Scheckel et al., 2016).

ELAVL in mRNA stability

The ELAVL family of RNA-binding proteins are mostly known for their role in mRNA stability. They primarily bind AU-rich elements (AREs) in the 3'UTR of their target mRNA to control target mRNA half-life (Bronicki & Jasmin, 2013). AU- rich elements are cis-regulatory elements found within intronic or untranslated regions of mRNA transcripts that are found in up to 10% of human transcripts (de Toeuf et al., 2018) and are divided into three classes: Class I consists of AUUUA pentamers found along the length of the 3'UTR, Class II consists of overlapping AUUUA motifs and Class III is U-rich (Ripin et al., 2019).

The most notable ARE- binding proteins (ARE-BPs) include Tristetrapolin (TTP), T-cell restricted antigen-1 (TIA1), AU-rich element RNA-binding protein 1 (AUF1), KH-type splicing regulatory protein (KSRP) and the ELAVL/Hu family of RNA binding proteins (Dolicka et al., 2020). TTP, AUF1, and KSRP are best known for destabilizing mRNA, whereas TIA1 is typically associated with translational repression (Dolicka et al., 2020). In contrast, the ELAVL family have almost exclusively been described as promoting mRNA stability, but accumulating evidence suggests that they can destabilize or translationally control target mRNA (Fukao et al., 2009; Ince-Dunn et al., 2012; Otsuka et al., 2019).

A feature of the ELAVL proteins is that they cooperatively form multimers when bound to an RNA target (Simone & Keene, 2013). This mechanism was found to be important for antagonizing the RNA-induced silencing complex (RISC) which relieves the target mRNA from degradation (Kundu et al., 2012). There is also evidence that the ELAVL proteins can promote stability by competing with destabilizing AU-RBPs (Bronicki & Jasmin, 2013). HuR was shown to interact with the destabilizing factors KRSP, AUF1, and TIA-1 and these proteins can bind shared regulatory elements in their common RNA targets, suggesting that there is a complex interplay between the stabilizing and destabilizing factors (Bronicki & Jasmin, 2013).

ELAVL proteins in translation

Eukaryotic mRNA translation is a complex system consisting of various initiation mechanisms including cap-dependent and cap-independent mechanisms (Shatsky et al., 2018). The main mechanism, cap-dependent translation, requires the m^7G cap located at the 5' end of mRNA. It requires the binding of the cap binding complex, the eukaryotic initiation factor 4F (eIF4F), consisting of three subunits: the cap-binding protein eIF4E, the RNA helicase eiF4A, and the scaffolding protein eIF4G. The pre-initiation complex is then recruited to scan the mRNA for the start codon to begin mRNA translation (Shatsky et al., 2018).

There is extensive evidence supporting a role for the ELAVL family of RBPs in regulating translation. HuD was shown to be important for stimulating cap-dependent and poly-A-dependent (Fukao et al., 2009). Wild type HuD was associated with heavy polysome fractions, suggesting that it is associated with mRNA transcripts undergoing translation. It was shown that RRM1 and RRM2 were dispensable for this interaction, however, the linker region and RRM3, were essential.

This was attributed to the poly-A tail binding properties of RRM3. This same study showed that HuD directly interacts with the RNA helicase eIF4A to promote translation. This interaction was required for neurite outgrowth of PC12 neuroblastoma cells (Fukao et al., 2009).

HuD was also shown to repress the translation of select targets. In the BTC6 pancreatic β cell line, HuD was shown to bind a 22-nucleotide sequence in the 5'UTR of the preproinsulin (*Ins2*) mRNA and repress its translation and was released upon glucose stimulation (E. K. Lee et al., 2012). HuD was also shown to bind the 5' UTR of p27 and repress its translation and p27 internal ribosome entry site (IRES)-mediated translation, suggesting that HuD is also involved in cap-independent translation mechanisms (Kullmann et al., 2002).

HuR was associated with promoting and suppressing translation of certain targets. It was shown to bind and promote translation of the tumour suppressor p53 transcript and the antiapoptotic gene, prothymosin alpha (ProTa) after exposure to UV (Mazan-Mamczarz et al., 2003). In contrast, in LPS-treated bone-marrow derived macrophages, HuR was shown to interact with the translational repressor TIA-1 to inhibit translation of *Tnfa* mRNA (Katsanou et al., 2005). HuR was also shown to bind the 3'UTR of its target c-Myc and repress its translation by recruiting let-7 miRNA and RISC (H. H. Kim et al., 2009). HuR is also implicated in cap-independent translation. For example, it binds the IRES of XIAP mRNA to promote cell survival (Durie et al., 2011). Like HuD, HuR also binds the 5'UTR to inhibit p27 translation through interaction with an IRES (Kullmann et al., 2002).

1.9 Post-translational control of ELAVL

The ELAVL proteins are involved in many cellular pathways including cell cycle control, inflammation, and neuronal development (Bronicki & Jasmin, 2013; Srikantan & Gorospe, 2012). In many cases, ELAVL proteins are regulated upstream through post-translational modifications (Bronicki & Jasmin, 2013; Srikantan & Gorospe, 2012). The post-translational control of HuR has been studied extensively, but less is known about nELAVL control (Grammatikakis et al., 2017).

HuD is known to be methylated by the coactivator-associated arginine methyltransferase 1 (CARM1)(Hubers et al., 2011). In mice, CARM1 methylates the residue Arg 248 resulting in inhibited binding to the cyclin dependent kinase inhibitor, *p21* mRNA, its destabilization and thus maintaining cellular proliferation (Hubers et al., 2011). HuD was also shown to represses translation of its target brain-derived neurotrophic factor (*Bdnf*). BDNF translation is enhanced by Protein kinase C (PKC)-mediated phosphorylation of HuD at Threonine 149 and 165 in mice, suggesting that HuD function may be inhibited by phosphorylation (Vanevski & Xu, 2015).

Several PTMs have been identified for controlling HuR function (Grammatikakis et al., 2017). The shuttling of HuR between the nucleus and the cytoplasm is well documented and is dependent on PTMs in its hinge region (Grammatikakis et al., 2017; Srikantan & Gorospe, 2012). Phosphorylation by the cyclin-dependent kinase CDK1 sequesters HuR in the nucleus thus inhibiting its ability to bind cytoplasmic mRNA (H. H. Kim et al., 2008). HuR phosphorylation by p38 mitogen-activated protein kinase (MAPK p38) at Threonine 118 is also induced by an IL1β-activated proinflammatory response (Liao et al., 2011). This leads to HuR increased binding to COX2 mRNA and its increased stability (Liao et al., 2011). HuR was also shown to undergo

poly(ADP-ribosyl)ation at aspartic acid D226 by poly-ADP-ribose polymerase 1 (PARP1). HuR underwent oligomerization/multimerization which was promoted by PARylation in TNF-α stimulated cells (Ke et al., 2021).

1.10 Cellular functions of ELAVL

1.10.1 HuR

HuR in development

HuR is essential for embryonic development and post-natal survival (Ghosh et al., 2009; Katsanou et al., 2005). Homozygous HuR-null mice display impaired placental development and total lethality by E14.5. Analysis at various embryonic stages of *HuR*$^{-/-}$ mice also indicated gross defects in skeletal and splenic development (Katsanou et al., 2009). In postnatal development, loss of HuR was associated with poor development of hematopoietic organs and loss of intestinal villi and death by post-natal day 10 (Ghosh et al., 2009).

HuR in inflammation

A well-characterized, and overarching function of HuR is its role in inflammation. Several studies have shown that HuR binds mRNA encoding cytokines like *COX2*, *TNFA*, *Il6*, and *IFN* (Srikantan & Gorospe, 2012). Most studies have shown that it binds the 3'UTRs to stabilize these targets (Srikantan & Gorospe, 2012). Interestingly, other studies strongly suggest that HuR inhibits production of proinflammatory mediators and attenuates the inflammatory response (Christodoulou-Vafeiadou et al., 2018; Katsanou et al., 2005; Yiakouvaki et al., 2012). Surprisingly, in LPS treated macrophages, overexpression of HuR was associated with enhanced mRNA stability, yet decreased translation of certain targets like *Tnf* and *Cox2* but coordinates with TIA1 to repress translation of *Tnfa* mRNA and possibly other targets requiring validation (Katsanou et al., 2005). In a mouse model of myeloid cell restricted HuR knockout, intraperitoneal injection of LPS resulted in lethality despite exposure to a sublethal dose (Yiakouvaki et al., 2012).

This correlated with enhanced serum levels of TNF-α, IL-6, IL-1β and Il-12, supporting a proinflammatory response. HuR also represses proinflammatory chemokines (Yiakouvaki et al., 2012). In LPS treated macrophages, HuR deficient conditions showed elevated levels of mRNAs like *Ccl2* and *Ccl7* that regulate chemotaxis in the context of acute inflammation (Yiakouvaki et al., 2012).

1.10.2 nELAVL

nELAVL in neuronal development

The expression of at least one of the nELAVL homologues appears to be essential for survival. Knockout of HuB results in a high death rate in recently weaned pups due to poor development (Mulligan & Bicknell, 2023), and double knockout of HuC and HuD is lethal at postnatal day 0 (Ince-Dunn et al., 2012). In primary human neuronal cells, depletion of HuB resulted in differential expression of targets involved in expected pathways such as synaptic and axonal function (Mulligan & Bicknell, 2023). Furthermore, it was shown that loss of HuC is important in the differentiation of inhibitory neurons with evidence suggesting that HuC plays a role in alternative polyadenylation where the longer 3'UTRs were associated with enhanced differentiation (Grassi et al., 2019). Transcriptomics from brains of *HuD*$^{-/-}$ mice also indicated alternative polyadenylation of targets involved in neuronal development and function (Sena et al., 2021). Loss of HuD in mice was associated with severe impairment in arborization of neurons in cortical and hippocampal regions (DeBoer et al., 2014). A role for HuD in neurogenesis was also exemplified by neurosphere assays. Neurospheres derived from neural stem cells (NSCs) lacking HuD showed a significant reduction in mature neurons compared to those derived from wild type NSCs (Akamatsu et al.,

2005). Analysis of embryos lacking HuD revealed fewer mature neurons, suggesting that HuD plays an important role in cell fate specification (Akamatsu et al., 2005).

nELAVL in neuronal function and activity

In the case of *HuC*$^{-/-}$ mice, splicing of transcripts related to glutamate signaling were impaired and the mice also exhibited spontaneous seizures (Ince-Dunn et al., 2012). *HuC*$^{-/-}$ mice also exhibit progressive axonal degeneration, cerebellar ataxia, tremor, postural reflex impairment, and motor deficits including poor performance on rotarod assay (Ogawa et al., 2018). These data suggest that HuC is important for maintaining neuronal function in the adult brain. In *HuD*$^{-/-}$ knockout mice, a hindlimb clasping phenotype, reminiscent of basal ganglia deficits were observed (Akamatsu et al., 2005). In between 20-26 weeks of age, *HuD*$^{-/-}$ mice also showed poor performance on rotarod and showed deficits in motor learning on the same task (Akamatsu et al., 2005). In another study, *HuD*$^{-/-}$ mice 2-3 months of age were significantly less active (DeBoer et al., 2014). In terms of behaviour phenotypes, loss of HuD was associated with inferior performance in the Morris Water Maze, suggesting impaired learning and memory skills (DeBoer et al., 2014). In the elevated plus maze test, *HuD*$^{-/-}$ mice surprisingly spent more time in the open arm, suggesting a decreased aversion to anxiety-inducing contexts (DeBoer et al., 2014). Interestingly, *HuD*$^{-/-}$ mice exhibited auditory-induced seizures rather than spontaneous (DeBoer et al., 2014).

1.11 ELAVL in Disease

1.11.1 HuR

HuR in Cancer

HuR has been strongly linked to various cancers including colorectal, pancreatic, breast and ovarian cancers (J. Wang et al., 2013). Within the cancer pathogenesis, HuR was linked to regulating proliferation, apoptosis, migration, angiogenesis, DNA damage, and drug resistance through control of various genes (J. Wang et al., 2013). For example, in colorectal cancer, HuR accumulation in the cytoplasm was associated with prolonged mRNA stabilization of *COX2* and the increased accumulation of HuR in the cytoplasm positively correlates with tumor stage (Blanco et al., 2016). In a model of colon cancer, the constitutive phosphorylation of nuclear HuR at S318 promoted proliferation of the cells (Doller et al., 2011). HuR S318-specific antibodies revealed high levels of phosphorylated HuR in patient samples of colon carcinoma (Doller et al., 2011).

HuR in inflammatory bowel disease

Microarray analysis of peripheral blood samples derived from Crohn's patients identified *HuR* as the most significant upregulated gene (H. Li et al., 2020). In comparisons of ulcerative colitis patients vs. Crohn's patients *ELAVL1/HuR* was among the four genes associated with Ulcerative colitis but was absent from the Crohn's profile (Burakoff et al., 2011). In intestinal biopsies, HuR was most abundant in the nucleus as expected, but in samples derived from Crohn's disease and Ulcerative Colitis patients, nuclear HuR remained abundant, yet cytoplasmic HuR was significantly increased in the intestinal epithelial cells (Lang et al., 2017). In animal models of inflammatory bowel disease elicited by chemical (DSS), *Citrobacter rodentium* infection, or TNF-

α, HuR was shown to have divergent roles in the intestinal epithelium and myeloid cells (Christodoulou-Vafeiadou et al., 2018). In the *C. rodentium* model, HuR was essential for epithelial barrier integrity through its positive effects on cellular proliferation and regeneration in intestinal epithelial cells (IEC). Intestinal tissue from IEC-*HuR*$^{-/-}$ mice indicated a more severe degenerative phenotype, hyperplasia, and enhanced expression of antimicrobial mRNAs *RegIIIβ* and *RegIIIγ*, but no increase in proinflammatory cytokine expression at acute time points. In contrast, myeloid cell depletion of HuR showed improved pathogen clearance, minimal degeneration, and hyperplasia. Interestingly, in the chemically induced colitis model, the initial days post-treatment showed divergent roles for *IEC-HuR*$^{-/-}$ vs. myeloid -*HuR*$^{-/-}$ but the phenotypes at end-point resembled each other. Specifically, both IEC and myeloid resulted in excessive, chronic inflammation, marked by elevated cytokines and tissue damage. These studies suggest that HuR is involved in IBD, but a solid understanding of its pathology in specific contexts is required to safely use it as a therapeutic target (Christodoulou-Vafeiadou et al., 2018).

1.11.2 HuD

HuD in neurodegenerative disease

While HuD is typically associated with neuronal development, a growing body of evidence suggests a role in maintaining neuron health into ageing (Silvestri et al., 2022). In human neuroblastoma cells, HuD was shown to bind and stabilize the amyloid precursor protein (*APP*), the precursor to the pathogenic peptide AB found in Alzheimer's Disease (AD) brains, and b-secretase protein 1 (*BACE1*) mRNA which are associated with AD (Kang et al., 2014a). The levels of HuD, APP, an BACE1 mRNA and protein were elevated in brains lysates derived from AD

patients compared to healthy controls (Kang et al., 2014a). A study investigating the RNA interactome of Fused in Sarcoma (FUS), an RNA-binding protein associated with Amyotrophic lateral sclerosis (ALS), found that FUS binds the 3'UTR of HuD and increases its protein levels in motor neurons expressing mutant FUS (De Santis et al., 2019a) . They further observe that HuD associates with mutant FUS in cytoplasmic speckles from FUS ALS patients and in TDP-43 positive inclusions in samples derived from sporadic patients (De Santis et al., 2019a). HuD is also implicated in spinal muscular atrophy (SMA) through its interaction with the causative SMN protein, where its interaction is impaired in patients and its overexpression rescues SMA-like phenotypes in motor neuron cells, suggesting a protective role (Hubers et al., 2011).

Finally, *HuD* has been genetically linked to Parkinson's disease in multiple studies, yet no mechanism has been elucidated. The first study mapped an age-of-onset modifier for PD at the *HuD* locus in an American and Australian population (Y.-J. Li et al., 2002). The *HuD* locus was also genetically associated with PD as a susceptibility gene for late-onset PD in an Icelandic population and was dubbed *PARK10* (Hicks et al., 2002). Single nucleotide polymorphisms in an intron and coding sequence of *ELAVL4* were identified as age-of-onset modifiers in a subsequent study (Noureddine et al., 2005). In contrast, a later study found no association of *ELAVL4* with Norwegian or American populations, but did note an association in an Irish cohort (Haugarvoll et al., 2007). Finally, another analysis in a Caucasian population found that an SNP previously identified by Nourredine et al, was replicated, and this has now been reproduced in three independent cohorts (DeStefano et al., 2008). Taken together, these genome-wide association studies suggest that HuD has a role in Parkinson's disease and should be characterized further.

1.12 Statement of Research

1.12.1 Rationale

Parkinson's disease is the second most common neurodegenerative disease yet has no cure. The *LRRK2 G2019S* mutation, conferring hyperactive kinase activity, is a common genetic cause of PD and large-scale efforts have been made to understand LRRK2 function, including in models of neurodegeneration and inflammation. A major challenge in the field has been defining its phosphorylation substrates. A *Drosophila* model of human mutant LRRK2 found that an ELAVL homologue, Rbp9, was required for LRRK2 induced pathology. Coincidentally, polymorphisms in the *HuD/ELAVL4* were associated with age-of-onset or susceptibility of PD.

1.12.2 Hypothesis

LRRK2 phosphorylates the ELAVL family of RNA-binding proteins to post-transcriptionally regulate gene expression of PD-relevant genes in neurons and immune cells.

1.12.3 Objectives

The chapters described in this thesis describe a collection of work aimed at understanding the function of the ELAVL-family of RNA-binding proteins in disease. The primary chapters (Ch.2 and 3) are focused on elucidating the role of the ELAVL proteins in LRRK2-dependent models of Parkinson's disease. Chapter 4 presents the characterization of HuD knockout in energy metabolism. Originally part of Chapter 2, the data led to new directions and is therefore described independently of LRRK2. The primary objective of each chapter is as follows:

- **Chapter 2 (manuscript in submission):**
    - Determine if LRRK2 phosphorylates the nELAVL proteins.

- Elucidate how loss of HuD modifies PD-like phenotypes in *Lrrk2-G2019S*-expressing mice.

- **Chapter 3:**
  - Investigate the role of the ubiquitous ELAVL homologue in cellular and mouse models of inflammation relevant to PD.

- **Chapter 4:**
  - Characterize the role of HuD in mouse metabolic phenotypes.

Chapter 2

Neuronal ELAVL RNA-Binding Proteins are Phosphorylated by LRRK2 and Regulate Genes and Phenotypes Relevant to Parkinson's Disease

Olanta Negeri[1,2*], Alyssa Pastic[1,2*], Aymeric Ravel-Chapuis[1,2], Alexandre Savard[1,2], My Tran Trung[1,2], Gareth Palidwor[3], Huishan Guo[1,2], Paul Marcogliese[4], James A. Taylor[1,2], Jean-François Couture[5], Hideyuki Okano[6], Laura Trinkle-Mulcahy[1], Bernard J. Jasmin[1,2], David Park[7], and Derrick Gibbings[1,2,8,9]

[1] Department of Cellular and Molecular Medicine, Faculty of Medicine, University of Ottawa, Ottawa, Ontario, Canada K1H 8M5
[2] University of Ottawa Brain and Mind Research Institute, University of Ottawa, Ottawa, Ontario, Canada K1H 8M5
[3] Ottawa Hospital Research Institute, Ottawa Hospital, Ottawa, Ontario, Canada
[4] Department of Biochemistry and Medical Genetics, Children's Hospital Research Institute of Manitoba, Winnipeg, Manitoba, Canada, R3E 3P4
[5]Department of Biochemistry, Microbiology and Immunology, Faculty of Medicine, University of Ottawa, Ottawa, Ontario, Canada K1H 8M5
[6]Keio University School of Medicine, Tokyo, 160-8582, Japan
[7] Hotchkiss Brain Institute, University of Calgary, Calgary, Alberta, Canada T2N 4N1
[8] Ottawa Institute for Systems Biology, University of Ottawa, Ottawa, Ontario, Canada K1H 8M5
[9]Eric Poulin Center for Neuromuscular Disease, University of Ottawa, Ottawa, Ontario, Canada K1H 8M5

Lead Contact: Derrick Gibbings (gibbings@uottawa.ca)

* Denotes co-first authors

2.1 Statement of Contributions

ON performed and analyzed PhosTag gels, immunoprecipitations of FLAG-HuB and phosphorylation assays, stereological counting of TH+ neurons, RT-PCR for splicing, microarray array validation experiments and wrote the manuscript. AP performed and analyzed all work in cell lines unless otherwise noted, western blots from mice, mutagenesis of HuD and immunoprecipitation of mutant HuD and phosphorylation assays. ARC designed splicing primers. MTT and AS helped generate mice and performed dissections. GP processed microarray data and performed analysis of nELAVLmotifs in microarray data and public datasets. HG performed proximity ligation assays, immunoprecipitation of LRRK2 and HuD, and HuD phospho-threonine. JT helped generate HuD mutants. HO generated and provided HuD knockout mice. LTM helped analyze mass spectrometry data. JFC analyzed phosphorylation sites on nELAVLs and generated crystal structure. BJ read and commented on the manuscript. DSP and PM conceived the project and helped design and interpret certain experiments. DG conceived the project, designed, and interpreted experiments including analysis of microarrays and patient data and wrote the manuscript. Text and figures in sections 2.2-2.7 were reproduced or adapted from Pastic, Negeri et al., *bioRxiv,* 2022 © pre-print with permission.

2.2 Abstract

Parkinson's disease (PD) is characterized by accumulation of α-synuclein and the loss of dopaminergic neurons. Many causative genes of Parkinson's disease have been identified including α-synuclein (SNCA) and *Leucine-Rich-Repeat Kinase-2* (*LRRK2*), while polymorphisms in others like *Embryonic Lethal Abnormal Vision-like 4* (*ELAVL4*) are considered risk factors for the disease. Since mutations which cause an increase in the kinase activity of LRRK2 are a major inherited cause of PD, factors that regulate LRRK2 levels and targets of LRRK2 phosphorylation may ultimately control PD. A genetic screen in *Drosophila* identified an ELAVL homologue as required for pathology instigated by human mutant LRRK2. We discovered that three nELAVLs including ELAVL4 (also known as HuD) bind to, and post-transcriptionally regulate mRNA encoding α-synuclein (*Snca*) and *Lrrk2*. We also show that LRRK2 phosphorylates HuD and its homologues HuB and HuC. This controls binding of nELAVLs to mRNA and post-transcriptionally regulates mRNA abundance and splicing including in the mouse midbrain. In mice, the complex regulatory loop connecting *Elavl4*, *Lrrk2 G2019S* and α-synuclein regulates LRRK2 and α-synuclein protein levels, loss of dopaminergic neurons and motor deficits. Targets of nELAVLs are also selectively misregulated in iPSC-derived neurons, and tissues from PD patients. Together, this suggests that misregulation of nELAVLs, which can be triggered by LRRK2 mutations among other factors, may contribute to the characteristic pathology of Parkinson's disease.

2.3 Introduction

Parkinson's disease is a progressive neurodegenerative disease, with both idiopathic and genetic causes. Pathology in patients with PD is primarily characterized by accumulation of α-synuclein and the progressive loss of dopaminergic neurons in the substantia nigra of the midbrain which leads to characteristic motor symptoms (Spillantini et al., 1997). Mutations in several genes can cause forms of PD (Bandres-Ciga et al., 2020; Klein & Westenberger, 2012). Duplication and triplication of the α-synuclein, *SNCA* (Chartier-Harlin et al., 2004; Ibáñez et al., 2004), or variants which increase its expression (Chiba-Falek, 2001) , can cause PD and its overexpression elicits Parkinson's-like symptoms in mice (Masliah et al., 2000), emphasizing the critical role of α-synuclein levels in PD. The most common cause of familial PD are mutations in *Leucine-Rich-Repeat Kinase 2* (*LRRK2*) gene (Paisán-Ruíz et al., 2004; Zimprich et al., 2004). Several mutations in *LRRK2* that cause PD result in over-active kinase activity, including the most common mutation, *LRRK2 G2019S* (West et al., 2005b). This suggests that target proteins phosphorylated by LRRK2 are a cause of patient pathology and symptoms. Recent unbiased phosphoproteomic studies have highlighted that LRRK2 phosphorylates RAB proteins including RAB10, RAB8a/b, RAB35, RAB12 and RAB29 to govern organelle dynamics and ciliogenesis (Imai et al., 2008; Martin et al., 2014) by locking RABs in a GTP-bound form. Other targets of LRRK2 kinase include WAVE2 (K. S. Kim et al., 2018b) and endophilin A which also regulate membrane dynamics (Jeong et al., 2018). Phosphorylation of targets including RAB10, and WAVE2 have been validated in patient cells (Atashrazm et al., 2019; K. S. Kim et al., 2018b). Phosphorylation of RABs by LRRK2 may mediate effects ascribed to LRRK2 at the cellular level including effects on autophagy (Arranz et al., 2014; Nirujogi et al., 2021) lysosomes, and vesicular trafficking (Giaime et al. 2017; Karayel et al. 2020).

While phosphorylation of RABs by LRRK2 is readily detected in cell lines like HEK-293, they are at low or undetectable levels in the brain (Orenstein et al., 2013; Steger et al., 2017), potentially due to the abundance of the relevant phosphatases (Berndsen et al., 2019). In cells and peripheral tissues where LRRK2 does phosphorylate RABs, the phosphorylated RABs only account for about 1% of total RABs (Berndsen et al., 2019; Steger et al., 2017). Phosphorylation of RABs by LRRK2 results in impaired endolysosomal trafficking relevant to PD, but their impact on dopaminergic neuron loss, accumulation of a-synuclein and motor deficits is unclear (Kuwahara & Iwatsubo, 2020). LRRK2 has also been reported to phosphorylate and/or interact with proteins regulating translation including the small ribosomal subunit 15 (Martin et al., 2014), Argonautes (Gehrke et al., 2010) and eIF4E-BP (Imai et al., 2008) but there is also debate about whether these are physiological substrates of LRRK2. Samples derived from idiopathic PD patients, and animal studies have provided evidence that LRRK2 activity is increased in PD pathogenesis irrespective of the presence of mutations (Di Maio et al., 2018). In post-mortem brain tissue, LRRK2 autophosphorylation, a marker of its activity, and phosphorylation of its target, RAB10, were increased in the substantia nigra from idiopathic PD patients. Similarly, rodent models of rotenone-induced oxidative stress and α-synuclein pathology noted increased LRRK2 activation (Di Maio et al., 2018), suggesting that controlling even wild-type LRRK2 levels or activity may protect from PD symptoms. Currently, an antisense oligonucleotide (BIIB094 Identifier: NCT03976349, clinical trial.gov) and kinase inhibitors targeting LRRK2 (DNL201, DNL151) are in clinical trials for both idiopathic patients and LRRK2-mutation carriers highlighting the central role LRRK2 is believed to have in a broad group of patients with PD pathology (Taymans et al., 2023).

Despite the association of LRRK2 mutations with PD, and the frequency of mutations like G2019S, these mutations have incomplete penetrance (Gasser, 2011). The incomplete penetrance associated with G2019S and other mutations in LRRK2 indicates that developing PD requires the presence of other risk factors which may include environmental toxins, age, lifestyle, and genetic modifiers (Gasser, 2011; Healy et al., 2008b; Trinh et al., 2022). Notably, studies in multiple independent patient cohorts found that single-nucleotide polymorphisms in the region of an *ELAVL* family member, *ELAVL4*, are linked with susceptibility to or age-of-onset of PD (DeStefano et al., 2008; Haugarvoll et al., 2007; Noureddine et al., 2005).Interestingly, a previous genome-wide screen in *Drosophila* expressing the human LRRK2-I2020T hyperactive kinase, identified Rbp9, an RNA-binding protein of the ELAVL (Embryonic Lethal Abnormal Vision) family as required for LRRK2 to induce retinal degeneration (Marcogliese et al., 2017). This suggests that ELAVL4 may impact PD pathogenesis and may control LRRK2-dependent pathology. The mechanisms by which ELAVL4 may be regulated in PD or impact processes or phenotypes associated with PD is not known.

ELAVL4 is more commonly known as HuD and is expressed nearly exclusively in neurons (Bronicki and Jasmin 2013). In mice and humans, HuD has two homologues, which are also preferentially expressed in neurons, called HuB and HuC (or ELAVL2 and ELAVL3). HuB, HuC and HuD bind U-rich and AU-rich motifs in the 3'UTR, 5'UTR and introns of mRNAs (Ince-Dunn et al., 2012; Scheckel et al., 2016). HuD contains three RNA-Recognition-Motifs (RRM). RRM1 and -2 bind to U-rich RNA motifs, while RRM3 binds to the poly(A) tail of mRNA (Fukao, Tomohiro, and Fujiwara 2021; Bronicki and Jasmin 2013; Chung et al. 1996). By binding to introns, HuC and HuD have important impacts on splicing of mRNAs to which they bind (Ince-

Dunn et al., 2012). In addition, HuC and HuD can either stabilize or destabilize mRNAs or regulate their translation (Bolognani, Contente-Cuomo, and Perrone-Bizzozero 2009; Pascale et al. 2005; Allen et al. 2013; Atlas et al. 2007; Kullmann et al. 2002). By binding to hundreds of mRNAs and controlling their splicing, stability, and translation HuB, -C and -D broadly regulate cellular processes (Bolognani et al., 2009; Ince-Dunn et al., 2012; Scheckel et al., 2016). mRNAs bound to and regulated by HuD include several involved in neuronal survival and formation of synaptic connections like Brain-Derived Neurotrophic Factor (BDNF) (Vanevski and Xu 2015). Neuronal cells lacking HuD have impaired dendritic outgrowth (Akamatsu et al. 2005; DeBoer et al. 2014; Vanevski and Xu 2015). Mice lacking HuD exhibit motor deficits such as hind-limb clasping phenotypes (Akamatsu et al. 2005; Ince-Dunn et al. 2012). The impact of loss of HuD on Parkinson's-like pathology and symptoms has not been previously investigated in detail, so it remains unclear to what extent HuB, HuC and HuD could contribute to Parkinson's disease.

Here, we demonstrate that *HuD*$^{-/-}$ mice show misregulation of α-synuclein and LRRK2, and behavioural changes. The neuronal ELAVL (nELAVL) proteins bind and regulate mRNAs encoding PD-relevant proteins, SNCA and LRRK2. We also show that LRRK2 phosphorylates and regulates RNA binding to HuB, C and D, creating a feedback loop whereby LRRK2 can regulate levels of LRRK2 and α-synuclein protein, in addition to other nELAVL targets. In *HuD*$^{-/-}$ mice, LRRK2 G2019S increases phosphorylation of HuB and HuC. This results in complex effects on levels of α-synuclein and LRRK2, loss of dopaminergic neurons, behavioural, and motor phenotypes that correlate with contrasting effects of LRRK2 G2019S on the splicing and mRNA stability of nELAVL targets.

2.4 Results

mRNAs bound by HuD are misregulated in patients with PD

Genetic data in *Drosophila* suggested that an ELAVL protein is essential for pathology induced by LRRK2 mutations and may be phosphorylated by LRRK2 (Marcogliese et al., 2017). As a surrogate of nELAVL function in PD samples, we queried whether targets of nELAVL were disproportionately misregulated in patient samples and patient-derived models of PD compared to healthy controls using public data. 3'UTRs were extracted from all mRNA detected in neural stem cells derived from induced pluripotent stem cells from LRRK2 G2019S patients vs. corrected LRRK2 wild-type (G.-H. Liu et al., 2012).The number of nELAVL binding motifs were normalized to the length of 3'UTRs. Among mRNAs downregulated in LRRK2 G2019S neural stem cells there is a significant enrichment in the density of nELAVL binding motifs (UUU*UUU) compared to mRNAs unaffected by LRRK2 G2019S (Fig. 2.4.1 a, $p=2.3^{-9}$, proportion test, 0.0021 vs 0.0019 motifs/length). To test whether misregulation of nELAVL binding mRNAs may thus be characteristic of broader groups of idiopathic PD patients, we queried this using mRNAs consistently dysregulated in the substantia nigra across multiple studies in PD patients (Mariani et al., 2016). Normalizing to 3'UTR length, the 3'UTRs of 782 unique mRNAs dysregulated in PD patients (Mariani et al., 2016)were significantly enriched in nELAVL binding motifs compared to all mRNAs detected (Fig.2.4.1 b, $p=1.51x10^{-6,}$ motifs/3'UTR length UUUNUUU: 0.0019873 vs. 0.0018528). To ensure the misregulation of mRNAs containing nELAVL-binding motifs was not due to a change in the cellular composition of degenerating substantia nigra, we analyzed data from purified dopaminergic neurons from a broad population of Parkinson's patients (Sandor et al., 2017). The 168 misregulated mRNAs in dopaminergic neurons from Parkinson's patients were

also enriched in nELAVL binding motifs compared to all detected mRNAs (Fig.2.4.1 c, $p=1x10^{-7}$, motifs/3'UTR UUUNUUU: 0.0022255 vs, 0.0018540). Together, this suggests that misregulation of nELAVL targets in neurons is characteristic of a broad population of patients with PD both with and without *LRRK2* mutations.

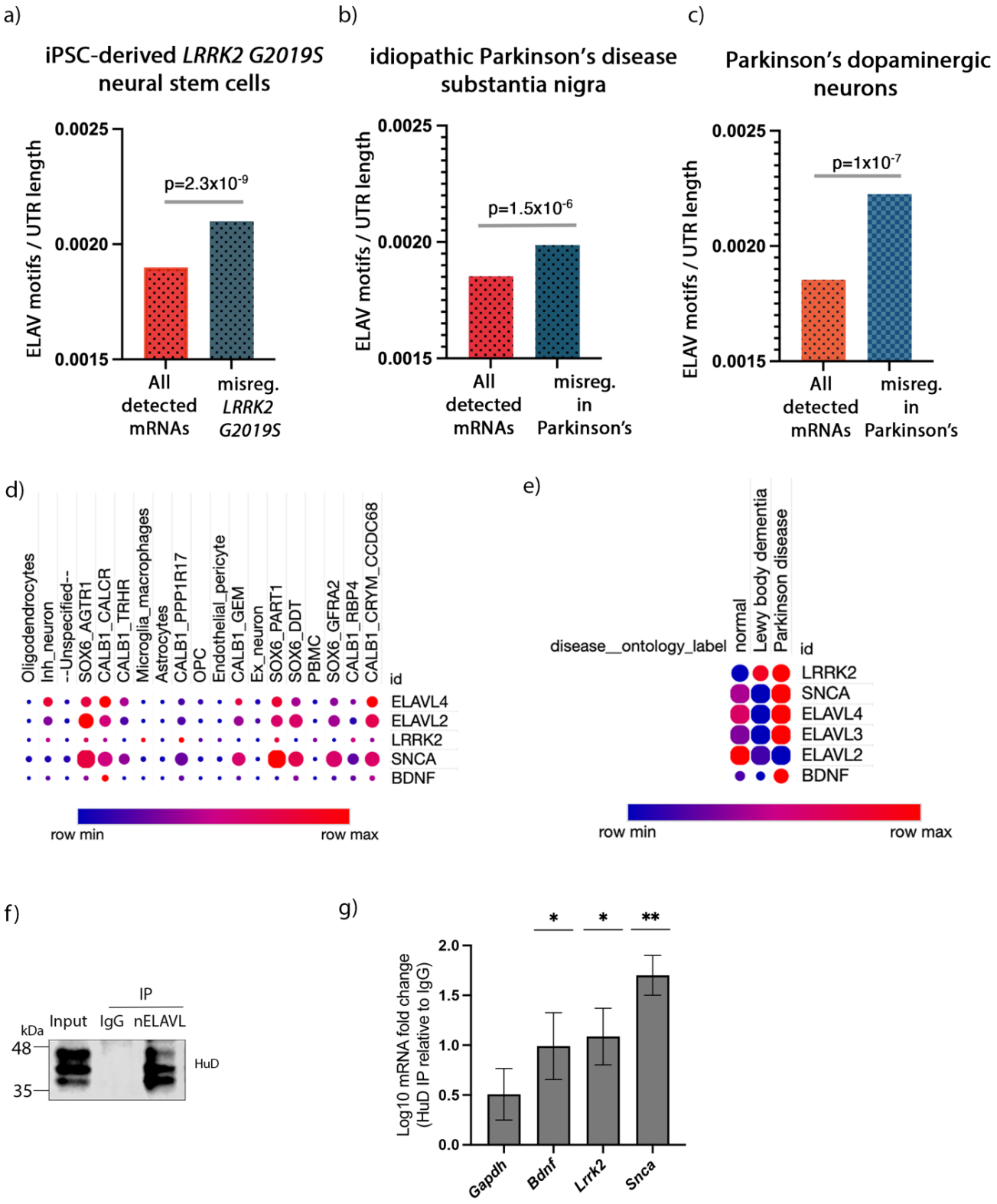
a)
iPSC-derived LRRK2 G2019S neural stem cells
ELAV motifs / UTR length
0.0025
0.0020
0.0015
p=2.3x10-9
All detected mRNAs
misreg. LRRK2 G2019S
b)
idiopathic Parkinson's disease substantia nigra
p=1.5x10-6
All detected mRNAs
misreg. in Parkinson's
c)
Parkinson's dopaminergic neurons
p=1x10-7
All detected mRNAs
misreg. in Parkinson's
d)
Oligodendrocytes
Inh_neuron
--Unspecified--
SOX6_AGTR1
CALB1_CALCR
CALB1_TRHR
Microglia_macrophages
Astrocytes
CALB1_PPP1R17
OPC
Endothelial_pericyte
CALB1_GEM
Ex_neuron
SOX6_PART1
SOX6_DDT
PBMC
SOX6_GFRA2
CALB1_RBP4
CALB1_CRYM_CCDC68
id
ELAVL4
ELAVL2
LRRK2
SNCA
BDNF
row min
row max
e)
disease__ontology_label
normal
Lewy body dementia
Parkinson disease
id
LRRK2
SNCA
ELAVL4
ELAVL3
ELAVL2
BDNF
row min
row max
f)
IP
kDa
Input
IgG
nELAVL
48
35
HuD
g)
Log10 mRNA fold change (HuD IP relative to IgG)
2.0
1.5
1.0
0.5
0.0
*
*
**
Gapdh
Bdnf
Lrrk2
Snca

Figure 2.4.1 nELAVL targets are misregulated in PD patient data.

a) mRNAs misregulated in LRRK2 G2019S iPSC-derived neural stem cells vs. LRRK2 corrected wild-type controls (G.-H. Liu et al., 2012) b) among 782 mRNAs misregulated in substantia nigra of idiopathic Parkinson's disease patients (Mariani et al., 2016) c) among 168 mRNAs misregulated in dopaminergic neurons of Parkinson's disease patients (Sandor et al., 2017). d) Single-nuclei RNA sequencing data of human midbrain. Size of dots indicates percentage of cells expressing the mRNA (Kamath et al., 2022). e) Single-nuclei RNA sequencing data from midbrain of neurotypical patients, Lewy body dementia patients and Parkinson's disease patients (Kamath et al., 2022). Size of dots indicates percentage of cells expressing the mRNA f) Western blot of nELAVL immunoprecipitates or an isotype control antibody (IgG) g) RT-qPCR of mRNAs enriched in nELAVL immunoprecipitates. Data were analyzed by One-Way ANOVA * $p<0.05$, ** $p<0.01$, *** $p<0.001$.

LRRK2 G2019S regulates expression of nELAVL targets in the mouse midbrain

Recent single-nuclei sequencing studies (Kamath et al., 2022) of dopaminergic neurons from the human midbrain identified a subpopulation expressing *AGTR1* that selectively expressed, at high levels, genetic risk factors for Parkinson's disease such as *SNCA*, and was selectively lost in Parkinson's disease. Expression of nELAVLs closely paralleled that of *SNCA* and was strongest in *AGTR1*+ subpopulation of dopaminergic neurons among all other subpopulations (Fig.2.4.1 d). In both Lewy body dementia and Parkinson's disease, expression of nELAVLs was strikingly misregulated, with all family members reduced in Lewy body dementia, and HuB levels strongly reduced in Parkinson's disease (Fig.2.4.1 e). Similarly, a single-cell RNA sequencing study of iPSC-derived dopaminergic neurons carrying a SNCA A53T mutation which causes PD, found that HuD was among the most downregulated genes (Fernandes et al., 2020). These data demonstrate that impaired regulation of nELAVL targets in PD patients (Fig.2.4.1 a-c) may be frequently caused by misregulation of nELAVLs, in ways that cannot be accounted for by loss of dopaminergic neurons.

The RNA-binding protein HuD binds mRNA encoding α-synuclein and LRRK2

High-throughput studies profiling mRNAs bound by HuD have identified *LRRK2* and *SNCA* among HuD target mRNAs, but this has not been experimentally validated (Bolognani et al., 2009; Scheckel et al., 2016). The 3'UTRs of mouse *Snca* and *Lrrk2* mRNA transcripts contain several canonical binding sites for nELAVLs (Supplementary Dataset 1). We immunoprecipitated nELAVL from wild-type mouse midbrain tissue and bound mRNAs were quantified by RT-qPCR (Fig. 2.4.1 f,g). mRNAs which do not bind HuD, like *Gapdh* mRNA, were not enriched in nELAVL immunoprecipitates (Fig.2.4.1 g). In contrast, *Bdnf*, a well-defined HuD target was

enriched in nELAVL immunoprecipitates compared to immunoprecipitates of control antibody (Fig.2.4.1 g) (Bolognani, Contente-Cuomo, and Perrone-Bizzozero 2009; Joseph, Orlian, and Furneaux 1998). This suggests that mRNAs encoding proteins relevant to PD may be regulated by HuD.

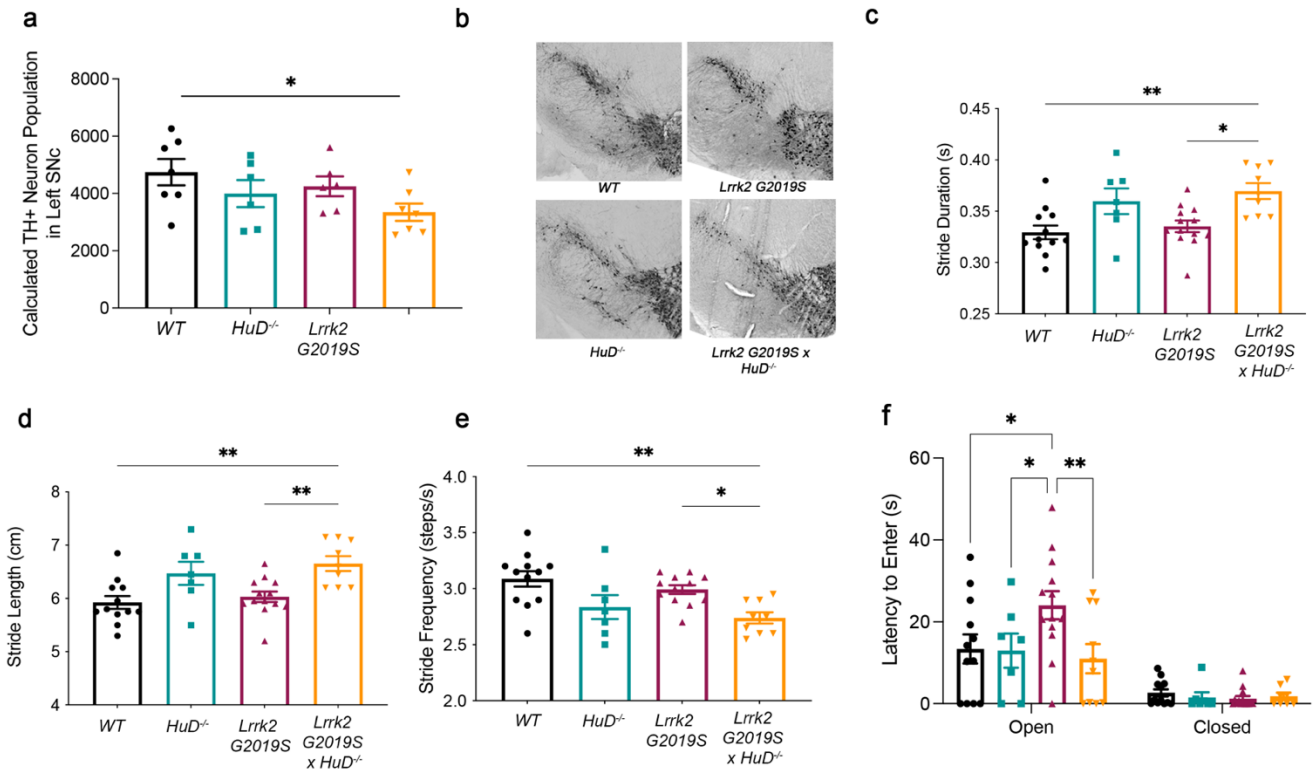

Figure 2.4.2 *Lrrk2 G2019Sx HuD*$^{-/-}$ mice exhibit loss of dopaminergic neurons and motor deficits.

(a,b) Stereological counting of Tyrosine-Hydroxylase+ dopaminergic neurons in serial sections of one half of the substantia nigra of *wild-type*, *HuD*$^{-/-}$, *Lrrk2 G2019S*, *Lrrk2 G2019SxHuD*$^{-/-}$ mice at one year of age. Error bars represent mean ± SEM. n=6-7. Data were analyzed by One-Way ANOVA followed by Dunnett's. * $p<0.05$ (b) Representative images of substantia nigra sections quantified in (a). c) Quantification of stride duration (d) length and (e) frequency in *wild-type*, *HuD*$^{-/-}$, *Lrrk2 G2019S*, *Lrrk2 G2019SxHuD*$^{-/-}$ mice at 26 weeks of age using a DigiGait analysis. (f) Latency to enter the open arm in Elevated Plus Maze tested at 26 weeks of age. Error bars represent mean ± SEM. n=7-13 Data were analyzed by One-Way ANOVA with Tukey's. * $p<0.05$, ** $p<0.01$, *** $p<0.001$.

Loss of HuD Elicits PD-like Phenotypes in Mice

As nELAVLs are frequently misregulated in PD (Fig.2.4.1 d,e), *HuD*$^{-/-}$ mice could model the impact of a partial loss of nELAVL function by eliminating one of three largely redundant nELAVL proteins. Crossing *Lrrk2 G2019S* with *HuD*$^{-/-}$ mice may additionally allow modeling of *ELAVL4* mutations as risk factors in PD patients that may increase the pathology and penetrance of *LRRK2* mutations. A key phenotype of PD is loss of dopaminergic neurons. Stereological counting of tyrosine hydroxylase-positive (TH+) dopaminergic neurons in serial sections of the substantia nigra of mice at 12 months showed insignificant differences in *HuD*$^{-/-}$ and *Lrrk2 G2019S* mice (Fig.2.4.2 a,b). However, *Lrrk2 G2019S xHuD*$^{-/-}$mice showed a modest but significant reduction in dopaminergic neurons in the substantia nigra, suggesting that partial loss of nELAVL function sensitizes *Lrrk2 G2019S* mice to PD-like phenotypes. Onset of motor symptoms in PD patients and mouse models usually occurs after loss of 30-50% (Cheng et al., 2010; Fearnley & Lees, 1991; Greffard et al., 2006) of dopaminergic neurons in the substantia nigra, like the amount of loss of these neurons observed in *Lrrk2 G2019S x HuD*$^{-/-}$mice. *HuD*$^{-/-}$ mice appeared to have altered gait, but this only reached significance in *Lrrk2 G2019S x HuD*$^{-/-}$ mice (Fig.2.4.2 c-e). PD patients may also present with non-motor symptoms including mood dysregulation (Blonder and Slevin 2011). In mice, anxiety-like phenotypes have been reported in some *Lrrk2 G2019S* models and are decreased in *HuD*$^{-/-}$mice (DeBoer et al., 2014; Lim et al., 2018). We therefore tested *Lrrk2 G2019S x HuD*$^{-/-}$ mice in the elevated plus maze for anxiety-related phenotypes. The total time spent, and the frequency of entry in the open arm were comparable (Supplementary Fig.2.1 a,b), however, the time to initial entry into the open arm was significantly higher in *Lrrk2 G2019S* mice compared to all groups (Fig.2.4.2 f), suggesting a subtle anxiety-like phenotype. In contrast to motor phenotypes and TH+ counts, this effect was rescued by loss of *HuD*, indicating a complex

genetic interaction between HuD and LRRK2 that may be due to divergent effects of LRRK2 on different pools of nELAVLs targets.

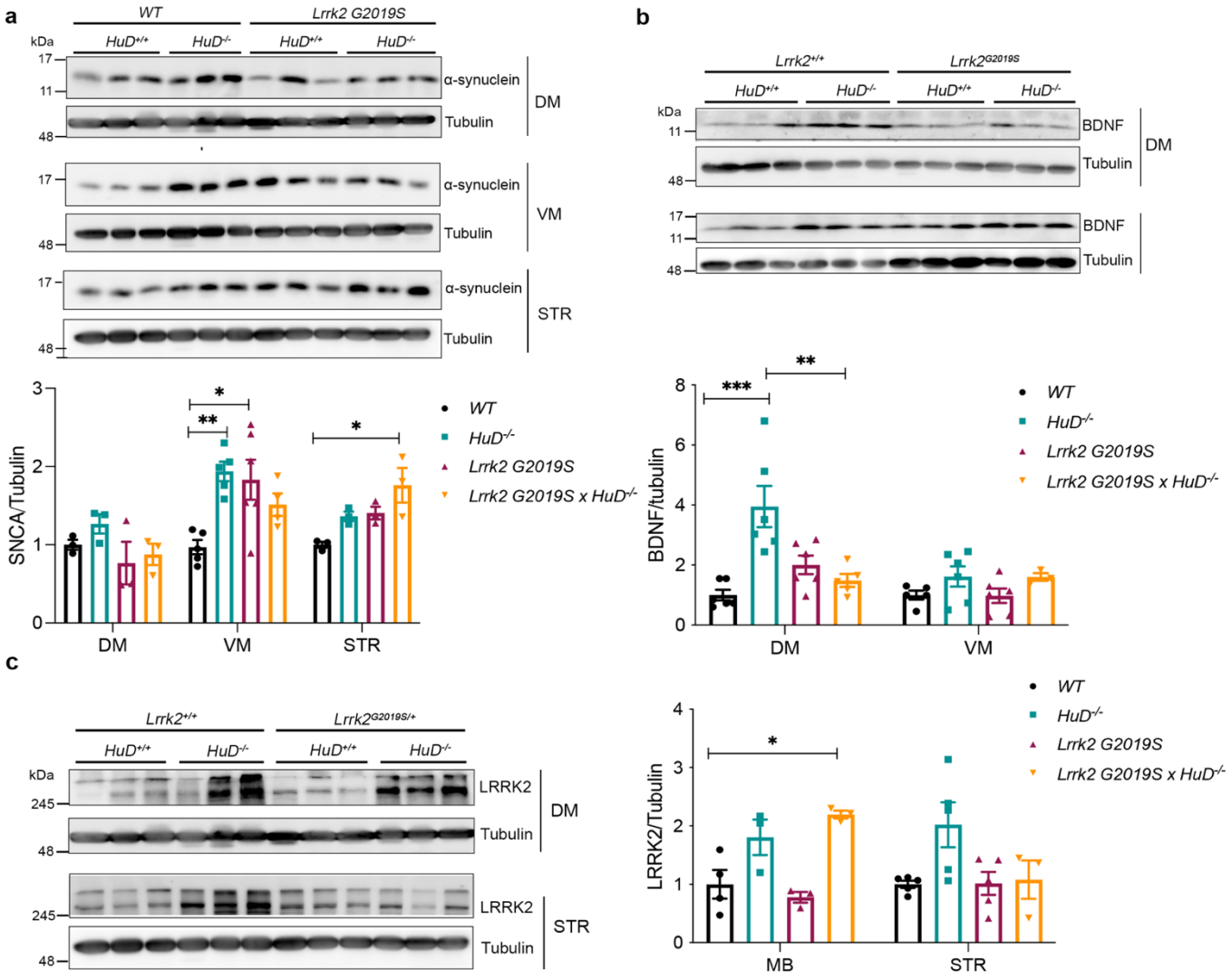

Figure 2.4.3 HuD and LRRK2 G2019S regulate α-synuclein, BDNF and LRRK2 protein levels in the mouse midbrain.

(a,b) Western blot (top) and quantification (bottom) of α -synuclein (a) and BDNF (b) in *wild-type*, *HuD*$^{-/-}$, *Lrrk2 G2019S*, and *Lrrk2 G2019SxHuD*$^{-/-}$ mice of 4 weeks of age with dorsal midbrain (DM), ventral midbrain (VM) and striatum (STR) samples normalized to tubulin (loading control). (c) Western blot (left) and quantification (right) of LRRK2 in *wild-type*, *HuD*$^{-/-}$, *Lrrk2 G2019S*, and *Lrrk2 G2019S x HuD*$^{-/-}$ mice of 4 weeks of age with dorsal midbrain (DM), and striatum (STR) samples normalized to tubulin (loading control). Note that blots for LRRK2 and α -synuclein were performed on the same membranes and therefore use the same tubulin control. Error bars represent mean ± SEM. n=3-6. Data were analyzed by One-Way ANOVA with Tukey's. * $p<0.05$, ** $p<0.01$, *** $p<0.001$.

The data in Fig. 2.4.1.-2.4.2 suggest that HuD is associated with phenotypes consistent with PD symptoms and loss of HuD can enhance some of the effects of *Lrrk2* mutations. Increased LRRK2 abundance and activity are associated with PD (Alessi and Sammler 2018). HuD bound mRNA encoding *Lrrk2* (Fig.2.4.1 f,g), suggesting HuD controls expression of *Lrrk2*. Resembling effects on other HuD targets, the levels of LRRK2 protein increased in midbrain and striatum of *HuD*$^{-/-}$ mice (Fig.2.4.3 c). Decreased levels of nELAVL proteins in PD patients (Fig.2.4.1 e) could therefore cause increases in *LRRK2* expression and activity, a known cause of PD. This provides a likely mechanism whereby *HuD*$^{-/-}$ could sensitize *Lrrk2 G2019S* mice to loss of dopaminergic neurons and motor phenotypes, and suggests mechanisms by which mutations in the HuD locus act as a risk factor for PD.

nELAVLs also bound mRNA encoding α-synuclein, and levels of α-synuclein protein were significantly increased in the ventral midbrain of *HuD*$^{-/-}$ mice and trended higher in the striatum. *Lrrk2 G2019S* modifies this effect (Fig.2.4.3 a). In dorsal midbrain, BDNF levels increased in *HuD*$^{-/-}$ mice and these effects were reduced by *Lrrk2 G2019S* (Fig.2.4.3 b). Mutations in the *HuD* locus could therefore additionally sensitize patients to PD by controlling levels of α-synuclein and other HuD targets.

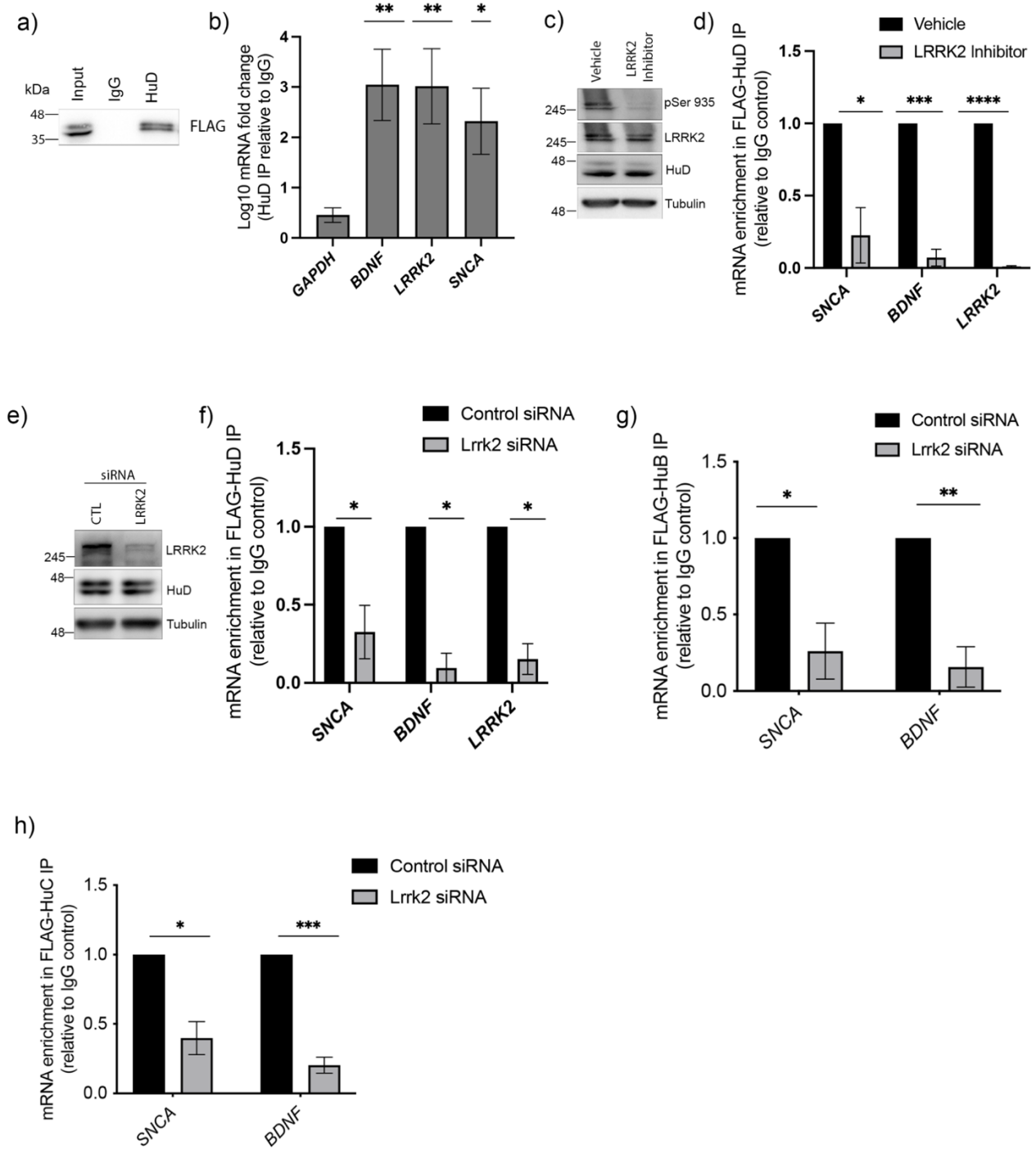
a)
kDa
Input
IgG
HuD
48
35
FLAG
b)
Log10 mRNA fold change (HuD IP relative to IgG)
**
**
*
GAPDH
BDNF
LRRK2
SNCA
c)
Vehicle
LRRK2 Inhibitor
245
pSer 935
245
LRRK2
48
HuD
48
Tubulin
d)
Vehicle
LRRK2 Inhibitor
mRNA enrichment in FLAG-HuD IP (relative to IgG control)
*
***
****
SNCA
BDNF
LRRK2
e)
siRNA
CTL
LRRK2
245
LRRK2
48
HuD
48
Tubulin
f)
Control siRNA
Lrrk2 siRNA
mRNA enrichment in FLAG-HuD IP (relative to IgG control)
*
*
*
SNCA
BDNF
LRRK2
g)
Control siRNA
Lrrk2 siRNA
mRNA enrichment in FLAG-HuB IP (relative to IgG control)
*
**
SNCA
BDNF
h)
Control siRNA
Lrrk2 siRNA
mRNA enrichment in FLAG-HuC IP (relative to IgG control)
*
***
SNCA
BDNF

Figure 2.4.4 LRRK2 controls binding of nELAVL proteins to mRNA.

(a) Western blot of immunoprecipitates of anti-FLAG antibody or an isotype control antibody (IgG) from cells transfected with plasmid expressing FLAG-HuD. (b) Log_{10} enrichment of the indicated mRNAs (x-axis) in immunoprecipitates of FLAG-HuD from SH-SY5Y cells normalized to levels in IgG control immunoprecipitates measured by RT-qPCR. n= 4-6. (c) Western blot of LRRK2 phosphoserine-935 in cell lysates after treatment with control vehicle or GSK2578215A LRRK2 kinase inhibitor. (d) Quantification of RNAs by RT-qPCR in FLAG-HuD immunoprecipitates from SH-SY5Y cells from cells treated with control vehicle or GSK2578215A LRRK2 kinase inhibitor. n=4. (e) Western blot of LRRK2 in cell lysates after treatment with control siRNA or LRRK2 siRNA. (f) Quantification of RNAs by RT-qPCR in FLAG-HuD immunoprecipitates from SH-SY5Y cells treated with control siRNA or LRRK2 siRNA. n=3-4. (g) Quantification of RNAs by RT-qPCR in immunoprecipitates of FLAG-HuB from SH-SY5Y cells treated with control siRNA or LRRK2 siRNA. n=4. (h) Quantification of RNAs by RT-qPCR in immunoprecipitates of FLAG-HuC from SH-SY5Y cells treated with control siRNA or LRRK2 siRNA. n=4. Error bars represent mean ± SEM. Data were analyzed by One-sample t-test. * $p<0.05$, ** $p<0.01$, *** $p<0.001$.

LRRK2 controls binding of nELAVL to target mRNAs

Predicted nELAVL target mRNAs appear to be dysregulated by LRRK2 in patient data and the encoded proteins are regulated by LRRK2 G2019S in the *HuD*$^{-/-}$ mouse brain, potentially by LRRK2 acting on the remaining nELAVLs, HuB and HuC. We therefore hypothesized that LRRK2 may affect nELAVL binding to mRNA. To test this, we used the human neuroblastoma cell line, SH-SY5Y expressing FLAG-HuD as a model. We first confirmed that FLAG-HuD binds mRNAs encoding *SNCA* and *LRRK2* in cells (Fig. 2.4.4 a,b). *BDNF*, *SNCA*, and *LRRK2* mRNAs were all significantly enriched, but not the negative control, *GAPDH* (Fig. 2.4.4 b). To test if LRRK2 controls HuD binding to target mRNA, SH-SY5Y cells were treated with a LRRK2 kinase inhibitor or siRNA. Treatment with the inhibitor decreased phosphorylation of LRRK2 at S935, which tightly correlates with LRRK2 kinase activity, as expected (Fig. 2.4.4 c). In FLAG-HuD immunoprecipitates, mRNA encoding *BDNF*, *SNCA*, and *LRRK2* detected by RT-qPCR were decreased when LRRK2 kinase was inhibited with GSK2578215A (Fig. 2.4.4 c,d). Ensuring this was not due to an off-target effect of the kinase inhibitor, silencing of LRRK2 with siRNA (Fig. 2.4.4 e) decreased binding of HuD to *BDNF*, *SNCA*, and *LRRK2* mRNAs (Fig. 2.4.4 e, f). Binding of the two HuD homologues, HuB and HuC, to *BDNF* and *SNCA* mRNAs was also reduced by LRRK2 siRNA (Fig. 2.4.4 g,h, Supplementary Fig. 2.1 d) or LRRK2 kinase inhibitor (Supplementary Fig.2.1 e-h).

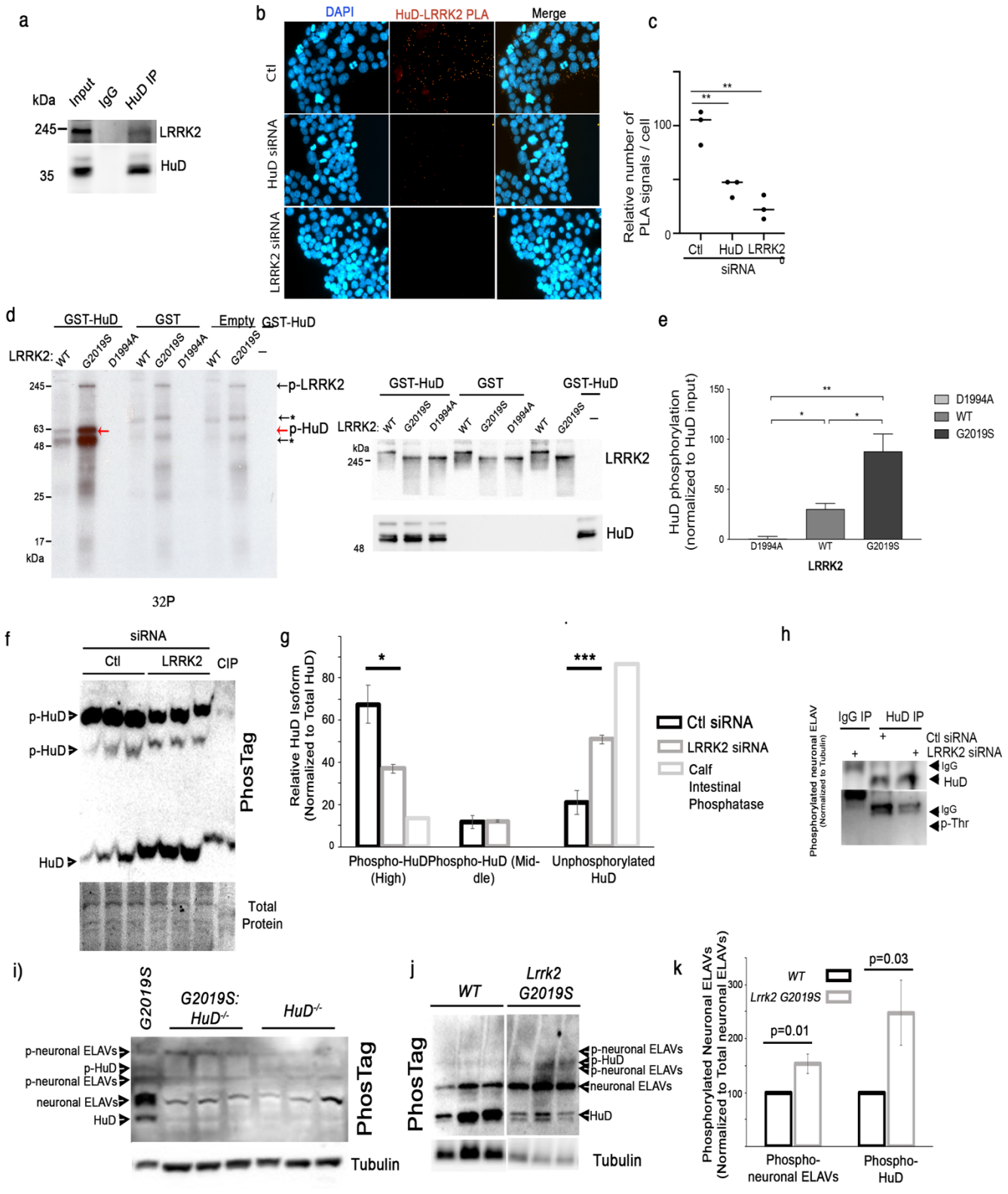
a
kDa
Input
IgG
HuD IP
245
LRRK2
35
HuD
b
DAPI
HuD-LRRK2 PLA
Merge
Ctl
HuD siRNA
LRRK2 siRNA
c
Relative number of PLA signals / cell
100
0
Ctl
HuD
LRRK2
siRNA
**
**
d
GST-HuD
GST
Empty
GST-HuD
LRRK2:
WT
G2019S
D1994A
WT
G2019S
D1994A
WT
G2019S
–
245
63
48
25
17
kDa
←p-LRRK2
←*
←p-HuD
←*
32P
GST-HuD
GST
GST-HuD
LRRK2:
WT
G2019S
D1994A
WT
G2019S
D1994A
WT
G2019S
–
kDa
245
LRRK2
48
HuD
e
HuD phosphorylation (normalized to HuD input)
150
100
50
0
**
*
*
D1994A
WT
G2019S
LRRK2
f
siRNA
Ctl
LRRK2
CIP
p-HuD
p-HuD
HuD
PhosTag
Total Protein
g
Relative HuD Isoform (Normalized to Total HuD)
80
60
40
20
0
*
***
Phospho-HuD (High)
Phospho-HuD (Middle)
Unphosphorylated HuD
Ctl siRNA
LRRK2 siRNA
Calf Intestinal Phosphatase
h
Phosphorylated neuronal ELAV (Normalized to Tubulin)
IgG IP
HuD IP
+
+
+
Ctl siRNA
LRRK2 siRNA
IgG
HuD
IgG
p-Thr
i)
G2019S
G2019S: HuD-/-
HuD-/-
p-neuronal ELAVs
p-HuD
p-neuronal ELAVs
neuronal ELAVs
HuD
PhosTag
Tubulin
j
WT
Lrrk2 G2019S
PhosTag
p-neuronal ELAVs
p-HuD
p-neuronal ELAVs
neuronal ELAVs
HuD
Tubulin
k
Phosphorylated Neuronal ELAVs (Normalized to Total neuronal ELAVs)
300
200
100
WT
Lrrk2 G2019S
p=0.01
p=0.03
Phospho-neuronal ELAVs
Phospho-HuD

Figure 2.4.5 LRRK2 phosphorylates nELAVL proteins *in vitro.*

(a) Western blot of LRRK2 and HuD in immunoprecipitates of endogenous HuD from Neuro2a cells. (b) Representative images of proximity ligation assays between HuD and LRRK2 in SH-SY5Y cells treated with control siRNA, HuD siRNA or LRRK2 siRNA. (c) Quantification of proximity ligation assays as shown in (b). (d) Autoradiographic exposure of SDS-PAGE gel after incubation of recombinant GST-HuD or controls with LRRK2 WT, LRRK2 G2019S and LRRK2 D1994A in the presence of γ-32P. Red arrow highlights phosphorylated HuD. Black arrows highlight autophosphorylated LRRK2, fragments of LRRK2, or contaminants are also observed by Coomassie total protein stain (Supplementary Fig.2 a). Below, Western blot of HuD and LRRK2 in samples from autoradiographic gels above. (e) Quantification of HuD phosphorylation on γ-32P gels as in (d) over n=3 independent experiments. γ-32P at the mass of GST-HuD was normalized to HuD detected by western blot in each experiment (f) Representative Western blot of PhosTag gels for FLAG-HuD (anti-FLAG) in SH-SY5Y cells treated with control or LRRK2 siRNA, or where lysates were treated with CIP (Calf Intestinal Phosphatase) to dephosphorylate FLAG-HuD. (g) Quantification of phosphorylated HuD in PhosTag blots of lysates of SH-SY5Y cells in (f). (h) Western blot phospho-Threonine on FLAG-HuD immunoprecipitates from SH-SY5Y cells treated with control siRNA or LRRK2 siRNA. (i) Representative Western blot of PhosTag gels for nELAVLs in midbrain of *Lrrk2 G2019S*, *HuD*$^{-/-}$ and *LRRK2 G2019Sx HuD*$^{-/-}$ mice, showing specificity of bands for HuD. (j) Representative Western blot of PhosTag gels for nELAVLs in midbrain of *wild-type* and *Lrrk2 G2019S* mice. Note, arrowheads and labels indicate bands for phosphorylated and unphosphorylated forms of HuD and nELAVLs as defined in (i). Blots are from the same membrane at the same exposure. (k) Quantification of phosphorylated HuD and phosphorylated nELAVLs in PhosTag blots of lysates of midbrain of *wild-type* and *Lrrk2 G2019S* (n=4). Data were analyzed by One-Way ANOVA followed by Tukey's where multiple groups were compared, t-test (two tailed assuming unequal variance) where two groups were compared * $p<0.05$, ** $p<0.01$, *** $p<0.001$.

LRRK2 phosphorylates nELAVLs

Since depletion of LRRK2 or inhibition of its kinase activity impacted HuD binding to target mRNA, we hypothesized that LRRK2 phosphorylates HuD. In cells, we found that LRRK2 was retrieved with HuD by immunoprecipitation (Fig. 2.4.5 a). Using Proximity Ligation Assay (PLA), we detected LRRK2 in proximity to HuD (Fig. 2.4.5 b,c), excluding a post-lysis artefact. siRNA targeting HuD or LRRK2 reduced these PLA signals, validating that HuD and LRRK2 were specifically detected in proximity to each other. This demonstrates that LRRK2 is positioned to phosphorylate HuD.

To test whether LRRK2 can directly phosphorylate nELAVLs we first utilized *in vitro* assays using recombinant wild-type LRRK2, the Parkinson's-linked hyperactive variant LRRK2 G2019S and the kinase-dead LRRK2 variant D1994A. LRRK2 autophosphorylation was observed, as expected, with equal amounts of wild-type LRRK2 and LRRK2 G2019S, but not the D1994A kinase-dead mutant (black arrows, Fig. 2.4.5 d). LRRK2 G2019S exhibited increased autophosphorylation compared to wild-type LRRK2 consistent with its hyperactive kinase activity (Fig. 2.4.5 d). Phosphorylation of some bands at sizes lower than full-length LRRK2 in preparations of purified LRRK2 were observed. These are likely autophosphorylated fragments of LRRK2 (asterisks, see "Empty" lanes, Fig. 2.4.5 d, Supplementary Fig. 2.2 a). When GST alone was added, no additional bands were noted demonstrating that GST is not phosphorylated by LRRK2. This also validates that LRRK2 retains specificity in this assay. GST-HuD, was phosphorylated by wild-type LRRK2 and LRRK2 G2019S but not kinase-dead LRRK2 D1994A (Fig. 2.4.5 d). HuB and HuC were phosphorylated by LRRK2 G2019S similarly to HuD (Supplementary Fig.2.2 b). Quantitatively, phosphorylation of HuD was increased 3-fold by LRRK2 G2019S compared to wild-type LRRK2

(Fig. 2.4.5 e), similar to the increased autophosphorylation of LRRK2 observed here, and the increased kinase activity of LRRK2 G2019S kinase on other substrates (West et al. 2005b).

Available antibodies detect all of the highly homologous nELAVLs (HuB, HuC and HuD) at slightly different masses (Ince-Dunn et al. 2012). As expected, in mouse midbrain, an antibody recognizing nELAVLs detected multiple bands for HuB, -C and -D some of which were absent in brain of *HuD*$^{-/-}$ mice and liver which does not express nELAVLs, validating these as HuD and nELAVLs respectively (Supplementary Fig. 2.2 c). To assess the impact of LRRK2 on phosphorylation of HuD in cells, we utilized PhosTag gels which cause a mass-shift in phosphorylated proteins (Fig. 2.4.5 f,g).Two higher mass bands of FLAG-HuD were detected on PhosTag gels, and these were nearly eliminated by dephosphorylation with Calf Intestinal Phosphatase (CIP), confirming their phosphorylation (Fig. 2.4.5 f,g). Unphosphorylated HuD was detected at the bottom of the gel. Resembling the effect of CIP, treatment of cells with LRRK2 siRNA reduced phosphorylation of one of the phospho-HuD species and caused an accumulation of unphosphorylated HuD. In SH-SY5Y cells, HuD was also detected using anti- phospho-Threonine in immunoprecipitates, and this signal was reduced when LRRK2 was silenced with siRNA (Fig. 2.4.5 h). Some phosphorylation of HuD on Threonines was still detected after depletion of LRRK2 potentially due to incomplete depletion of LRRK2 by siRNA, or the phosphorylation of HuD by other kinases in addition to LRRK2.

To assess the impact of LRRK2 on phosphorylation of nELAVLs in mice, we utilized PhosTag gels (Fig. 2.4.5 i,j). Several mass-shifted bands were detected with antibody recognizing nELAVLs in *Lrrk2 G2019S* mice. These mass-shifted bands were eliminated when lysates were dephosphorylated with CIP, validating these as *bona fide* phosphorylation events on nELAVLs

(Supplementary Fig.2.2 d). In *HuD*$^{-/-}$ and *Lrrk2 G2019S x HuD*$^{-/-}$ mice, one unphosphorylated band and one mass-shifted band were absent, validating these as unphosphorylated and phosphorylated HuD respectively (Fig. 2.4.5 i), indicated by arrowheads and labels. An additional two mass-shifted bands, presumably phosphorylated versions of HuB and/or HuC, were also detected at higher mass with anti-neuronal ELAVL antibodies (Fig. 2.4.5 i). Having validated the specificity of the PhosTag analysis for HuD and *bona fide* phosphorylation, we quantified the effect of *Lrrk2 G2019S* on phosphorylation of nELAVLs. The phosphorylation of HuD was increased over 2-fold in midbrain of *Lrrk2 G2019S* mice compared to wild-type littermates (Fig. 2.4.5 j,k) consistent with 2-3-fold increase in kinase activity of LRRK2 G2019S vs. wild-type LRRK2 (West et al., 2005b).The phosphorylation of a band corresponding to other nELAVLs was also significantly increased in *Lrrk2 G2019S* compared to *wild-type* controls (Fig. 2.4.5 j,k).

Together, this demonstrates that LRRK2 can directly phosphorylate multiple nELAVLs, and their phosphorylation is increased by LRRK2 *in vitro* (Fig. 2.4.5 d,e), in neuronal cell lines (Fig. 2.4.5 f-h) and by LRRK2 G2019S in mouse midbrain (Fig. 2.4.5 j,k) using three independent types of experiments (i.e., *in vitro* kinase assay, phospho-threonine antibodies, and PhosTag gels).

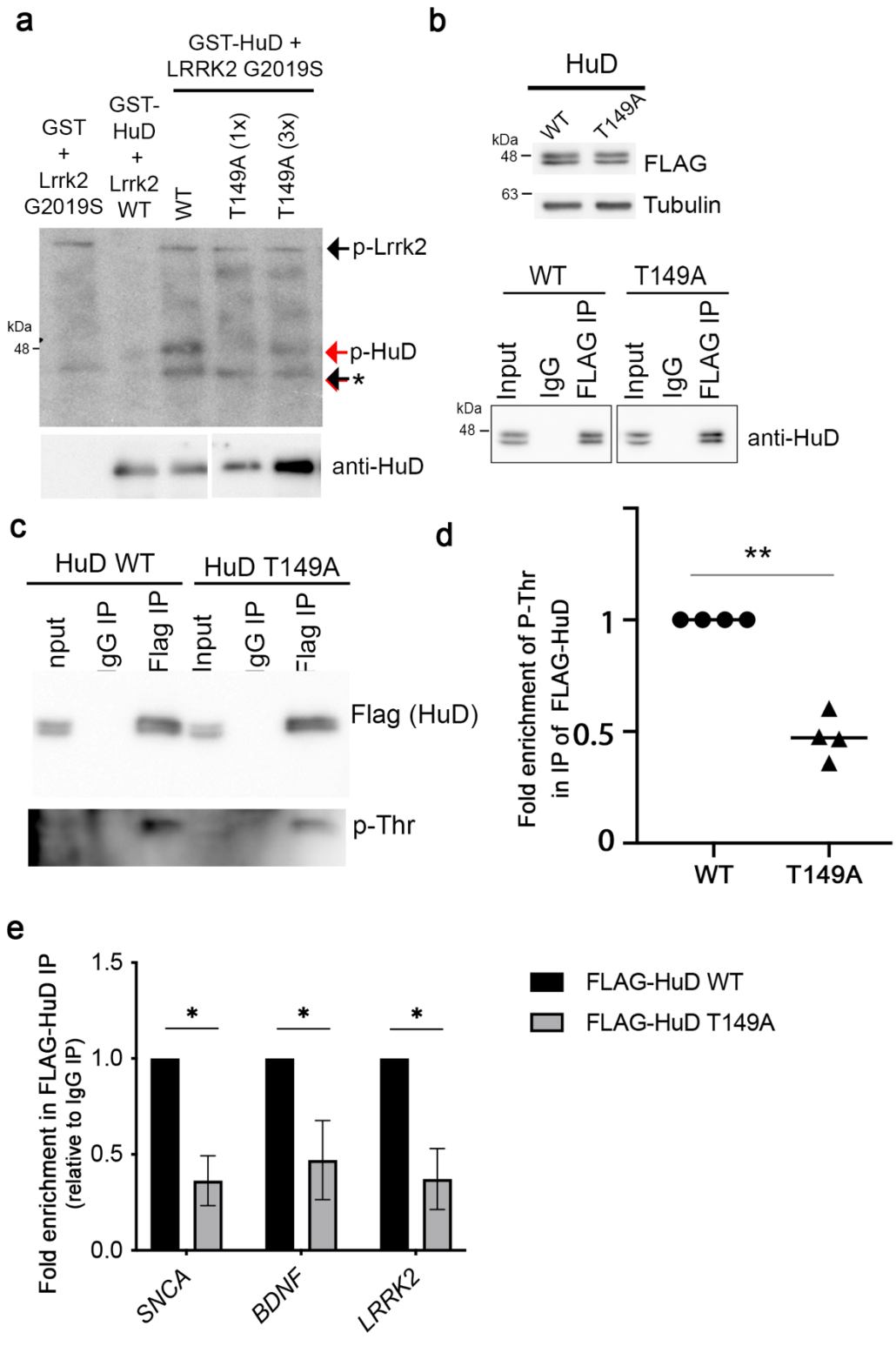
a
GST-HuD + LRRK2 G2019S
GST + Lrrk2 G2019S
GST-HuD + Lrrk2 WT
WT
T149A (1x)
T149A (3x)
kDa
48
p-Lrrk2
p-HuD
*
anti-HuD
b
HuD
WT
T149A
kDa
48
FLAG
63
Tubulin
WT
T149A
Input
IgG
FLAG IP
Input
IgG
FLAG IP
kDa
48
anti-HuD
c
HuD WT
HuD T149A
nput
gG IP
Flag IP
Input
gG IP
lag IP
Flag (HuD)
p-Thr
d
Fold enrichment of P-Thr in IP of FLAG-HuD
**
1
0.5
0
WT
T149A
e
Fold enrichment in FLAG-HuD IP (relative to IgG IP)
1.5
1.0
0.5
0.0
*
*
*
SNCA
BDNF
LRRK2
FLAG-HuD WT
FLAG-HuD T149A

Figure 2.4.6 LRRK2 phosphorylates T149 on HuD to control its binding to RNA.

(a) Autoradiography of HuD phosphorylation with γ-32P by LRRK2. SDS-PAGE gel exposed to film after incubation of LRRK2 wild-type or G2019S with γ-32P and wild-type HuD, or equal amounts of HuD T149A mutant (1x) or 3-fold as much HuD T149A mutant. Below, Western blot of HuD was run with the identical samples, in parallel, on a separate gel. Blots are from the same membrane at the same exposure. (b) (Above) Western blot of FLAG in total cell lysates of cells expressing wild-type or T149A-FLAG-HuD, or (Below) immunoprecipates of FLAG from the same cells. (c) Western blot for phospho-Threonine (p-Thr) in immunoprecipitates of wild-type or T149A FLAG-HuD (d) Quantification of phospho-Threonine in immunoprecipitates of wild-type or T149A FLAG-HuD over three experiments. One sample t-test e) RT-qPCR quantification of mRNAs in immunoprecipitates of wild-type or T149A FLAG-HuD. * $p<0.05$, one-sample t-test.

We sought to identify the sites in HuD phosphorylated by LRRK2. Mass spectrometry was performed on nELAVL immunoprecipitates from mouse brains to identify physiologically relevant phosphorylation sites on HuD for the serine/threonine kinase activity of LRRK2 (West et al., 2005b). Phosphorylation at T149, T174 and S233 of nELAVLs was observed across different animals in the mouse brain. To test whether LRRK2 was capable of phosphorylating these sites directly, mass spectrometry was performed on recombinant HuD after incubation with LRRK2 G2019S or kinase-dead LRRK2 with peptide coverage of 65-68%. Phosphorylation of HuD at T149 was consistently increased after incubation with LRRK2 G2019S over three independent replicates (Supplementary Fig.2.2e). While it is possible that LRRK2 G2019S phosphorylates HuD on additional sites, we focused our attention on T149 because it was the only site both consistently phosphorylated by LRRK2 G2019S *in vitro* and phosphorylated in the mouse brain. T149 is also conserved in HuB, and replaced by a serine in HuC which could also be phosphorylated by the serine/threonine kinase activity of LRRK2 (Supplementary Fig.2.2 b,f). T149 and its surrounding sequence is also highly conserved in ELAVLs through zebrafish, *C.elegans* and *Drosophila* (Supplementary Fig.2.2 f). T149 is located on an accessible surface of HuD within the RNA-binding RRM2 domain (Supplementary Fig. 2.2 g,h). This suggests that T149 is available for phosphorylation by LRRK2, and this could cause the effects on HuD binding to RNA induced by LRRK2 (Fig. 2.4.4 c-f).

To verify that T149 is phosphorylated by LRRK2 G2019S, this site was mutated to alanine. Phosphorylation of recombinant, purified, HuD T149A by LRRK2 G2019S *in vitro* was strongly reduced compared to wild-type HuD in the *in vitro* kinase assay (Fig. 2.4.6 a). Some residual phosphorylation of HuD was nonetheless noted in T149A mutants, and suggests LRRK2 may

phosphorylate additional sites on HuD, such as T174. Phosphorylation of HuD T149A was still reduced when a 3-fold excess of the protein was added to the assay (Fig. 2.4.6 a). This demonstrates that *in vitro* LRRK2 G2019S may phosphorylate multiple sites on HuD at a low rate, but the principal site of phosphorylation is T149. In cells, the HuD T149A mutation did not affect levels of HuD, suggesting it has no major impact on protein stability or folding (Fig. 2.4.6 b). Detection of HuD with antibodies specific for phospho-Threonine was also significantly reduced by the T149A mutation (Fig. 2.4.6 c,d). Collectively, this demonstrates that T149 on HuD is phosphorylated in cells, and that this is the dominant site on HuD phosphorylated by LRRK2. Mutation of T149 reduced binding of HuD to target mRNAs including *SNCA*, *BDNF* and *LRRK2* mRNA (Fig. 2.4.6 e), closely resembling the effects of LRRK2 siRNA and kinase inhibitors (Fig. 2.4.4 c-f). This suggests that LRRK2 phosphorylates HuD at T149 to increase its binding to RNA (Fig. 2.4.4-6).

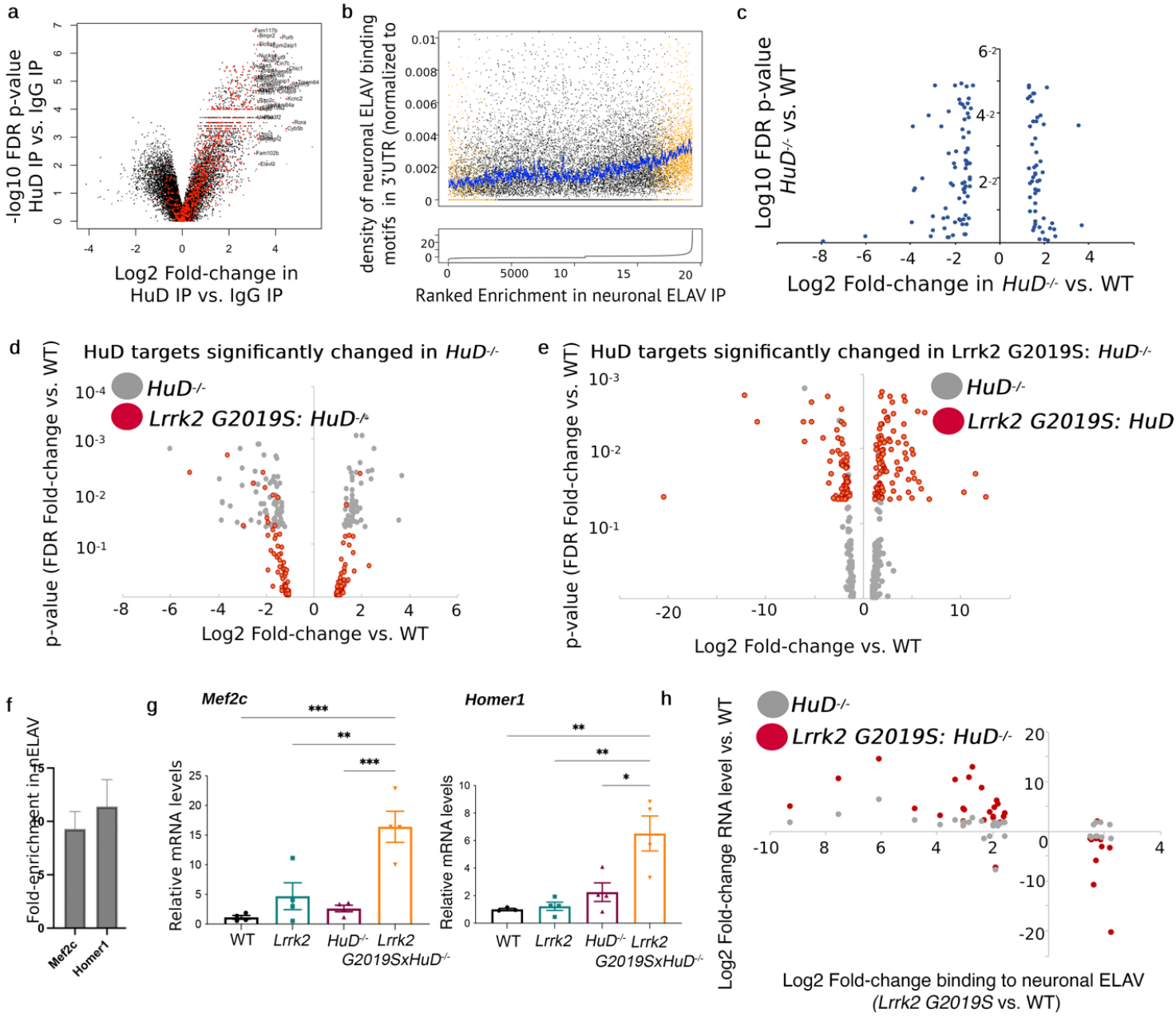
a
-log10 FDR p-value
HuD IP vs. IgG IP
Log2 Fold-change in
HuD IP vs. IgG IP
b
density of neuronal ELAV binding
motifs in 3'UTR (normalized to
Ranked Enrichment in neuronal ELAV IP
c
Log10 FDR p-value
HuD-/- vs. WT
Log2 Fold-change in HuD-/- vs. WT
d
HuD targets significantly changed in HuD-/-
HuD-/-
Lrrk2 G2019S: HuD-/-
p-value (FDR Fold-change vs. WT)
Log2 Fold-change vs. WT
e
HuD targets significantly changed in Lrrk2 G2019S: HuD-/-
HuD-/-
Lrrk2 G2019S: HuD
p-value (FDR Fold-change vs. WT)
Log2 Fold-change vs. WT
f
Fold-enrichment in nELAV
Mef2c
Homer1
g
Mef2c
Homer1
Relative mRNA levels
WT
Lrrk2
HuD-/-
Lrrk2 G2019SxHuD-/-
h
HuD-/-
Lrrk2 G2019S: HuD-/-
Log2 Fold-change RNA level vs. WT
Log2 Fold-change binding to neuronal ELAV
(Lrrk2 G2019S vs. WT)

Figure 2.4.7 LRRK2 G2019S exaggerates the effects of *HuD*$^{-/-}$ on targets of nELAVLs in the mouse midbrain. (a) Volcano plot of Log2-enrichment vs. p-value of mRNAs in immunoprecipitates of nELAVLs from mouse midbrain. Red dots, enriched in the present nELAVL immunoprecipitates, represent mRNAs identified as bound to nELAVLs in published nELAVL CLIPseq from cortex (b)(Ince-Dunn et al., 2012) Increased density of nELAVL binding motifs (UUU*UUU) (Ince-Dunn et al., 2012)in mRNAs enriched in nELAVL immunoprecipitates. On the bottom, mRNAs are ordered by their enrichment in nELAVL immunoprecipitates and in the top graph the density of nELAVL binding motifs in these mRNAs are plotted with those significantly enriched or depleted from nELAVL immunoprecipitates colored in orange. The blue line plots the moving average density of nELAVL binding motifs. Note the increase in the blue line when enrichment in nELAVL immunoprecipitates increases (orange dots). (c) Inverted volcano plot of fold-change in mRNA levels vs. significance (FDR p-value) in *HuD*$^{-/-}$ mice for all mRNAs in nELAVL immunoprecipitates (>2 log2 vs. IgG, FDR p>0.01). Levels of mRNAs bound to nELAVL either increase or decrease in midbrain of *HuD*$^{-/-}$ mice. (d) Volcano plot of all mRNAs in nELAVL immunoprecipitates (>2 log2 vs. IgG, FDR p>0.01) that are also significantly altered (p>0.05) in *HuD*$^{-/-}$ mice. Changes in nELAVL target levels in *HuD*$^{-/-}$ mice is largely lost in *Lrrk2 G2019SxHuD*$^{-/-}$ mice. (e) Volcano plot of all mRNAs in nELAVL immunoprecipitates (>2 log2 vs. IgG, FDR p>0.01) that are also significantly altered (p>0.05) in *Lrrk2 G2019SxHuD*$^{-/-}$ mice. Despite being bound to nELAVLs, levels of these RNAs are only altered in *Lrrk2 G2019SxHuD*$^{-/-}$ mice and rarely in *HuD*$^{-/-}$ mice. (f) Fold-enrichment of *Mef2c* and *Homer1* mRNAs in IPs of nELAVLs from mouse midbrain normalized to immunoprecipitation with control IgG. (g) RT-qPCR quantification of the levels of *Mef2c* and *Homer1* in samples from mouse midbrain of the indicated genotypes. (h) Plot of Log2 Fold-change in RNA level vs. Log2-Fold change in binding to nELAVLs (Lrrk2 G2019S vs wild-type). Only RNAs bound to nELAVLs (>4-fold, FDR>0.01), whose binding to nELAVLs was altered more than Log(2)x1.5 in LRRK2 G2019S, and whose expression was significantly altered (p>0.05) in *Lrrk2 G2019SxHuD*$^{-/-}$ mice are plotted. Note that decreased binding to nELAVLs in *Lrrk2 G2109S* results in increased levels of RNA in *Lrrk2 G2019S x HuD*$^{-/-}$ mice. Conversely, increased binding to nELAVLs in *Lrrk2 G2109S* results in decreased levels of RNA in *Lrrk2 G2019SxHuD*$^{-/-}$ *mice*.

LRRK2 G2019S regulates expression of nELAVL targets in the mouse midbrain

We next sought to ascertain the impact of LRRK2 G2019S on nELAVL targets in a genome-wide fashion. Others have reported that nELAVLs (HuB, C and D) can either increase or decrease mRNA stability and translation by binding U-rich sequences in the 3'UTR of mRNAs (Tebaldi et al. 2018; Ince-Dunn et al. 2012). To define nELAVL targets, RNA from nELAVL immunoprecipitates from mouse midbrain was quantified. Neuronal ELAVLs bound 2078 RNAs in mouse midbrain with a minimum 4-fold enrichment vs. IgG control including mRNA encoding a-synuclein (FDR p>0.01, Supplementary Table 1,2). Neuronal ELAVL immunoprecipitates were enriched in binding motifs for nELAVLs and mRNAs previously identified to bind nELAVLs by CLIPseq (Ince-Dunn et al., 2012) (Fig.2.4.7 a,b).

Total RNA from midbrain of *wild-type*, *HuD*$^{-/-}$, *Lrrk2 G2019S* and *Lrrk2 G2019S x HuD*$^{-/-}$ mice was also analyzed (four mice per group, Supplementary Table 1). In mice expressing *Lrrk2 G2019S*, no significant changes in RNA abundance were recorded compared to wild-type mice (Supplementary Table 1). In a genome-wide manner *HuD*$^{-/-}$ mice and *Lrrk2 G2019S x HuD*$^{-/-}$ mice exhibited changes in the levels of many mRNAs (Supplementary Table 1, Supplementary Fig.2.3). Focusing on targets of nELAVLs, in midbrain from *HuD*$^{-/-}$ mice, 127 RNAs that were significantly bound to nELAVLs were also significantly upregulated or downregulated (FDR >0.05, Fig. 2.4.7 c, Supplementary Table 3). These RNAs were significantly enriched in RNA and DNA binding proteins (Supplementary Table 5), and this may cause secondary effects on the other RNAs that do not bind nELAVLs but are misregulated in *HuD*$^{-/-}$ mice (Supplementary Table 1).

LRRK2 can phosphorylate HuB and HuC, like HuD, to regulate their binding to RNAs (Fig.2.4.4 g,h, Supplementary Fig.2.1 d-h). This would empower *Lrrk2 G2019S* to either rescue the effect of *HuD*$^{-/-}$ on RNA, if it phosphorylates and promotes HuB and HuC function, or alternatively exacerbate the effect of *HuD*$^{-/-}$ if it inhibits HuB and HuC, mimicking total loss of nELAVL function. Changes in the levels of the 127 mRNAs significantly bound to nELAVLs and significantly altered in *HuD*$^{-/-}$ mice were largely reversed in *Lrrk2 G2019S x HuD*$^{-/-}$ mice (Fig.2.4.7 d, Supplementary Table 3). A unique subset of 171 RNAs which bound to nELAVLs was not significantly changed in *HuD*$^{-/-}$ mice but became significantly different in *Lrrk2 G2019S x HuD*$^{-/-}$ mice (Fig.2.4.7 e, Supplementary Table 3). These RNAs were found in pathways involved in neurons, synapses and post-synapses (Supplementary Table 6).

We validated these microarray results. *Mef2c* and *Homer1* mRNAs, bound nELAVLs (Fig.2.4.7 f). Their levels in total RNA were subtly increased in *HuD*$^{-/-}$ mice, and strongly increased in *Lrrk2 G2019Sx HuD*$^{-/-}$ mice as detected in genome-wide analyses (Fig.2.4.7g, Supplementary Table 1). MEF2C impacts motor function, learning and memory in mice and patients (Barbosa et al., 2008; Zweier et al., 2010), and Homer1 regulates survival of dopaminergic neurons in models of PD (T. Chen et al. 2013; Szumlinski et al. 2004).

To gain insight into the mechanism by which LRRK2 G2019S exerts these effects, we examined the effects on RNAs whose binding to nELAVLs was altered in *Lrrk2 G2019S* mice vs. *wild-type* mice. mRNAs whose binding to nELAVLs was decreased by *Lrrk2 G2019S* had subtly increased levels in *HuD*$^{-/-}$ mice that were further increased by co-expression of *Lrrk2 G2019S* (Fig.2.4.7 h). This suggests that nELAVLs are destabilizing this group of mRNAs and mutant LRRK2 inhibits

nELAVLs and this destabilization, phenocopying an nELAVL loss of function. Conversely, RNAs whose binding to nELAVLs was increased by LRRK2 G2019S, had their levels decreased by LRRK2 G2019S in *HuD*$^{-/-}$ mice (Fig.2.4.7 h). Both examples suggest that LRRK2 G2019S changes which RNAs are bound to and destabilized by nELAVLs.

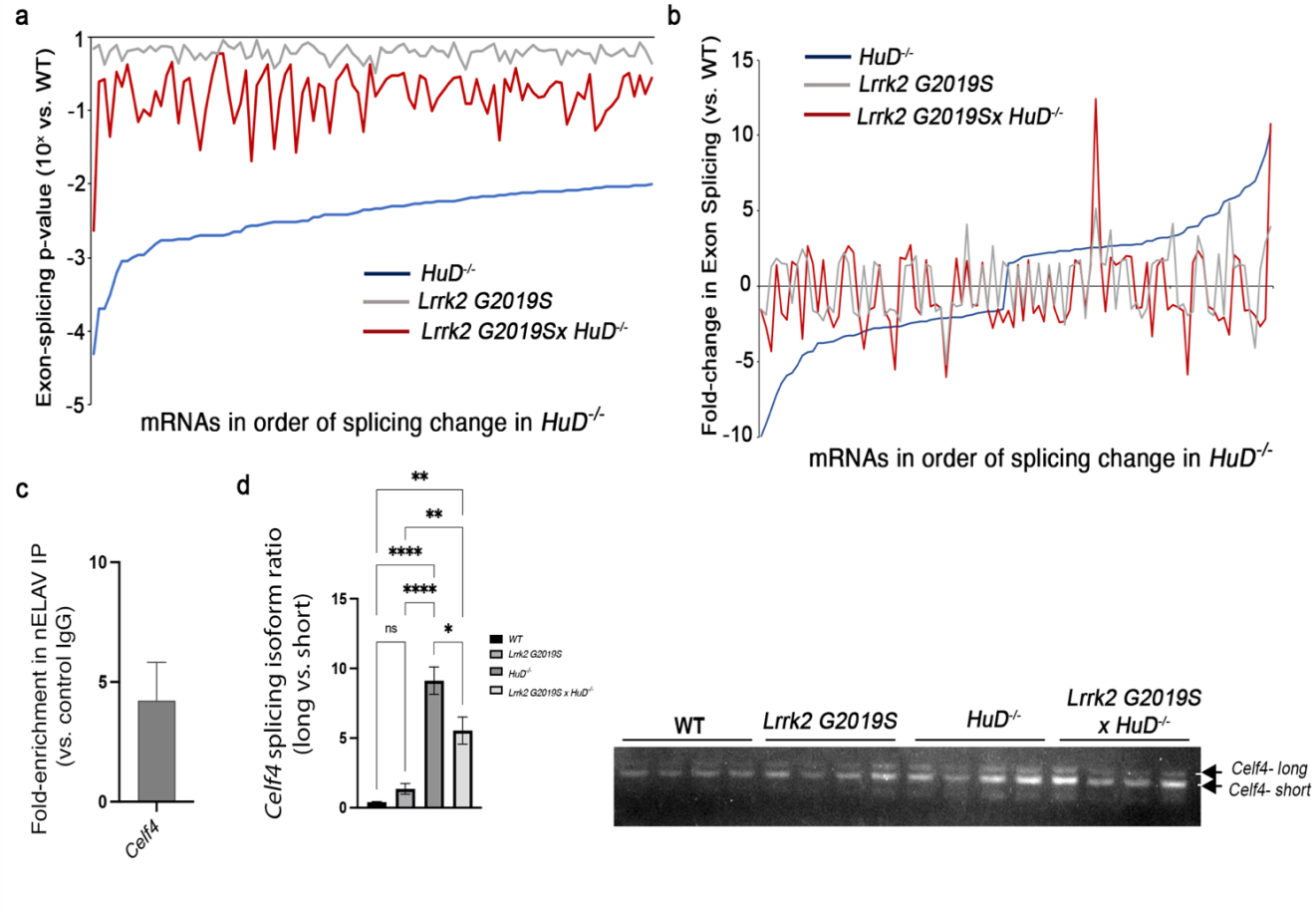

Figure 2.4.8 LRRK2 G2019S minimizes splicing defects caused by loss of *HuD*.

(a) Rank-order of all significant (FDR<0.01) splicing changes in *HuD*$^{-/-}$ mouse midbrain by p-values. Note mRNAs whose splicing is significantly altered in *HuD*$^{-/-}$ mice are nearly all reversed by *Lrrk2 G2019S*. (b) Rank-order of all significant (FDR<0.01) splicing changes in *HuD*$^{-/-}$ mouse midbrain by fold-change in exon-splicing. Note amplitude of effect on mRNA splicing in *HuD*$^{-/-}$ mice is diminished by *Lrrk2 G2019S*. (c) Fold-enrichment of *Mef2c* and *Homer1* mRNA in nELAVL immunoprecipitates quantified by RT-qPCR. (d) (Left) Quantification of *Celf4* splice variants (long vs. short form) n=4. (Right) *Celf4* splice variants amplified by RT-PCR and analyzed by agarose gel. Data were analyzed by One-Way ANOVA with Tukey's. * p<0.05, ** p<0.01, *** p<0.001, **** p<0.0001.

LRRK2 G2019S corrects splicing defects in *HuD*$^{-/-}$ mice

The results above demonstrate that LRRK2 regulates RNA levels of nELAVL targets in mice and patient cells. Neuronal ELAVLs also control mRNA splicing (Ince-Dunn et al., 2012). In mouse midbrain, LRRK2 G2019S had no independent effects on splicing of mRNAs that bind nELAVLs (Supplementary Table 7). As previously reported, *HuD*$^{-/-}$ mice exhibited extensive changes in mRNA splicing, with 1125 mRNAs exhibiting significant differences in splicing ($p<0.01$, Supplementary Table 8). These mRNAs differentially spliced in *HuD*$^{-/-}$ mice were enriched in factors involved in motor function, gait disturbance, brain atrophy and higher mental functions (Supplementary Table 9). Among these alternatively spliced mRNAs, 100 were also bound by nELAVLs and likely directly regulated by HuD ($p<0.01$, Fig 2.4.8 a,b, Supplementary Table 10). Remarkably, 92% of these splicing changes of nELAVL targets in *HuD*$^{-/-}$ mice were prevented by co-expression of *Lrrk2 G2019S*, whether analyzed as p-value or fold-change in splicing (Fig.2.4.8 a,b, Supplementary Table 10). This effect was validated on a predicted splice variant in *Celf4*. Neuronal ELAVLs in the mouse midbrain bound to *Celf4* mRNA (Fig.2.4.8 c). A long splice isoform of *Celf4* was induced in *HuD*$^{-/-}$ mice and this splice variant was reduced by co-expression of *Lrrk2 G2019S* (Fig.2.4.8 d). This demonstrates that while phosphorylation by LRRK2 inhibits the function of nELAVLs on mRNA levels and translation (Fig.2.4.3, Fig.2.4.7), it promotes the functions of nELAVLs in mRNA splicing (Fig.2.4.8). Collectively, these results demonstrate that the *Lrrk2 G2019S* mutation may exacerbate some effects while reducing other effects in *HuD*$^{-/-}$ mice, paralleling the effects we observed on motor impairment and behaviour (Fig.2.4.2).

2.5 Discussion

Like many proteins which post-transcriptionally regulate gene expression, ELAVL family proteins regulate both mRNA stability and translation through processes that intimately link translational inhibition and mRNA decay (Fukao et al., 2021b; Selbach et al., 2008). In these cases, effects on mRNA levels can often be more subtle than the effects on protein levels (Selbach et al., 2008). This is likely why HuD associates with hundreds, or even thousands of mRNAs, but the mRNA levels of only about 10% of these are measurably changed in *HuD*$^{-/-}$ mice (Supplementary Table 1), but differences are observed in protein levels of HuD targets like α-synuclein, BDNF and LRRK2 itself (Fig.2.4.3, Fig.2.4.7).

LRRK2 phosphorylates HuD on T149, a major site of HuD phosphorylation in the mouse brain defined by mass spectrometry. T149 is on an exposed loop in its RRM2 domain which mediates binding to U-rich RNA motifs (Chung et al., 1996; Park et al., 2000). Stable binding of HuD to U-rich RNA motifs requires all three RRMs, and notably RRM2 (Park et al., 2000), suggesting a mechanism by which phosphorylation of HuD on T149 in RRM2 can regulate its binding to mRNA. HuD has been documented to promote mRNA stability and destabilization (Aranda-Abreu et al., 1999; Bolognani et al., 2009; Ince-Dunn et al., 2012), and to promote translation through binding to eIF4a (Fukao et al., 2009) or Y-RNAs (Tebaldi et al., 2018). The RRM2 and its neighboring linker region to RRM3 also regulate its effects on translation (Tiruchinapalli, Caron, and Keene 2008; Fukao et al. 2009; Tebaldi et al. 2018).The RRM2 domain thus appears to be central to most of the effector functions of HuD, and a potent point for regulation by a kinase like LRRK2. While T149 appears to be the principal site of phosphorylation for LRRK2 on HuD, it is

possible that phosphorylation of HuD on additional sites contributes to the observed effects in cells and mice.

In agreement with previous publications (Ince-Dunn et al., 2012; Tebaldi et al., 2018), we found that mRNAs directly bound and regulated by nELAVLs were divided into three pools which either decreased or increased in the midbrain of *HuD*$^{-/-}$ mice or were differentially spliced (Fig.2.4.7-8). Phosphorylation by LRRK2 G2019S appears to redirect nELAVL function among these pools. It reinforces nELAVL effects on splicing, while impairing nELAVL effects on mRNA (de)stabilization. These contrasting effects on splicing and mRNA (de)stabilization were paralleled in impacts on levels of α-synuclein, BDNF and LRRK2 in mouse brain (Fig.2.4.3). In some brain regions LRRK2 G2019S exacerbated the effects on levels of these HuD targets in *HuD*$^{-/-}$ mice, while in other brain regions LRRK2 G2019S reversed the effects on protein levels of HuD targets in *HuD*$^{-/-}$ mice.

When levels of nELAVLs were reduced in *HuD*$^{-/-}$ mice, LRRK2 G2019S increased the phosphorylation of the remaining nELAVLs (Supplementary Fig.2.2 b, Fig.2.4.5 j,k) further inhibiting nELAVL activity on mRNA expression and levels of BDNF and α-synuclein in some brain regions (Fig.2.4.3). This suggests that LRRK2 hyperactivity will preferentially elicit nELAVL-dependent phenotypes in regions, or in patients, where nELAVLs are less abundant. One might expect that *Lrrk2 G2019S* mice would exhibit at least in part the phenotypes of *HuD*$^{-/-}$ mice. We observed control of nELAVL function by LRRK2 in contexts where expression of nELAVLs was limiting. For example, experiments in cell culture were performed in the neuroblastoma cell line SH-SY5Y where endogenous nELAVL expression was low. In the brain, three nELAVLs are

expressed, frequently at high levels, while LRRK2 levels in neurons are low (Fig. 2.4.1 d). Intriguingly, studies in mouse and human have noted that nELAVLs are expressed at low levels in the midbrain (Okano & Darnell, 1997; Uhlén et al., 2015), the region principally affected in PD, and tend to decrease further with age (Okano & Darnell, 1997), making the midbrain particularly susceptible to decreased expression or inhibition of nELAVLs. The role of the SNPs identified in the *ELAVL4* locus are not yet known, but it is possible that they decrease HuD expression, and modify age-of-onset of PD through this mechanism.

The capacity of nELAVLs to bind and regulate mRNAs encoding LRRK2 and α-synuclein (Fig.2.4.1, Fig.2.4.3-4, Supplementary Table 1) could control levels of these proteins which are critical for PD. Loss of nELAVL expression or function would increase levels of α-synuclein and LRRK2 and could thereby materially contribute to PD pathology. Our evidence also shows that increased LRRK2 expression or activity would also feedforward to further inhibit nELAVL function, reinforcing and exacerbating increases in levels of α-synuclein and LRRK2. LRRK2 kinase activity has previously been shown to regulate the levels of LRRK2 protein (Herzig et al., 2011) and α-synuclein pathology in mice (O'Hara et al. 2020; Bieri et al. 2019).One mechanism by which LRRK2 G2019S could contribute to the accumulation of α-synuclein and LRRK2, and the acceleration of α-synuclein and LRRK2-dependent pathology is by inhibiting nELAVLs.

LRRK2 G2019S effects on proteins other than nELAVLs likely contribute to the phenotypes observed in this study. However, our data demonstrates that LRRK2 G2019S increased phosphorylation of nELAVLs in the mouse brain (Fig.2.4.5 j,k) and specifically exacerbated changes in expression of one pool of mRNAs bound by nELAVLs in *HuD*$^{-/-}$ cells while rescuing

the effects of *HuD*$^{-/-}$ on another pool of their targets. Neuronal ELAVL targets were also selectively misregulated in sporadic PD and neurons derived from patients carrying LRRK2 G2019S mutations. Together, this suggests that at least part of the PD-relevant phenotypes induced by *Lrrk2 G2019S* in *HuD*$^{-/-}$ mice are due to misregulation of other nELAVLs. Nonetheless, it is also likely that nELAVLs and LRRK2 G2019S contribute to these phenotypes in mice via pathways operating independently of one another, including the phosphorylation of other substrates by LRRK2.

Phosphorylation of any single target by LRRK2 is unlikely to account for aspects of the symptoms and pathology in PD. Several molecular mechanisms have been proposed to be a root cause of PD including disruptions in mitochondrial dynamics, vesicle-trafficking, autophagy, inflammation, and accumulation of a-synuclein (Alessi and Sammler 2018). Recent literature has demonstrated that LRRK2 can phosphorylate RAB proteins involved in organelle trafficking to impact some of these pathways in cell models (Taylor and Alessi 2020). ELAVL proteins, by binding and regulating hundreds of mRNAs, also regulate mitochondrial dynamics (Carrascoso et al., 2017), autophagy (C. Kim et al., 2014) , inflammation (Katsanou et al., 2005) and α-synuclein and LRRK2 expression (Fig.2.4.3). Indeed, we also identified several RAB proteins, including RAB10 among nELAVL targets (Supplementary Table 1). Alongside its regulation of RABs, LRRK2 could also impact this broad range of pathways with roles in PD in part by phosphorylating ELAVL proteins to control their mRNA targets.

Mouse models expressing PD-linked mutations in LRRK2 at near physiological levels, such as the mice studied here, have shown minimal or no loss of dopaminergic neurons or motor phenotypes

(Herzig et al., 2011). This is also consistent with low penetrance of LRRK2 suggesting the presence of genetic or environmental triggers to elicit disease. The loss of *HuD*$^{-/-}$ in the presence of mutant LRRK2 induced PD-relevant phenotypes including loss of dopaminergic neurons, accumulation of α-synuclein in some tissues, and motor phenotypes (Fig.2.4.2-3). This models findings in patients where mutations in the nELAVL locus are risk factors for PD that may accelerate age-of-onset, penetrance, or pathology in patients, including those with LRRK2 mutations. If LRRK2 kinase activity is increased in a large majority of patients with idiopathic PD as reported (Di Maio et al., 2018), alterations in the *HuD* locus could thereby contribute to PD in many patients.

Are nELAVLs actually misregulated in patients with PD? We demonstrated that nELAVL target mRNAs were selectively dysregulated across studies of iPSC-derived neural stem cells from patients, substantia nigra, and isolated dopaminergic neurons from PD patients. This provides evidence that nELAVLs are misregulated in both patients with *LRRK2 G2019S* mutations and patients with idiopathic PD, independent of any change in cell composition of tissues. Together, this suggests that downregulation of nELAVL expression or loss of nELAVL function, by LRRK2 phosphorylation or other mechanisms, may be common in PD and contribute to its characteristic pathology.

2.6 Supplementary Data

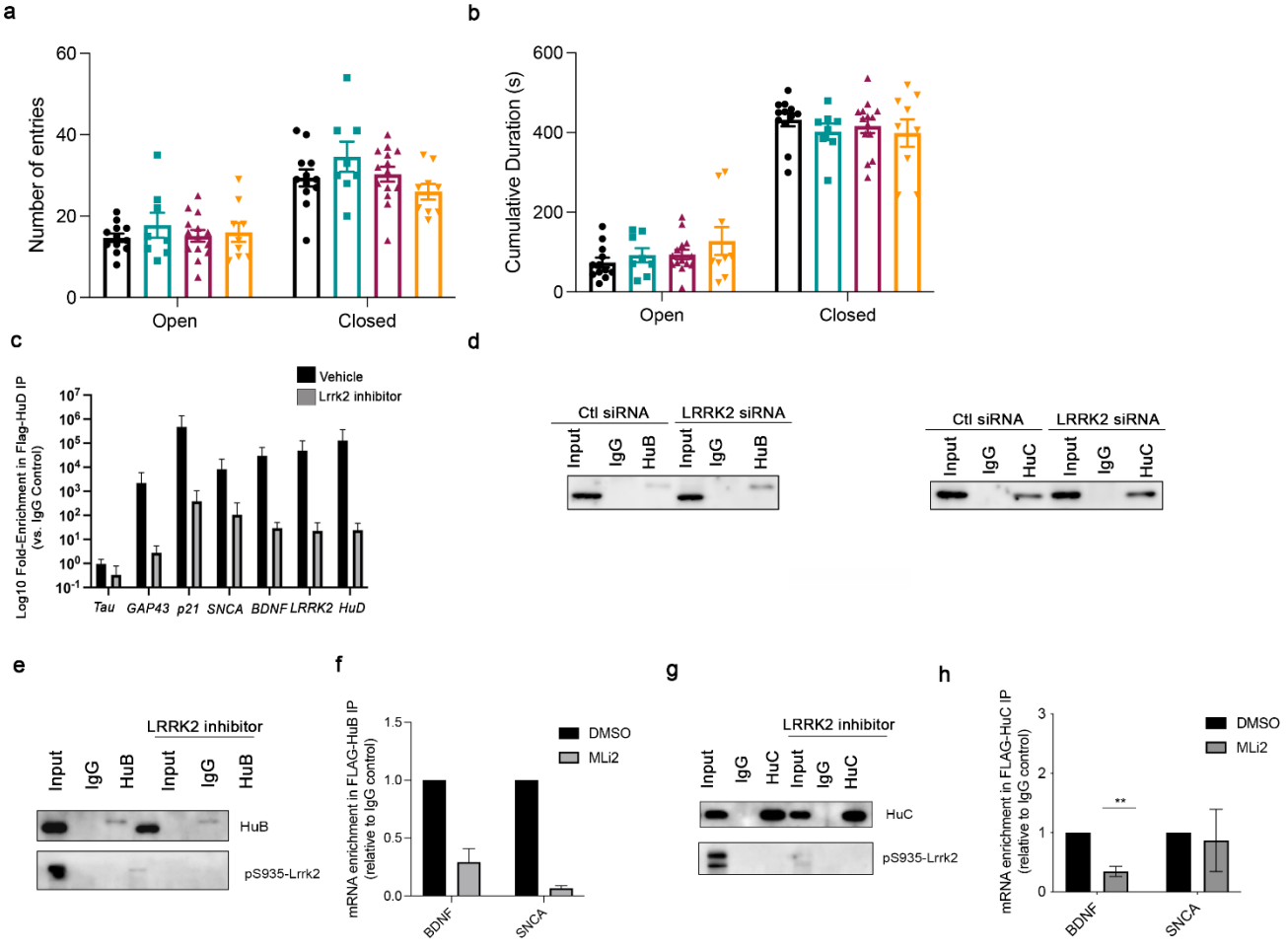

Supplementary Figure 2.1

(a,b) Elevated plus maze on 26-month old mice (a) number of entries into the open or closed arm (b) cumulative duration spent in either open or closed arm. (c) Log10 fold-enrichment of mRNAs in FLAG-HuD immunoprecipitated (vs. IgG control immunoprecipitated) after treatment of cells with vehicle of LRRK2 kinase inhibitor (d) Western blot of FLAG in immunoprecipitates of FLAG-HuB or FLAG-HuC from SH-SY5Y cells treated with control siRNA or LRRK2 siRNA. (e)Western blot of FLAG and LRRK2 phosphoserine-935 in SH-SY5Y cell lysates and immunoprecipitates of FLAG from cells transfected with FLAG-HuB (e) or FLAG-HuC (g). (f,h) Quantification of RNAs by RT-qPCR in immunoprecipitates of FLAG-HuB (f) or FLAG-HuC (h) from SH-SY5Y cells treated with vehicle or MLi2 LRRK2 kinase inhibitor. Error bars represent mean ± SEM. n=2-3. *$p<0.05$, ** $p<0.01$, *** $p<0.001$.

a

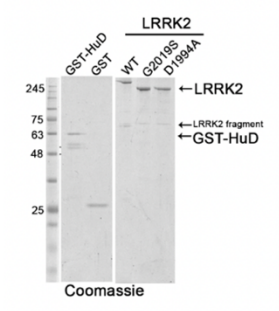

b

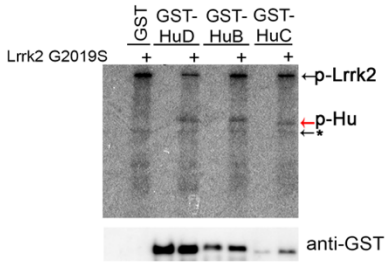

c

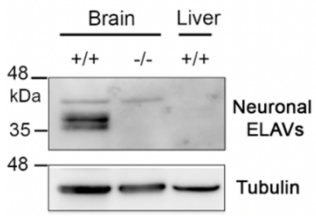

d

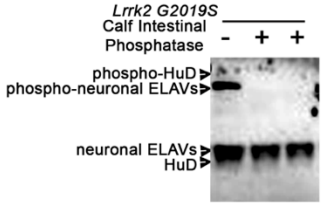

e

Phosphorylation in HuD (Phosphorylated peptide/Total HuD peptides)				
HuD residue (mouse)	No LRRK2	LRRK2 D1994A	LRRK2 G2019S	P-value
T63	-	-	0.022	0.21
S69	0.321	0.056	0.181	0.48
S133	-	-	0.050	0.21
T147	-	-	0.015	0.21
T149	**-**	**-**	**0.062**	**0.04***
T174	**-**	**-**	**0.030**	**0.05***
S222	-	-	0.026	0.21
S223	-	-	0.040	0.09
S233	**-**	**-**	**0.034**	**0.02***
Y259	-	-	0.037	0.07

f

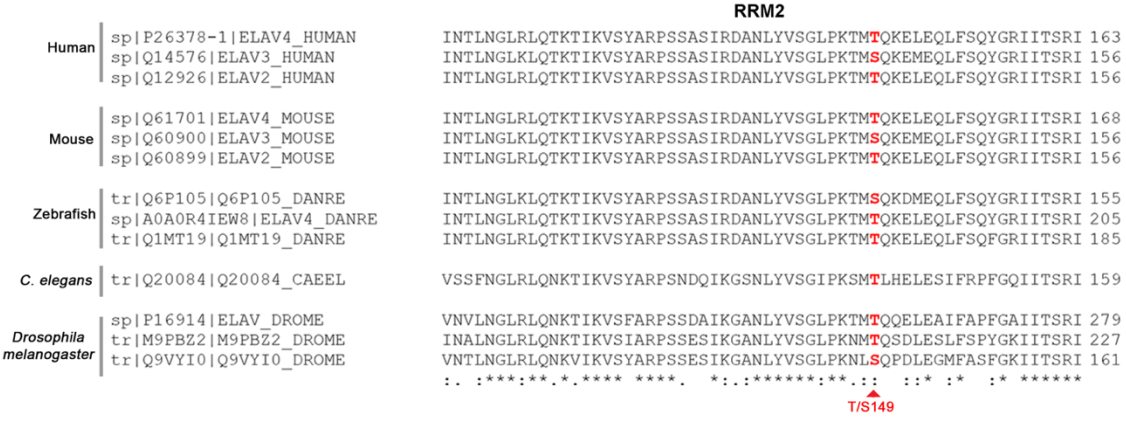

g

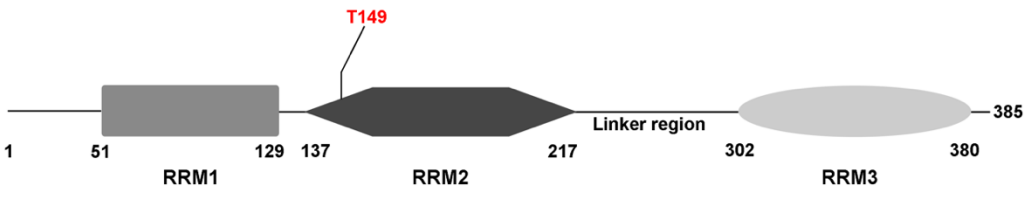

h

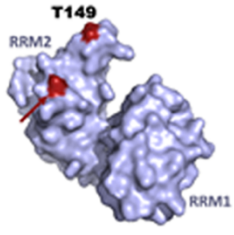

Supplementary Figure 2.2

(a) Coomassie total protein stain from recombinant proteins used in *in vitro* kinase assays. (*) non-specific bands indicating fragments of LRRK2. (b) Autoradiographic exposure of SDS-PAGE gel after incubation of recombinant GST-HuB, -HuC, and -HuD with vehicle or LRRK2 G2019S in the presence of γ-^{32}P. (c) Western blot of nELAVLs in brain and liver of wild-type and *HuD*$^{-/-}$ mice. (d) Western blot of nELAVLs from the midbrain of *Lrrk2 G2019S* mice separated on a PhosTag gel. Equal amounts of samples were left untreated or treated with Calf Intestinal Phosphatase to dephosphorylate proteins and validate detection of phosphorylated nELAVLs on PhosTag gels. (e) Quantification of recombinant HuD phosphorylation on specific sites by MS/MS (phosphorylated peptide count/Total HuD peptide count) after incubation alone, with kinase-dead LRRK2 D1994A or with LRRK2 G2019S. Peptides significantly phosphorylated after incubation with LRRK2 G2019S vs. D1994A are shown in bold. (f) Alignment of mouse, human, zebrafish, *C.elegans* and *Drosophila* ELAVL homologues highlighting conservation of LRRK2 phosphorylation site at T149. (g) Domain map of nELAVLs indicating the location of T149. (h) Crystal structure of HuD protein indicating T149 site.

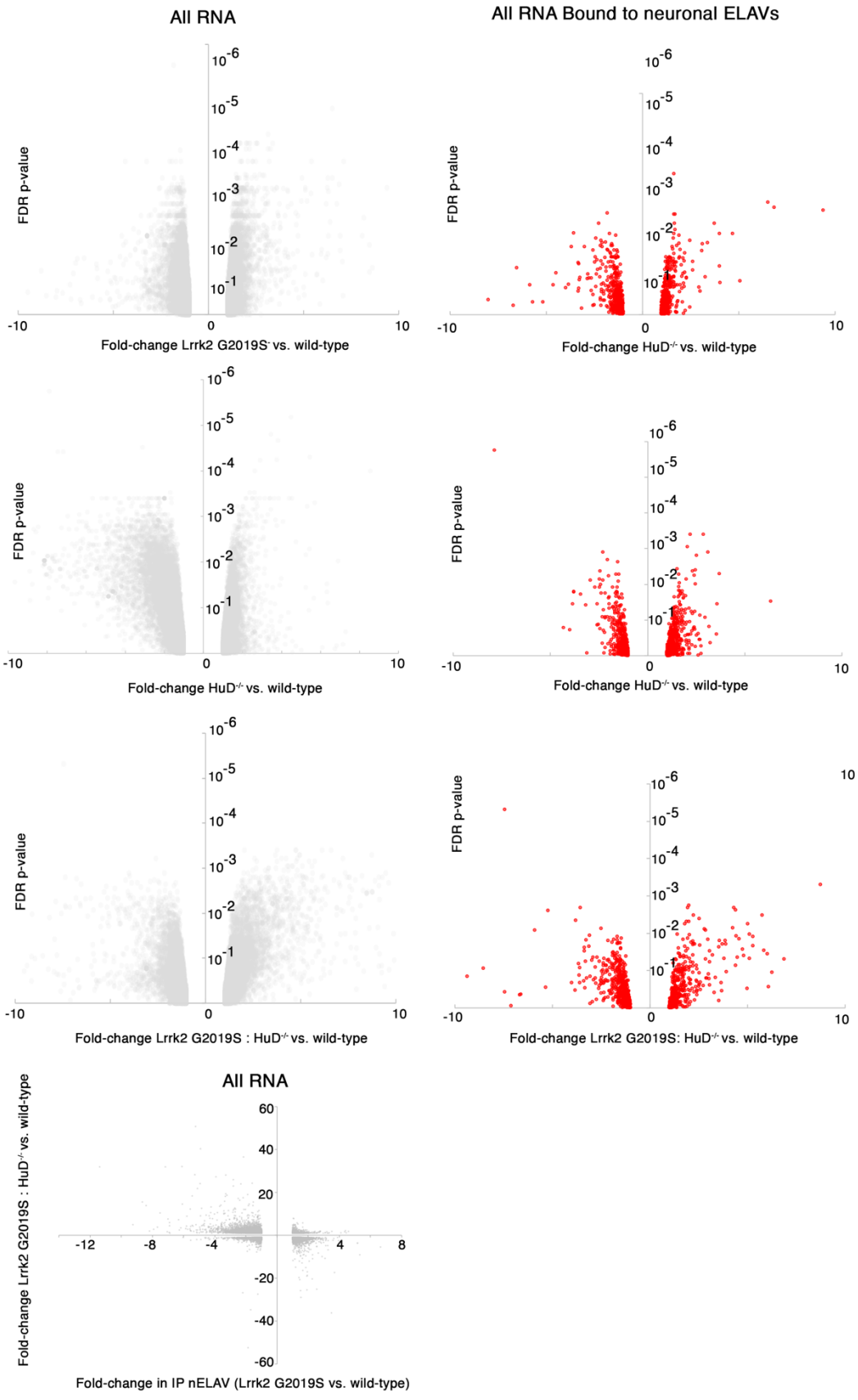
All RNA
All RNA Bound to neuronal ELAVs
FDR p-value
Fold-change Lrrk2 G2019S vs. wild-type
Fold-change HuD-/- vs. wild-type
Fold-change Lrrk2 G2019S : HuD-/- vs. wild-type
Fold-change Lrrk2 G2019S: HuD-/- vs. wild-type
Fold-change in IP nELAV (Lrrk2 G2019S vs. wild-type)

Supplementary Figure 2.3

mRNA expression in midbrain of *Lrrk2 G2019SxHuD*$^{-/-}$ and *HuD*$^{-/-}$ mice. Volcano plot of the Log2 fold-change in mRNA levels (x-axis) vs. the p-value of the fold-change in *Lrrk2 G2019S x HuD*$^{-/-}$ and *HuD*$^{-/-}$ mice.

2.6.1 Online Supplementary Tables

Impact of HuD and LRRK2 G2019S on RNA Levels (Tables 1-6)

Supplementary Table 1. All RNA Expression Data.

Supplementary Table 2. All RNAs Bound to Neuronal ELAVLs (>log2, FDR<0.01).

Supplementary Table 3. All RNAs Bound to Neuronal ELAVLs (>log2, FDR<0.01) and Differentially Regulated in *HuD*$^{-/-}$ vs. WT midbrain.

Supplementary Table 4. All RNAs Bound to Neuronal ELAVs (>log2, FDR<0.01) and Differentially Regulated in *LRRK2 G2019S x HuD*$^{-/-}$ vs. WT midbrain (FDR<0.05).

Supplementary Table 5. GO-Term analysis of All RNAs Bound to Neuronal ELAVLs (>log2, FDR<0.01) and Differentially Regulated in *HuD*$^{-/-}$ vs. WT midbrain (FDR<0.05).

Supplementary Table 6. GO-Term analysis of All RNAs Bound to Neuronal ELAVLs (>log2, FDR<0.01) and Differentially Regulated in *LRRK2 G2019S x HuD*$^{-/-}$ vs. WT midbrain (FDR<0.05).

Impact of HuD and LRRK2 G2019S on RNA Splicing (Tables 7-10)

Supplementary Table 7. All Splicing Data including exon identifications.

Supplementary Table 8. All RNAs Differentially Spliced in *HuD*$^{-/-}$ vs. WT midbrain (FDR<0.01).

Supplementary Table 9. GO-Term analysis of All RNAs Differentially Spliced in *HuD*$^{-/-}$ vs. WT midbrain (FDR<0.01).

2.7 Materials & Methods

Cell Culture and Treatments

Mouse neuroblastoma Neuro2A cells and human neuroblastoma SH-SY5Y cells were cultured in DMEM (Wisent) supplemented with 10% fetal bovine serum (FBS), 100U/mL penicillin and 100 µg/mL streptomycin at 37°C with 5% CO_2. Transient DNA transfection was performed 24 hours post-seeding in low-serum (2-5% FBS), antibiotic-free DMEM using Lipofectamine 2000 (Catalogue 11668-019, Thermo Fisher Scientific). FLAG/HA-HuD was expressed using the pFRT-DestFLAGHA_HuD plasmid (Addgene #65760); a gift from Thomas Tuschl (Rockefeller University, NY, USA), comparing to a control transfection with pcDNA3-EGFP plasmid (Addgene #13031) a gift from Doug Golenbock. Silencer® Select siRNAs (Thermo Fisher Scientific; Appendix - Table 1) were transfected at a concentration of 10nM using RNAiMax (Catalogue 13778150, Thermo Fisher Scientific). Co-transfection of DNA and siRNA was performed using Lipofectamine 2000 and cells were harvested for analyses 60-72h post-transfection. All siRNA sequences are available in Table 1.

For total protein collection, cells were washed twice in cold PBS, scraped, and incubated in lysis buffer [50mM Tris-HCl (pH 7.4), 75mM NaCl, 0.5mM EDTA, 0.5% Triton-X, 1X protease inhibitor cocktail (Catalogue 4693159001, Sigma Aldrich), 1X phosphatase inhibitor cocktail (Catalogue 4906837001, Sigma Aldrich)] at 4°C for 20 min with moderate tumbling. Lysates were centrifuged for 5000 x g for 10 min and supernatants were stored at -20°C. For total RNA collection, 1mL TRIzol reagent (Catalogue 15596-018, Thermo Fisher Scientific) was added directly to cells following two PBS washes. For experiments involving LRRK2 kinase inhibition, cells were treated with 1 µM of DMSO-dissolved LRRK2 inhibitor GSK2578215A (Catalogue

4629, Tocris), or 2 μM LRRK2 inhibitor HG-10-102-01 (Catalogue 438195, EMD Millipore) for 3 hours immediately before cell harvest. Control cells were simultaneously treated with equivalent amounts of DMSO vehicle.

Mice

C57BL/6 *HuD*$^{-/-}$ (Akamatsu et al., 2005)mice were previously generated by Hideyuki Okano (Keio University, Tokyo). Mice with the LRRK2 G2019S mutation knocked into the endogenous loci were a kind gift of Novartis (Herzig et al., 2011).Experimental mice were bred in two groups C57BL/6 *HuD*$^{+/-}$ x Lrrk2$^{+/+}$ were crossed with C57BL/6 HuD$^{+/-}$ x Lrrk2$^{+/+}$ to generate C57BL/6 HuD$^{-/-}$ x Lrrk2$^{+/+}$and C57BL/6 HuD$^{+/+}$ x Lrrk2$^{+/+}$. C57BL/6 HuD$^{+/-}$ x Lrrk2$^{G2019S/G2019S}$ were crossed with C57BL/6 HuD$^{+/-}$ x Lrrk2$^{G2019S/G2109S}$ to generate C57BL/6 HuD$^{-/-}$ x Lrrk2$^{G2019S/G2019S}$ and C57BL/6 HuD$^{+/+}$ x Lrrk2$^{G2019S/G2019S}$. Mice were randomized into cages at weaning.

Western Blotting

Cortex, ventral midbrain, dorsal midbrain and striatum tissues were harvested from mice at approximately 4 weeks of age. Tissues were flash frozen and stored at -80°C. For protein analysis, a fraction of each brain region was re-suspended in homogenization buffer [50mM Tris-HCl (pH 7.4), 140mM NaCl, 1% SDS, 1% Triton-X and 1X protease inhibitor cocktail] in 2.0mL tubes containing stainless steel beads. Tubes were placed in a MagNA lyser for two rounds of rapid oscillation at 7000rpm for 15 sec. Tissues were then incubated with gentle shaking at 4°C for 20 min and centrifuged twice at 10,000 x g for 10 min. Tissue lysates were stored at -80°C until further use.

Protein concentration was estimated using the Bradford Protein Assay (Catalogue 500-0122, Biorad). Lysates were diluted in Laemmli loading buffer [50mM Tris (pH 6.8), 2% SDS, 10% glycerol, 5% β-mercaptoethanol, 0.1M DTT] denatured at 99°C for 8-10 min and separated by 10% polyacrylamide gel electrophoresis (SDS-PAGE). Proteins were transferred to polyvinylidene fluoride (PVDF) membranes (Catalogue IPVH00010 , Fisher Scientific) and membranes were blocked in 5% milk for 1 hour at room temperature. All antibodies used are available in Table 2. Proteins were visualized using Luminata Crescendo Western HRP chemiluminescent substrate (Catalogue WBLUR0500, Fisher Scientific) to the membrane on an Image Quant LAS4010 Biomolecular Imager (GE Healthcare). Quantitative analyses on band intensity levels were performed using the Histogram function on Photoshop CS6 software with an area of fixed size. Mean band intensity was normalized to Tubulin or Actin levels.

Enzyme-Linked Immunosorbent Assay (ELISA)

Seventy-two hours after transfection cell culture media was centrifuged at 1500 x g for 10 min and supernatants were immediately used in the Quantikine Human BDNF Immunoassay (Catalogue DBD00, R&D Systems). Values of a media blank were subtracted before calculating BDNF concentration based on a standard curve.

Immunoprecipitation

For RNA immunoprecipitation, IP lysis buffer also contained 40units/mL of RNaseOUT Recombinant Ribonuclease Inhibitor (Catalogue 10777019, Thermo Fisher Scientific). To pre-clear cell lysates, 10uL of washed Dynabeads® Protein-G magnetic beads (Catalogue 10004D, Thermo Fisher Scientific) were added to each lysate and discarded 20 min later. To immunoprecipitate the protein-complexes, 2 µg of antibody to the protein of interest or 2 µg of

mouse IgG control antibody (eBioscience) was added to 800 µg-900 µg of protein lysate and incubated at 4°C for 2 hours. To capture the antibody-protein complexes, 20 µL of magnetic beads were washed and then added to each IP. After 1 h samples were washed (5 min) with increasing NaCl concentration for each wash (150mM, 175mM and 200mM). For RNA-protein immunoprecipitations, 10% of the beads were resuspended in 20uL IP lysis buffer and Laemmli buffer for western blot, while remaining beads were resuspended in TRIzol reagent.

Phosphorylation assay

GST-tagged mouse HuD or GST control proteins were a gift from Dr. Jocelyn Coté. Wild-type LRRK2, recombinant G2019S LRRK2 (aa. 970-2527) and recombinant D1994A LRRK2 (aa. 970-2527) human proteins were obtained from Thermo Fisher Scientific (A15197, PV4881 and PV6051). In vitro phosphorylation assays were carried out in a 25 µL volume by combining 1.5 µg of GST-HuD (or GST control) with 60 ng of wild-type, G2019S or D1994A LRRK2 in phosphorylation buffer (20mM HEPES (pH 7.5), 10mM $MgCl_2$, 1mM EGTA, 2mM DTT, 1% DMSO and 1X PhosSTOP™ phosphatase inhibitor cocktail). To initiate phosphorylation, 10µM ATP and 10µCi [γ-^{32}P]ATP (Catalogue BLU002A500UC, Perkin Elmer) was added to each tube and reactions were incubated at 30°C for 1hr. Reactions were performed in parallel but without [γ-^{32}P]ATP to confirm equal amounts of HuD and LRRK2 in each reaction by Western blot. Reactions were terminated by the addition of 1X Laemmli loading buffer and were subsequently boiled at 99°C for 5 min. Membranes were dried and exposed to autoradiography film for 24-72 hours before imaging.

Phos-Tag

Phos-Tag SDS-PAGE gels consisted of a 12% acrylamide resolving gel containing 50 μM Phos-tag Acrylamide (Catalogue AAL-107S1, Wacko) and 100 μM $ZnCl_2$. Gels were washed in transfer buffer with 10 mM EDTA (3 x 10 min) followed by one 10 min wash in transfer buffer without EDTA. Samples were transferred using Western blot protocol above.

Splicing RT-PCR

cDNA synthesis was performed using the iScript cDNA synthesis kit (Catalogue 170-8891, BioRad) and PCR using Taq DNA polymerase (Catalogue HTD0078, Biobasic). Primer sequences are available in Table 3. The cycling conditions were as follows: 95°C, 3min, [95°C for 30 sec, 55°C for 30 sec, 72°C for 30 sec] x 35 cycles, 72°C for 5 min. Samples were run on a 2% Agarose gel.

Protein identification by LC-MS/MS

Samples were prepared in a sterile work environment and separated on 4-20% Mini-PROTEAN TGX Pre-cast Protein Gels (Catalogue 165-3366, BioRad). Proteins were visualized using the PlusOne Silver Staining Kit (Catalogue, 17-1150-01, GE Healthcare Life Sciences), excised from gels and stored in 1% acetic acid. Proteins were digested in-gel using trypsin (Promega). Peptide extracts were concentrated by Vacufuge (Eppendorf). LC-MS/MS was performed using a Dionex Ultimate 3000 RLSC nano HPLC (Thermo Scientific) and Orbitrap Fusion Lumos mass spectrometer (Thermo Scientific) by the Ottawa Hospital Proteomics Core Facility. MASCOT software version 2.6 (Matrix Science, UK) was used to infer peptide and protein identities from the mass spectra. The observed spectra were matched against mouse sequences from SwissProt

(version 2016-09) and also against an in-house database of common contaminants. The results were exported to Scaffold PTM Viewer (Proteome Software, USA) for analysis.

RNA Extraction and RT-qPCR

Total RNA: from cells and tissues was extracted with TRIzol reagent following the manufacturer's instructions (Catalogue M0253L, Thermo Fisher Scientific). RNA was reverse transcribed using M-MuLV reverse transcriptase (New England Biolabs) supplemented with Oligo$(dT)_{18}$ and dNTP mix (Catalogue R0192, Thermo Fisher Scientific) following the manufacturer's protocol. qPCR reactions were carried out using GoTaq ® qPCR master mix (Catalogue A6002, Promega). Cycling conditions for all primer sets was as follows: 95°C for 2 min, (95°C for 15 sec, 60°C for 40 sec) x 40 cycles. All primer sequences are available in Table 3. Fold changes in mRNA levels were calculated using the ΔΔCt method. For SH-SY5Y experiments, mRNA levels were normalized to GAPDH and TBP mRNA, while in mice Actin was used for normalization.

Immunoprecipitated RNA : cDNA was prepared from 7 µL of RNA using iScript Reverse Transcription Supermix (Catalogue 1708840, BioRad) according to manufacturer's instructions. qPCR reactions were carried out using SsoAdvanced Universal SYBR Green Supermix (Catalogue 1725271, BioRad). Cycling conditions for all primer sets was as follows: 95°C for 3 min, (95°C for 10 sec, 60°C for 20 sec, 72°C for 20 sec) x 40 cycles. Technical replicates that produced undetectable Ct values or multiple/incorrect melt curve peaks were omitted from analysis. mRNA levels in HuD immunoprecipitations were normalized to levels in control IgG samples and expressed as fold change relative to the IgG. In experiments comparing mRNA enrichment in different conditions, mRNA quantities were normalize to the amount of HuD immunoprecipitated (using band intensity from western blots.)

Microarray

Total RNA and RNA extracted from HuD immunoprecipitates from the midbrains of 4 week old mice was sent to the Centre for Applied Genomics at Sick Kids Hospital (Toronto, Canada) for microarray analysis. For immunoprecipitated RNA, equal volumes of RNA was reversed transcribed into cDNA. For total cellular RNA, 8000 pg RNA was reverse transcribed into cDNA. All DNA was prepared using the Affymetrix GeneChip™ Whole Transcriptome (WT) Pico Kit (Thermo Fisher Scientific) and labelled with biotin allonamide triphosphate. Labelled target DNA was hybridized for 16-18h at 45°C to Clariom™ D Mouse Pico GeneChip™ (Thermo Fisher Scientific). GeneChip assays were scanned using an Affymetrix GeneChip Scanner 3000.

Bioinformatics analysis

Analysis of microarray data was performed using the Affymetrix Transcriptome Analysis suite v 4.0.1, and MTA 1.0 r3 annotations by Gareth Palidwor at the Ottawa Bioinformatics Core. Fold change analysis was performed using RMA-normalized (Robust Multi-array Average) conditions for both immunoprecipitated RNA and total RNA samples. The g:Profiler tool [https://biit.cs.ut.ee/gprofiler/] was used for gene ontology analysis (Reimand et al., 2016).

The density of nELAVL binding motifs in 3'UTRs was quantified by extracting the 3'UTR from all known mRNAs detected in the dataset. Then, the number of nELAVL binding motifs (UUU*UUU)(Ince-Dunn et al., 2012) was quantified per mRNA and normalized to the total 3'UTR length of the given mRNA. Analysis of single-nuclei RNA sequencing data (Kamath et al., 2022) was performed using the Broad Single Cell Portal.

Site-directed mutagenesis

The human FLAG-HA-HuD plasmid was used to create mutations in the sites corresponding to mouse T149 (Human T144). Mutations were created with primers in the Reagents section below. Primers were designed to anneal 'back-to-back' on opposing DNA strands in a non-overlap extension site-directed mutagenesis using Q5 High-fidelity DNA polymerase (Catalogue M0491L, New England Biolabs).

Gateway cloning and protein purification

Wild-type and mutant pFRT-DestFLAGHA-HuD plasmids were used to produce GST-HuD and GST-HuD-T149A bacterial expression plasmids using Gateway cloning. pENTR4-ELAVL2 (Addgene #65752) and pENTR4-ELAVL3 (Addgene #65752) were used as Entry plasmids for Gateway cloning to produce GST-HuB and GST-HuC, respectively. Plasmids were transformed in BL21 (DE3) competent E.coli. An overnight culture was diluted 1 in 100 in LB broth including ampicillin and protein expression was induced at OD_{600} 0.4 with 0.2 mM Isopropyl β-D-1-thiogalactopyranoside for four hours at 30 degrees Celsius. Bacterial culture was centrifuged at 10,000 x 30 min (4°C) and lysed with 1 mg/mL Lysozyme in resuspension buffer (50mM Tris, pH 8, 200 mM NaCl, 1mM EDTA, 1mM DTT, 1% Triton, 5% glycerol and protease inhibitor tablet). Lysate was sonicated and centrifuged at 12,000xg for 30 min. Supernatant was loaded on a Glutathione-agarose column and eluted with 10 mM reduced glutathione in resuspension buffer.

Behaviour and Motor Co-ordination Analysis

Behaviour analysis was completed in a dark light cycle to which mice were acclimated for 2 weeks prior to testing. Mice were acclimated to the test room for 30-60 min prior to testing. Mice were tested at 26 weeks of age. Mice were randomized into group cages at weaning based on randomized

numbered ear tags by independent personnel (MTT, AS) to enable blinded testing by ON and personnel of the University of Ottawa Behaviour Core Facility.

DigiGait

Mice were individually placed on the DigiGait belt with a speed of 18cm/sec at an 8-degree incline. Video data lasting at least three seconds was used in the analysis, averaging data for right and left limbs for each mouse. Analysis showed no significant difference between left and right limbs in any group.

Elevated Plus Maze (EPM)

Mice were tested on an Elevated Plus Maze apparatus composed of acrylic plastic material. The maze is constructed with a removable white floor, and two arms measuring 6 cm wide and 75 cm long. The arms are crossed perpendicularly and are open at the junction point. One arm is open and the other is enclosed by walls measuring 20 cm in height. The maze is raised 74 cm off the floor and is set in a room with overhead light intensity of 100 lux. During the test, mice are placed in the center of the maze and are permitted to explore freely for 10 minutes. Mouse behaviour is observed on a computer from outside of the testing room during the 10-minute test period.

Immunohistochemistry and Stereology

Mice were anesthetized with 5% isofluorane and transcardially perfused with PBS. The right side of the brain was immediately frozen in liquid nitrogen for analysis of proteins and RNA and the left side of the brain was taken for histology. Brains were fixed in 4% PFA overnight and

cryoprotected with 30% sucrose solution until the brains sank. Brains were frozen with isopentane and the substantia nigra was sectioned at 40 ìm using a cryostat.

Free-floating sections were washed with PBS, and endogenous peroxidases were blocked using 0.9% H2O2 in PBS for 10 min. Tissue was blocked in 10% normal goat serum for 30 minutes. Tissue was incubated in rabbit anti-Tyrosine Hydroxylase primary antibody (AB152, Abcam) at 1:5000 with 1% normal goat serum and 0.3% Triton-X at 4°C overnight. Tissue was incubated in goat biotinylated anti-rabbit secondary antibody at 1:225 (BA-1000 Vector Laboratories) with 0.3% Triton-X and 10% normal goat serum for 1.5 hours at room temperature. Signal amplification was achieved with an avidin-biotin complex kit (ABC kit PK-6100 Vectastain) for 1.5 hours at room temperature. Colour was developed with 0.2 mg/mL of 3'3-diaminobenzidine for 10 minutes. Unbiased stereological estimation was used to count TH+ cells of the substantia nigra in a genotype-blinded manner. Every sixth section of the substantia nigra was used for stereology. Stereological counts were obtained with Stereo Investigator software (MBF BIOSCIENCE).

Statistical Analysis

Statistical analysis was performed with GraphPad Prism. One sample t-tests were performed in cases comparing two independent groups of data. For data with more than two independent groups, a one-way ANOVA (analysis of variance) test was performed with a Tukey post-hoc test. Hypergeometric tests were performed to identify statistical significance in microarray experiments. Statistical significance was represented with the following notation: *$p<0.05$; **$p<0.01$, ***$p<0.001$, etc.

Acknowledgements

ON was funded by the Toth Family Fellowship (2017) and the Audrey Grant Scholarship (2018) from the Parkinson's Research Consortium (Ottawa). AP was funded by NSERC Graduate Student Scholarship. Research in the Gibbings and Park lab was funded by an award from the Canadian Institutes for Health Research. The authors thank Mirela Barclay and Christine Luckhart of the University of Ottawa Animal Behaviour Core Facility for performing behavioural testing. The authors thank Novartis for the kind gift of LRRK2 G2019S mice.

Conflicts of Interest

The authors declare they have no conflict of interest.

Table 2.7.1 siRNA sequences

Target gene	siRNA ID	Catalog #	Antisense sequence (5'-3')
Elavl4 (mouse)	s67974	4390771	AAAUUGUCCAGCCUGAAUCuu
LRRK2 (human)	s42413 s42415	4392420 4392420	UUCGGUUAUAAGGCACAGCct AGUUGUAAUAAUCGUUUCCgg
Negative control	N/A	4390847	N/A

Table 2.7.2 Antibodies

	Dilution	**Vendor**	**Catalogue #**
Primary			
α-synuclein	1:5000	Cell Signalling Technology	2628
α-Tubulin	1:20,000	Thermo Fisher Scientific	PA5-22060
β-Actin	1:10,000	Sigma	A5441-.2ML
BDNF	1:3000	Abcam	Ab205067
FLAG (M2)	1:5000	Sigma	F1804-IMG
HuD (H-9)	1:5000	Santa Cruz	sc48421
HuD	1:3000	Abcam	Ab96474
LRRK2 (MJFF2[c41-2])	1:1000	Abcam	Ab133474
LRRK2 PSer935 (UDD2-10(12))	1:1000	Abcam	Ab13340
P-Thr (H2)	1:1000	Santa Cruz	sc5267
Tyrosine Hydroxylase	1:5000	Abcam	AB152
Goat anti-rabbit biotinylated secondary	1:225	Vector Laboratories	BA-1000

Goat anti-mouse	1:5000	Jackson ImmunoResearch	115-035-174
Goat anti-rabbit	1:5000	Jackson ImmunoResearch	111-035-144
Isotype control (for immunoprecipitation)			
Mouse IgG1 K immunoglobulin	N/A	eBioscience	14-4714-82
Goat anti-rabbit	N/A	Jackson ImmunoResearch	111-035-144

Table 2.7.3 Primers

Target gene	Species	Sequence (5' – 3')		Application
Actb	Mouse	Fwd	AGATCAAGATCATTGCTCCTCCT	RT-qPCR
		Rev	ACGCAGCTCAGTAACAGTCC	
BDNF	Human	Fwd	GGCGGCAGACAAAAAGACTG	
		Rev	CACTGGGAGTTCCAATGCCT	
Bdnf	Mouse	Fwd	TGCGGATATTGCGAAGGGTT	
		Rev	ACCTGGTGGAACATTGTGGC	
ELAVL4	Human	Fwd	GCGTAAAGAGACTGATGTCTGGA	
		Rev	CACTCTCATCGGAATCGGGG	
Elavl4	Mouse	Fwd	GCTTGTATGTGTAGCGGTGC	
		Rev	TGGTGCTAATTATCATCTTCAAGCC	
ELAVL1	Human	Fwd	GGCGCAGAGATTCAGGTTCT	
		Rev	CCAAACGGCCCAAACATCTG	
GAP43	Human	Fwd	CAAACAGAATTAAAAGGGAACCTGG	
		Rev	TTAAGCAAGGGCTGAGGTGT	
GAPDH	Human	Fwd	ATCACCATCTTCCAGGAGCGA	
		Rev	TCTCCATGGTGGTGAAGACG	
Gapdh	Mouse	Fwd	CCCTTAAGAGGGATGCTGCC	
		Rev	TACGGCCAAATCCGTTCACA	
		Fwd	GCACAGCTAGGAAGCCTTAAA	

LRRK2	Human	Rev	GGAAGATTGATGTCCCAAACGG	
LRRK2	Mouse	Fwd	CTCACCCCCACTTCATGACC	
		Rev	GAAGAGGCACGAGCCTTGAT	
MAPT	Human	Fwd	TGACCCAAGAGCCTGAAAGT	
		Rev	TGTGTCCTCAGGTCCTGTCC	
SNCA	Human	Fwd	GCAACAGTGGCTGAGAAGAC	
		Rev	AATTCCTTCCTGTGGGGCTC	
Snca	Mouse	Fwd	ACCAGATGGGCAAGGGTGAG	
		Rev	GAACTGAGCACTTGTACGCC	
TBP	Human	Fwd	AGTGACCCAGCATCACTGTTT	
		Rev	CGCTGGAACTCGTCTCACTA	
Celf4	Mouse	Fwd	ACGCTGGAGTGCAGCAGTAT	RT-PCR
		Rev	GCCTCTTCATGCCTATCTGG	
HuD-T144A (mouse HuD T149A)		Fwd	GCCCAGAAGGAACTGGAGCAACTTTTCTCGCA	Site-directed mutagenesis
		Rev	CATGGTTTTGGGAAGGCCGCTAACATAGAGGT	
ELAVL4 - Sequence 1			GGAGTCTCTTCGGGAGCATTGG	DNA sequencing
ELAVL4 - Sequence 2			GTTAGCGGCCTTCCCAAAAC	

Chapter 3

Investigating the role of the RNA-binding protein HuR in LRRK2-dependent models of inflammation

3.1 Statement of contributions

James Taylor performed site-directed mutagenesis on HuR plasmids to generate HuR mutant sequences. Lrrk2 knockout CRISPR clones were a gift from Erwin Schurr Lab. Lrrk2 knockout MEFs were a gift from David Park lab. Kristofferson Tandoc performed RT-qPCR and mRNA decay assay in Fig 3.6 b,c. Rudolf Mueller performed histopathology on DSS gut tissues. Zhibin Ning of the uOttawa Proteomics Core performed mass spectrometry analysis. Kaela O'Connor ran the MiST program on mass spectrometry hits. Olanta Negeri designed and performed experiments. Derrick Gibbings designed experiments.

3.2 Introduction

Emerging evidence suggests that inflammation is a driving factor in PD pathology. Inflammation has been associated with neurodegenerative diseases through several mechanisms including via the "gut-brain axis," a mode of communication between the central nervous system and the gut (Houser & Tansey, 2017; Mulak & Bonaz, 2015). The bidirectional communication between the brain and the gut is mediated by the vagus nerve, which innervates the gastrointestinal tract to regulate functions such as digestion and immune responses (Bonaz et al., 2018). In the other direction, the gut microbiota communicate with the brain through the production of neuroactive metabolites stimulating the vagus nerve (Bonaz et al., 2018). It is also hypothesized that a disruption in the gut microbiome promoting intestinal inflammation can lead to an overproduction of proinflammatory cytokines in the periphery (H. Lee et al., 2017). The cytokines arising from sustained peripheral inflammation are hypothesized to cross the blood-brain barrier and "prime" the microglia. Microglia priming would result in exaggerated inflammatory responses leading to dopaminergic neuron death in Parkinson's disease (H. Lee et al., 2017; Su & Federoff, 2014). Braak's hypothesis posits that α-synuclein eventually spreads to the midbrain through the enteric nervous system (Braak et al., 2003), where α-synuclein pathology can be detected in the GI tract years before the onset of motor symptoms in PD patients (S.-J. Chen & Lin, 2022) . Further evidence for peripheral synuclein pathology comes from prodromal and clinical stage PD samples that indicate the accumulation of α-synuclein in the vermiform appendix, an organ with roles in pathogen control (Killinger et al., 2018). This gut-brain connection therefore acts as a link for inflammatory responses between the periphery and the brain.

Interestingly, one of the earliest symptoms described in PD patients is intestinal dysfunction such as constipation and inflammation of the bowel (Houser & Tansey, 2017). Biopsies of intestinal tissue from PD patients indicate elevated levels of proinflammatory cytokines such as Il-1β, IL-6, IFN-γ, and TNF-α (Lebouvier et al., 2010). These cytokines are also elevated in the brains and cerebrospinal fluid of PD patients, including asymptomatic *LRRK2-G2019S* carriers, suggesting that systemic inflammation is an important feature of the disease (Dzamko et al., 2016; Lebouvier et al., 2010; Mogi et al., 1994, 1996; Mount et al., 2007; Nagatsu et al., 2000).

Mutations in the *Leucine-rich-repeat kinase 2* (*LRRK2*) gene are associated with PD, Crohn's disease (CD), and Leprosy- three seemingly unrelated diseases (Russo et al., 2022). Crohn's is an inflammatory bowel disease causing chronic inflammation of the gastrointestinal tract (Baumgart & Sandborn, 2012), whereas Leprosy is caused by a *Mycobacterium leprae* infection (Fava et al., 2020). Inflammation is therefore the common feature between these distinct illnesses, suggesting that LRRK2 is implicated in the immune response. Interestingly, patients with inflammatory bowel disease such as Crohn's are ~30% more susceptible to developing PD (Peter et al.., 2018). In cells, elevated levels of *LRRK2* mRNA and protein have been reported in the immune cells of PD and CD patients (D. A. Cook et al., 2017). Furthermore, LRRK2 levels are increased in immune cells upon stimulation with pathogens, suggesting that LRRK2 participates in regulating inflammation (Hakimi et al., 2011).

In mice, overexpression of WT LRRK2 and LRRK2 G2019S in mice showed aggravated intestinal inflammation compared to wild-type mice in models of dextran sodium sulfate (DSS) induced colitis, suggesting that LRRK2 kinase activity potentiates an exacerbated inflammatory response

(Cabezudo et al., 2023; C. Lin et al., 2022; Takagawa et al., 2018). An earlier DSS study in *Lrrk2* knockout mice showed that loss of LRRK2 resulted in a more severe colitis phenotype (Liu et al., 2011); however, a more recent study reported an attenuated colitis response in mice lacking LRRK2 (Yan et al., 2022), supporting the findings that LRRK2 is associated with a proinflammatory response. The variable conclusions between studies may be partially explained by mouse housing conditions and differences in experimental design (e.g., DSS concentrations, length of study).

A major initiative in the LRRK2 field is identifying its phosphorylation substrates. Mechanisms implicating LRRK2 in inflammation include autophagy, phagocytosis, and cell signaling via pattern recognition receptors (Wallings et al., 2020). Many of these mechanisms are dependent on LRRK2 kinase activity, including through the phosphorylation of RAB proteins, WAVE2, RCAN1 (Atashrazm et al., 2019; Han et al., 2017; K. S. Kim et al., 2018), and potentially other undefined substrates.

An important regulator of inflammation is the RNA-binding protein HuR. HuR has been shown to directly bind and stabilize the mRNAs encoding key inflammatory factors including TNF- α, IL-6 and IFN- γ in macrophages (Chen et al., 2009; Dean et al., 2001). In humans, HuR is associated with inflammatory bowel disease (IBD), as it was found to be increased in the cytoplasm of intestinal epithelial cells isolated from patients with IBD (Lang et al., 2017). Most studies investigating HuR function in inflammation suggest that it promotes expression of proinflammatory cytokines (Srikantan & Gorospe, 2012). In contrast, overexpression of HuR in myeloid cells shows that it acts as a negative modulator of inflammation. HuR synergizes with

TIA-1, a translational inhibitor, to suppress translation of inflammatory regulators such as TNF-α, IL-6, IL-1, TGF- β1 (Katsanou et al., 2005a). The observed differences could be due to several factors such as different subtypes of immune cells as well as studies done in fibroblasts and cancer cells, and cell lines vs. primary cells. A compelling follow up study reported that loss of HuR in myeloid cells aggravates inflammation in LPS challenged mice (Yiakouvaki et al., 2012). Loss of HuR also sensitizes mice to an exaggerated colitis phenotype when treated with dextran sodium sulfate (DSS), corroborating the same lab's earlier findings that HuR tempers inflammation (Yiakouvaki et al., 2012).

We previously showed that LRRK2 phosphorylates the neuronal homologues of the ELAVL family of RNA-binding proteins to control their binding to mRNA targets (Chapter 2). The ELAVL family, including the ubiquitously expressed homologue HuR, share ~70% sequence homology (Okano & Darnell, 1997). Interestingly, HuR was among the identified targets phosphorylated by LRRK2 in a phosphoproteomic screen (Steger et al., 2016). Given the role of both LRRK2 and HuR in controlling immune responses, and its homology with the nELAVL proteins, we hypothesized that LRRK2 phosphorylates HuR to control inflammatory phenotypes relevant to Crohn's and Parkinson's.

3.3 Results

LRRK2 phosphorylates HuR *in vitro*

In our previous study, outlined in Chapter 2, we showed that LRRK2 phosphorylates the HuR homologues HuB, HuC and HuD in vitro and in the mouse brain. We therefore hypothesized that LRRK2 would phosphorylate HuR. To test this, we generated recombinant GST-HuR and incubated it with either the kinase dead mutant, LRRK2 D1994A, WT LRRK2 or overactive kinase mutant LRRK2 G2019S with γ-32P ATP. Recombinant GST was used as a negative control. As expected, HuR is not phosphorylated by the kinase dead mutant but is by WT LRRK2 and this is further phosphorylated by LRRK2 G2019S (Fig. 3.3.1 a).

Given the extent of homology among the ELAVL protein family, within, and across species (Fig. 3.3.1 b), we hypothesized that LRRK2 phosphorylates HuR at residues homologous to HuD. Using mass spectrometry, we identified T144 and T169 (T149 and T174 in mouse) as the LRRK2 target sites in HuD (mouse and *in vitro*). We therefore generated HuR mutants with threonine to alanine substitutions at the corresponding residues in HuR, T118 and T143. We found a non-significant decrease in phosphorylation with each mutant; however, phosphorylation was completely ablated with the double mutant, suggesting that T118 and T143 are the residues phosphorylated by LRRK2 (Fig. 3.3.1 c-e).

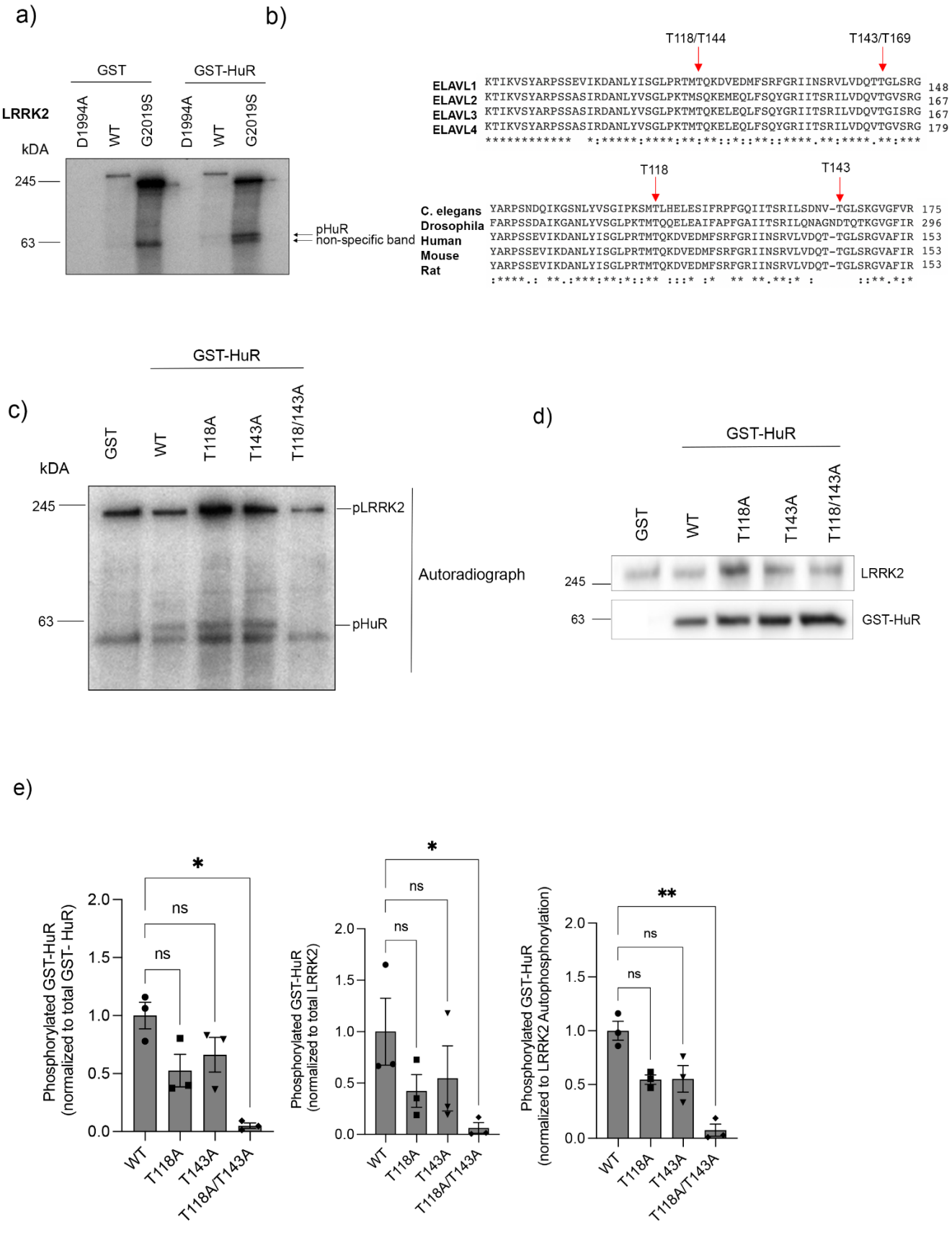
a)
GST
GST-HuR
LRRK2
D1994A
WT
G2019S
D1994A
WT
G2019S
kDA
245
63
pHuR
non-specific band
b)
T118/T144
T143/T169
ELAVL1 KTIKVSYARPSSEVIKDANLYISGLPRTMTQKDVEDMFSRFGRIINSRVLVDQTTGLSRG 148
ELAVL2 KTIKVSYARPSSASIRDANLYVSGLPKTMSQKEMEQLFSQYGRIITSRILVDQVTGVSRG 167
ELAVL3 KTIKVSYARPSSASIRDANLYVSGLPKTMTQKELEQLFSQYGRIITSRILVDQVTGISRG 167
ELAVL4 KTIKVSYARPSSASIRDANLYVSGLPKTMTQKELEQLFSQYGRIITSRILVDQVTGVSRG 179
T118
T143
C. elegans YARPSNDQIKGSNLYVSGIPKSMTLHELESIFRPFGQIITSRILSDNV-TGLSKGVGFVR 175
Drosophila FARPSSDAIKGANLYVSGLPKTMTQQELEAIFAPFGAIITSRILQNAGNDTQTKGVGFIR 296
Human YARPSSEVIKDANLYISGLPRTMTQKDVEDMFSRFGRIINSRVLVDQT-TGLSRGVAFIR 153
Mouse YARPSSEVIKDANLYISGLPRTMTQKDVEDMFSRFGRIINSRVLVDQT-TGLSRGVAFIR 153
Rat YARPSSEVIKDANLYISGLPRTMTQKDVEDMFSRFGRIINSRVLVDQT-TGLSRGVAFIR 153
c)
GST-HuR
GST
WT
T118A
T143A
T118/143A
kDA
245
63
pLRRK2
pHuR
Autoradiograph
d)
GST-HuR
GST
WT
T118A
T143A
T118/143A
245
63
LRRK2
GST-HuR
e)
Phosphorylated GST-HuR (normalized to total GST- HuR)
Phosphorylated GST-HuR (normalized to total LRRK2)
Phosphorylated GST-HuR (normalized to LRRK2 Autophosphorylation)
*
**
ns
2.0
1.5
1.0
0.5
0.0
WT
T118A
T143A
T118A/T143A

Figure 3.3.1 LRRK2 phosphorylates HuR at T118 and T143.

a) *In vitro* kinase assay with GST-HuR, incubated with LRRK2 D1994A or LRRK2 G2019S and γ-^{32}P ATP. b) Sequence alignment of ELAVL homologues in humans (top), Sequence alignment of ELAVL homologues across species highlighting conserved residues. (bottom) c) *In vitro* kinase assay with wild-type vs. mutant GST-HuR and recombinant LRRK2 incubated with γ-^{32}P ATP. d) Corresponding western blot for (c). e) Quantification of (c). Error bars represent mean ± SEM. n=3 Data were analyzed by Kruskal-Wallis followed by Dunn's test. n=3, * $p<0.05$, ** $p<0.01$, ***$p<0.001$, ****$p<0.0001$.

LRRK2 inhibits HuR binding to U-rich motifs

We previously showed that LRRK2 kinase activity controls nELAVL binding to target mRNAs. To test if LRRK2 phosphorylation directly controls HuR binding to canonical binding motifs, we employed gel shift assays. We first investigated if LRRK2 controls HuR binding to a validated AU-rich elements (ARE) derived from the 3'UTR of *Tnfa* mRNA, a well characterized target of HuR (Chae et al., 2009; Dean et al., 2001). GST and GST-HuR were incubated with LRRK2 D1994A or LRRK2 G2019S in a phosphorylation assay prior to incubation with the AU-rich, γ-^{32}P -labelled, RNA probe or scrambled control (Fig. 3.3.2 a). Background binding was detected to the negative control probe in lanes with HuR that is of similar length to the ARE probe and 58% composed of As and Us; however, less free probe is detected in *Tnfa* ARE lanes, suggesting increased ratio of bound/free RNA, and a degree of specificity for binding of HuR to the *Tnfa* ARE. The ELAVL proteins can multimerize along the length of the 3'UTR, including the *Tnfa* ARE (Dean et al., 2001; Ke et al., 2021a), which contains several AUUUA canonical binding motifs interspersed across the sequence. We observed multiple size-shifted RNA complexes, suggestive of HuR oligomerization on the *Tnfa* ARE, that became more apparent in the presence of more HuR (Fig. 3.3.2 b). LRRK2 did not affect binding of HuR or any of its putative multimer forms to the *Tnfa* ARE (Fig. 3.3.2 b,c). AU-rich elements are separated into three classes and are distinguished by AU or U-rich motifs present (Barreau, 2005). Class III, consisting of only U-rich motifs, were confirmed to be the dominant binding site for HuR in both CLIPseq and RNAcompete-S methods, where HuR was shown to preferentially bind a heptamer of Us (Cook et al. 2017). To test if LRRK2 controls binding to the poly-U motif, we designed a probe with tandem repeats of U-heptamers to allow for oligomerization, and to circumvent the need for a particular known HuR mRNA target (Fig. 3.3.3 a). In contrast to the *Tnfa* results, HuR binding to a U-rich

motif was significantly decreased by ~30% when phosphorylated by LRRK2, suggesting that LRRK2 could control HuR binding to a specific subset of RNAs (Fig. 3.3.3 b).

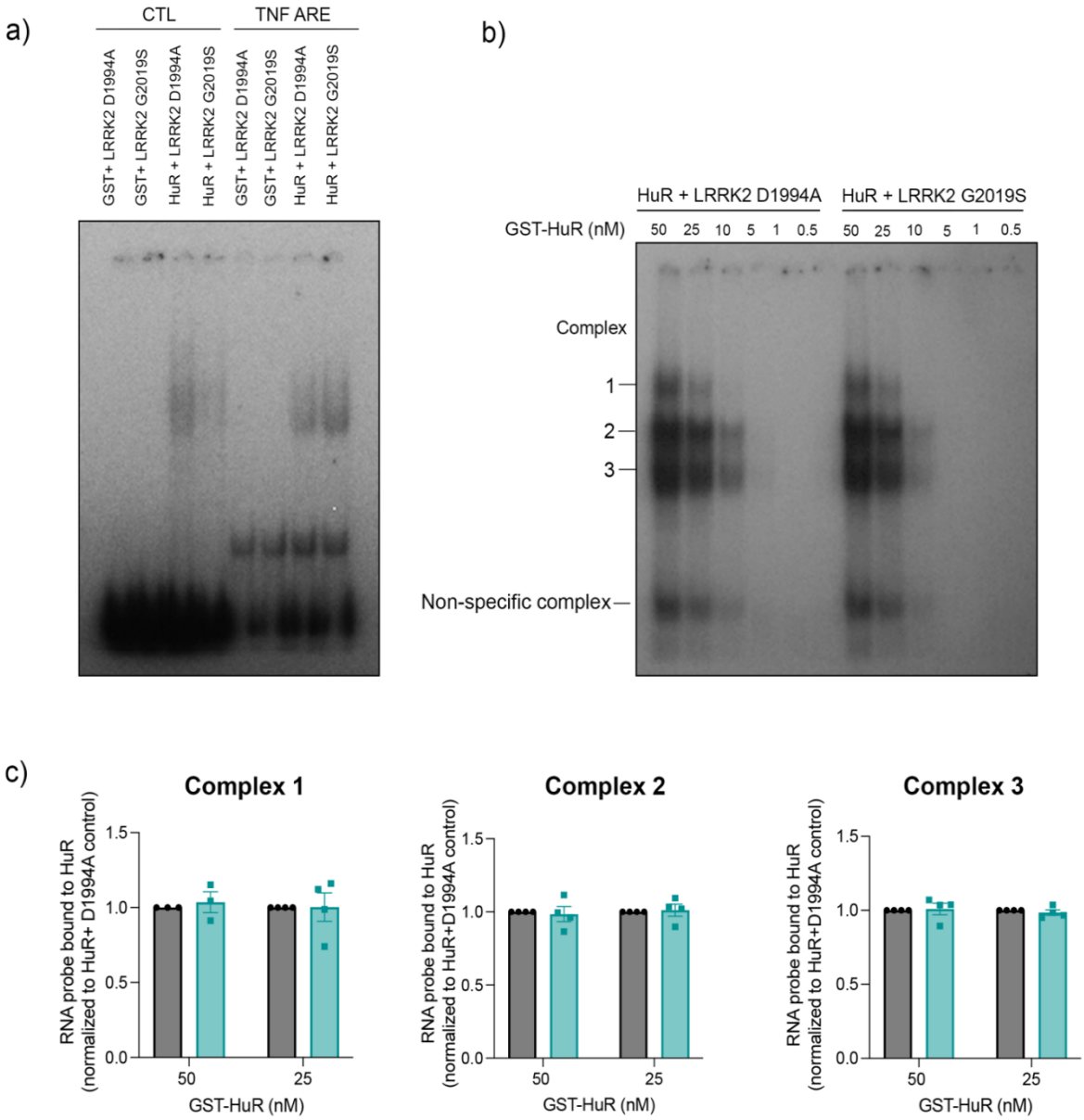

Figure 3.3.2 LRRK2 does not control HuR binding to AU-rich motifs.

a) Autoradiograph of gel shift assay. GST only or GST-HuR were incubated with LRRK2 D1994A or LRRK2 G2019S, and γ-^{32}P ATP- labelled scrambled RNA probe vs. probe with known HuR AU-rich binding site derived from *Tnfa* mRNA. b) Autoradiograph of gel shift with decreasing concentrations of GST-HuR (nM) with LRRK2 D1994A or LRRK2 G2019S recombinant proteins. c) Quantification of b. Error bars represent mean ± SEM. n=4. Data were analyzed by Two-way ANOVA followed by Holm-Sidak's. * $p<0.05$, ** $p<0.01$, ***$p<0.001$, ****$p<0.0001$.

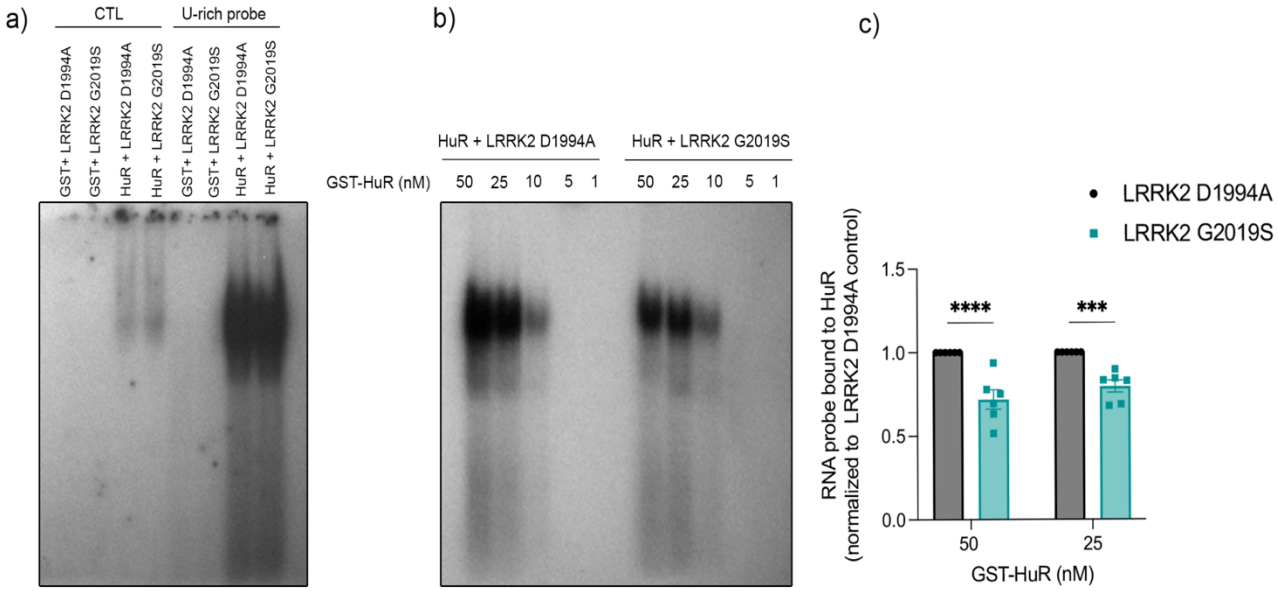

Figure 3.3.3 LRRK2 controls HuR binding to U-rich motifs.

a) Autoradiograph of gel shift assay. GST only or GST-HuR were incubated with LRRK2 D1994A or LRRK2 G2019S, and γ-^{32}P ATP- labelled scrambled RNA probe vs. probe with consecutive Us. b) Autoradiograph of gel shift with decreasing concentrations of GST-HuR (nM) with LRRK2 D1994A or LRRK2 G2019S recombinant proteins. c) Quantification of b. Error bars represent mean ± SEM. n=6. Data were analyzed by Two-way ANOVA followed by Holm-Sidak's. * $p<0.05$, ** $p<0.01$, ***$p<0.001$, ****$p<0.0001$.

We then asked if alanine substitutions resulting in phospho-dead mutants would increase binding to U-rich RNA. When incubated with the U-rich probe, we observed a slight increase in binding with the GST-HuR-T118A and GST-HuR-143A mutants, suggesting that loss of phosphorylation increases binding as in Fig 3.3.3, but this did not reach significance. Binding of the double mutant HuR T118A/T143A to U-rich RNA, in contrast, was significantly decreased suggesting that loss of both phosphorylation sites decreases RNA-binding properties (Fig. 3.3.4 a-c). Like the homologous sites in HuD, T118 and T143 are located on exposed loops within the second RNA-recognition motifs (RRM2) of HuR (Fig 3.3.4 d). RRM2 coordinates with RRM1 to undergo a conformational change that stabilizes HuR binding to target mRNA (Wang et al., 2013a). The double mutant, operating independently of phosphorylation, likely results in ablation of this conformational change and results in impaired binding, contrary to the expected increase in binding with loss of phosphorylation in accordance with Fig 3.3.3.

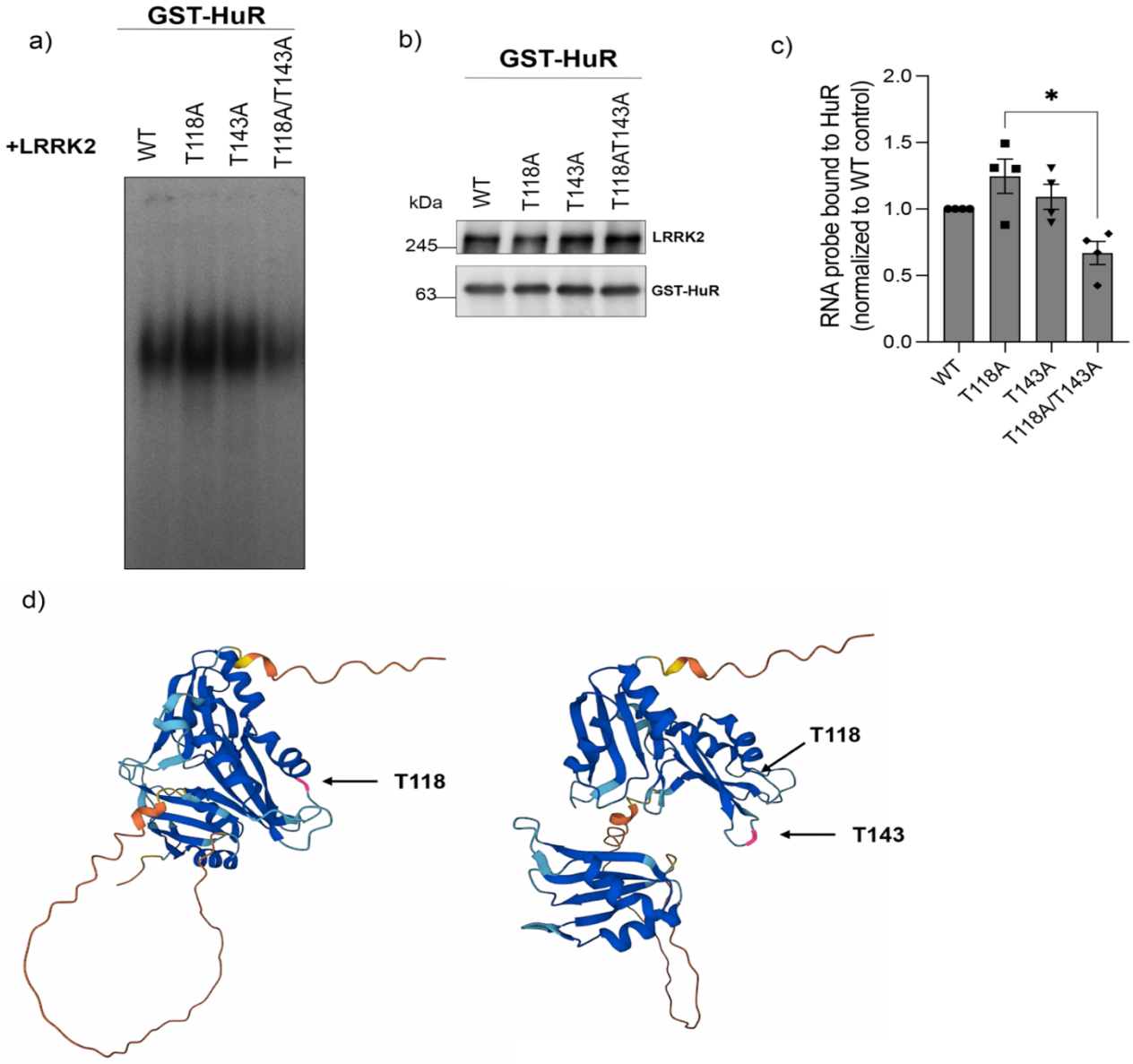

Figure 3.3.4 RRM2 mutations impact HuR binding to mRNA.

a) Autoradiograph of gel shift assay. GST only, WT GST-HuR or mutant GST-HuR were incubated with γ-^{32}P ATP- labelled U-rich RNA probe and WT LRRK2 b) Corresponding WB of (a) c) Quantification of (a). Error bars represent mean ± SEM. n=4. Data were analyzed by Two-way ANOVA, followed by Holm-Sidak's. * $p<0.05$, ** $p<0.01$, ***$p<0.001$, ****$p<0.0001$. d) Human HuR protein structure modeled using AlphaFold. Arrows are pointing to residues phosphorylated by LRRK2.

LRRK2 phosphorylates HuR in cells

While the above data shows that LRRK2 phosphorylates HuR *in vitro* and directly controls its binding to RNA, we sought to test if HuR is a physiological substrate of LRRK2. HuR was among the candidate proteins identified as a LRRK2 substrate in a phosphoproteomic screen from mouse embryonic fibroblast cells (MEFs) (Steger et al., 2016), thus we sought to confirm this in *Lrrk2*$^{-/-}$ MEFS.

To test this, we employed the PhosTag gel system to distinguish between phosphorylated and unphosphorylated species of endogenous HuR in MEFs derived from wild-type and *Lrrk2*$^{-/-}$ mice. We first confirmed that the cells are devoid of LRRK2 and express HuR (Fig. 3.3.5 a). HuR is phosphorylated by several kinases at various residues (Abdelmohsen et al., 2007; Lafarga et al., 2009; Reglero et al., 2020; Schulz et al., 2013), and as expected more than one phosphorylated form was detected as indicated by the presence of multiple bands (O'Donoghue & Smolenski, 2022). Band 1 was absent in MEFs lacking LRRK2, indicating that LRRK2 phosphorylates HuR in cells, in addition to recombinant proteins (Fig. 3.3.5 b,c).

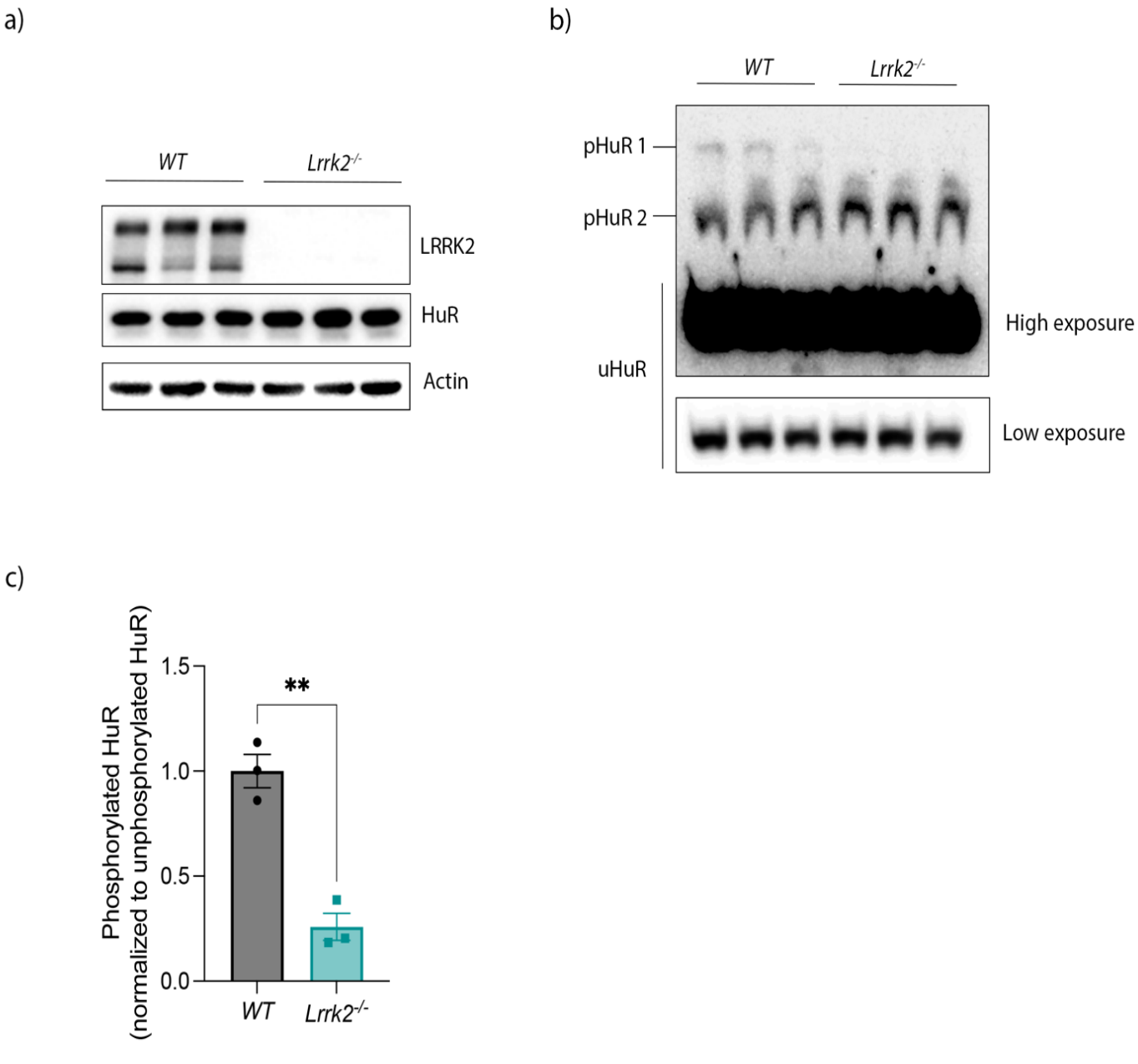

Figure 3.3.5 LRRK2 phosphorylates HuR in cells.

a) Phos-tag gel analysis of mouse embryonic fibroblasts (MEFs) derived from wild-type or *Lrrk2*$^{-/-}$ mice. Bottom panel is the lower exposure of unphosphorylated HuR on the same gel. b) Corresponding western blot of lysates used for Phos-tag gel. c) Quantification of (b). Error bars represent mean ± SEM. n=3. Data were analyzed by unpaired t-test using Welch's correction. * $p<0.05$, ** $p<0.01$, ***$p<0.001$, ****$p<0.0001$.

LRRK2 does not control cytokine response in LPS challenged cells

As HuR is primarily nuclear, and LRRK2 is cytoplasmic, the majority of HuR molecules are not amenable to LRRK2 phosphorylation under normal conditions. HuR shuttles to the cytoplasm under stress, including in response to proinflammatory stimuli (F.-Y. Lin et al. 2006; Zha et al. 2010; Dickson et al. 2012). Thus, it is possible that under situations of cell stress that LRRK2 would phosphorylate HuR to control relevant pathways. To test this, we moved into a model of inflammation where HuR was shown to shuttle to the cytoplasm in response to inflammatory stimuli, like lipopolysaccharide (LPS) (Zha et al., 2010), where it is more likely to interact with LRRK2, and be relevant to Crohn's and PD.

To test this, we first sought to establish a system in which a LRRK2 response to an inflammatory stimulus is elicited using RAW 264.7 mouse macrophage-like cells as a model system. More recent work investigating the role of LRRK2 in inflammation showed that LRRK2 was required for NF-kB activation and subsequent TNF-α release via Dectin-1 signalling in primary dendritic cells (Takagawa et al., 2018). We therefore tested if LRRK2 would control TNF-α release to Zymosan depleted (Zymosan D), an ultra-pure Dectin-1 ligand derived from yeast which is devoid of Toll-like receptor stimulating properties (Takagawa et al., 2018). We treated RAW 264.7 cells with 100 µg/mL Zymosan D for 24 hours and saw no difference in extracellular TNF-α levels. Data in the literature suggests that in RAW 264.7 cells, stimulation of Dectin-1 alone will not elicit a cytokine response and requires a crude extract that maintains TLR2/TLR4 stimulating properties (Walachowski et al., 2016). We then pre-treated cells with 1 ng/mL LPS overnight to stimulate TLR4 signaling, followed by Zymosan D for 2, 6, and 24 hours in parallel with Zymosan alone or LPS alone (Fig. 3.3.6 a). We found that TNF-α release was due to LPS alone, and no additive effect of Zymosan was observed. The dose of LPS-B5 used to prime the cells stimulates TLR4

only and would require a 100-fold increase to stimulate TLR2 and it is possible that the Dectin-1 signaling required both.

Several studies have reported conflicting results on LRRK2 effects on LPS-induced responses in models of neuroinflammation or peripheral inflammation (Lee, James, and Cowley et al., 2017); however, our preliminary findings showed a significant decrease in TNF-α release in *Lrrk2*$^{-/-}$ cells in response to LPS (Fig. 3.3.6 a) and was pursued for downstream experiments. While HuR is often described as a proinflammatory mediator, two compelling studies suggest that HuR suppresses inflammation (Katsanou et al.., 2005; Yiakouvaki et al.., 2012). Thus, we hypothesized that LRRK2 phosphorylates HuR and inhibits its function as a negative regulator of inflammation, which would result in less TNF-α production in *Lrrk2*$^{-/-}$ cells. Later attempts to recapitulate effects of LRRK2 on TNF-α release, total *Tnfa* mRNA levels, and mRNA stability tested by Actinomycin D assay failed to reproduce an effect of LRRK2 (Fig. 3.3.6 b-d). In all assays, TNF-α expression was significantly ($p<0.05$) elevated over baseline, suggesting that the lack of differences observed is not due to poor induction of TNF-α.

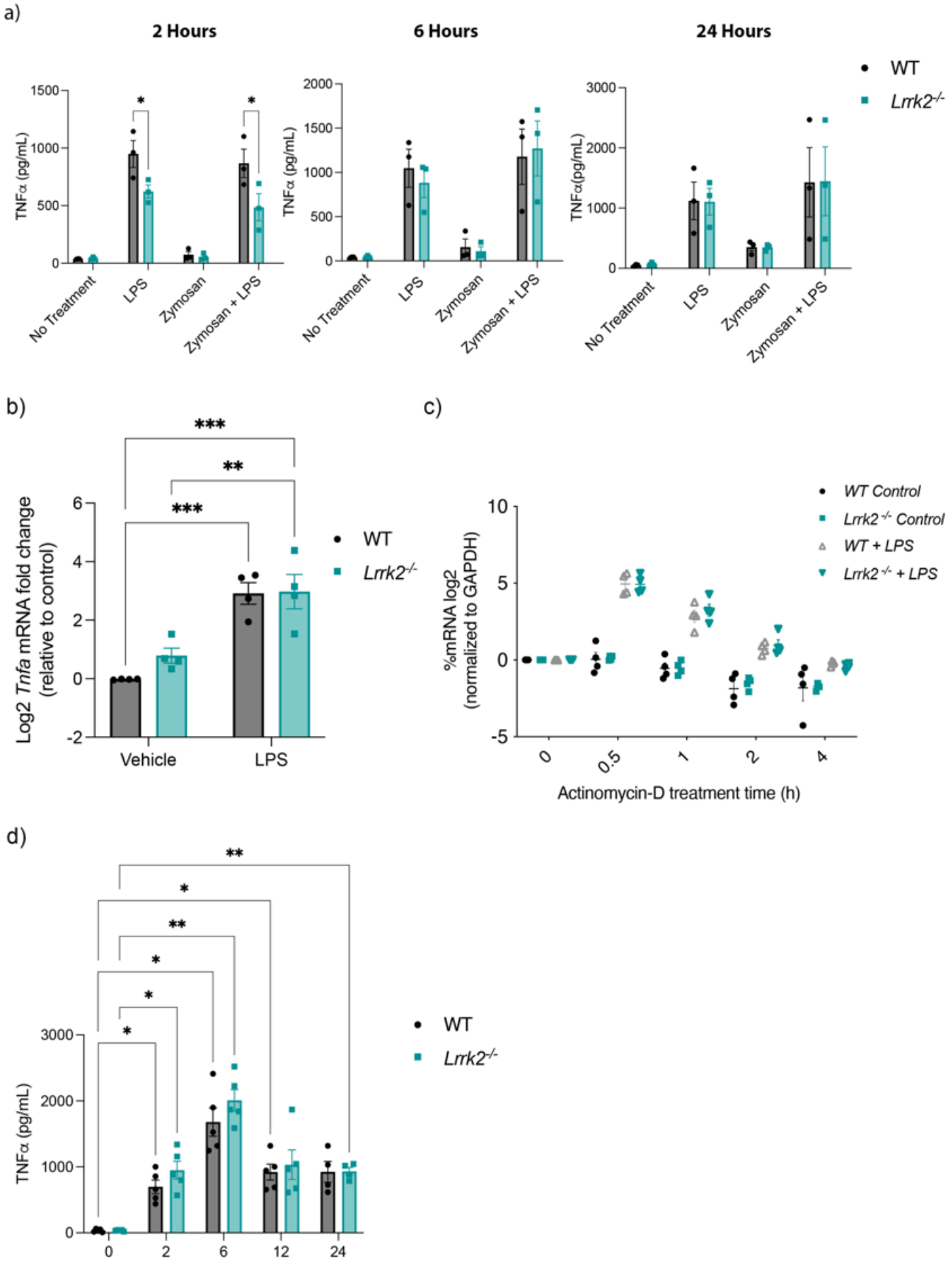
a)
2 Hours
6 Hours
24 Hours
TNFα (pg/mL)
TNFα(pg/mL)
WT
Lrrk2-/-
No Treatment
LPS
Zymosan
Zymosan + LPS
b)
Log2 Tnfa mRNA fold change (relative to control)
Vehicle
LPS
c)
WT Control
Lrrk2 -/- Control
WT + LPS
Lrrk2 -/- + LPS
%mRNA log2 (normalized to GAPDH)
Actinomycin-D treatment time (h)
d)
TNFα (pg/mL)

Figure 3.3.6 LRRK2 does not control LPS cytokine response in RAW cells.

a) RAW 264.7 cells were treated with 1 ng/mL LPS, 100 µg/mL Zymosan D, or primed with 1 ng/mL LPS (24h) followed by 100 µg/mL Zymosan D for the indicated times. n=3. Error bars represent mean ± SEM. Two-Way ANOVA followed by Holm-Sidak's b) RT-qPCR of *Tnfa* mRNA after 2 hours of LPS treatment. Data were analyzed by One-Way ANOVA followed by Holm-Sidak's c) RT-qPCR analysis of *Tnfa* mRNA decay assay. Cells were pre-treated with LPS followed by 5 µg /mL Actinomycin D and LPS for the duration of the experiment. d) TNF-α ELISA performed at 2,6,12, and 24 hours post-LPS treatment. Error bars represent mean ± SEM. n= 4. Data were analyzed by repeated measures Two-Way ANOVA followed by Holm-Sidak's. All data were derived from two wild -type and two *Lrrk2*$^{-/-}$ CRISPR clones. * $p<0.05$, ** $p<0.01$, ***$p<0.001$, ****$p<0.0001$.

To ensure that the opposite was not true, where LRRK2 controlled HuR to promote inflammation, we inhibited HuR function in wild-type vs. *Lrrk2*$^{-/-}$cells by employing the HuR-mRNA interaction inhibitor, CMLD-2 (Wu et al., 2015). Since this inhibitor has not been previously tested in RAW 264.7 cells, we selected a dose by measuring mRNA levels of known HuR targets inhibitors after 24 hours of treatment. We noted that 30 μM was the maximum dose that significantly decreased mRNA levels of HuR targets and did not result in excessive cell death (Supplementary Fig.3.1 a,b), which occurred at 50 μM. While significant cell death was observed at the selected dose, it was not exacerbated by LPS (Supplementary Fig.3.1 b), nor did it elicit an inflammatory response as measured by *Tnfa* levels in RAW cells (Fig.3.3.7 a). After treating wild-type and *Lrrk2*$^{-/-}$ cells with LPS and CMLD-2 we still did not observe a significant effect of LRRK2. This data also suggests that HuR is not acting as a positive regulator of *Tnfa* either. Together, this suggests that LRRK2 and HuR are not controlling *Tnfa* response under these experimental conditions.

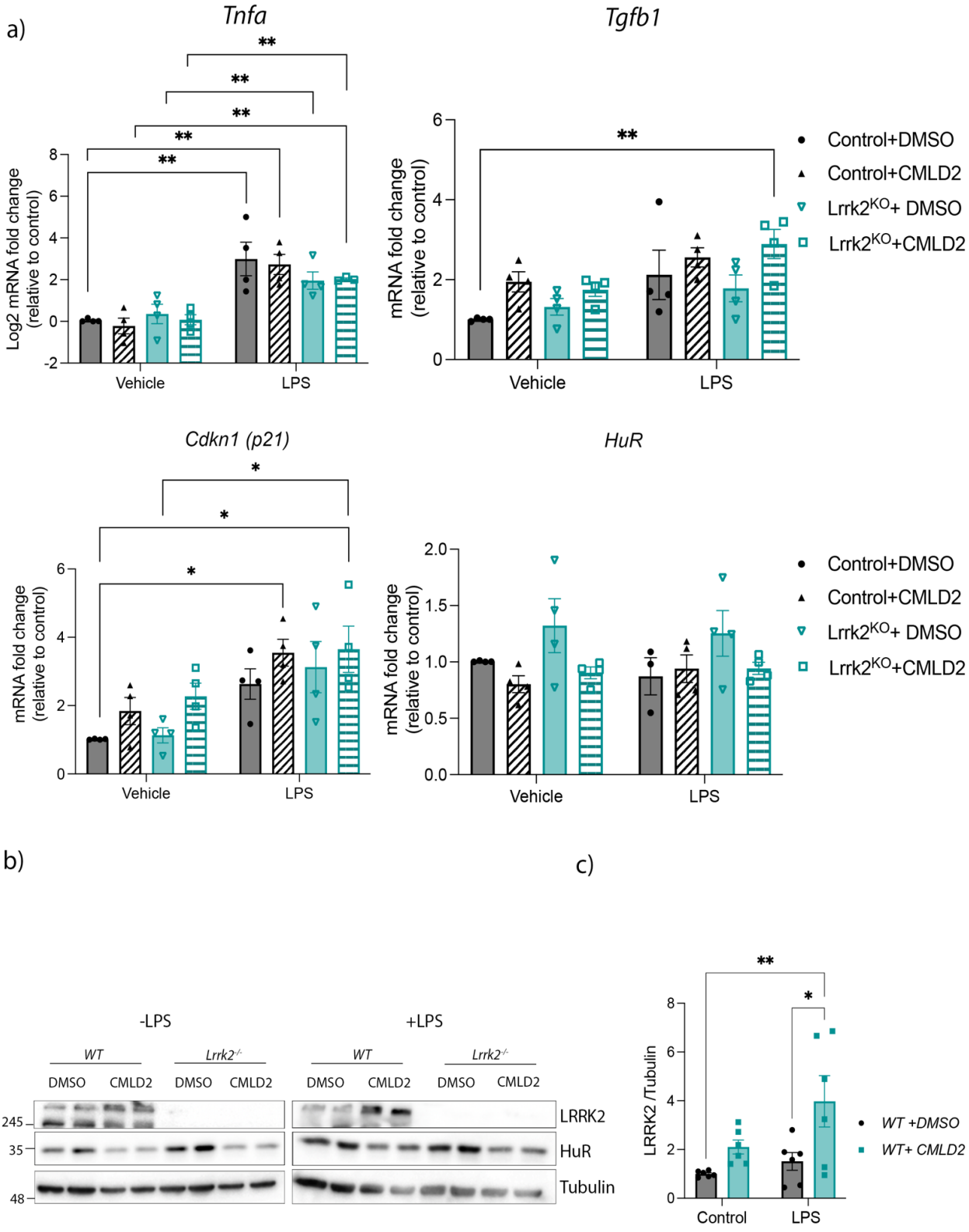
a)
Tnfa
Log2 mRNA fold change (relative to control)
Vehicle
LPS
Tgfb1
mRNA fold change (relative to control)
Control+DMSO
Control+CMLD2
Lrrk2KO+ DMSO
Lrrk2KO+CMLD2
Cdkn1 (p21)
HuR
b)
c)
-LPS
+LPS
WT
Lrrk2-/-
DMSO
CMLD2
245
35
48
LRRK2
HuR
Tubulin
LRRK2 /Tubulin
Control
LPS
WT +DMSO
WT+ CMLD2

Figure 3.3.7 HuR inhibition increases LRRK2 protein levels in LPS treated cells.

a) RAW 264.7 cells were pre-treated with the HuR inhibitor, CMLD-2 (30 μM), for 24 hours followed by LPS (1 ng/mL) for 2 hours prior to harvesting. a) RT-qPCR of known HuR mRNA targets following LPS treatment and 24-hour CMLD-2 (30 μM) treatment. Error bars represent mean ± SEM. n=4. Data were analyzed by Three-way ANOVA with Holm-Sidak's. * $p<0.05$, ** $p<0.01$, ***$p<0.001$, ****$p<0.0001$. b) Western blot of treated cells. c) Quantification of (b). Error bars represent mean ± SEM. n=6. Data were analyzed by Two-Way ANOVA with Holm-Sidak's post hoc. * $p<0.05$, ** $p<0.01$, ****$p<0.001$, ****$p<0.0001$.

Inhibiting HuR increases target mRNA levels in LPS treated cells

In support of other studies (Dzamko et al., 2012; Hakimi et al., 2011), our findings indicated that LRRK2 does not control cytokine responses in macrophage-like cells in response to the tested stimuli. We further investigated the effects of the HuR inhibitor on other targets of HuR with relevance to inflammation. *Tgfb1*, *p21*, and *HuR* all showed a significant effect of CMLD-2 treatment (Three-Way ANOVA, $p<0.01$ and 0.05, respectively) (Fig.3.3.7 a). *p21* and *Tgfb1* showed a significant effect of LPS treatment (Three- Way ANOVA, $p< 0.0001$, and 0.05, respectively) and were elevated nearly 3-fold in LPS treated cells. Both *p21* and *Tgfb1* have been linked to controlling macrophage polarization (Rackov et al., 2016; Zhang et al., 2016). Elevated levels of both targets shift macrophage cells from an M1, proinflammatory profile to an M2, anti-inflammatory profile. No significant differences were observed between wild-type and *Lrrk2*$^{-/-}$ cells, but both targets were only significantly upregulated over baseline in *Lrrk2*$^{-/-}$ cells. Interestingly, HuR has been linked to controlling macrophage polarization (Yiakouvaki et al., 2012). The overall significant effect of CMLD-2 treatment inhibiting HuR function on mRNA targets controlling polarization suggests that HuR could regulate this pathway and warrants further investigation.

We previously showed that loss of HuD increases LRRK2 protein levels in mice. To test if HuR also controls LRRK2 protein levels, we inhibited HuR in untreated vs. LPS treated RAW cells. Loss of HuR function resulted in a non-significant 2-fold increase in LRRK2 levels, and this was further increased by LPS treatment (Fig.3.3.7 b). Furthermore, the LPS effect was significantly different between wild-type and *Lrrk2*$^{-/-}$ cells, suggesting that HuR controls LRRK2 levels in response to proinflammatory stimuli.

HuR protein-protein interactions are mediated by LRRK2 kinase activity

The data above suggests that LRRK2 phosphorylates HuR, but this does not control cytokine expression in response to LPS treatment. Since LRRK2 did not significantly control HuR mRNA targets, we sought to test if LRRK2 controls its protein-protein interactions. HuR co-immunoprecipitations from LPS treated RAW 264.7 cells were analyzed by mass-spectrometry and candidate targets were assigned MiST scores, a composite score of target specificity, abundance, and reproducibility (Jäger et al., 2012). A MiST score >0.70 was considered a hit (Table 3.3.1). As expected, many proteins bound by HuR are known regulators of translation. Interestingly, in cells treated with the specific LRRK2 kinase inhibitor, MLi-2 (Fell et al., 2015), many of these candidate targets were associated with lower MiST scores, suggesting that LRRK2 promoted interactions with these proteins. Stress granule associated proteins, G3BP-1, G3BP-2, and Caprin-1 (Yang et al., 2020) were among the top targets in vehicle treated cells with lower MiST scores in MLi-2 treated cells, suggesting a possible role for LRRK2 and HuR in translational control during microbial infection. We confirmed HuR interaction with these proteins in U2OS cells overexpressing either G3BP-2 or Caprin-1 (Supplementary Fig.3.2), but this requires validation in LPS treated RAW cells with LRRK2 inhibition.

Table 3.3.1 HuR Mass Spectrometry Hits

HuR immunoprecipitation from RAW 264.7 cells pre-treated with 50 nM MLi2 or DMSO control. All samples were treated with 1 ng/mL LPS ± MLi-2 for 2 hours. Samples without MiST scores were left blank in the table. Targets associated with a MiST score above 0.7 in either DMSO or MLi2 treated IPs were included in the table.

Uniprot ID	Protein	Function	MiST Score			
			DMSO		MLi2	
			HuR IP	IgG	HuR IP	IgG
P97379-2	G3BP-2-G3BP Stress Granule Assembly Factor 2	Stress Granule Formation	0.89093		0.071	
P61514	RPL37A-60S ribosomal protein L37a	Translation	0.83972			0.03773
Q3TLH4-5	PRC2C-Proline Rich Coiled-Coil 2C	Stress Granule Formation	0.83923			
P42125	ECI1-Enoyl-CoA Delta Isomerase 1)	Lipid metabolism	0.83885			
O35286	Dhx15-DEAH-Box Helicase 15	RNA Helicase (Immunity)	0.83878	0.39972	0.61	0.60098

Q9D0M5	DYL2-Dynein light chain 2	Translation	0.83789			0.11102
Q6ZQ58	LARP1 La Ribonucleoprotein 1, Translational Regulator	Translation	0.83658			
P07091	S100-A4-Calcium Binding Protein A4	Motility, Differentiation, Apoptosis, Autophagy	0.83598	0.0196	0.024	0.25245
Q91WK2	EIF3H-Eukaryotic Translation Initiation Factor 3 subunit H	Translation	0.83213			
Q99PL5-6	RRBP1-Ribosome-binding protein 1	Protein Transport	0.83213			
Q60865	CAPR1-Caprin-1	Translation	0.8197	0.00883	0.284	0.00204
P67984	RPL22-60S ribosomal protein L22	Translation	0.80288	0.03568	0.071	0.25775
Q9CXY6	ILF2-Interleukin enhancer-binding factor	Transcription (T-cells)	0.7988		0.395	0.0363

P62082	RPS7-40S ribosomal protein S7	Translation	0.77962	0.23525	0.442	0.23584
P97855	G3BP-1-Stress Granule Assembly Factor	Stress Granule Formation	0.77206	0.00968	0.418	0.00202
Q9EPU0-2	UPF1- UPF1 RNA helicase and ATPase	RNA Helicase (NMD pathway)	0.7458		0.414	
Q02105	C1QC-Complement C1q	Serum Complement System	0.74405	0.25323	0.305	0.36938
P62911	RPL32-60S ribosomal protein L32	Translation	0.73957	0.2459	0.47	0.38518
P25444	RPS2-40S ribosomal protein S2	Translation	0.73641	0.18673	0.458	0.00818
P62908	RPS3-40S ribosomal protein S3	Translation	0.73322	0.22898	0.516	0.32606
Q91VM5	Rbmxl1-Retrogene of RNA binding	Splicing	0.73112	0.22851	0.438	0.30795

	motif protein, X-linked-like 1					
P97461	RPS5-40S ribosomal protein S5	Translation	0.72587	0.21943	0.524	0.33147
Q8K363	DDX18-DEAD-Box Helicase 18	RNA Helicase	0.71613	0.00807	0.536	0.03053
Q6ZWN5	RPS9-40S ribosomal protein S9	Translation	0.71571	0.17255	0.508	0.33266
Q9D0T1	NHP2-Nucleolar Protein Family A, Member 2	RNA Processing	0.71204	0.21143	0.415	0.21708
Q3TLE4	TAF15-TATA-box binding protein associated factor 15	Transcription	0.71157	0.2108	0.561	0.21013
P43274	H14-Histone H1.4	Nucleosome Structure	0.70806	0.22639	0.331	0.48191
P70372	HuR-Human antigen R	Translation, Cell proliferation, Inflammation	0.70484	0.15174	0.548	0.26584

P99027	RLA2-60S acidic ribosomal protein P2	Translation	0.70418	0.27276	0.485	0.36772
P62270	RPS18-40S ribosomal protein S18	Translation	0.70413	0.2317	0.501	0.35598
Q6A0A9	F120A-constitutive coactivator of PPAR-gamma-like protein 1	RNA Transport (Oxidative Stress)	0.7016		0.525	
Q6ZWV7	RL35-60S ribosomal protein L35	Translation	0.70022	0.25244	0.543	0.01685
Q9D8M4	RL7L-60S ribosomal protein L17-like 1	Translation	0.57035	0.01116	0.708	0.0146
Q9CPR4	RPL17-60S ribosomal protein L17	Translation	0.5603	0.01178	0.704	0.21077
Q00PI9	HNRL2-heterogeneous nuclear	RNA metabolism	0.52664		0.721	0.01067

	ribonucleoprotein U Like 2					
Q8VHM5	hnRNPR-heterogeneous nuclear ribonucleoprotein R	RNA metabolism	0.5067		0.749	0.0095
Q3UBP6	Uncharacterized-Actin Family	Cytoskeletal Organization	0.49899	0.12047	0.721	0.36147
Q9EQ61	PES1-Pescadillo Ribosomal Biogenesis Factor 1	Ribosome Assembly (PeBoW Complex)	0.46019		0.727	0.02599
Q9D0I8	MRTO4-mRNA turnover protein 4 homolog	Ribosome Assembly	0.43355	0.00978	0.71	0.02107
Q8BL97-3	SRSF7-Serine/arginine-rich splicing factor 7	Splicing	0.38435	0.18161	0.773	0.35377
P0DP28	CALM3-calmodulin-3	Calcium Binding	0.38397	0.00999	0.73	0.25385

P18760	COF1-Cofilin-1	Cytoskeletal Organization	0.383	0.01683	0.746	0.02469
P62849-2	RPS24-40S ribosomal protein S24	Translation	0.371		0.773	
Q9Z1N5	DX39B-DExD-Box Helicase 39B	RNA helicase (Splicing)	0.34936		0.82	
Q9CR47	NSA2- Ribosome biogenesis protein homolog	rRNA maturation	0.34906		0.797	
Q99JY9	Actr3-Actin related protein 3	Cytoskeletal Organization	0.32431		0.737	
Q91YU8	SSF1-Suppresor of SWI4 1 homolog	Cell growth	0.14417		0.784	
Q9CPT5	NOP16-Nucleolar protein 6	Nucleolar Protein 6	0.13559		0.793	
P51410	RPL9-60S ribosomal protein L9	Translation	0.12966		0.746	0.04192
Q9WV32	ARPC1B-Actin-related protein 1B	Cytoskeletal Organization	0.10725		0.784	0.04196
Q8BG05-2	hnRNPA3-heterogeneous	RNA Transport,	0.1063		0.792	0.03422

	nuclear ribonucleoprotein A3	Splicing (predicted)				
Q8C2Q3	RBM14-RNA Binding Protein 14	Splicing	0.03435		0.932	0.02613
P08752	GNAI2-G protein subunit alpha I2	GTPase Activity			0.75	0.07843

DSS-colitis is exacerbated by loss of LRRK2

A study investigating the role of HuR in a DSS-model of colitis reported a protective role of HuR in inflammation (Yiakouvaki et al., 2012). More specifically, mice with conditional knockout of HuR in myeloid cells developed a more severe colitis phenotype. This effect was rescued in HuR overexpressing mice, suggesting that HuR negatively regulates inflammation. Based on the study in LRRK2 transgenic mice and myeloid cell–specific HuR-deficient mice, we hypothesized that LRRK2 promotes colitis by inhibiting HuR function as a negative regulator of inflammation.

We tested a pilot cohort of male and female, WT vs *Lrrk2*$^{-/-}$ mice using dextran sodium sulfate (DSS) at 1.5% and 3.0% for one week to determine experimental conditions. We found that 1.5% DSS only induced a modest colitis phenotype, but at 3.0% the colitis phenotype was achieved as indicated by the ~20% decrease in body weight (Supplementary Fig. 3.3 a). To validate these findings, we ran a second cohort of DSS-treated mice. No significant differences were observed (Fig. 3.3.8 a); however, a trend in which *Lrrk2*$^{-/-}$ were slightly more resistant to weight loss was apparent in both cohorts. DSS-induced colitis has been previously reported to cause a more severe phenotype in male mice (Bábíčková et al., 2015). We observed this trend, but by day 8, only *Lrrk2*$^{-/-}$ mice showed a significant sex effect (Supplementary Fig. 3.3 b).

We therefore asked if there were differences in TNF-α levels in colon tissue from these mice. TNF-α levels were significantly increased in the colon homogenates of *Lrrk2*$^{-/-}$ mice, suggesting that there are observable differences in colitis severity between genotypes (Fig. 3.3.8 b). Since the involvement of HuR was previously described in a model of DSS-colitis, we asked if LRRK2 and HuR interact to control this response. In WT, untreated colon homogenates, LRRK2 was co-

immunoprecipitated with HuR (Fig. 3.3.8 c), indicating that the proteins interact under normal conditions. We then immunoprecipitated HuR from colon tissue of DSS treated mice, and quantified *Tnfa* mRNA, bound by HuR. *Tnfa*, but not the negative control *Gapdh*, was significantly enriched in HuR RNA-immunoprecipitations (R-IPs) over IgG controls (Fig. 3.3.8 d,e). *Tnfa* was not enriched in HuR R-IPs from *Lrrk2*$^{-/-}$ mice, suggesting that LRRK2 controls binding of HuR to *Tnfa* mRNA to control inflammatory responses in mice. These findings contradict the *in vitro* gel-shift assays where LRRK2 did not control HuR binding to the TNF ARE. It is possible that the presence of other factors like RNA-binding proteins mediate the LRRK2 effect *in vivo*.

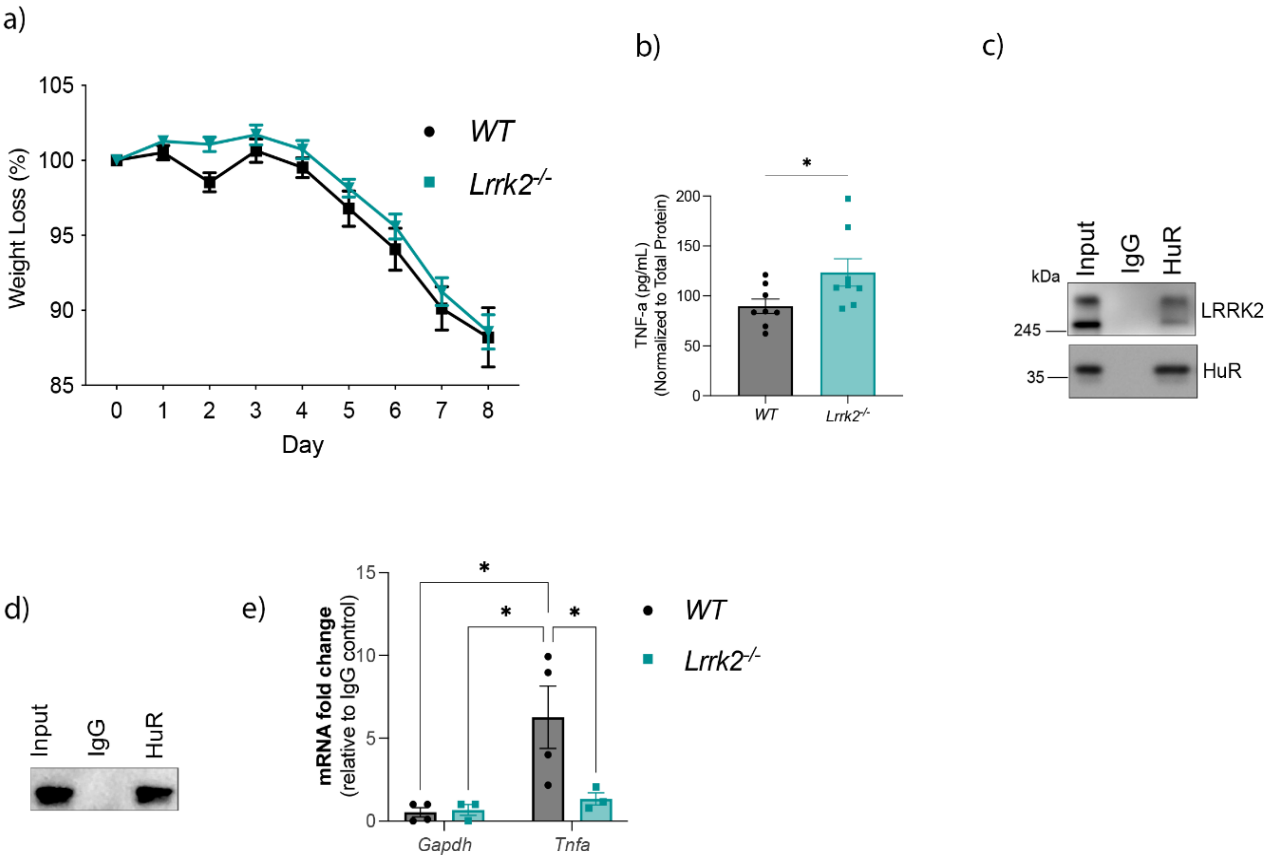

Figure 3.3.8 LRRK2 and HuR interact in mouse colon tissue.

Mice were treated with DSS in drinking water for 7 days and sacrificed on day 8. a) Animal weight in WT vs. *Lrrk2*$^{-/-}$ DSS-treated mice over the course of the study presented as a percentage of starting weight. n=6-11 b) TNF-α protein levels in colon lysates from WT vs. *Lrrk2*$^{-/-}$ DSS-treated mice. n=8 c) Co-immunoprecipitation of HuR and LRRK2 in colon lysates from WT, untreated mice. d) Western blot corresponding to RNA-immunoprecipitation of HuR in (e). e) RT-qPCR of *Tnfa* and *Gapdh* mRNA immunoprecipitated with HuR from WT vs. *Lrrk2*$^{-/-}$ DSS-treated mice. Error bars represent mean ± SEM. n= 3-4. Data were analyzed by Two-Way ANOVA with Holm-Sidak's. * $p<0.05$, ** $p<0.01$, ***$p<0.001$, ****$p<0.0001$.

We next asked if the effects on TNF-α control were reflected in histopathology. Colon sections from control and DSS animals were evaluated and scored for hallmarks of colitis pathology including edema, loss of goblet cells and infiltration of immune cells (Erben et al., 2014). Histopathology analysis indicated no genotype dependent differences in colon sections in water treated control mice. *Lrrk2*$^{-/-}$ DSS treated mice exhibited significantly more edema, loss of goblet cells and immune cell infiltration in both mucosae and muscularis tissues (Fig. 3.3.9 a,b), indicating more severe destruction of the epithelial barrier and subsequent inflammation. Furthermore, lesser described phenotypes described in IBD patients like vasculitis, dilated lymph, and pathology of the serosa ganglia were also observed in *Lrrk2*$^{-/-}$ mice, suggesting that gut motility may be altered (Britzen-Laurent et al., 2023; Kurowski et al., 2021; Lakhan & Kirchgessner, 2010; Sahin et al., 2018). Together, these findings suggest that loss of LRRK2 in DSS treated mice is associated with several markers of inflammation and pathology.

a)

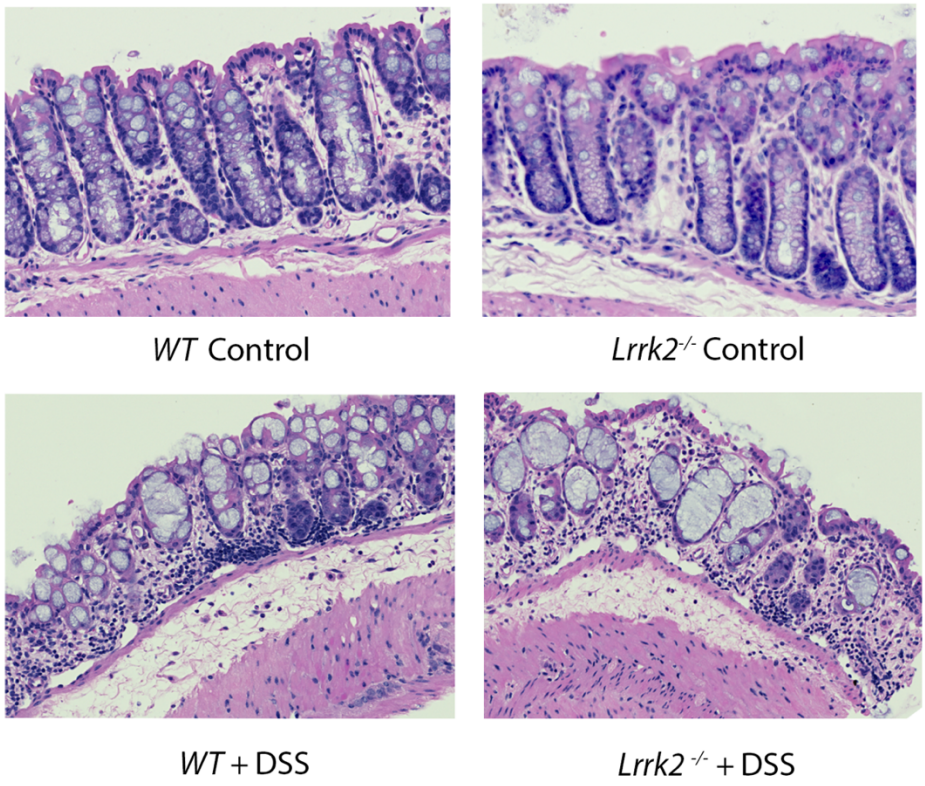
WT Control
Lrrk2-/- Control
WT + DSS
Lrrk2 -/- + DSS

b)

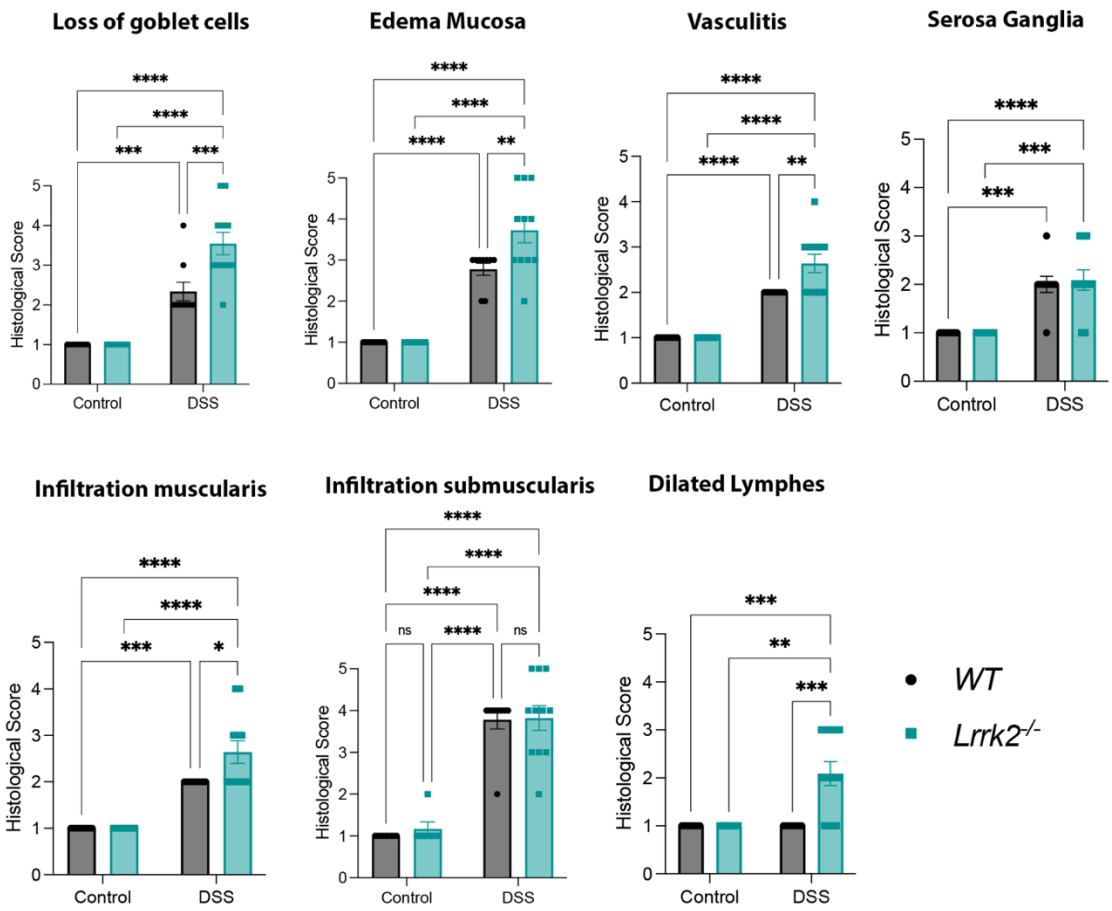
Loss of goblet cells
Edema Mucosa
Vasculitis
Serosa Ganglia
Infiltration muscularis
Infiltration submuscularis
Dilated Lymphes
Histological Score
Control
DSS
WT
Lrrk2-/-

Figure 3.3.9 Histopathology analysis of DSS colitis in WT vs. *Lrrk2*$^{-/-}$ mice.

Mice were treated with DSS in drinking water for 7 days and sacrificed on day 8. a) Representative images of colon tissue. b) Histopathology analysis of colon sections. Error bars represent mean ± SEM. n=6-11. Data were analyzed by Two-Way ANOVA followed by Holm-Sidak's post-hoc * $p<0.05$, ** $p<0.01$, ***$p<0.001$, ****$p<0.0001$.

LRRK2 phosphorylates HuR in spleen tissue

A commonly described feature of DSS-colitis is enlarged spleen, which is often correlated with disease severity (Chassaing et al., 2014), and is presumably caused by the proliferation of immune cells (Nunes et al. 2018). The spleen acts as a primary site for both innate and adaptive immunity, with roles in clearing the blood of old blood cells and pathogens (Mebius & Kraal, 2005). During DSS treatment, bacterial translocation from the gut to the spleen is observed, indicating a damaged epithelial barrier (Laukens et al.., 2014). A role for LRRK2 or HuR in the spleen during DSS-colitis has not been previously investigated; however, LRRK2 is highly expressed in peripheral tissues including the spleen and its mRNA and protein are increased in response to pathogens (Hakimi et al., 2011). To determine if LRRK2 and HuR might play a role in the spleen during DSS colitis, we performed PhosTag gel analysis. Interestingly, we observed a treatment effect in DSS treated animals on HuR phosphorylation, and this was significant in WT DSS-treated mice compared to controls (Fig. 3.3.10 a,b), suggesting that LRRK2 could phosphorylate HuR to control pathways in the spleen in response to intestinal inflammation. Multiple bands were detected (Fig. 3.3.10 a), indicating more than one phosphorylation site, but only one was controlled by LRRK2, suggesting the presence of other kinases phosphorylating HuR. No significant differences were observed in total HuR or LRRK2 levels, or LRRK2 kinase activity inferred by pSer935 levels (Fig. 3.3.10 c,d), suggesting that HuR phosphorylation was modified by DSS treatment. Given the role of LRRK2 in pathogen responses, it would be worthwhile to investigate this interaction further.

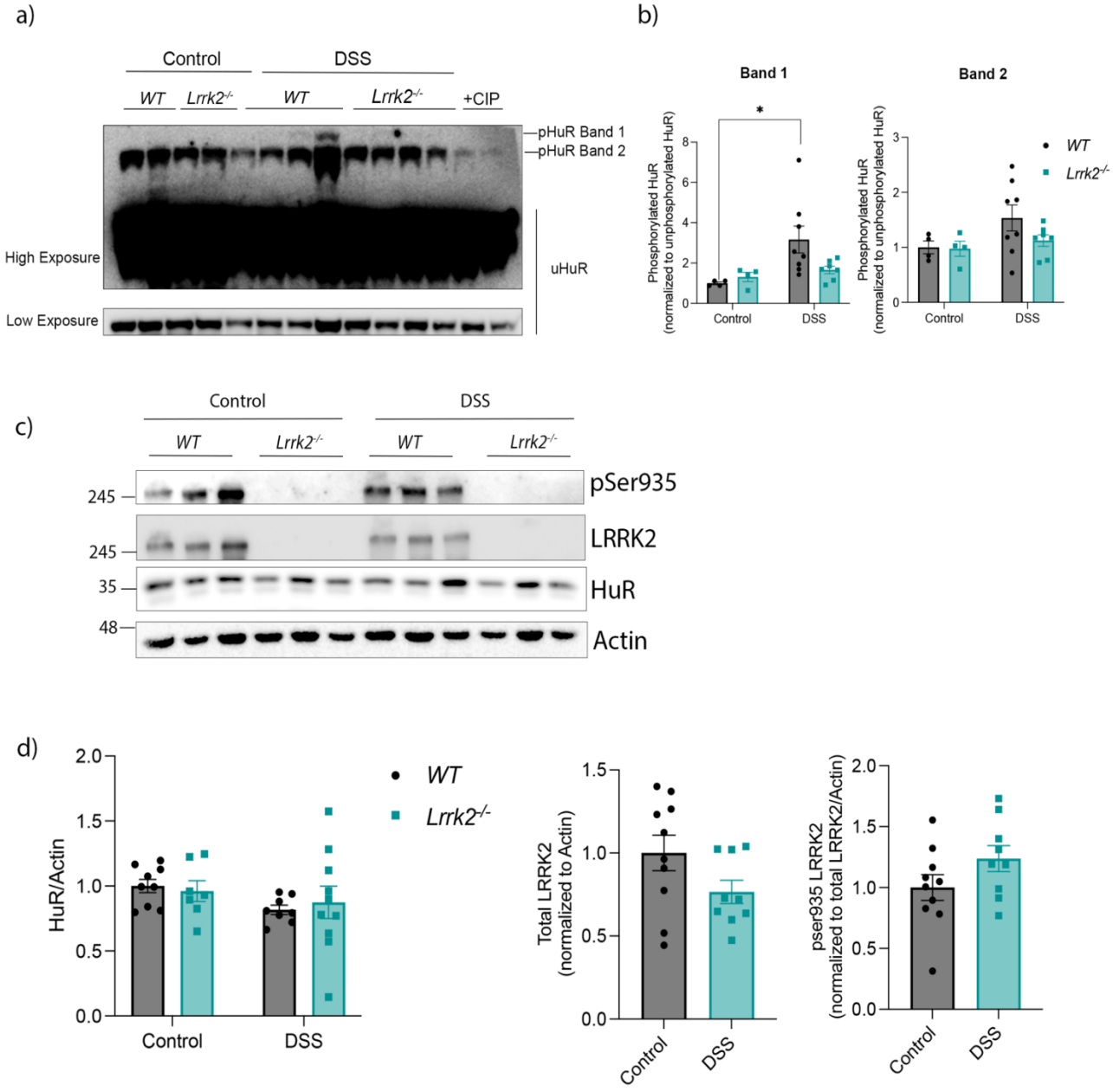

Figure 3.3.10 LRRK2 phosphorylates HuR in spleens of DSS-treated mice.

a) Phos-tag gel analysis of spleen tissue from control and DSS treated WT vs. *Lrrk2*$^{-/-}$mice. Error bars represent mean ± SEM. n=4-8. Data were analyzed by Two-Way ANOVA followed by Holm-Sidak's. * $p < 0.05$. b) Quantification of (a). c) Total protein blot of spleen tissue. d) Quantification of (c). Error bars represent mean ± SEM. n= 7-10. Data were analyzed by Two-Way ANOVA followed by Holm-Sidak's. * $p < 0.05$.

DSS increases α-synuclein in *Lrrk2*$^{-/-}$ brains

The data in Fig. 3.3.8-10 suggest that LRRK2 controls colitis-like phenotypes in mice by phosphorylating and controlling HuR binding to cytokine mRNA in the periphery. Given the growing evidence linking the gut-brain axis to pathology in IBD and PD, we asked if the peripheral inflammation induced by DSS might promote LRRK2-dependent neuroinflammation. We quantified the levels of proinflammatory cytokines *Il1b*, *Il6*, and *Tnfa* in the cortex, midbrain and striatum and found that in the cortex, there was a treatment effect of *Il1b* mRNA in DSS treated mice (Two-way ANOVA, $p<0.01$) suggesting trends towards minor neuroinflammation, but this was not controlled by LRRK2 (Fig. 3.3.11 a).

We also evaluated α-synuclein pathology in the brains of DSS-treated mice. While no effect was observed in *Snca* mRNA, we observed a subtle, but significant increase in α-synuclein protein levels in the cortex, but not the midbrain or striatum of *Lrrk2*$^{-/-}$ mice treated with DSS, suggesting a region-specific effect on translation or turnover (Fig. 3.3.11 b). Since cytokine mRNA levels were not significantly changed in the brains of WT vs. *Lrrk2*$^{-/-}$ mice, it is difficult to ascertain if the α-synuclein effect is promoted by neuroinflammation.

a)

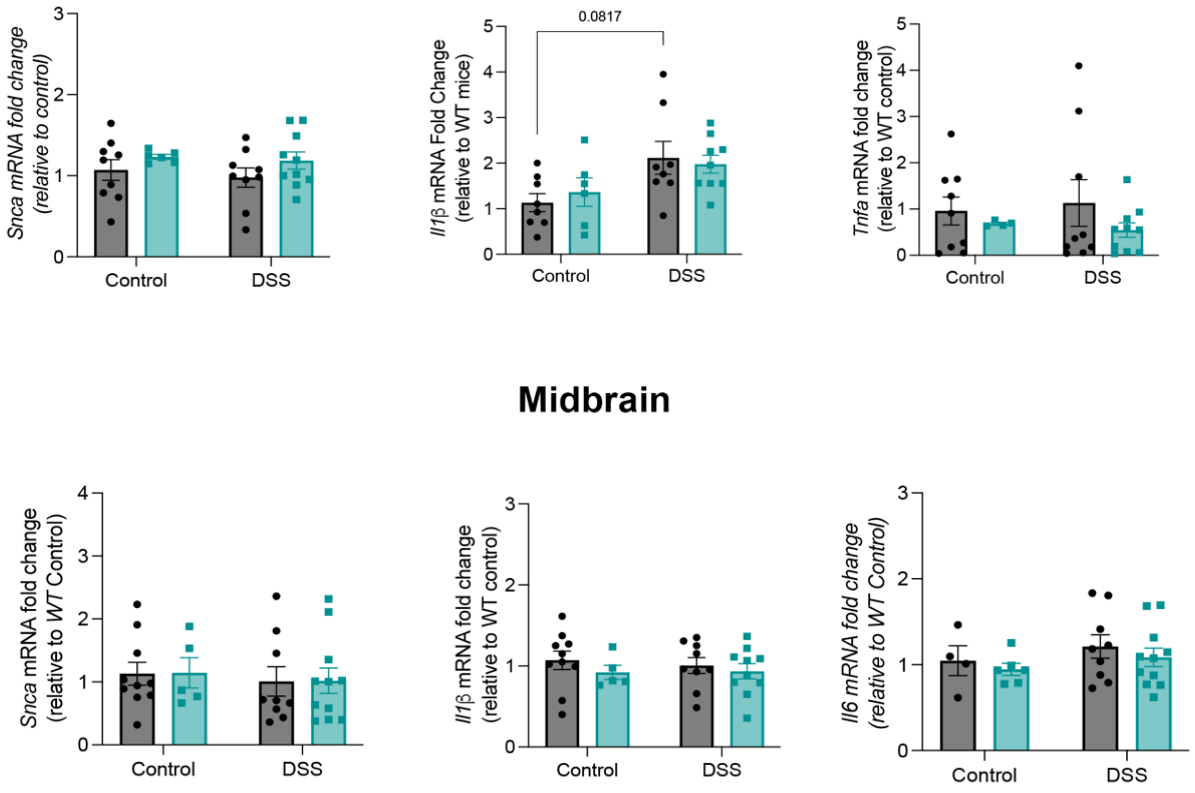
Cortex
Snca mRNA fold change (relative to control)
Il1β mRNA Fold Change (relative to WT mice)
0.0817
Tnfa mRNA fold change (relative to WT control)
Control
DSS
Midbrain
Snca mRNA fold change (relative to WT Control)
Il1β mRNA fold change (relative to WT control)
Il6 mRNA fold change (relative to WT Control)

b)

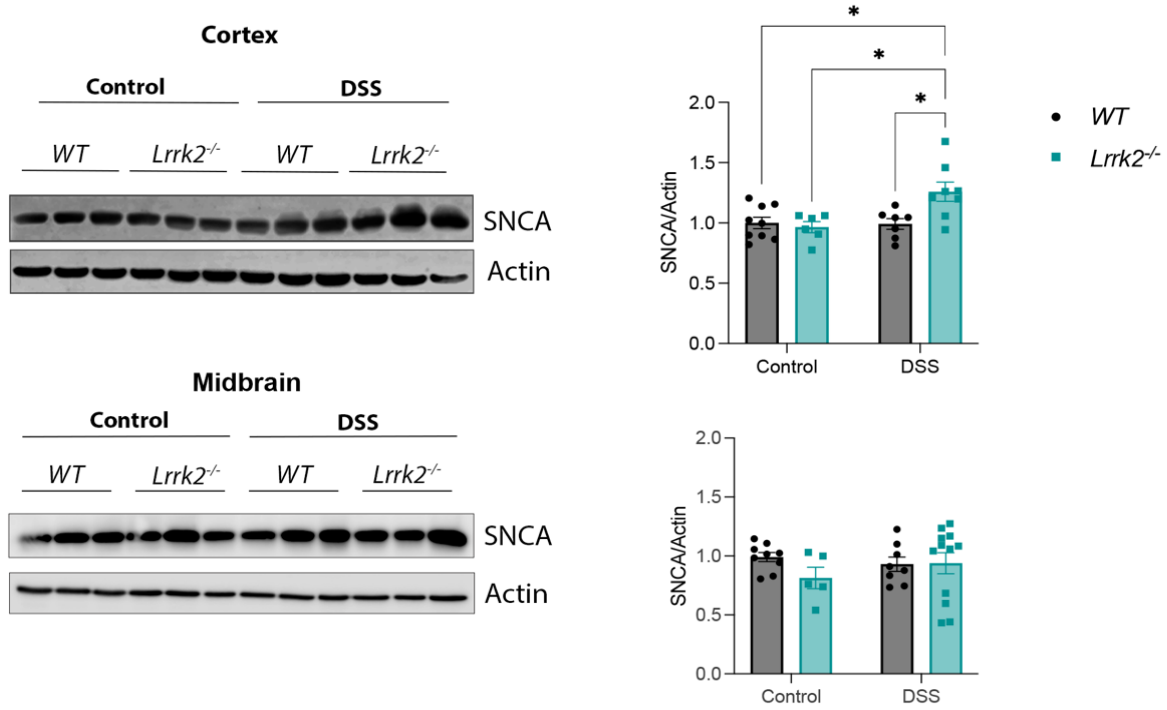
Cortex
Control
DSS
WT
Lrrk2-/-
SNCA
Actin
Midbrain
SNCA/Actin
WT
Lrrk2-/-

Figure 3.3.11 Alpha-Synuclein is increased in cortex of DSS-treated *Lrrk2*$^{-/-}$ mice.

a) Cytokine mRNA levels in brains of DSS treated mice. b) Western blot of α-synuclein in brains of DSS treated mice. Error bars represent mean ± SEM. n=4-11. Data were analyzed by Two-way ANOVA with Holm-Sidak's. * $p<0.05$, ** $p<0.01$, ***$p<0.001$, ****$p<0.0001$.

3.4 Discussion

We previously showed that LRRK2 phosphorylates the nELAVL proteins to control their binding to mRNA targets and this ultimately controlled RNA metabolism at both the level of splicing and post-transcriptional stability/translation. Here we show that LRRK2 phosphorylates and controls the ubiquitously expressed homologue, HuR at sites that are conserved in nELAVL (Fig. 3.3.1). *In vitro* experiments indicated that LRRK2 controlled HuR binding to a U-rich probe and had no significant effect on its binding to the TNF ARE (Fig.3.3.2- 3.3.4). Binding of HuR to the TNF ARE has been replicated in many contexts, as confirmed here, but several studies indicate that HuR shows greater affinity for U-rich sequences (Barker et al., 2012; Chae et al., 2009; K. B. Cook et al., 2017; H. S. Kim et al., 2011; Schulz et al., 2013), and U-rich motifs could be preferentially regulated by LRRK2 *in vitro*.

The identified phosphorylation sites, T118 and T143, lie within the second RNA recognition motif. *In vitro* studies show that RRM1 is the essential RNA-binding domain for HuR, and RRM2 increases affinity for its target mRNAs by inducing a conformational change to the protein structure in coordination with RRM1 (Wang et al., 2013b). The modest ~30% decrease in RNA-binding to the U-rich probe by HuR in the presence of LRRK2 may be explained by the fact that it is phosphorylated in the second RRM. In contrast, data from mouse colon tissue indicates that HuR binding to *Tnfa* mRNA was ablated in mice lacking *Lrrk2*. LRRK2 and HuR physically interacted by co-immunoprecipitation (Fig.3.3.8 c-e), suggesting that LRRK2 directly controls HuR binding to various species of mRNA *in vitro* and *in vivo* and can may have target-dependent effects.

The discordant data may be described by a few reasons. Firstly, the GST-tag used to improve solubility is not negligible at a molecular weight of 27 kDa and may impact HuR properties. Furthermore, *in vitro* experiments lack other factors controlling RNA-binding, including co-regulators or antagonizing factors. Studies have also shown that phosphorylation of specific residues can influence the binding preference of HuR for specific AU-rich or U-rich elements (Schulz et al., 2013). Finally, the various post-translational modifications on HuR may have broader control of HuR function *in vivo*, in addition to phosphorylation by LRRK2.

Data in cells indicated that LRRK2 did not control expression of HuR target mRNAs including *Tnfa*, *p21*, *Tgfb* or *HuR* itself. The lack of LRRK2 dependent response on TNF-α suggests that LRRK2 is dispensable for cytokine production of HuR targets in RAW cells treated with LPS (Fig 3.3.6-3.3.7). In agreement, human iPSC-derived monocytes and macrophages expressing the LRRK2 G2019S hyperactive kinase show significantly increased levels of proinflammatory cytokines in response to LPS treatment, but Lrrk2 knockout cells have no effect (Ahmadi Rastegar et al., 2022). Furthermore, no LRRK2-dependent effect on HuR target levels were detected when HuR was inhibited in cells treated with LPS for 2 hours (Fig 3.3.7 a). In myeloid cells, loss of HuR was dispensable for the initiation of inflammation but was required for its resolution (Yiakouvaki et al., 2012), thus it is possible that LRRK2 could control HuR responses and its targets at time points beyond 2-hours. In particular, targets like *Tgfb* are associated with chronic responses, and should be re-evaluated at later time points (Christodoulou-Vafeiadou et al., 2018).

We did not observe compelling effects of LRRK2 and HuR on gene expression in cells; however, data from LPS treated RAW cells revealed insights into HuR protein-protein interactions that are

mediated by LRRK2 (Table 3.3.1). When LRRK2 kinase activity was inhibited by MLi-2 treatment, many translation-associated proteins had lower MiST scores, suggesting weaker interactions with HuR. Of note, all cells were treated with LPS, thus it is possible that interactions impacted by LPS treatment were missed. Nevertheless, stress granule associated proteins including G3BP1-2, and Caprin-1 were associated with lower MiST scores in LRRK2 inhibited cells. Stress granules are membraneless cytoplasmic complexes formed in response to cellular stress and are partially comprised of RNA-binding proteins bound to translationally stalled mRNA transcripts (Li & Wang, 2023). Little is known about stress granule formation in response to non-viral microbial structures, however, evidence suggests that they do form in response to bacterial infection (Tweedie & Nissan, 2021), and may be triggered by the *E.coli*-derived LPS. Stress granule assembly requires at least one of G3BP1 or G3BP2 and includes other proteins like Caprin-1 (Li & Wang, 2023). HuR is among the RNA-binding proteins found within stress granules (Li & Wang, 2023) and may have a role in stress granules associated with bacterial infection.

Interestingly, HuR itself was among the targets that were bound by HuR in control cells (MiST >0.70) but associated with a lower score in LRRK2 inhibitor treated cells. ELAVL proteins interact to produce multimers along the 3'UTR of target mRNAs to exert their effects on mRNA stability and translation. A decrease in oligomerization inhibits their effects on protein production of bound targets (Kundu et al., 2012). The HuR linker domain and RRM3 were found to be essential for HuR oligomerization (Fialcowitz-White et al., 2007; Ke et al., 2021b; Toba & White, 2008), and LRRK2 phosphorylates HuR in RRM2, which impacts RNA-binding affinity (Wang et al., 2013b). It is possible that the effects of LRRK2 on protein-protein interactions are indirectly due to a

decrease in HuR-mRNA target interactions rather than a direct effect on oligomerization or protein complex formation.

Both LRRK2 and HuR have been ascribed various functions in controlling inflammatory responses. In myeloid cells, HuR plays a role as a negative regulator of inflammation, where it binds to *Tnfa* mRNA to suppress its translation (Katsanou et al., 2005b). Evidence from macrophage-like cells and mouse colon tissue supports this hypothesis. Firstly, its decreased association with *Tnfa* mRNA in *Lrrk2*$^{-/-}$ colon tissues coincided with increased TNF-α protein levels in DSS treated *Lrrk2*$^{-/-}$ mice (Fig 3.3.8 b,d,e). Secondly, inhibition of HuR resulted in increased LRRK2 protein levels in response to LPS in RAW 264.7 cells (Fig 3.3.7 b,c), and *LRRK2* expression is upregulated in response to proinflammatory stimuli (Gardet et al., 2010; Hakimi et al., 2011). In colitis models, however, the data on LRRK2 has been conflicting. The earliest study suggested that loss of LRRK2 results in the nuclear translocation of NFAT which then promotes transcription of proinflammatory cytokines, resulting in an exacerbated phenotype (Liu et al., 2011). In a later study, *Lrrk2* transgenic mice exhibited a worsened phenotype that was kinase dependent (Takagawa et al., 2018). More recent data also suggests that the hyperactive kinase mutant LRRK2 G2019S promotes an exacerbated phenotype, and loss of LRRK2 attenuates pathology (Cabezudo et al., 2023; C. Lin et al., 2022; Yan et al., 2022). Here we show that LRRK2 deficiency is associated with increased markers of inflammation at the molecular level and tissue level (Fig 3.3.8-9), in agreement with Liu et al. 2011. The disparate data are difficult to reconcile as all the studies varied in experimental design. For example, the DSS administered varied from 2-3% (w/v), the length of consecutive treatment days and recovery days prior to tissue harvest were variable, and both acute and chronic models were evaluated.

Most of the literature has focused on its pathogenic functions, but accumulating evidence from bacterial and viral infections indicate that LRRK2 is protective in certain contexts. For example, *Salmonella typhimurium* induced sepsis showed that infection was poorly controlled in *Lrrk2*-deficient mice, and myeloid cell expression of the G2019S mutant conferred increased pathogen clearance and survival (Shutinoski et al., 2019). Furthermore, mice lacking *Lrrk2* showed increased susceptibility to an enteric infection of *Listeria monocytogenes* as evidenced by an increased bacterial load in the liver and feces, with similar trends in the spleen (Q. Zhang et al., 2015). Interestingly, the gut-spleen axis has been modeled in DSS treated mice in which splenectomy mice exhibited an exacerbated colitis response, and bacteremia due to loss of pathogen control (Q. Zhang et al., 2015). Endotoxemia is also reported in patients with inflammatory bowel disease, highlighting the systemic consequences of poor pathogen control in the gut (Gardiner et al., 1995). Given the growing evidence for the role of LRRK2 in microbial infections, and the crosstalk between the spleen and the gut during infection, we asked if LRRK2 could phosphorylate HuR in the spleen. The Phos-tag gel of spleen lysates showed multiple bands of phosphorylated HuR (Fig 3.3.10). Phosphorylation of HuR has been shown to be regulated by kinases like p38, CHK2, and PKC, including at T118 in response to various stimuli (Abdelmohsen et al., 2007; Lafarga et al., 2009). We observed a significant increase in HuR in WT DSS treated mice, and a partial decrease in phosphorylated HuR in *Lrrk2*-deficient mice, suggesting that other kinases simultaneously regulate HuR in the spleen. These findings indicate that it would be worthwhile to investigate if LRRK2 and HuR coordinate inflammatory responses in the spleen.

With respect to the PD gut-brain axis model, we evaluated markers of neuroinflammation and synuclein pathology. Surprisingly, we found significantly increased levels of α -synuclein protein in the cortex of *Lrrk2*$^{-/-}$ mice in response to acute, systemic inflammation induced by DSS

(Fig.3.3.11 b). We also noted no significant increase in proinflammatory cytokine mRNA between genotypes; however, we did observe a significant treatment effect on *Il1b* mRNA in the brains of DSS treated mice (Fig.3.3.11 a). The equal cytokine mRNA expression between genotypes suggests that localized synthesis of proinflammatory cytokines is not the cause of synuclein accumulation. For example, it is possible that circulating cytokines from the periphery elicited this response. Evidence suggests that synuclein accumulation begins in the gut and spreads to the brain via the vagus nerve, and this has been confirmed by vagotomy in mouse models of synuclein pathology (S. Kim et al., 2019). A recent study found that a chronic mild DSS-induced colitis in *Lrrk2 G2019S* mice resulted in increased colonic synuclein levels though it was not reported if there were any effects in the brain, whereas another reported dopaminergic neuron death (Cabezudo et al., 2023; C. Lin et al., 2022), confirming that LRRK2 can control gut-brain inflammation. Further investigation is required to delineate the exact role for HuR in these LRRK2 associated phenotypes described, but the data from this study suggests that LRRK2 and HuR interact to regulate inflammatory responses in cells and in mice.

3.5 Supplementary Data

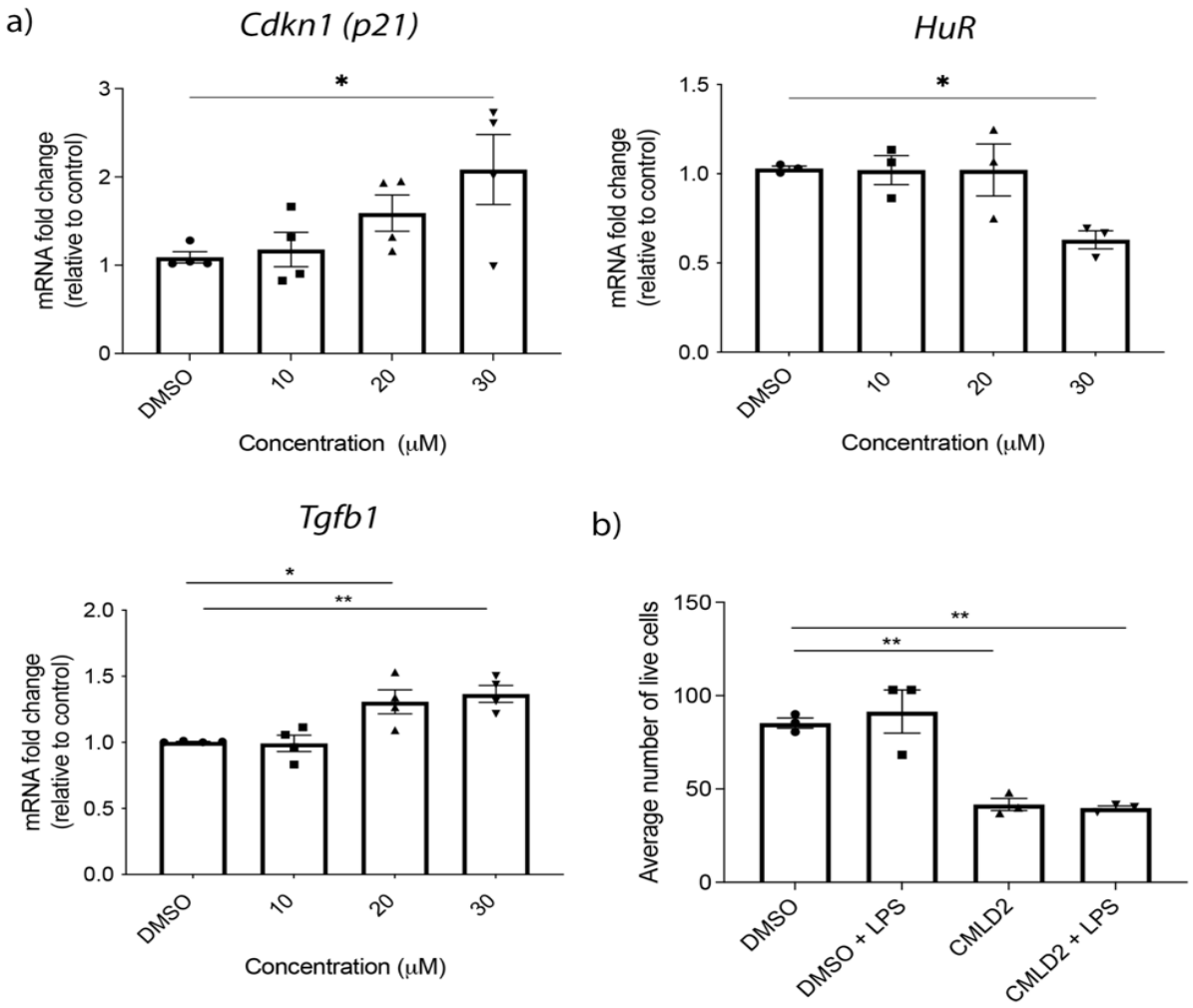

Supplementary Figure 3.1 Validation of CMLD-2 inhibitor.

a) RT-qPCR of HuR mRNA targets following 24 hours of treatment with 10-30 μM inhibitor vs. DMSO control. b) Quantification of live cells following co-treatment with CMLD-2 and LPS for 24 hours. Live cells were evaluated using Trypan blue. Error bars represent mean ± SEM. n= 3-4. Data were analyzed by One-Way ANOVA followed by Holm-Sidak's. * $p<0.05$, ** $p<0.01$, ***$p<0.001$, ***$p<0.0001$

Supplementary Figure 3.2. HuR interacts with G3BP2 and Caprin-1

a) Co- immunoprecipitation of G3BP2 from U2OS cells overexpressing GFP-G3BP2 and HuR

b) Co-immunoprecipitation of Caprin-1 from U2OS cells overexpressing GFP-Caprin-1 and HuR.

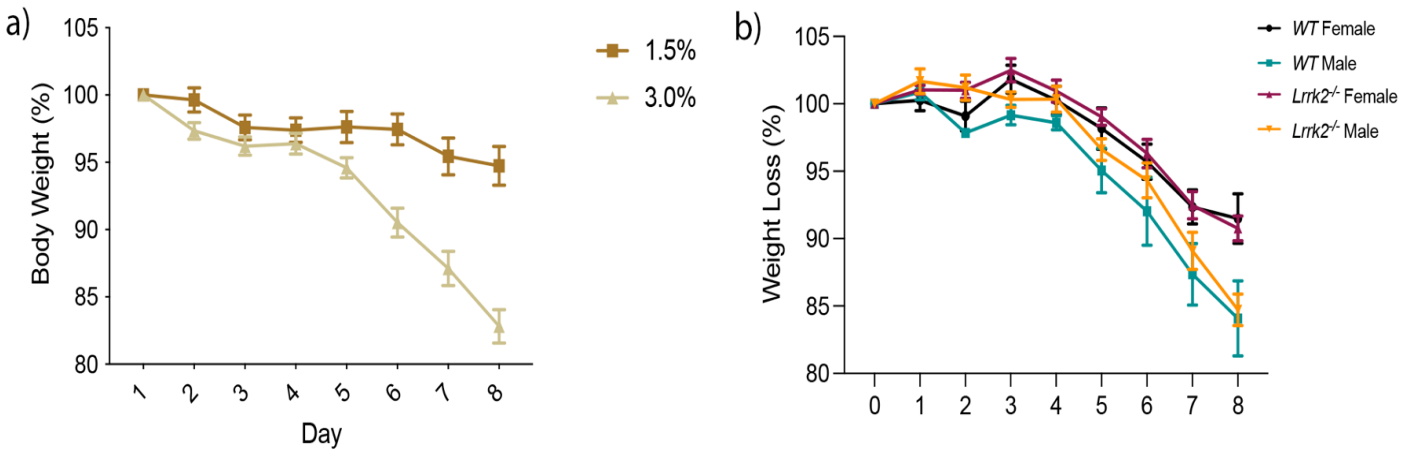

Supplementary Figure 3.3 Weight loss in DSS treated mice.

a) Pilot study in a cohort of mice to determine DSS concentration. Mice were treated with either 1.5% or 3.0% DSS for 7 days and evaluated on the 8th b) Analysis of sex-differences in mice treated with 3.0% DSS. n=4-5. Data were analyzed by repeated measures Two-way ANOVA.

3.6 Materials & Methods

Cell Culture

RAW 264.7 CRISPR cells were a gift from Erwin Schurr Lab. Two independent clones were used for each experiment. Cells were cultured in DMEM supplemented with 10% fetal bovine serum, 100 U/mL penicillin and 100 µg/mL streptomycin at 37°C with 5% CO_2. MLi-2 inhibitor (Cat. No. 5756, Tocris) was used at a concentration of 50 nM. RAW 264.7 cells were pre-treated with 1 ng/mL LPS-B5 (Catalogue #tlrl-b5lps, InvivoGen) for 24 hours, followed by 100 µg/mL Zymosan depleted (Catalogue #tlrl-zyd, InvivoGen) or only 1 ng/mL LPS or 100 µg/mL Zymosan depleted for the indicated periods. Lrrk2 knockout MEFs were a gift from David Park lab. Cells were culture as described above.

Mice

Lrrk2 $^{-/-}$ mice were bred on a C57BL/6 background from Charles River. Experimental mice were bred by crossing heterozygous mice to generate wild type and knockout littermates and were randomized into cages at weaning. All animal procedures were approved by the University of Ottawa Animal Care Committee.

Dextran Sodium Sulfate (DSS)-induced Colitis

Mice aged 10-11 weeks were used in a pilot study to determine appropriate dextran sodium sulfate (DSS) salt concentrations to induce colitis phenotype. Mice were treated with 1.5% or 3.0%DSS (Catalogue # ICN16011080, MP Biomedical) in sterile drinking water for 7 days and sacrificed on the eighth day. A second cohort of mice was treated with 3.0% DSS for 7 days and sacrificed on

the eighth day. Disease activity indices were monitored daily for the duration of the study. Mice were anesthetized with sodium pentobarbital and transcardially perfused with PBS. Spleen, brain, and distal colon tissue were flash frozen in liquid nitrogen for RNA and protein analysis. The remaining colon sections were gently rinsed in HBSS and prepared into Swiss rolls with the proximal end centered.

Histopathology

Colon tissue were fixed in 10% formalin then transferred to 70% ethanol prior to paraffin embedding. 40 µM sections were used for hematoxylin and eosin (H&E) staining. Tissue sections were scored for disease severity in a blinded manner by an independent pathologist. Pathology was described as 1=0%, 2= 0-25%, 3= 25-50%, 4= 50-75%, 5=75-100% of the field.

RNA-Immunoprecipitation

Tissue used for RNA-immunoprecipitation (R-IP) were lysed in R-IP buffer [50 mM Tris, (pH 7.4), 150 mM NaCl, 1% NP-40 and 1X cOmplete ™protease inhibitor cocktail (Catalogue # 4693159011)] tumbled for 20 min at 4°C and centrifuged at 10,000xg for 10 min. Supernatants were pre-cleared using 10 µL wet volume of Dynabeads ™Protein G magnetic beads (Catalog # 10004D, Thermo Fisher). RNA-protein complexes were immunoprecipitated using 750-1000 ug of pre-cleared supernatants incubated with 4 µg HuR (sc-5261, Santa Cruz) antibody vs. mouse IgG control for 2 hours at 4°C. RNA-protein complexes were captured by adding 25 µL wet volume of beads and tumbled for 1 hour at 4°C. Complexes bound to beads were washed (3 min x 5) in wash buffer [50 mM Tris, (pH 7.4), 150 mM NaCl, 0.1% NP-40] and resuspended in wash

buffer. Ten percent of IP was used for western blot detection and remaining beads were resuspended in TRIzol for RNA isolation following manufacturer's protocol.

RT-qPCR

Equal volumes of RNA from control and experimental immunoprecipitates were used to generate cDNA using the iScript cDNA synthesis kit (Catalogue 170-8891, BioRad). For total RNA, 500 ng of RNA was used in a mMulv RT cDNA synthesis reaction. qPCR was performed using GoTaq ® qPCR master mix (Catalogue A6002, Promega). The cycling conditions were as follows 95°C, 2min, [95°C for 15 sec, 60°C for 1 min,] x 40 cycles. RNA levels from experimental immunoprecipitates were normalized to IgG control and expressed as a fold change relative to IgG R-IP. RNA levels were normalized to band intensity of respective IP to control for the amount of immunoprecipitated proteins between control and experimental groups. Total RNA was normalized to housekeeping genes Gapdh and Actb. Fold change was calculated using the $2^{\wedge-\Delta\Delta Ct}$ method. Primer sequences are in Table 3.6.1.

Western Blot and Phos-tag SDS-PAGE

Total protein collection from cells was performed with two washes of PBS or 1X TBS for Phos-tag samples, scraping and lysis in buffer [50 mM Tris, pH 8.0, 150 mM NaCl, 10mM EDTA, 1% Triton X-100, and 1X cOmplete ™protease inhibitor cocktail (Catalogue # 4693159011) and 1X PhosSTOP phosphatase inhibitor (Catalogue # 4906845001]. Lysates were tumbled for 20 min at 4°C, and centrifuged at 10, 000xg for 10 min. EDTA was omitted in samples prepared for Phos-tag gel analysis according to manufacturer's protocol. Supernatant concentration was estimated

using the RC DC ™ Protein Assay (Catalogue 500-0122, BioRad) and diluted in Laemmli sample buffer.

Tissue samples were lysed in buffer [50 mM Tris, pH 8.0, 150 mM NaCl, 10mM EDTA, 1% Triton X-100, and 1X cOmplete ™protease inhibitor cocktail (Catalogue # 4693159011) and 1X PhosSTOP phosphatase inhibitor (Catalogue # 4906845001], tumbled for 20 min at 4°C, and centrifuged at 10, 000xg for 10 min. EDTA was omitted in samples prepared for Phos-tag gel analysis according to manufacturer's protocol. Supernatant concentration was estimated using the RC DC ™ Protein Assay (Catalogue 500-0122, BioRad) and diluted in Laemmli sample buffer. Antibodies used are listed in Table 3.6.2.

Samples for western blot were run on 10% polyacrylamide gels and transferred to PVDF membranes. Membranes were blocked in 5% milk for 1 hour at room temperature and incubated in primary antibody overnight followed by secondary antibody for 1 hour at room temperature. Images were obtained using the Image Quant LAS4010 Biomolecular Imager (GE Healthcare). Protein quantification was performed using Image J (Fiji) to calculate mean band intensity normalized to the mean intensity of a housekeeping gene.

Phos-tag ™ SDS- PAGE gels were cast with a 12% acrylamide resolving gel using 50 µM PhosTag Acrylamide (Catalogue AAL-107S1, Wacko) and 100 µM $ZnCl_2$ in 1.0 mM cassettes to improve transfer efficiency. Samples were run at 70V for stacking and 100V for resolving until the dye front reached the end of the gel. The gel was washed 3x10 min in 1X Transfer buffer with 10 mM EDTA followed by 1x10 min wash in 1X transfer buffer without EDTA. Proteins were

transferred to PVDF membranes for 90 min at 100V in 1X transfer buffer [25 mM Tris, 192 mM glycine], with 10% methanol. Blocking and antibody incubation were performed as described above. Negative control samples were treated with calf intestinal alkaline phosphatase for 30 min at 37°C at a concentration of 1U/10 ug of lysate. Western blot or Phos-tag SDS-PAGE images were obtained using the Image Quant LAS4010 Biomolecular Imager (GE Healthcare). Protein quantification was performed using Image J (Fiji) to calculate mean band intensity.

Enzyme-Linked Immunosorbent Assay (ELISA)

Cells were treated with 1 ng/mL LPS-B5 (Standard) (Catalogue # tlrl-b5lps) for 2,6,12, and 24 hours. Cell culture medium was collected and diluted 20X in assay diluent provided with the kit. Mouse TNF-α ELISA (Catalogue # 430904, Biolegend) was used according to manufacturer's instructions. Absorbance was measured at 450 nm and 570 nm using the Synergy H1 Multi-Mode Plate Reader (BioTek).

Gateway cloning and protein purification

Wild-type pENTR4_ELAVL1 (Plasmid # 106103) were a gift from Thomas Tuschl (Addgene) and was used to generate HuR mutants using site-directed mutagenesis. Mutant and wild-type pENTR4_ELAVL1 plasmids were used to generate GST-HuR, GST-HuR-T118A, GST-HuR-T143A and GST-HuR-T118A/T143A bacterial expression plasmids using Gateway cloning. Plasmids were transformed in BL21 (DE3) competent E. coli. An overnight culture was diluted 1 in 100 in LB broth including ampicillin and protein expression was induced at OD_{600} 0.4 with 0.2 mM Isopropyl β-D-1-thiogalactopyranoside for four hours at 30 degrees Celsius. Bacterial culture was centrifuged at 10,000 x 30 min (4°C) and lysed with 1 mg/mL Lysozyme in resuspension

buffer (50mM Tris, pH 8, 200 mM NaCl, 1mM EDTA, 1mM DTT, 1% Triton, 5% glycerol and protease inhibitor tablet). Lysate was sonicated and centrifuged at 12,000xg for 30 min. Supernatant was loaded on a Glutathione-agarose column and eluted with 10 mM reduced glutathione in resuspension buffer.

Phosphorylation assay

GST-tagged human HuR or GST control proteins were generated as described above. Wild-type LRRK2, recombinant G2019S LRRK2, and recombinant D1994A LRRK2 (aa. 970-2527) human proteins 37°C were obtained from Thermo Fisher Scientific (A15197, A15201 and PV6051). In vitro phosphorylation assays were carried out in a 25 µL volume by combining 1.0 µg of GST-HuR, GST-HuR mutants or GST control with 20 ng of wild-type, G2019S or D1994A LRRK2 in phosphorylation buffer (20mM HEPES (pH 7.5), 10mM MgCl2, 1mM EGTA, 2mM DTT, 1% DMSO and 1X PhosSTOP ™ phosphatase inhibitor cocktail). To initiate phosphorylation, 10µM ATP and 10µCi [γ-32P]-ATP (Catalogue # BLU002A500UC, Perkin Elmer) was added to each tube and reactions were incubated at 30°C for 1hr. Reactions were performed in parallel but without [γ-32P]-ATP to confirm equal amounts of HuR and LRRK2 in each reaction by Western blot. Reactions were terminated by the addition of 1X Laemmli loading buffer and were subsequently boiled at 99°C for 5 min. Membranes were dried and exposed to autoradiography film for 24-72 hours before imaging.

Gel-Shift Assay

10 pmol of RNA probes were 5'-labelled with 25 pmol of [γ-^{32}P]ATP (3,000Ci/mmol, 10 mCi/ml, PerkinElmer) and T4 Polynucleotide Kinase (NEB) at 37°C. Phosphorylation assays were

performed in 25 µL as described above with 1.0 µg of GST-HuR or GST, 20 ng of wild-type, G2019S or D1994A LRRK2 recombinant proteins, 10 µM of ATP, in phosphorylation buffer. Binding assays were incubated at room temperature for 30 min with 2 µL of phosphorylation assays and 35 fmol of RNA probes in binding buffer (20 mM Tris pH 7.4, 1 mM EDTA, 100 mM KCl, 1 mM DTT, 5% Glycerol) in a total volume of 20 µL. Reactions were terminated with 2.5 µl of 10X loading buffer (100 mM Tris pH 7.4, 10 mM EDTA, 50% Glycerol, 0.1 % Xylene Cyanol, 0.1 % Bromophenol Blue) and 10 µL were loaded and separated on a 6% acrylamide:bisacrylamide (29:1) gel. After electrophoresis, gels were dried on 3MM Whatman papers and autoradiographed using X-ray films. The RNA probe sequences are in Table 3.6.1.

Mass Spectrometry

R-IP samples were prepared for Mass spectrometry analysis with an on-bead digestion method. After last wash with R-IP wash buffer, beads were washed twice on ice with 20mM TrisHCl pH 8.0 + 2mM $CaCl_2$. A small volume of sample was removed for western blot validation. The liquid-free beads were then resuspended in 9 µL of 20mM Tris-HCl pH 8.0 with 1.6 µL of 25mM DTT, followed by a 30 min incubation period at room temperature with gentle agitation. 1.2 µL of 50mM iodoacetamide was added for an additional 10 minutes at room temperature and incubated with agitation. 10 µL of 100 ng/µL mass-spectrometry grade trypsin (Worthington Biochemical, catalogue no. LS02122) was added to each sample at a final concentration of 45 ng/µL and incubated at 37°C on a rotator overnight. Supernatant was removed and an additional 500ng of trypsin was added to each sample for 4 hours at 37°C with gentle agitation. Reactions were terminated by adding formic acid to a final concentration of 2%.

Desalting was performed using Sep-Pak tc18 1cc cartridges (Waters, catalogue no. WAT054960) following manufacturer's instructions. Cartridges were conditioned in 900 µL of 100% acetonitrile (ACN) followed by 300 µL of 50% ACN, 0.5% acetic acid (HAcO). Cartridges were then equilibrated with 900 µL of 0.1% trifluoroacetic acid (TFA) and samples concentration was adjusted to 0.4% TFA prior to cartridge filtration. Desalting was performed with 900 µL of 0.1% TFA. Washes were performed with 90 µL of 0.5% HAcO and elution with 500 µL of 50% ACN, 0.5% HAcO. Samples were analyzed by Liquid-Chromatographs Mass-Spectrometry. Sample analysis was performed by the uOttawa Proteomics Resource Centre. Raw sample files were analyzed by MaxQuant (version 1.5.2.8), and candidate targets were selected for further analysis using Mass Spectrometry interaction STatistics (MiST) (Jäger et al., 2012).

Statistical Analyses

Statistical analysis was performed using GraphPad Prism 9. Two-tailed t-test with Welch's correction was performed when comparing two independent groups. Non-parametric datasets were analyzed using Kruskal-Wallis with Dunnett's post-hoc test. Two-way ANOVA (analysis of variance) with Holm-Sidak post-hoc test when two independent variables were evaluated or Three-Way ANOVA when three independent variables were evaluated. All data were represented as mean ± SEM. Statistical significance was represented with the following notation: *$p<0.05$; **$p<0.01$, ***$p<0.001$, ****$p<0.001$.

Table 3.6.1 Primers and RNA probes

Primers			
Gene	**Application**	**Sequence (5'-3')**	**Citation**
Actb	qPCR	F-ACTGCCGCATCCTCTTCCTC	
		R- GGATGCCACAGGATTCCATACC	
Cdkn1 (p21)	qPCR	F-CATTCAGAGCCACAGGCACC	
		R-ACGAAGTCAAAGTTCCACCGT	
Il1b	qPCR	F-TGCCACCTTTTGACAGTGATG	
		R- TGATGTGCTGCTGCGAGATT	
Il6	qPCR	F-TCCTCTCTGCAAGAGACTTCC	
		R- GGTCTGTTGGGAGTGGTATCC	
Gapdh	qPCR	F- ATGGCCTTCCGTGTTCCTACC	
		R- GTAGCCCAAGATGCCCTTCAG	
Lrrk2 KO	Genotyping	mF80- GGC TCT GAA GAA GTT GAT AGT CAG GCT G	Jie Shen
		neoLKF1- CCC AAG CTA GCT TTA TCG ATA AGC TTG A	
		mR52- CTG TAC ACT GGC AAC TCT CAT GTA GGA G	
Lrrk2	qPCR	F- TCTGGCTGGAACCCTGCTAT	Hakimi et al. 2011
		R- AACTGGCCATCTTCATCTCC	
Snca	qPCR	F-CCTTCAGAGGAAGGCTACCAAG	

		R-TGACTGGGCACATTGGAACT	
Tgfb1	qPCR	F- TTGCTTCAGCTCCACAGAGA	
		R-TGGTTGTAGAGGGCAAGGAC	
Tnfa	qPCR	F-CCTCACACTCACAAACCACCA	
		R-GTGAGGAGCACGTAGTCGG	
RNA Probes			
TNF ARE	Gel shift	AUAUUUAUAUUUGCACUUAUUAUUUAUUAUUUAUUUAUUAUUUAUUUAUUG	
TNF Neg Control	Gel shift	AUCUCUAGAUGUGCACUCAUCAGUGAUCACUGAGUCAAUAGUCAAUGAGUCGAGUCGA	
PolyU	Gel shift	UUUUUUUUUUUUUUUUU	
PolyU Neg	Gel shift	ACGUGACCUAACGUCA	

Table 3.6.2 Antibodies

Antibody	Dilution	Vendor	Catalogue #
Primary			
α-synuclein	1:2000	BD Transduction	610787
α-Tubulin	1:10,000	Sigma	T6199
β-Actin	1:10,000	Sigma	A5441-.2ML
GST (B-14)	1:5000	Santa Cruz	Sc-138
HuR/ELAVl (3A2)	1:5000	Santa Cruz	Sc-5261
LRRK2 (MJFF2[c41-2])	1:4000	Abcam	Ab133474
LRRK2 pSer935 (UDD2-10(12))	1:4000	Abcam	Ab13340
HRP-secondary			
Goat anti-mouse	1:7500	Jackson ImmunoResearch	115-035-174
Goat anti-rabbit	1:7500	Jackson ImmunoResearch	111-035-144
Isotype control (for immunoprecipitation)			
Mouse IgG	N/A	Thermo Fisher Scientific	02-6502

Chapter 4

Characterization of the neuronal RNA-binding protein HuD in mouse energy metabolism

4.1 Statement of Contributions

Christine Luckhart and Mirela Barclay of the uOttawa Behaviour and Physiology Core facilitated EchoMRI and indirect calorimetry experiments. Arul Vadivel performed pulse oximetry experiments. Olanta Negeri designed and conducted experiments. Derrick Gibbings designed experiments.

4.2 Introduction

Metabolic disturbances are often associated with neurological and neurodegenerative diseases; however, the metabolic changes are often not considered as part of the core causes or consequences of the disease (Menzies et al., 2021; Santiago et al., 2017; Santiago & Potashkin, 2021). In neurodevelopmental disorders such as Down Syndrome and Fragile X disease, metabolic changes like obesity, insulin resistance, diabetes, and cardiovascular impairments are often observed (Dierssen et al., 2020; Irving & Chaudhari, 2012; Utari et al., 2010). These findings are recapitulated in mouse models of neurodevelopmental disorders including Down Syndrome, Fragile X Syndrome, and Autism Spectrum Disorder where impaired energy metabolism, altered body composition, and dysregulation of key metabolites associated with mitochondrial function have been reported (Menzies et al. 2021).

In contrast to neurodevelopmental disorders, obesity, diabetes, and insulin resistance are considered risk factors for neurodegenerative diseases including Parkinson's disease (PD) and Alzheimer's disease (AD), (Arvanitakis et al. 2004; Park et al. 2022; Labandeira et al. 2022) highlighting the crosstalk between metabolism and neuronal function. As PD progresses, patients may present with significant metabolic impairment including weight loss and an increased resting metabolic rate (Femat-Roldán et al. 2020). In the case of AD, significant weight loss is a common feature of advanced disease (Poehlman & Dvorak, 2000), which may be caused in part by reduced movement (Franssen et al., 1999), but some reports suggest that patients also exhibit increased energy expenditure (Doorduijn et al., 2020) in addition to brain hypometabolism (Zilberter & Zilberter, 2017). Metabolic disorders are linked to impaired mitochondrial function, oxidative stress, and excessive inflammation (Bhatti, Bhatti, and Reddy 2017; Hotamisligil 2006), and the

association between these mechanisms and cell death in neurodegenerative diseases has been well established through numerous models (Muddapu et al., 2020). Given the high energy demands of the brain, neurons are particularly susceptible to disruptions in energy balance (Muddapu et al., 2020).

The RNA-binding protein HuD (ELAVL4) is a pivotal regulator of RNA metabolism and is most often associated with its roles in regulating neuronal development and synaptic plasticity(Silvestri et al., 2022). In the adult brain, HuD has been mechanistically linked to disease processes in Alzheimer's disease (Kang et al. 2014), and in recent years, both Amyotrophic Lateral Sclerosis (ALS) (De Santis et al. 2019), and Parkinson's disease (Chapter 2). In all instances, HuD was linked to the accumulation of toxic proteins; however, the implications of its aberrant expression or regulation in neuronal energy metabolism are unknown.

HuD expression is primarily restricted to neurons, but it has also been ascribed functions outside of the CNS (Jung & Lee, 2021). In the pancreas, HuD was shown to bind to the 5' end of insulin mRNA in β cells and inhibit its translation, suggesting that HuD is required for glucose homeostasis (E. K. Lee et al., 2012). In patient data, HuD was identified in gene networks linked to Type II diabetes in human-derived pancreatic islet cells (Taneera et al., 2012). Together, these findings imply that HuD may play an important role in metabolic disorders.

Interestingly, GWAS data has also linked HuD to obesity (Locke et al. 2015), suggesting that it may control other metabolic pathways. While accumulating evidence points to a role for HuD in metabolic processes, effects of its loss on systemic energy metabolism have not yet been elucidated. We therefore sought to investigate the effect of HuD knockout in mouse energy metabolism and its association to metabolic changes relevant to CNS disorders.

4.3 Results

Body composition is altered in *HuD*$^{-/-}$ mice

Several neurological and neurodegenerative diseases are associated with metabolic disorders and changes in body composition (Menzies et al. 2021; Femat-Roldán et al. 2020; Poehlman and Dvorak 2000. To determine if *HuD*$^{-/-}$ mice exhibit altered phenotypes in body composition, we used EchoMRI to evaluate fat mass, lean mass, and total body weight in a cohort of mice at 4 months of age and again at 8 months of age (Fig. 4.3.1 a,b). Mice were fed a pulverized standard chow diet ad libitum and had access to a running wheel in CLAMS cages. At 4 months, no significant differences were observed in fat mass (Fig. 4.3.1 a); however, by 8 months, female and male knockout mice showed a decrease in fat (Fig. 4.3.1 b), but this was more pronounced and significant in males, suggesting an age-related, and sex-specific effect. Lean mass was significantly decreased in both male and female knockout mice at 4 months of age, and this was conserved at 8 months in males (Fig. 4.3.1 b). Together, the differences in fat and lean mass led to an effect on total weight with *HuD*$^{-/-}$ mice being smaller. When body fat percentage was evaluated, we observed a significant decrease in male body fat percentage in *HuD*$^{-/-}$ mice suggesting that they are proportionally leaner and not just smaller (Supplementary Fig. 4.1).

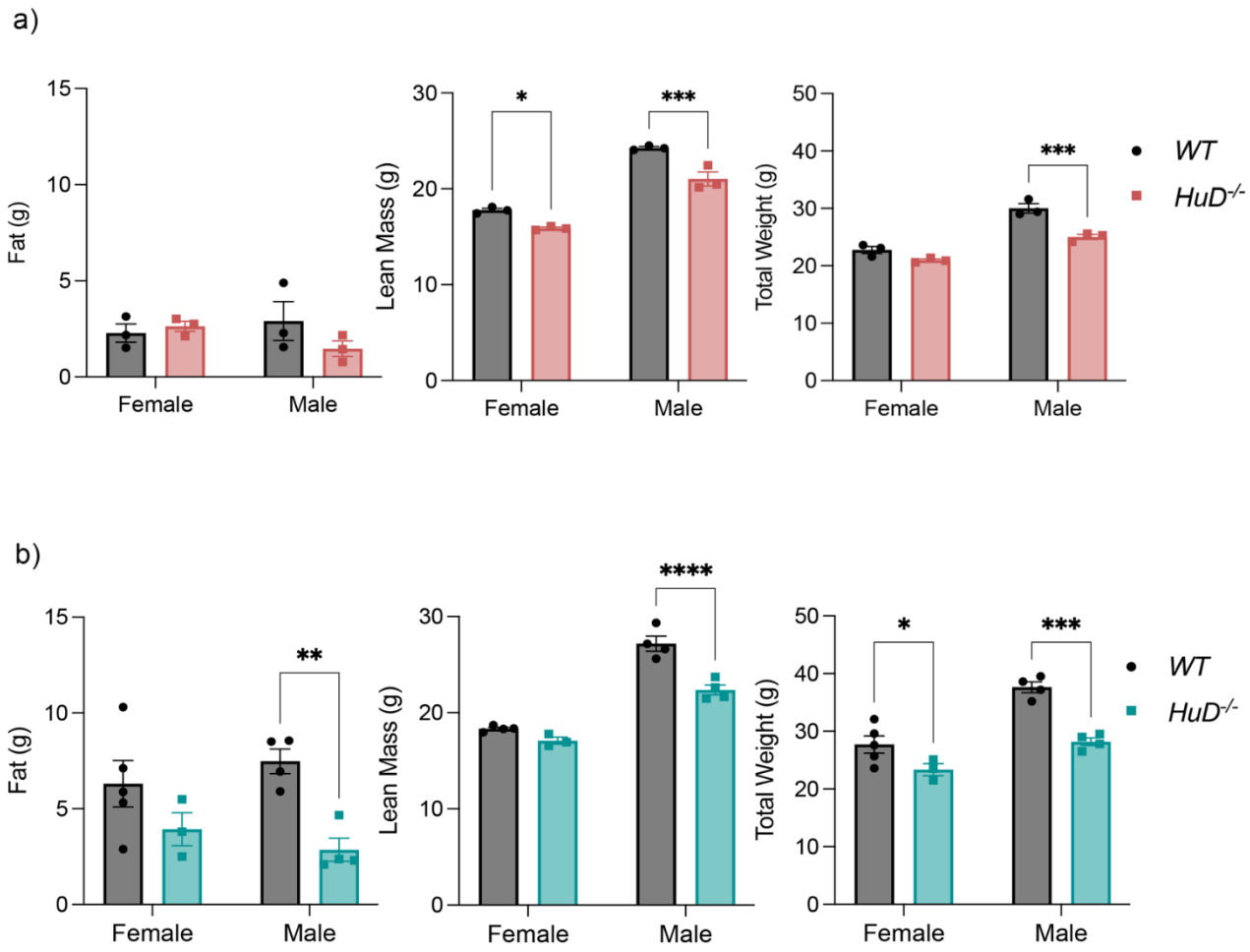

Figure 4.3.1 Body composition measured by EchoMRI.

a,b) Fat mass, lean mass , and total animal weight are compared in male vs. female mice at 4 months (a) or 8 months (b) of age. Error bars represent mean ± SEM. n=3-4. Data were analyzed by two-way ANOVA with Holm-Sidak's. * $p<0.05$, ** $p<0.01$, ***$p<0.001$, ****$p<0.0001$.

Energy metabolism is impaired in *HuD*$^{-/-}$ mice

To determine if HuD knockout led to metabolic changes we performed indirect calorimetry using the Oxymax Comprehensive Lab Animal Monitoring System (CLAMS) (Fig. 4.3.2). Indirect calorimetry is a noninvasive method to infer energy metabolism by measuring gas exchange (i.e., oxygen consumption and carbon dioxide production) (Speakman 2013). We therefore first evaluated the volume of oxygen consumption (VO_2) in WT vs. *HuD*$^{-/-}$ mice in 12-hour cycles presented as dark (active) vs. light cycles. The data were normalized to lean body mass (LBM) as it is considered the active metabolizing tissue (Speakman 2013).

At 4 months, the volume of oxygen (VO_2) trended lower in knockout mice during the active cycle. This effect was accentuated and reached significance by 8 months of age (Fig. 4.3.2 a). While the VO_2 of WT mice remained the same at ~4800 mL/Kg/Hr at both time points, the VO_2 of knockouts decreased by another ~10% by 8 months, indicating a possible age-related decline in energy metabolism. In contrast, the volume of carbon dioxide produced (VCO_2), appeared to be slightly decreased in *HuD*$^{-/-}$ mice in both groups but this was not significant (Fig. 4.3.2 b).

We next evaluated the respiratory exchange ratio (RER), which describes the metabolic production of carbon dioxide relative to oxygen intake and serves as an indirect measurement of metabolic substrate oxidation (Farinatti et al., 2016). An RER close to 1 indicates the metabolism of predominantly carbohydrates, and an RER close to 0.7 indicates the metabolism of fats as a fuel source. Interestingly, the RER of *HuD*$^{-/-}$ mice was significantly increased in both age groups, suggesting a shift towards mainly carbohydrate metabolism (Fig. 4.3.2 c). RER may be influenced by several factors including food consumption, sedentarism, insulin sensitivity, and acid/base

imbalance in the blood which may be caused by conditions like high intensity exercise, sepsis, or mitochondrial disease (C.-H. Lee et al. 2006; Steiner et al. 2017; Farinatti, Castinheiras Neto, and Amorim 2016; Ramos-Jiménez et al. 2008; Chinnery 1993).

To determine the cause of the elevated RER, we first evaluated the total food consumed over the 24-hour test period and found a trend toward decreased food consumption during the dark cycle in *HuD*$^{-/-}$ mice at 4 months of age, but not at 8 months of age (Fig. 4.3.2 d), indicating that the increased RER is likely unrelated to food consumed. We then asked if the elevated RER was due to aberrant insulin sensitivity as HuD has been previously linked to insulin regulation in pancreatic β cells in HuD transgenic mice (Lee et al. 2012). To determine if insulin regulation is impaired in *HuD*$^{-/-}$ mice, we challenged the mice to a glucose tolerance test. Mice at 8 months of age were fasted for 16 hours and administered glucose via oral gavage. Surprisingly, glucose utilization was equal between WT vs. *HuD*$^{-/-}$ mice at 8 months, and 4 months (Fig. 4.3.2 e, Supplementary Fig. 4.2), suggesting that insulin was not meaningfully misregulated in the knockout mice. Differences in the route of administration may be the underlying cause of this discrepancy. Lee et al., used an intraperitoneal glucose tolerance test which relies on a non-physiological route of administration and has been reported to induce higher plasma glucose levels and a delayed insulin response when compared to OGTT (Andrikopoulos et al. 2008; Small et al. 2022).

Volume of Oxygen

a)

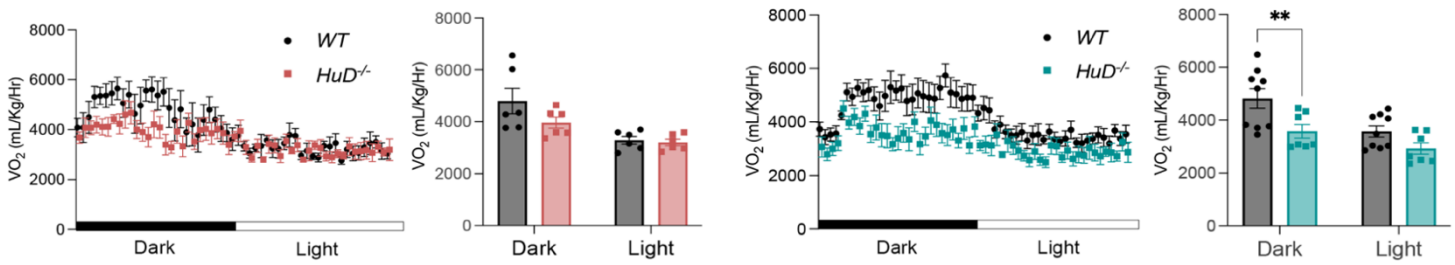

Volume of Carbon Dioxide

b)

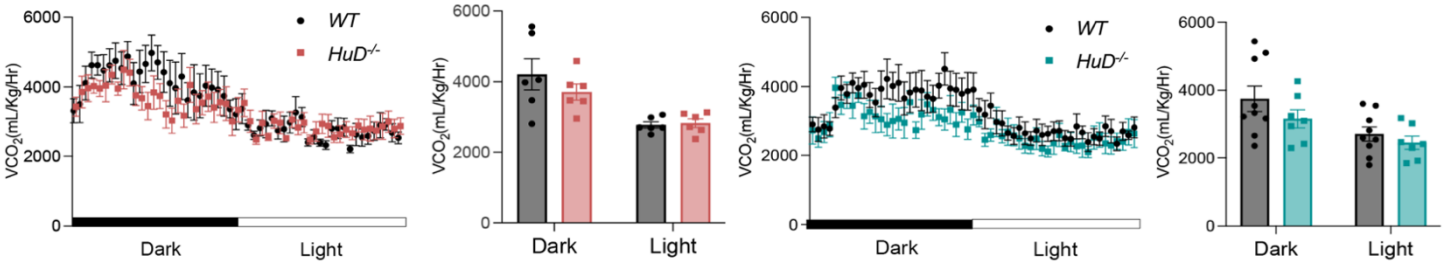

Respiratory Exchange Ratio

c)

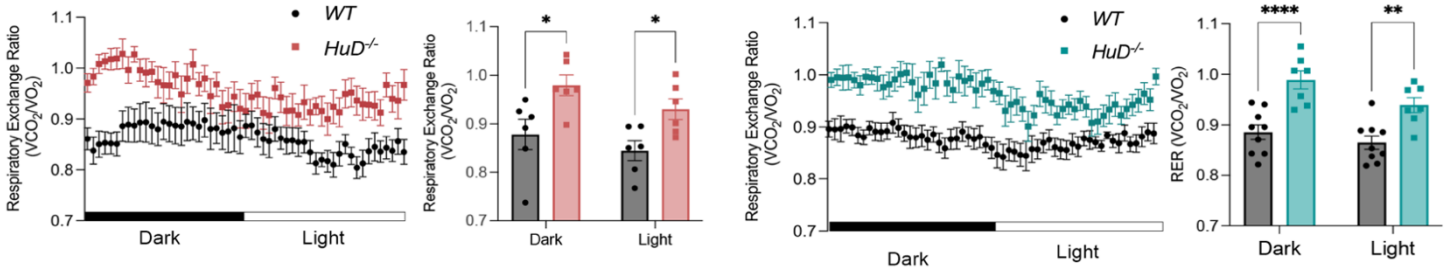

d)

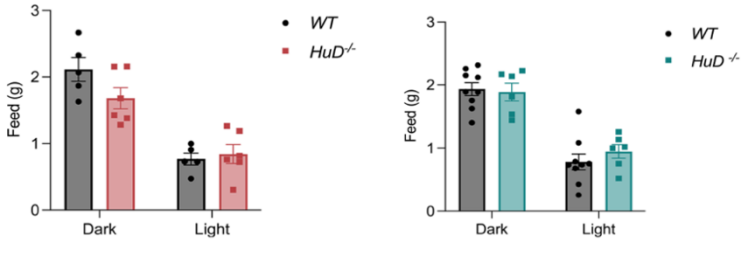

e)

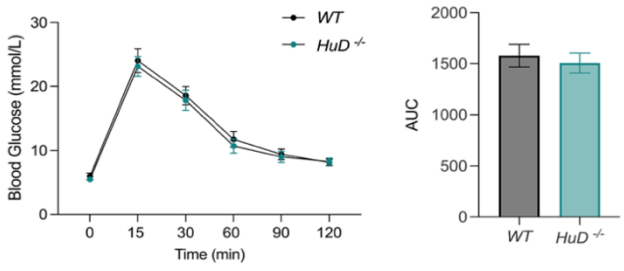

Figure 4.3.2 Energy metabolism is impaired in *HuD*$^{-/-}$ mice.

a) Oxygen consumption (VO_2) in 4 month (red) and 8-month-old mice (blue). b) Volume of carbon dioxide (VCO_2) exchange in 4 month and 8-month-old mice. (a,b) Data are presented over a 24 - hour period (left panel) or as dark cycle vs. light cycle. c) Respiratory exchange ratio in 4-month-old mice (left panel, circadian, right panel dark vs. light) and 8-month-old mice. d) Powdered food consumed over 12-hour cycles in 4-month-old and 8-month-old mice. Error bars represent mean ± SEM. n=6-9. Data were analyzed by Two-way ANOVA with Holm- Sidak's. * $p<0.05$, ** $p<0.01$, ***$p<0.001$, ****$p<0.0001$. e) Oral glucose tolerance test following 16-hour fast in 8-month-old mice. Error bars represent mean ± SEM. n=6-9. Glucose clearance presented on the left panel and calculated area under the curve (AUC) on the left. Data were analyzed by unpaired t-test with Welch's correction.

Energy expenditure is decreased in *HuD*$^{-/-}$ mice

We next sought to evaluate activity levels in the context of CLAMS metabolic chambers. *HuD*$^{-/-}$ have been previously shown to be less active (DeBoer et al., 2014). The horizontal ambulatory activity, vertical movement, and running wheel activity confirmed that HuD knockout mice are significantly less active during the dark cycle (Fig. 4.3.3 a,b).

The energy expenditure calculated as heat (Kcal/Kg/Hr) normalized to LBM, was decreased in *HuD*$^{-/-}$ mice in both groups, however like the VO_2 (Fig. 4.3.2 a), this was exacerbated by ~10% in 8 months vs. 4 months and reached significance in this group, suggesting a progressive decline in energy metabolism (Fig. 4.3.3 c). As expected, the effects on energy expenditure were exaggerated during the dark cycle, when the mice were most active.

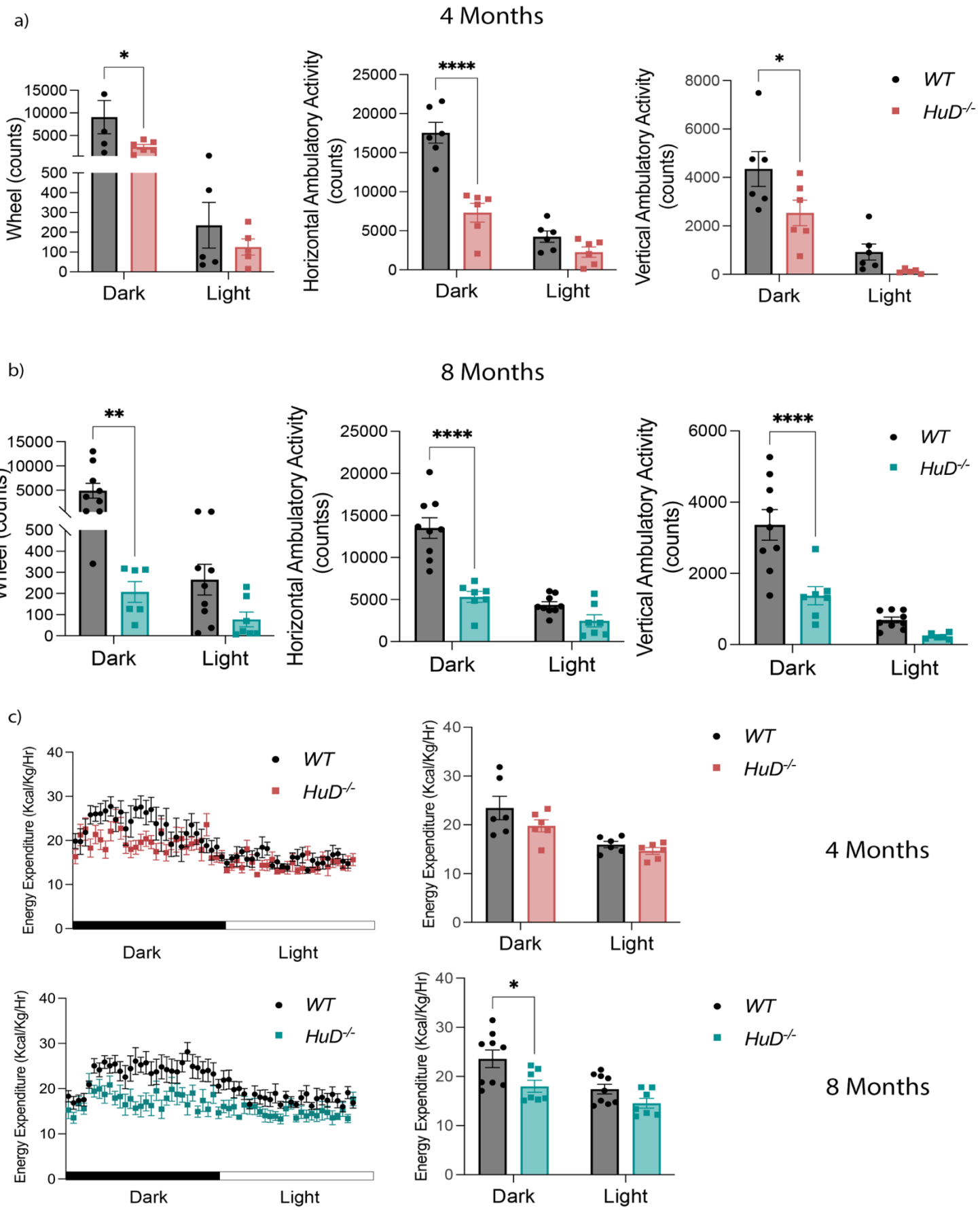
a)
4 Months
Wheel (counts)
Horizontal Ambulatory Activity (counts)
Vertical Ambulatory Activity (counts)
Dark
Light
WT
HuD-/-
b)
8 Months
Horizontal Ambulatory Activity (countss)
c)
Energy Expenditure (Kcal/Kg/Hr)
4 Months
8 Months

Figure 4.3.3 Energy expenditure is decreased in *HuD*$^{-/-}$ mice.

a) Physical activity in 4 month and b) 8-month-old mice. Left to right: Running wheel activity, horizontal ambulatory activity, and vertical ambulatory activity. c) Energy expenditure calculated as heat (Kcal/Kg/Hr) in 4-month-old mice (red) and 8-month-old mice (blue). Circadian data is plotted on the left panel, and dark vs. light cycle on the right. Error bars represent mean ± SEM. n=6-9. Data were analyzed by Two-way ANOVA with Holm- Sidak's. * $p<0.05$, ** $p<0.01$, ***$p<0.001$, ****$p<0.0001$.

Reduced breath rate in *HuD*$^{-/-}$ mice

To gain insight into the underlying cause for decreased movement, energy expenditure and decreased oxygen consumption, we evaluated pulmonary function using pulse oximetry. Intriguingly, breath rate was significantly decreased in *HuD*$^{-/-}$mice (Fig. 4.3.4 a), and this was associated with an elevated heart rate (Fig. 4.3.4 b). The low breath rate resulted in a slight decrease in blood oxygen saturation (Fig. 4.3.4 c); however, this was not significantly decreased, and is still within the range considered healthy ≥95% (Hafen & Sharma, 2023), suggesting that the deficits in energy metabolism are not caused by impaired lung function.

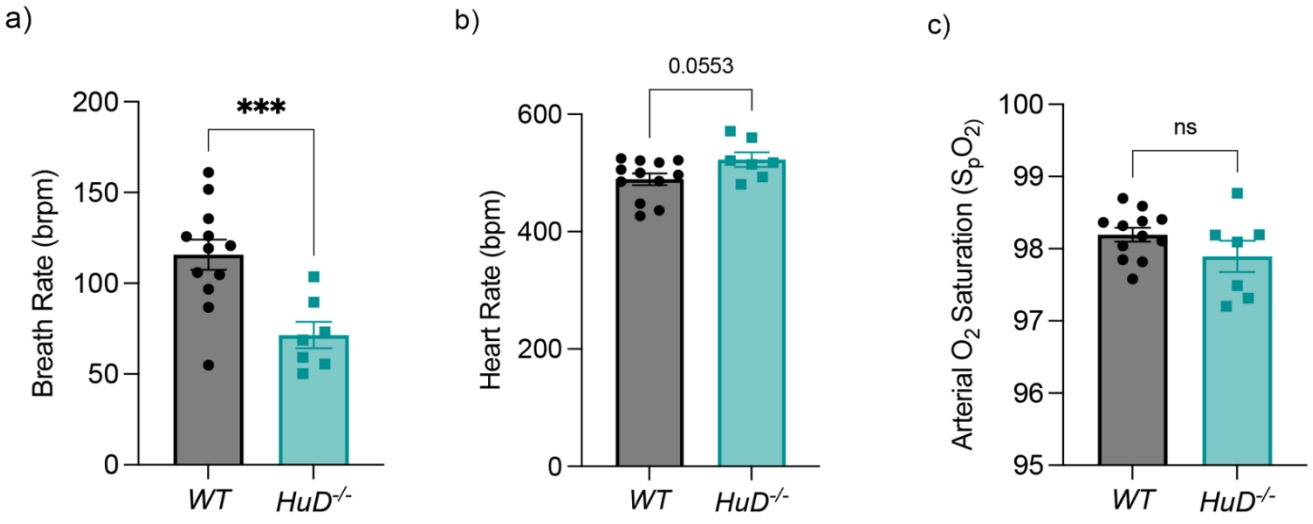

Figure 4.3.4 Loss of *HuD* function alters breath rate.

a) Breath rate (breaths per minute) b) Heart rate (beats per minute) c) Blood oxygen saturation (S_pO_2) were measured by pulse oximeter for a minimum of 30 seconds. Error bars are represented by mean ± SEM. n=6-9. Data were analyzed by unpaired t-test with Welch's correction. * $p<0.05$, ** $p<0.01$, ***$p<0.001$, ****$p<0.0001$.

HuD binds and regulates gene controlling mitochondrial dynamics and mitophagy

The low activity levels, decreased energy expenditure, and increased RER (Fig. 4.3.2-3) suggest that the *HuD*$^{-/-}$ mice are exhibiting deficits in energy metabolism consistent with mitochondrial impairment. To investigate the underlying mechanisms, we first sought to determine if HuD might control genes regulating mitochondrial homeostasis. To do this, we examined HITS-CLIP and microarray datasets from nELAVL (nELAVL) immunoprecipitations in mouse or human brain tissue for relevant targets (Bolognani, Contente-Cuomo, and Perrone-Bizzozero 2009; Ince-Dunn et al. 2012; Scheckel et al. 2016); Chapter 2). Interestingly, the datasets revealed that in human brain tissue, mRNAs encoding proteins regulating mitochondrial dynamics or mitophagy were bound by nELAVL proteins (Scheckel et al. 2016; Chapter 2. Specifically, we found that the dynamin-related GTPases, Mitofusins 1 and 2 (*Mfn1/2*), and Optic Atrophy 1 (*Opa1*) regulating outer mitochondrial membrane fusion, and inner mitochondrial membrane fusion, respectfully, along with the mitochondrial fission regulator, mitochondrial fission factor (*Mff*) (Tilokani et al., 2018) were all bound and regulated by nELAVL proteins. Optic Atrophy 3 (*Opa3*), a protein whose function is still unclear, but is also associated with fragmented mitochondria (Bagli et al., 2017) was also bound. Furthermore, the gene encoding Parkin (*Park2*), an E3 ubiquitin ligase protein involved in the PINK1/Parkin mitophagy pathway, the selective degradation of damaged mitochondria (Seirafi, Kozlov, and Gehring 2015), was among the targets bound by nELAVL. We then mapped out the putative nELAVL U-rich binding sites defined in Scheckel, 2016., and found that they were primarily within the intronic regions and 3'UTRs of the candidate genes (Supplementary Table 4.1), consistent with their roles in regulating splicing as well as mRNA stability and translation.

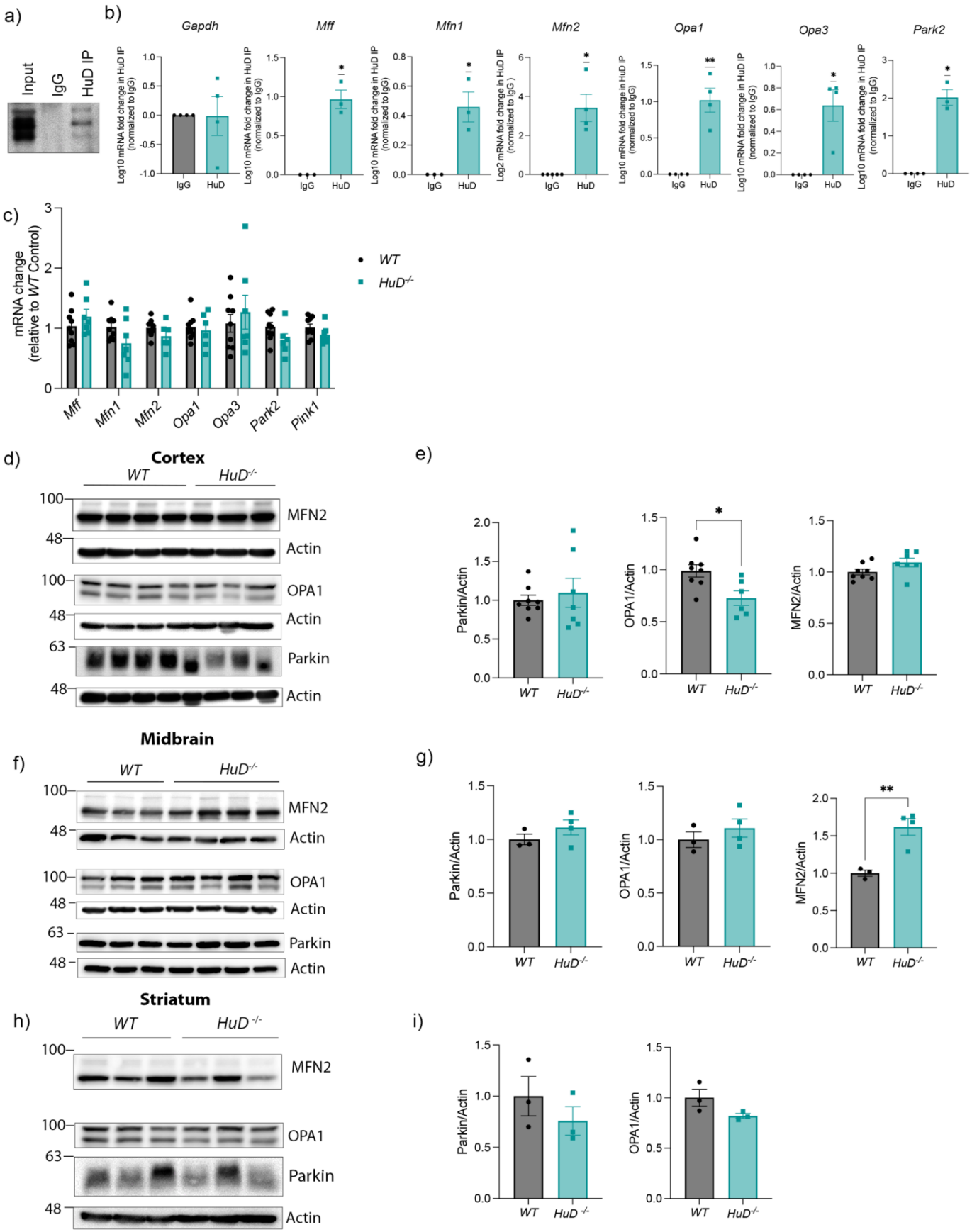
a)
Input
IgG
HuD IP
b)
Gapdh
Mff
Mfn1
Mfn2
Opa1
Opa3
Park2
Log10 mRNA fold change in HuD IP (normalized to IgG)
Log2 mRNA fold change in HuD IP (normalized to IgG)
IgG
HuD
c)
mRNA change (relative to WT Control)
WT
HuD-/-
Mff
Mfn1
Mfn2
Opa1
Opa3
Park2
Pink1
d)
Cortex
WT
HuD-/-
MFN2
Actin
OPA1
Parkin
e)
Parkin/Actin
OPA1/Actin
MFN2/Actin
f)
Midbrain
g)
h)
Striatum
HuD -/-
i)

Figure 4.3.5 HuD regulates genes important for mitochondrial homeostasis.

a) Neuronal ELAVL (nELAVL) RNA-immunoprecipitations in mouse cortex. b) mRNAs bound to nELAVL R-IPs normalized to IgG control R-IPs and quantified by RT-qPCR. Data were analyzed by one sample t-test. c) Total mRNA in mouse cortex quantified by RT-qPCR. d) Western blot analysis of candidate genes in mouse cortex. e) Quantification of (d) f) Western blot analysis of candidate genes in mouse midbrain g) Quantification of (f) h) Western blot analysis of candidate genes in mouse striatum i) Quantification of (h). Error bars represent mean ± SEM. n=3-8. Data were analyzed by unpaired t-test with Welch's correction. * $p<0.05$, ** $p<0.01$, ***$p<0.001$, ****$p<0.0001$. Note: Loading control for Striatum MFN2 was unavailable. Unquantified MFN2 was left in for reference purposes.

Table 4.3.1 Genes regulating mitochondrial homeostasis are misregulated in *HuD*$^{-/-}$ mice.

Genes bound in nELAVL IPs in (Scheckel et al. 2016; Chapter 2) are shown with corresponding gene expression fold change or exon splicing index identified by microarray (Chapter 2).

* Not a direct target of nELAVL

Gene	Fold Change *HuD*$^{-/-}$ vs. *WT* (Log2)	Fold Change FDR p.value	Exon Splicing Index *HuD*$^{-/-}$ vs. *WT*	Splicing FDR p.value
Mitochondrial Fission Factor (*Mff*)	-1.16	0.3942	-2.06	0.0291
Mitofusin 1 (*Mfn1*)	-1.14	0.9896	1.62	0.0196
Mitofusin 2 (*Mfn2*)	1.8	0.001	-2.35	0.0044
Optical Atrophy 1 (*Opa1*)	-1.05	0.7318	-2.65	0.1282
Optical Atrophy 3 (*Opa3*)	1	0.7503	-1.69	0.2706
Parkin (*Park2*)	-1.16	0.0892	1.78	0.0513
PTEN induced kinase 1 (*Pink1*) *	2.05	0.0073	2.92	0.001

To validate these targets, we performed nELAVL IPs (Fig. 4.3.5 a) in mouse brain tissue. Bound mRNAs were quantified by RT-qPCR and candidate mRNAs *Mff*, *Mfn1*, *Mfn2*, *Opa1*, *Opa3*, and *Park2* were all significantly enriched over IgG control IPs, but not the negative control mRNA, *Gapdh*. (Fig. 4.3.5 b). The microarray data from our group suggest that gene expression and/or splicing of these targets is misregulated (Table 4.3.1) (Chapter 2). In the cortex, we measured total mRNA levels and found no significant differences in gene expression (Fig. 4.3.5 c), suggesting that mRNA stability was not misregulated. We then evaluated protein levels across the cortex, midbrain, and striatum of WT vs. *HuD*$^{-/-}$ mice. In cortical tissue, we found a significant decrease in OPA1 levels in *HuD*$^{-/-}$ tissue, suggesting that mitochondrial fusion is impaired in *HuD*$^{-/-}$ mice (Fig. 4.3.5 d,e). Surprisingly, the OPA1 levels were unchanged in the midbrain and striatum, however, MFN2 was significantly increased in the midbrain of knockout mice (Fig. 4.3.5 f,g), suggesting that mitochondrial fusion is still impaired. Parkin levels were variable in the cortex of *HuD*$^{-/-}$ mice, but unchanged in the midbrain and striatum (Fig. 4.3.5 h,i). The lack of differences in Parkin protein levels may be explained by the fact that 13 of the 14 putative bindings sites lie within intronic sequences, whereas in MFN2 and OPA1 mRNA, the binding sites were found only in the 3'UTR or both in introns and 3'UTR, respectively (Supplementary Table 4.1). The microarray data suggests that *Park2* is misspliced in *HuD*$^{-/-}$ mice (Table 4.3.1), consistent with the high density of intronic binding sites. Since the motifs were identified in human prefrontal cortex, we asked if the 3'UTR binding sites were conserved in the mouse transcripts and found that many of these were (Supplementary Dataset 4.1), suggesting that the nELAVL proteins coordinate mitochondrial dynamics in neurons in an evolutionarily conserved manner.

Expression of the RNA-binding protein HuD is primarily restricted to neurons, with expression also detected in endocrine cells in the pancreas, testes, and adrenal gland (Bergman et al., 2017; E. K. Lee et al., 2012). Minor discrepancies about its expression at the organ level have been reported (Abdelmohsen et al., 2010; E. K. Lee et al., 2012), therefore, we confirmed the lack of *HuD* expression in tissues relevant to the observed metabolic phenotypes (Figures 4.3.1-.4, Supplementary Figure 4.3). While we cannot rule out the role of HuD in neurons innervating other tissues, or in endocrine cells, we focused our attention on neuronal tissues given the relatively high expression of *HuD* in brain tissue (Supplementary Figure 4.3), the remarkably high energy demands of the brain at 20% of the body's total oxygen metabolism (Watts et al., 2018), and the undetectable levels of HuD protein in other organs relevant to the observed phenotypes (Supplementary Figure 4.3). Taken together, it is plausible that loss of $HuD^{-/-}$ in neurons results in disrupted mitochondrial quality control pathways leading to a global deficit in energy metabolism.

4.4 Discussion

High throughput analyses of the nELAVL family of RNA-binding proteins has revealed that they preferentially bind U-rich motifs in introns and 3'UTRs of target mRNAs to regulate several aspects of RNA metabolism (Ince-Dunn et al. 2012; Scheckel et al. 2016). The most well characterized of the homologues, HuD (ELAVL4), has been mostly attributed roles in neuronal development, however, its misregulation has also been linked to aberrant neuronal function in models of Alzheimer's disease, ALS, and Parkinson's disease (De Santis et al. 2019; Kang et al. 2014; Chapter 2). A few studies have implicated HuD in regulating metabolic pathways including insulin translation and triglyceride production in the pancreas (C. Kim et al., 2016; E. K. Lee et

al., 2012), however, to date, the effect of loss of HuD on energy metabolism in a whole animal has not been investigated.

Here we evaluated global energy metabolism in *HuD*$^{-/-}$ mice for the first time and found that loss of HuD is associated with changes in energy metabolism, respiratory rate, and body composition. More specifically, we observed a surprisingly elevated respiratory exchange ratio in *HuD*$^{-/-}$ mice compared to WT mice (Fig. 4.3.2 c). In ~50% of the knockout mice, the RER surpassed 1.0 at 8-months, which is typically only observed during intense exercise as carbohydrates are burned for quick fuel and the body produces more lactic acid as a byproduct (Ramos-Jiménez et al. 2008). As previously described (DeBoer et al., 2014), and as confirmed in this study, the knockout animals are significantly less active than wildtypes (Fig. 4.3.3 a,b), and this is therefore not the cause of the high RER. Paradoxically, an elevated RER is also associated with sedentarism. The link between low activity levels and high RER is described in the case of obesity(Ramos-Jiménez et al., 2008). The EchoMRI results indicate that *HuD*$^{-/-}$ mice exhibit decreased fat mass, (Fig. 4.3.1 a,b, Supplementary Fig. 4.1) suggesting that the altered body composition in *HuD*$^{-/-}$ mice is not driving the elevated RER. The data on food consumption, glucose tolerance test, and pulse oximetry (Fig. 4.3.2-4) suggest that the elevated RER and decreased energy expenditure in *HuD*$^{-/-}$ mice is not caused by impaired glucose homeostasis, feeding habits nor impaired lung function. Furthermore, the decreased VO_2, breath rate, and energy expenditure could be a consequence of decreased movement, however, there should be a concomitant and proportional decrease in VCO_2 and heart rate. The presence of an elevated heart rate, and increased RER suggest that the *HuD*$^{-/-}$ mice are exhibiting a metabolic phenotype. We therefore hypothesized that it was associated with mitochondrial impairment.

To test this, we evaluated several datasets for nELAVL binding to mitochondrial genes and found that HuD or its homologues bind to introns or 3'UTRs of mRNAs encoding proteins required for mitochondrial dynamics including the fission and fusion factors *Mff*, *Mfn1/2*, *Opa1/3* or mitophagy (*Park2*) and these were validated by RNA-immunoprecipitation (R-IP) in mouse brain tissue (Fig. 4.5 a,b) (Bolognani, Contente-Cuomo, and Perrone-Bizzozero 2009; Ince-Dunn et al. 2012; Scheckel et al. 2016; Chapter 2). Data from our previous study indicated that these targets were differentially expressed or misspliced in the brains of *HuD*$^{-/-}$ mice (Table 4.3.1). Furthermore, *Pink1*, which is part of the PINK1/Parkin mitophagy pathway, was among the differentially expressed and spliced targets, however, it is not directly bound by nELAVL. In humans, mutations in PINK1 and Parkin are associated with early onset Parkinson's disease, suggesting that HuD may be implicated in PD through various mechanisms (Chapter 2).

While the splicing data still requires experimental validation, we evaluated protein levels in the cortex, striatum, and midbrain of one year old mice and found that OPA1 was significantly decreased in the cortex, and MFN2 was significantly increased in the midbrain (Fig. 4.3.5 d-g), suggesting that mitochondrial fusion is impaired in both regions of the brain. A recent study also found that MFN2 expression was controlled by HuD in pancreatic β cells (Hong et al., 2020), suggesting that HuD could also regulate mitochondrial dynamics in neurons. OPA1 controls inner mitochondrial membrane fusion, whereas MFN2 controls outer membrane fusion (Tilokani et al., 2018). The inner mitochondrial membrane is the site of the respiratory chain complexes responsible for oxidative phosphorylation (OXPHOS), and the outer membrane coordinates mitochondrial dynamics and serves as a receptor site for mitophagy (Kühlbrandt 2015; Xian and

Liou 2021). The high energetic demands of neurons is dependent on oxidative phosphorylation, and dysregulation of this pathway is associated with neurological and neurodegenerative diseases (Zheng et al. 2016). Therefore, loss or gain of function of key mitochondrial proteins could have catastrophic effects on neuronal bioenergetics.

In the absence of oxygen, or in cases of impaired OXPHOS, the cells will undergo a metabolic shift towards glycolysis to sustain energy demands (Ait-Aissa et al., 2019). Glycolysis, which is entirely reliant on carbohydrate metabolism, will produce lactic acid as a byproduct (Yellen, 2018). This accumulation of lactic acid triggers the bicarbonate buffering system, thereby increasing the VCO_2 relative to VO_2 and driving the RER to 1.0 or above (Korkmaz Eryılmaz et al. 2018), as we have observed. While we noted a significant decrease in oxygen consumption in older *HuD*$^{-/-}$ mice (Fig. 4.3.2 a), the pulse oximetry data showed normal oxygen saturation levels (Fig. 4.3.4 c), suggesting that tissue hypoxia was not occurring in *HuD*$^{-/-}$ mice.

Impaired OXPHOS is a defining characteristic of metabolic disorders, which are caused by mutations in mitochondrial DNA or in nuclear genes encoding mitochondrial proteins, and many of these disorders present with neurological disabilities (Gorman et al., 2016). In mitochondrial disorders involving the CNS, diagnostic testing may reveal elevated levels of lactate in the blood and the cerebrospinal fluid (Chinnery, 1993) , indicative of deficits in mitochondrial respiration. Collectively, mitochondrial disorders may present with an array of symptoms and manifestations including encephalopathy, seizures, fatigue, cardiac arrhythmias including tachycardia, impaired breathing like bradypnea, an inability to gain weight, and lactic acidosis (Anglin et al., 2012; Finsterer, 2008; Koene et al., 2013; Koenig, 2008; Lindenschot et al., 2018; Monlleo-Neila et al.,

2013; Shah, 2017; Thomas et al., 2015). In mice, loss of HuD resembles a mitochondrial disorder, as we have observed significantly decreased motor activity, decreased body weight, bradypnea, and tachycardia (Fig. 4.3.1-4). Interestingly, mice lacking HuC or HuD have been previously reported to experience seizures (DeBoer et al., 2014; Ince-Dunn et al., 2012), which we have also observed in mice as young as weanlings. Taken together, the data suggests a potential model in which HuD is required for coordinating mitochondrial dynamics and mitophagy in neurons by binding and regulating splicing or gene expression of key mitochondrial proteins to control energy metabolism. Future directions required to validate this model include analysis of metabolites like blood and CSF lactate concentrations, and the effect of HuD knockout on cellular metabolism and mitochondrial dynamics in primary neurons. Furthermore, the predicted nELAVL binding sites (Supplementary Dataset 4.1) in mouse mitochondrial RNAs should be validated.

4.5 Supplementary Data

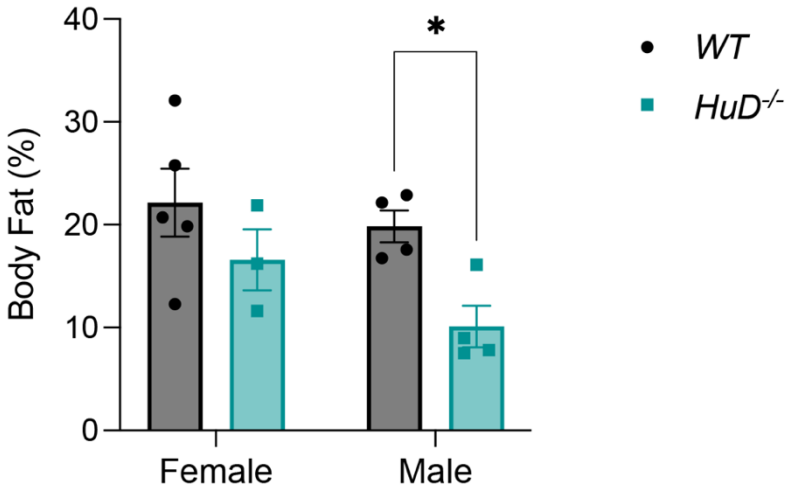

Supplementary Figure 4.1 Body fat percentage is decreased in *HuD*$^{-/-}$ mice.

Body fat calculated as a percentage of total mass in 8-month-old mice. * $p<0.05$, Two-Way ANOVA with Holm-Sidak's post-hoc test. n=3-4.

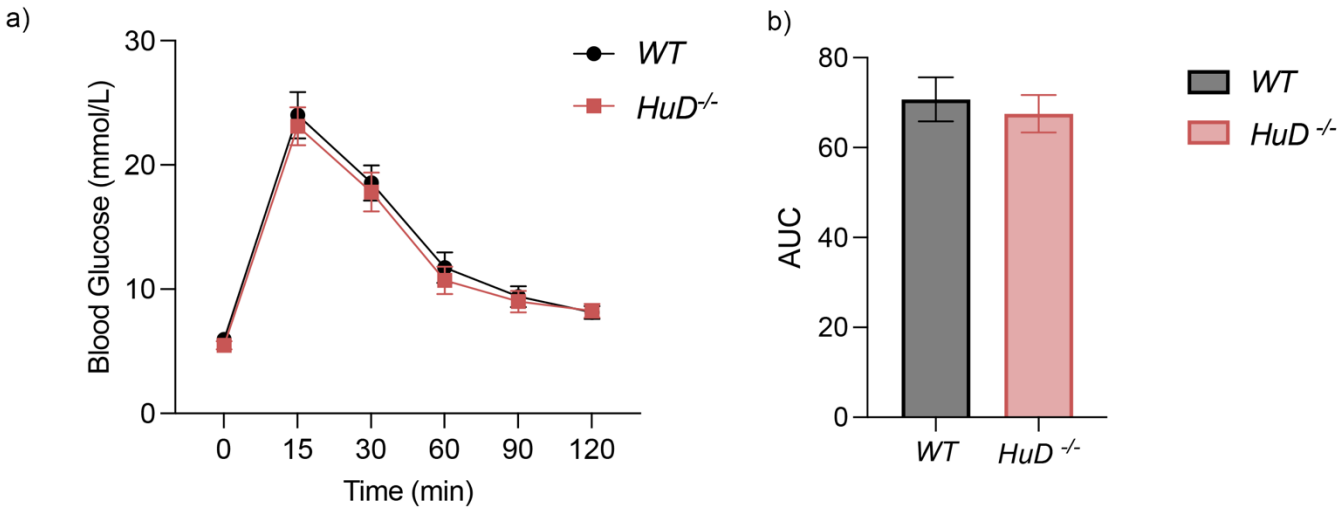

Supplementary Figure 4.2 Blood glucose levels are unchanged in *HuD*$^{-/-}$ mice.

Four-month-old, male, and female mice were fasted for 6 hours prior to an oral glucose tolerance test. Mice were administered a 2 mg/g bolus of 20% glucose solution by oral gavage. a) Saphenous vein blood samples were taken at 0, 15, 30, 60, 90, and 120 minutes and blood glucose levels were read by a glucometer. b) Data represented as area under the curve (AUC). n=5-6.

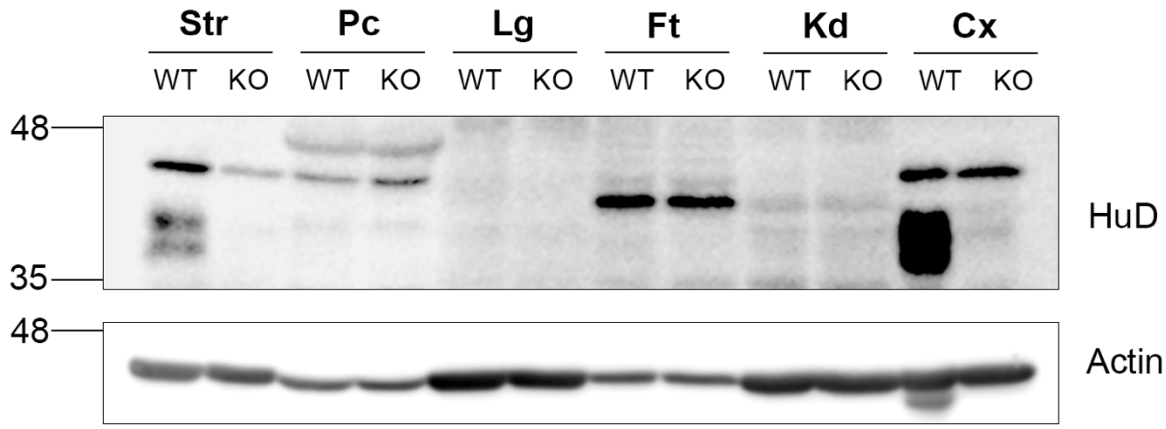

Supplementary Figure 4.3 *HuD* expression across tissue types.

Western blot screening of HuD expression across tissues relevant to *HuD*$^{-/-}$ phenotypes. Knockout tissues were used as an antibody control. Striatum (Str), Pancreas (Pc), Lung (Lg), Fat (Ft), Kidney (Kd), Cortex (Cx).

Supplementary Table 4.1

nELAVL binds genes regulating mitochondrial homeostasis. Genomic coordinates of nELAVL binding sites identified by HITS-CLIP in prefrontal cortex of human post-mortem brain tissue (Scheckel et al. 2016). Specific binding sequences were identified using NCBI Genome Data Viewer using Genome Reference Consortium Human Build 37 (GRCh37) as the reference genome.

Gene	Chr_hg19	Start_hg19	End_hg19	Strand	Region	Binding Site
MFF	chr2	228191511	228191519	+	intron	UUUGUUUUU
MFF	chr2	228193251	228193262	+	intron	UUUUCUUUCUUU
MFF	chr2	228193808	228193813	+	intron	UAUAGU
MFF	chr2	228193874	228193875	+	intron	UU
MFF	chr2	228194297	228194298	+	intron	GA
MFF	chr2	228197199	228197210	+	CDS	UAAACCCCUGGC
MFF	chr2	228206459	228206467	+	intron	UUUUCUUUU
MFF	chr2	228206623	228206624	+	intron	UA
MFF	chr2	228206806	228206807	+	intron	UU
MFF	chr2	228207410	228207413	+	intron	CUUU
MFF	chr2	228207564	228207565	+	intron	AA
MFF	chr2	228207820	228207822	+	intron	UAU
MFF	chr2	228207888	228207890	+	intron	UUU

MFF	chr2	228208321	228208322	+	intron	CC
MFF	chr2	228208507	228208511	+	intron	UUGUU
MFF	chr2	228210428	228210429	+	intron	UA
MFF	chr2	228210764	228210766	+	intron	UUU
MFF	chr2	228211750	228211751	+	5'UTR	AG
MFF	chr2	228221929	228221930	+	3'UTR	UA
MFF	chr2	228222133	228222134	+	3'UTR	CA
MFF	chr2	228222455	228222457	+	3'UTR	AAA
MFN1	chr3	179086264	179086273	+	intron	UUUUUACUUU
MFN1	chr3	179086958	179086959	+	intron	UCU
MFN1	chr3	179088807	179088808	+	intron	UU
MFN1	chr3	179089345	179089354	+	intron	AUUUUCUUAU
MFN1	chr3	179090622	179090624	+	intron	UUU
MFN1	chr3	179092898	179092901	+	intron	UCUU
MFN1	chr3	179110138	179110139	+	3'UTR	UG
MFN1	chr3	179110235	179110240	+	3'UTR	CAUGGG
MFN1	chr3	179110384	179110395	+	3'UTR	UUUAUUCCCGUU
MFN1	chr3	179110686	179110689	+	3'UTR	UUUU
MFN2	chr1	12071779	12071788	+	3'UTR	CUUAUUUUCC
MFN2	chr1	12073426	12073427	+	3'UTR	UU
OPA1	chr3	193337717	193337719	+	intron	UGC
OPA1	chr3	193337797	193337801	+	intron	UGACC

OPA1	chr3	193338301	193338306	+	intron	UCUUUG
OPA1	chr3	193376745	193376758	+	CDS	UAUUUUAUGGAAGA
OPA1	chr3	193384109	193384116	+	CDS	UUUUGGCG
OPA1	chr3	193412465	193412466	+	3'UTR	UU
OPA1	chr3	193412751	193412753	+	3'UTR	UUU
OPA1	chr3	193412909	193412918	+	3'UTR	UAUUCACCAC
OPA1	chr3	193413121	193413123	+	3'UTR	UAC
OPA1	chr3	193413332	193413338	+	3'UTR	UCCCCCU
OPA1	chr3	193413571	193413572	+	3'UTR	UA
OPA1	chr3	193414082	193414083	+	3'UTR	CA
OPA1	chr3	193414302	193414303	+	3'UTR	UU
OPA1	chr3	193414522	193414528	+	3'UTR	UUUGUUU
OPA1	chr3	193414785	193414788	+	3'UTR	UUUU
OPA1	chr3	193414991	193414992	+	3'UTR	UG
OPA1	chr3	193415252	193415257	+	3'UTR	AUUUUG
OPA1	chr3	193415313	193415315	+	3'UTR	CAC
OPA3	chr19	46053416	46053430	-	3'UTR	UUCUUUUCUUUUCUU
PARK2	chr6	161769910	161769932	-	3'UTR	AGCUUUUUUUUCAGCC AUUC
PARK2	chr6	162154068	162154069	-	intron	UU
PARK2	chr6	162167523	162167536	-	intron	GGUUGAUUUUUCUC
PARK2	chr6	162334286	162334295	-	intron	UGCUGAUUUU

PARK2	chr6	162821526	162821533	-	intron	UUUUUACU
PARK2	chr6	162852603	162852604	-	intron	UG
PARK2	chr6	162855079	162855091	-	intron	AUGGAAUGUUUCU
PARK2	chr6	162928436	162928450	-	intron	UUUUUUUGAGAGACA
PARK2	chr6	162935088	162935096	-	intron	UUUCUUUUU
PARK2	chr6	162985385	162985400	-	intron	UGCUGAUUUU
PARK2	chr6	163009421	163009442	-	intron	UGUUUGCUUUUUUUUU UUGUUA
PARK2	chr6	163019891	163019903	-	intron	CUUUUUUUUUUUU
PARK2	chr6	163026764	163026779	-	intron	UUUGUUUUCUUUUUAG
PARK2	chr6	163044012	163044017	-	intron	GUUUUG

Supplementary Dataset 4.1. Predicted binding sites for nELAVLs (nELAVL) in the 3'UTR of human and mouse mitochondrial mRNAs. AU-rich and U-rich nELAVl binding sites were identified by HITS-CLIP (Scheckel et al. 2016). Human and mouse 3'UTRs were aligned using Clustal Omega. Only regions with predicted binding sites are shown.

Mitochondrial Fission Factor (MFF)

Human Transcript: ENST00000304593.14

Mouse Transcript: ENSMUSU00000162003.8

```
Human      UUCUUUGUUUCUGUCUCUGCAUUGUAUGCCAUUUUAUAGUCCACACCCUGAAAAUGUAUU     116
Mouse      UUCAUUGUUUCUGUCUUUGCAUCAUC-------GUAU---GACGGCCCUGAAAAUGUAUU     110
           *** ************ *****  *          ***        ***************
Human      UCUUCCAGAAAGUCUGGAGGAAGGACCUAUAUUUGUAGAAGUAAAGGUAUAUUCUGUCAC     176
Mouse      UCUC-CAGAGUGC---AGGGAAGGCCCUGUAUCUGUAGA-GUGAAGGCCUGUGGUGCUGC     165
           ***  ****  *      ****** *** *** ****** ** ****  * *  **   *
Human      UCAGCUGUAUUCACGUCUGAGCAGUUCUGCAGUAACACCUGCUUAAAAUUCUCCCUUUGC     236
Mouse      UGA------UGGGCGUUCAGCCAGUUGUGCAGUGGCACCUA---UACACUCUCCUUUUGC     216
           * *      *   ***     ***** ******  *****     * * ***** *****
Human      AUGUUUUGUAAAUAGGCUCCAGUUUUGUUUU---UUAAAAGGAAUUUAU--UUUUUGCCU     291
Mouse      AUGUCUUGUAAAUAGGCUCUAGGUUUGUUUUGUUUUUAAAGAAAAUAAUUUUUGUGGCCU     276
           **** ************** ** ********   ** **** ** * **  ** * ****
Human      CAUCAGUCCACCCAACUGAUUCUGAAUGGGAGA----GAGUCUGUAGAGAAUUGAUUCAG     347
Mouse      CACCAGUCUGUACAGCUAAUUCUCUAAACAGAAAUGGCAGU-CAUAAAGAGUGAGUUUAG     335
           ** *****    ** ** *****  *      *     ***   ** *** *   ** **
Human      AAAAGUGUCUGUGAAAGAAAAACAAUUAUUUUGUCCUGUUUCUCAAACAGUGUUAAGCAG     407
Mouse      AAAACUGUCUGUGAAAGAAAA----GUGUUUUGUCCUGUUUUC-AG--AUGAUGAAGCGA     388
           **** ****************     * *************   *   *   * ****
Human      UUUUGUUAAUAGACA-UUUUUGCAUCGACACUUCAACAUUAACACUUUCAAAGUCAUGGU     466
Mouse      UUUCUUUGAUAGAUGCUUUUUGUAUCUACAUCUCAACUGUAAUGCUUUCUAAGUCACAGU     448
           ***  ** *****   ****** *** ***  *****  ***  ***** ******  **
Human      CUGGUGCCAGAUUUAAGAAACUCGAACCACCUAAUAUUUCAUAACCUUCUUCAUUAGGUA     526
```

```
Mouse       GCUGUGCAGGACUGAA----GUCAAACCACCUGACU---------CUGCUUCAUCGCCUA      495
               ****  ** * **     ** ******** *           ** ******    **
Human       CUUGUACAGA--------UUAAUUUCUAACAUUGCAGCAGUUUCAUAUGUGUGCAAUAUG      578
Mouse       CCUGCACAGGCGGGGCUAAAAACUCCUAACAGUUCAGCAGUCU-GUCUGUGUGCAAUGCU      554
            * ** ****           ** * ****** * ******* *  * **********
Human       UGCAUUCUUUCAUUUUAGUUUUGCACUUGGUUUUCUAUAAAGUACGUUUUUACUCAGUUC      638
Mouse       -----------GUUUUGACUUUCAUCUUAGUUUUCUAUCAAGUAUGUUUUUACCAAGUCC      603
                     ****   ***   *** ********* ***** ********  *** *
Human       AUGCGUGAACAAUUUAAAAAACGACAGAAUAAGGUACAAAUGUAGUGUAUUUAAUAAACU      698
Mouse       AUGUGUGAAUGAUUUAAAAACCUAAAAAAUAAGGUAUAAAUGUAGUGUAUUUAAUAAACU      663
            *** *****  ********* * * * ********* ************************
Human       GUCAACCAAAGAA- 711
Mouse       GUCAACCAAAGCAA 677
            *********** *
```

Mitofusin 1 (MFN1)

Human Transcript: ENST00000471841.6

Mouse Transcript: ENSMUSU00000091257.1

```
Human      GAGCCUUUCAUCUUCUUUCUCAAAACUAGUUUUUGAUGCUUUCUUUCAUGGGAAUAGUCA     396
Mouse      --CCUUUUCAUC--CUUUCUCAGUGCUAGUUCUUGAUGCU-UCUUUAAUGGGAAUAGUGA     388
              * *******  ********   ****** ******** ***** ********** *

Human      CUUUUUUAUUUAGUAAAUCGCAUUGCUGGAACCACCAAGGAGUGUGGAAUGUCCUUGAGU     456
Mouse      ACUUGUUU----AUAAGCCGAUUUGCUCAAACC----AGGGGUGUGGGCUGCUCCUGGGG     440
             ** **      ***  **  *****  ****    *** ******  **  * ** *

Human      GUAUUAUUUAUGCAAGUCACAGUCACGUUGCCAUCAUGGCAGCUAUGUGAAACACUAAUA     516
Mouse      GGGUCC-----------UGCAAUCACUCUGUCCUCACAGCAAGGAUGU-AACCACUACUA     488
           *  *               ** ****  ** * ***  ***   **** ** ***** **

Human      AAUGUGUUUUUACU---UUUUAUUCCCGUUAAAACUGAUGUAAAACAGGAUAAAGGCUUG     573
Mouse      AACA-GUUUUUACUUUCUUUUAUUCCCAUUAAAGCUGAUGUGAAAUAGUAACGAGGCCUA     547
           **   *********   ********** ***** ******* *** ** *   **** *

Human      UUA---UAGUCACUUAU-AAGUAUCUGGGUCUAAGUAAUUUCCUUAGAUGUUUCUAAAGA     629
Mouse      UCAUUGUAGCCACGCAUGAAGUAUUUGGGUCUG----CUUUCCUGCUCUCUCUCUUUAGA     603
           * *   *** ***  ** ****** *******      ******    * * ***  ***

Human      AACAUUUUCAGCUUUGCUCCCAUUAUGAUUCCAAUAAGGAACGCUUUCCUAGUGCAAUUU     689
Mouse      CACAUUUUCAGCCUUG-----------AGUCCAGCAAGGAGAGCUUUUCUGCCUAAGUGU     652
            *********** ***           * ****  *****  ***** **     * * *

Human      UAGGAGUAAAGUUUGAAGAGAUAAAAAUAGCCAAAGAUA------GGAGACGUCUGAAUU     743
Mouse      GAAGUGGAAGGUCUGAAGGGGUGAAAUGGGA-GCAGAAAGUGUGUGGAGUGGAGUG----     707
            * * * ** ** ***** * * ***   *    *** *      ****  *  **

Human      UUGAAUGAUAAACAGUGAUGUUUUAAAAAAGCUGUUGUUCUUCAGGAGG-CAUUUGCCUA     802
Mouse      --GAGUGUGGUGCAGUGACUGUGG----CAACUGGU---UCUCAGCAGGACACUCACCGA     758
             ** **     ******   *       * *** *     **** *** ** *  ** *

Human      G-------GAUAUUGCUGGAUUAUACCCCAUUGGAGGCUUUUAAUUUUAUUUGUAUGAAU     855
Mouse      GACCCUGGGCGUGUCCAGGCGU-GUCCCCACUGGAAGCUUUG-AUUUGAAUUACAUGAAU     816
           *       *    * * **  *   ***** **** *****  **** * **
```

Mitofusin 2 (MFN2)

Human Transcript: ENST00000235329.10

Mouse Transcript: ENSMUSU00000030884.10

```
Human      GCACCCAGUCUCGUACCAUUUUGAGCCCUCCAGCACUACUUAUUUUCCCCCACCUUUGCC     177
```

```
Mouse      GCACCCAGUCUUGUACCAGUUACUCCC----------------------UAC-------      118
           *********** ****** **    **                        **
Human      UGCUGUUGCUGGAAGA--GCUGGCUCAUACCCCCAAAGGACACUUUCAGCGACAGCUAUG      235
Mouse      --CCCCUGCAGGAAGACCCCUGGCUCAUACCC-UAAUGGAGACCAACAAGG-----ACUG      170
             *   *** ******   *************  ** *** **   **  *       **
Human      GACAGCAUGGUACCAAGGAGUUAAGUUGA-GGCUUUUUCCAGCUUUCUCUGGUUCAUU--      292
Mouse      GACAGCUCGGCUCCAAGGAGUUAUGCAUGUGUCUGUGUC-UGC-UCCUCACGCUCACCCG      228
           ******  **  *********** *     * ** * **  ** * ***  * ***
Human      --------UGAU----UGCUUGAUAAGG----CCUCAGGAUCUCAGCAUUGCACAAUGCC      336
Mouse      GUUGAAAGUCACUGUGCAUUUGAUAAAGUUUUCCUCAGAAUGGCACC-CUGCAGAAUGAC      287
                  * *        ******* *    ****** **  ** *  **** **** *
Human      UCAUGGAAGCCUUUGAGGGUAUCACACAGACACCCCCACCUUCCUCCAGCCUGUGCGCAC      396
Mouse      UGAUGGGCGCCUUCACAGGCAUCAGGCAGCCACUCCUAC-UUUCUCCAGCCUGAGCACAC      346
           * **** *****    ** ****  *** *** ** ** ** ********** ** ***
Human      CUGCCCUCCUUGCAGCCCAGCACACCUGCAGGUGUAAGG---------GACGAUUGGAGU      447
Mouse      CUACAGA---------GAGACAGUGUUGGGGGUGACAGGAUGCCCCAGAAAAAUUCAGGA      397
           ** *               **    **  ****  ***          *  ***   *
Human      UUCUUCCCAGAG-----AGUCUGUCCCAGAAGGACUGUGGCUUGUGUGUGUCCAUCUCGC      502
Mouse      UACUUCUGAAAUUGCCAUGUUUGUCUCAGAACU--UGUAUCUUGCGUUUGGCCCU-----      450
           * **** * *       ** **** *****    ***  **** ** ** ** *
Human      CUGUUGGCUCAGUGCUUCAUCCCAUUUGCAGAGCCUCAGACACGU-CUUGGUGGUGAGGC      561
Mouse      ---CAGCUUUAGCACUUUUUCCCACUUGCAGAGUCUUUCAGUUGUGCUUGGUAGCCAGGC      507
                *  * **  ***  ***** ******** **   *   ** ****** *  ****
Human      UCAGUUACCCCUGGGCUUAGGCUGAGGCGGGCCCUGUGCUGGGGGUGGUAGAAAGGAUGC      621
Mouse      UCAACACACCGGGGCUUUAGACUCAAGCAGCUUAUAUG----------------GGAAGC      551
           ***     **  **  **** ** * ** *    * **               *** **
Human      UGCUG-----AGGCAGCUGGAGGAGUGGGAGUAGCUCAGAGG--GGAG-GGCUGUUGGAU      673
Mouse      UGGAGACCCCUGCCAGCCAGAGCACAGUAA-GGGCUCGGAGAAGGUAUGUGAACUAGGGU      610
           **  *      * ****  *** *  *  *   **** ***   * *   *   * ** *
Human      GUAUGGGGAGCUGGCAGAGCAGGUGGCAGUCACUGGGACAAGGAGGGACUUGCCUCUCUU      733
Mouse      AUCUGAUGUGGUAGUGCAGUUGGUGUCUGGCAUUGUGACGACAAGGGACUUGCCUCCCUU      670
            * **  * * * *   **  **** * * ** ** *** *  ************* ***
Human      CUCAUUAUUGUGUCCUUUGCUUUAGUGUCAGUCCUGGACUUGUGCAGGCCUGUUUUGUGU      793
Mouse      CUUGCCACUGAGGCCCUUGCUUUUCCUUCAGCUCUUGGCCUGUUGG-UCCGGUUU-----      724
           **    * ** * ** *******    ****  ** * * ***     ** ****

Human      AGAUCUGUUUUGGAAGAUGGCAUGGUCUAGGUGGUUGAAGGAUGUAGUAGAAGGAUGGAU      853
Mouse      -----AUUAGUGAGAGCUAGUUUGCUCCAGGUGGUUAAAGGAUGUAGCAGGAG---GAAU      776
                  *  **  ** * *  ** ** ******** ********** ** **   * **

Human      GGUGGAAGGUGGGGACGUUGGUGGCUGGCUGAGGUGCAUGGGCCCCACACAGGACAGCUG      913
Mouse      GGUGGAAGAUGGGAGCU-----GCCCGGGUU-------------------AGUACAGA--      810
```

```
          ******** ****  *      * * ** *                    ** ****
Human     GAGAAUGGGCCGUCCACUUGGCCUCGUUCUGCGAGGGGCUCAUGGGUCUGAGAGCCCCCA     973
Mouse     ---AGAGGUCUGUCUAUCUGACCUAGCACUG--AGGGGUUCACAAACCUGUGAGGUGCAC     865
             *  ** * *** *  ** *** *  ***  ***** ***     *** ***   *
Human     CCCACUAGGCUUGAUUGCAUCCCUGUUGUGCCCUUUAAGAGACAUGUUUCCACCCCACCC     1033
Mouse     CUCACUAAUUUUGGC-UCAUCCCUGCCUUGC--UACAAGCUCCCUGUGGCCACC------     916
          * *****   ***    ********   ***  *  ***   * ***  *****
Human     CCAACCUUGUCCCAAGUGCCCUGGACUAAAUUUCCUGUGCCAGUGACUGCAGUUGGCCAA     1093
Mouse     ---------------AUUCUCUGGACU----GUACCGUGCUGAUGACUGCAGCUGGCUAC     957
                        * * *******     * * ****   ********* **** *
Human     GGGACAAUGUGGAAAACC---CAGUGUCCAU-----CUUUCCACCCUCC----------C     1135
Mouse     AAAACAGCAUGAGAACCUGGCCGCUGUUCUCCUACUGCCUCCACCCUCAGGCAGGCCUCC     1017
             ***   **  ** *    *  *** *          *********          *
Human     UGAUCU------CCAGAA------------------------------CCUUCGACUGA     1158
Mouse     UCCUCUUCUGCCCCUGAAGCCUCCUGCUGCUUGCUCCUCCUGCCUCCACCCUCAGGCAGG     1077
          *  ***      ** ***                                  ***  * * *
Human     CCCCCUU-----------------------------------------GUCUUUAUGCU-     1176
Mouse     CCUCCUCCUCUUCUGCCCCUGAAGCCUCCUGCUGCUGCUCCUCCACCUCAGUCAGUGCUG     1137
          ** ***                                             *   ****
Human     --------GAUGUUGAGUUUUGGGAUUGUUACUGGUUGAAGUGGGGGGCAGAUGCCUGUCA     1228
Mouse     AACUUCUCACUGUUGAGUGUUGAAAUUGUUAAUGGUCAAAGCAG-GGAGGAUGCCAGUCA     1196
                    ******** ***  ******* ****  ***  * **  ****** ****
Human     CCAAGGUGUUGACUGUGUGAGAAAAGCAGUUU--GGGUGACAAAUCCUGUGUGGCACAAG     1286
Mouse     CCAAGG--UUGAUUGUCUUGGGAAAGCAGUUUUAGAGUGAUGAAUCCUUUGUAGGACAGG     1254
          ******  **** *** *  * **********  * ****  ****** *** * *** *
Human     UUGGAUCGCUUCCUAGAAAUAAGCAACACCUCUCCCAAAAAGCAGCCCACAAGGCAGGGG     1346
Mouse     UA-GAGAGUAUCUUAGAGAUAAAAAAA---------------------------------     1280
          *  **  *  ** **** ****  **
Human     CCCAGCAGCCCAGCCAUCACUCAUCUUUGAGGAAAUGAGUUGGUAGCCUCUGUGCACUGU     1406
Mouse     ------------------------------------UG--------GGCUAUGUCCUCU--     1295
                                              **        * ** *** * **
Human     UUGGUGGCCACAUCACAGGUGAUGUCCUGUUCACAUACCUGCUUGUAUUUAAAGCCCUCA     1466
Mouse     --CCUG------------CCCAUGUCUUGUGCUCACU--------------CGCCCCUCA     1327
              **               ***** *** * **                   ******
Human     GUCUGUCCUGUUGUGUGGGGCGAAGUGAUGGACUCUGCCAG-GUGGACAUGCUGUGGGUG     1525
Mouse     GUCUACCCUUUUUGCUGGG--ACAGUGAUGGUCUUGGCCAAGGUCAGCAUGUAAUGGAAA     1385
          ****  *** **   ****    ******** **  ****  **   ****   ***

Human     GAUGUUCCCGGCGUGUGCCGGGCCUGAAUGGACAGGGGCCACUUCACAGCAUGUCAG-GG     1584
Mouse     GA------CAGUGUAUUGCCAGGCUGGAUAGAU-GGGGUCAUCUCACAGUGGGUCACGUG     1438
          **      * * ** *  *  * *** ** **  **** **  ******   ****   *
Human     AAAAUCACUGUCACACAAUUCCAAUGGAUUUUGUGCUCUUUUUGAAAAAAAAAAAAUUCUU     1644
```

```
Mouse       AAAAUCAGUGUCACGUAGUCCCAGUGAAUGUUGUGUUCUUUCUGGGGGGAGG--GGGGAA     1496
            ******* ******  * * *** ** ** ***** ***** **     *
Human       UAGCGUAAACAUGAAUUUUUUUUUCAAUGUAGCCCCUGGGGAAUGAAUGAAAUUUUGAGCU     1704
Mouse       UAGAAUAAACUCAAAUUCUUUUUCAGUAUAGCCCCUGAGUAAUGAAUGAAAAUUUGAGCU     1556
            ***  *****   **** ******* * ********* * ********** ********
Human       UCUUCAAUACGUAAAAUUAAAUUUAUACCACUGAGGGAGAGACCCUUUCUGAAAGAAGUA     1764
Mouse       UAUG---UAAGUAAAGAUUCAUUUAUGCCACC-AGGGAGAGCCUGUAUCUGAGAGACAUU     1612
            * *    ** ***** *  ****** ****  ******** *  * ***** ***  *
Human       UGGCCAAAAGCACUUUAAU-----GCUGCUGACAUUGUUGUUUUUAUGUUCAUUUGCUGG     1819
Mouse       UAGCAGAGAGCACUUUAGUUUUUUGCUGCUAACU--GU----UGUGUGAUCCUUUGCUGG     1666
            * **  * ********* *     ****** **   **    * * ** ** ********
```

Optic Atrophy 1 (OPA1)

Human: ENST00000361510.8

Mouse: ENSMUSU00000160597.8

```
Human       UUUGUCCAGCCUCUUUUCUUCUGCUGUUCCACCUUUCUAAACAUACAAUAAAGUCAUGG     115
Mouse       UUUGUCCUGCCUCCUUCCUC---CCGUUCUACCCUUUUCCGUGCAAAAUAAAGUCACAG     115
            ******* ***** *** **    * **** *** ** *      * **********  *

Human       GAUAAAAAUAAUCGAUGUAUGUUACGGGCGCUUUAACCAUCAGCUGCCUCUCGAAUGGAA     175
Mouse       GGUAAAAGUCAUGUACGUGUGUUCCAGGCACU-UAACCUGCAGCUGCCGUUUGAGCAGAA     174
            * ***** * **  * ** **** * *** ** *****  ********  * **   ***

Human       GAACAGUGGUAAUGG-AUUAACAUCCUAUUUUGUUGUACUAAAGUGACAAAUCGGAAUAA     234
Mouse       GAGCCCUGGACGUGGCAUCCACGGUCUGUGAGCUCGUGCUGACGGCAGACAUUGGGAAAA     234
            ** *  ***   *** **  **   ** *    * ** ** * *  * * ** ** * **

Human       UAUAAUUGGUAUGGCCAUUAGGUUCAGUCCUUGAAGAUAAGAAACUUGUUCUCUGUUUGU     294
Mouse       CAUCACUGGUGUGGCCGUGAGGCUUAGUCCUCAGAGAUUAAGAAGUUGCUCUCUGA----     290
             ** * **** ***** * *** * ******   **** *  ** *** ******

Human       UGUCUUAUUUGUGGUGGCACUCGUUUAAUGGAUUAACUGAGGUUGCUCAAUGUUCAGUUU     354
Mouse       -GUCGUGUUUGUGGUGGCACUGAUGUGA----UUCACUAUGGCUGG--------------     331
             *** * ***************  * * *    ** ***  ** **

Human       CUUUUCCAGAAAUACAAUGCUAGGUGUUUUGAAAUAAAACUUAUAUAGCAAUUGUU-UAA     413
```

```
Mouse       ---UAUCACACGUACAGUGGUAGCUGCUCUGGAAUAAAACUUAC--AGUAAUUUUUUAAA      386
               *  ** *  **** ** *** ** * ** ***********   ** **** **  **

Human       AGUUAUCAAUUGUAUAUAA---AAUCACAGUAGCCUGCUAAAUCAUUGUAUGUGUCUGUA      470
Mouse       AGGCAUCAAUUGUAUAUGACAAGAUGACAGUU-ACUGCUAAACCAUCA----UGUCUACA      441
            **  ************* *    ** *****   ******** ***      *****  *

Human       GUAUUCUAUUCCCAGAAACUAUUUGACCAUGAUAAUUCAGUUUAUAUUCACCACAUGAAA      530
Mouse       GUGUUCUGUAUUCAGGAACGCUUUGACUGUAAACACUCAGUUUAUGUUCACCACAUGAAA      501
            ** **** *   *** ***  ******  * *  * ********* **************

Human       GAAAAAUGGGUAACAGAAGAACCCUUAAAACAGGUUAAUUUGGAUUGUAA----------      580
Mouse       GAAAGCUGGUUUAUAAACAGAUGCUUCAGCUGGGUUAAUUUAUGUUGGGCAGUUCAGUGU      561
            ****  *** * * * *   *  *** *    *********   ***

Human       -CGUUCAGUGAAAGAAAUUUCAACCCUUCAUAGCCAGCGAAGAAAUUUGCCUUGGAAGCC      639
Mouse       AUAUUCAGUGAAAGAAACAUCCACCCUCCAUUGCCAGCUUAGAAACUCGCCUUGGAAGCC      621
               **************  ** ***** *** ******  ***** * ************

Human       AAGUCAGUACCAGCUUACCUAUUUGAUUCAGUUGCUGUUUUCUCACUCUCUAUAUCCAUU      699
Mouse       AAC--CGCAGCAGCGUGC-------AGUCCAUCGCUGCUUUUGC--GCCCUGUAUCCGUG      670
            **    * * **** * *       * **  * **** ***  *   * ** ***** *

Human       UGAAAUUGAUUUAUUUUAGAUGUUGUAUACUUA-CGUUAGGCUUUCUGUUAAUAGUGGUU      758
Mouse       UGCACUUAGUUCAGUUUGAAUAUUGUGUGCUCUCAGUCAGGCUUUCUGGAA-CAGUAGG-      728
            ** * **  ** * ***  ** **** * **    ** **********  *  *** *

Human       UUUCUCCUGUUGACAGAGCCACCGGAUUAUGACACAGGAUGAGGAAGAUUAAGGAUAAUC      818
Mouse       UCUCUCCUGGUGACACAGCCAUUGAAUUAUGACCCACGCUGGAGAAGACUAAAGACCACC      788
            * ******* ***** *****  * ******** ** * **  ***** *** **  * *

Human       AAUUGACUAAUUUCAUUUAGAAUAUUAUCAAACAUUUCAACUAGGUAUCAGAAAAAGGCU      878
Mouse       AGUUGACGAAUUUCAUUUAGAGUGCUAUCAAAUGUCUGAACUAGGCGUCAGGGAAAGGUU      848
            * ***** ************* *  *******  * * *******  ****  ***** *

Human       UUCUU------UCAUAAGACUAUUUUAAAUAGAAAUUAUUUCAACAAUUAAAGUAAUGUU      932
Mouse       UCACAAUAGCCCUCAAACACUAUUUUAAAGAAAAAUUAUUCUAACAAGGGAA-AAAUGUU      907
            *              ** ********** * ********  *****   **  ******

Human       GACCAUCCCCCUCUC--AGCUGAAUAAAGAAAAAUUUAGUUCAAUUUAUUGCAAUUUAAU      990
Mouse       GACCCACUCCCACUUAAAGCUG--------AAAAUUCUGUUUAAUUCAUUGCAGUUAUAG      959
            ****  * *** **   *****        ******  *** **** ****** **  *
```

```
Human       UACAAUACUACCUUCACAACAUUUUCAUGUGUUUUAAAUAAAUAUUUUUUAAUUGGCUAA      1050
Mouse       UA----AUAACCUUCAUAAUAUUUUCAUGCGCUUUAUAUAAAAU----UACGUUGGUUAA      1011
            **    *  ******* ** ********* * **** *****      *   **** ***

Human       AGGACAUUCAAGCAAAGAAAUGCU--UUCUUUACUUAAAAUGUCUAUCUCAUUUGCUGCC      1108
Mouse       AAAAGCUUAAGGCAAACA-GUACUUCAUAUUUACUUCAAAUGUCUUUUUCAUCUGCCACC      1070
            *  *  ** * ***** *  * **   * ******* ******** * **** ***  **

Human       UU-UUCACUAAGCCUUUACUUUGUUAAUAAAAGUGUCCAUUGUGUGAUGUUUUUGAUUUU      1167
Mouse       UUUUUUAUUAAGGCUUUACUGUUCUGGUAAAAACACCCAGGGUUGC-AGUUCUU--AUUU      1127
            ** ** * **** ******* *  *  *****    ***  **     *** **   ***

Human       ACAGUUUGC--UAAAUCUUAUUUUCUUGGAGUUGCUUUUUGGUAACAGCCCCAUUGCUAC      1225
Mouse       ACAGUUAAUUUUAUAACCAGUUUCCUUGGAAAUGUUUUU----------------------      1166
            ******     ** * *   *** ******  ** ****

Human       UCCCCAUUUUAUUGUUUUACAUCAAUGCAUGCUUCGUUGUGAUCCCUCAAGAUGUAACAC      1285
Mouse       ----------G---------------------UUUAUGAUUCCCUCGAAUCUGACAG      1192
                      *                     ** **** **     ** * ***

Human       UUGGUAUGCUCGGUUGAGGAUAUGAAAAAAUACUUCCGAAACCAGGAAUUCAAUGUAUGU      1345
Mouse       U----AUGGAAGG------------GGCAGUGUUUCAGAAACCAUGAAUUCAAUAAGUAC      1236
            *    ***   **               * *  *** ******* *********   *

Human       UUGUUUUAUACUGUUUGAUAAGAAAAGUAGGUCCAGCCUUAAGC-------AGCACAGAU      1398
Mouse       UCUAUUUAAA-UUAUCAAUAAGAAGCCUGGGUGCAAUUCUCAGAGCUACGACGAACAGUG      1295
            *   **** * *  *  *******   * *** **    * **         * ****

Human       GCGCUGGUAGAUGCAUAGUCAGGAACUUUUUUUAUUUCUUUUAGGUCUAGGGACAGGAGU      1458
Mouse       ---CC----CAUCCUUCCCUAGGACAAAUGU--GCAGGUUGUAGGUGU-GGGACAGUAGC      1345
               *      ** * *    ****    * *       ** ***** * ******* **

Human       GAAUAGAAAGGGAGGAGAGCUCUAUUAUGUUCUAUACACAGAUUAGGAGAUGACCUUACU      1518
Mouse       GAACAGAAGCUCUAGAGAGCCCUGGGCUGAUUCCCACAGCCAUGAGGAUAUGCUCGUCCU      1405
            *** ****      ****** **    ** *    ***   ** **** ***  * * **

Human       GGGUACAC-CCCUCUAACCAGUGCU---------UACAGGUUAAUGCAUGUUAAUGAAU-      1567
Mouse       AAGCCAGUGGUCCUCAACCUGUGGGCCAAGAGCACUUUGGGGGCUGCAUAUCAGCUACUU      1465
              *        *   **** ***              **    ***** * *   * *

Human       AUUUUUGCAGUUGU-------AAAGCAUAACAAUUAC-----AACUACACAUCUAUUUC-      1614
```

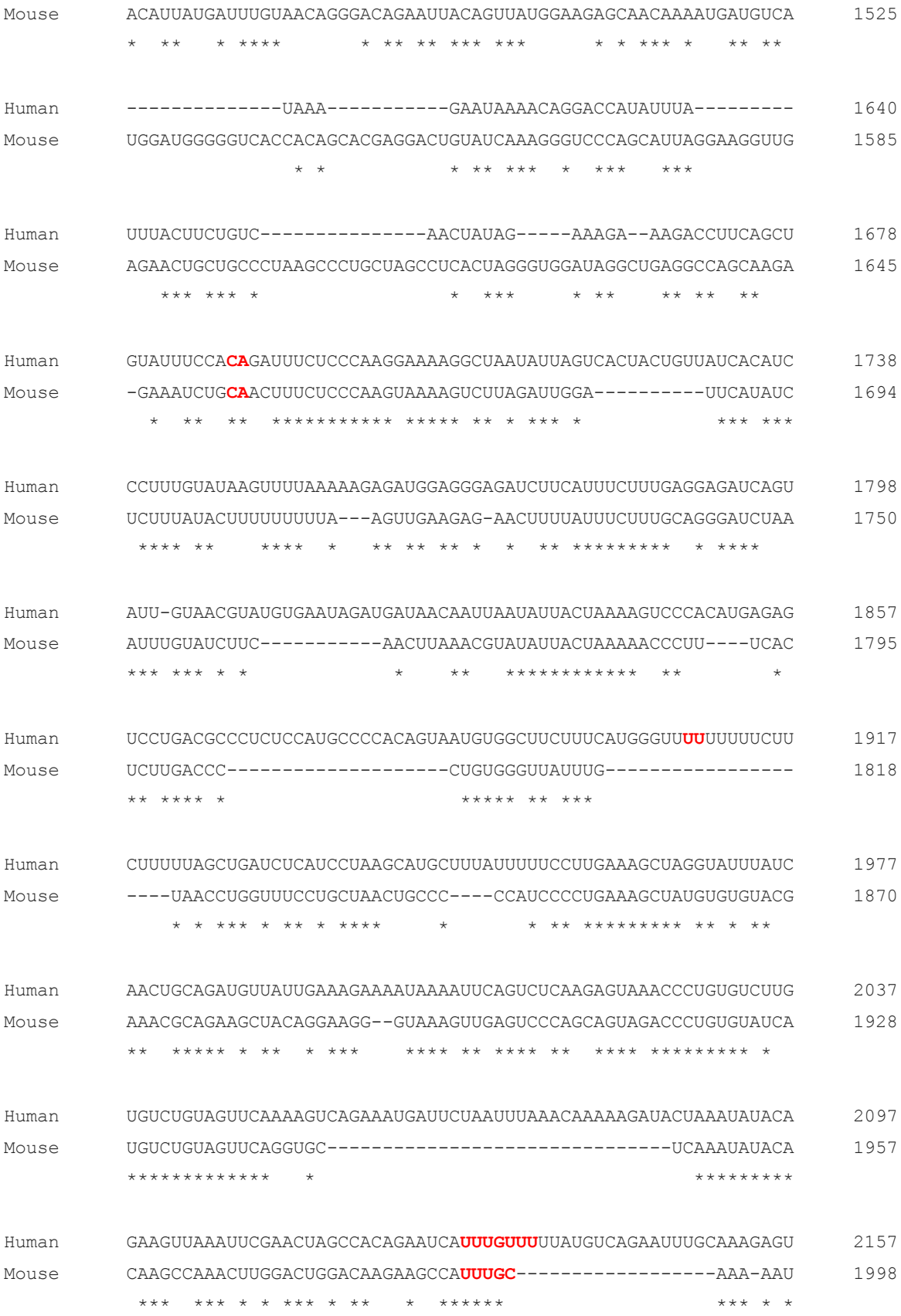
Mouse ACAUUAUGAUUUGUAACAGGGACAGAAUUACAGUUAUGGAAGAGCAACAAAAUGAUGUCA 1525
Human --------------UAAA-----------GAAUAAAACAGGACCAUAUUUA--------- 1640
Mouse UGGAUGGGGGUCACCACAGCACGAGGACUGUAUCAAAGGGUCCCAGCAUUAGGAAGGUUG 1585
Human UUUACUUCUGUC---------------AACUAUAG-----AAAGA--AAGACCUUCAGCU 1678
Mouse AGAACUGCUGCCCUAAGCCCUGCUAGCCUCACUAGGGUGGAUAGGCUGAGGCCAGCAAGA 1645
Human GUAUUUCCACAGAUUUCUCCCAAGGAAAAGGCUAAUAUUAGUCACUACUGUUAUCACAUC 1738
Mouse -GAAAUCUGCAACUUUCUCCCAAGUAAAAGUCUUAGAUUGGA----------UUCAUAUC 1694
Human CCUUUGUAUAAGUUUUAAAAAGAGAUGGAGGGAGAUCUUCAUUUCUUUGAGGAGAUCAGU 1798
Mouse UCUUUAUACUUUUUUUUUA---AGUUGAAGAG-AACUUUUAUUUCUUUGCAGGGAUCUAA 1750
Human AUU-GUAACGUAUGUGAAUAGAUGAUAACAAUUAAUAUUACUAAAAGUCCCACAUGAGAG 1857
Mouse AUUUGUAUCUUC----------AACUUAAACGUAUAUUACUAAAAACCCUU----UCAC 1795
Human UCCUGACGCCCUCUCCAUGCCCCACAGUAAUGUGGCUUCUUUCAUGGGUUUUUUUUUCUU 1917
Mouse UCUUGACCC--------------------CUGUGGGUUAUUUG----------------- 1818
Human CUUUUUAGCUGAUCUCAUCCUAAGCAUGCUUUAUUUUUCCUUGAAAGCUAGGUAUUUAUC 1977
Mouse ----UAACCUGGUUUCCUGCUAACUGCCC----CCAUCCCCUGAAAGCUAUGUGUGUACG 1870
Human AACUGCAGAUGUUAUUGAAAGAAAAUAAAAUUCAGUCUCAAGAGUAAACCCUGUGUCUUG 2037
Mouse AAACGCAGAAGCUACAGGAAGG--GUAAAGUUGAGUCCCAGCAGUAGACCCUGUGUAUCA 1928
Human UGUCUGUAGUUCAAAAGUCAGAAAUGAUUCUAAUUUAAACAAAAAGAUACUAAAUAUACA 2097
Mouse UGUCUGUAGUUCAGGUGC------------------------------UCAAAUAUACA 1957
Human GAAGUUAAAUUCGAACUAGCCACAGAAUCAUUUGUUUUUAUGUCAGAAUUUGCAAAGAGU 2157
Mouse CAAGCCAAACUUGGACUGGACAAGAAGCCAUUUGC-----------------AAA-AAU 1998

```
Human      GGAGU-------------------GGACAAAGCUCUGUAUGGAAGACUGAACAA-CUGUA      2197
Mouse      GGAGUGGAUAGGUUUUUCUUUUUUAGACAAAAUUUUAUUUGGAGAACUAAGGGAUUUUUA      2058
           *****                  ******  * * * ****  *** *   *  * **

Human      AAUAGAUGAUAUCCAAACUUAAUUUGGCUAGGACUUCAAUUUUAAAAAUCAGUGUACCUA      2257
Mouse      AAUACAUCAUAAGCAAAAUGA-CUUGGUCAGAAUGUCAGUUAUGAA--------CCCCUA      2109
           **** ** ***  **** * *  ****  ** *  *** ** * **          ****

Human      GGCAGUGCACAGCACGAAAUAAGUG----GCCCUUGCAGCUUCCCCGUUUAACCC----A      2309
Mouse      GUCUGUGUGCAGCAUGAACCACAGGAAGCAAGCUUGCUGCUUCAGCCACACACCAAGCAA      2169
           * * ***  ***** ***  *   *       ***** *****  *     ***     *

Human      CUGUGCUAUAGUUGCGGGUGGAACAGUCA--ACCUUUCUAGUAGUUUAUGAUAUUGCCCU      2367
Mouse      UCUUCAGUUAGUUACAGGUGCAGCAGUCUGGGCCUUCCUCUUCGUCUCU--------CCU      2221
              *    ***** * **** * *****    **** **  * ** * *        ***

Human      CUUUGUAUUCCCAUUUUCUACAGUUUUUUCCGCAGACUUCUUUCUGCAAAUUAUUCAGCC      2427
Mouse      CAUCG-GGCCCCGUUUUCCAGGCUGUAGUCAGUGGACUC----CCACAGAUUCCUCAGUG      2276
           * * *    *** ***** *   * *  ** *  ****     *  ** ***  ****

Human      UCCAAAUGCAAAUGAAUGAUAUAAAAAUAAGUAGGGAA----CAUGGCAGAGAGUGGUGC      2483
Mouse      ACCAAAUGGAAAGGGUUGGUGUGGAAGCAAGUGAGACUUCCUAACUGUACAGCGUGGGAU      2336
            ******* *** *  ** * *  **  ****  *        *  * * ** ****

Human      UUCCCAGC----------------------------CUCACAA------------------      2498
Mouse      GUCACAUGCAGGAUUCAGGUGGCAGAAGCAGGACAGUCACAAGUCAAAGGCAAGCCUGAG      2396
            ** **                               ******

Human      -----------------UGUGGGAAUUUGACAUAGGAUGAGAGUCAGAGUAUAGGUUUAA      2541
Mouse      CUACAUAGGGACACCCCUGUCUCAAAAACAAAAAUAACAAAAUUAAGACUUUAGGCUCAG      2456
                        ***   **    * * *  *  * * * *** * **** * *

Human      AAGAUAAA-AUCUUUAGUUAAUAAUUUUGUAUUUAUUUAUUCUAGAUGUAUGUAUCUGAG      2600
Mouse      AAAGCAAAUUUCUUAUGUAGUUAAUUUUGUAUUUAUUUAUUUCAGAUGUAUUUAUCUGAU      2516
           **   ***  ****  **   ********************  ******** *******

Human      GAAAGAAAUCUGGUAUUUUUGCUUUCCAAUAAAGGGGAUCAAAGUAAUGGUUUUUCUCUC      2660
Mouse      AAAAGAAACUU---UUUUUCUCUCUCCAAUAAAUGAGAUCACGGUACUGGUGUGU--CUC      2571
            *******  *    ****  ** ********* * *****  *** **** * *  ***
```

```
Human       AGUUCUCUAAGCUGGUCUAUGUUAUAG---------CUCUAGCAGUAUGGAAAUGUGCUU      2711
Mouse       CAUCCUCUACGCUGGUGUAUGGUAGAUUGUCUUAUACUGUAGCAA-CUGGAAAUGUGCUU      2630
              * ***** ****** **** ** *          ** *****   *************

Human       UAAAAUAUGCUUACCUUUUGAAUGAUCAUGGCUAUAUGUUGUUGAGAUAUUUGAAACUUA      2771
Mouse       GAAAAUAUGCUUACCUUCUAAACGAUCAUGGCUAUUUGAUAUCUAAAUAUUUAAAACUUA      2690
             ***************** * ** ************ ** * *  * ****** *******

Human       C-CUUGUUUUCACUUGUGCACUGUGAAUGAACUUUGUAUUAUUUUUUUAAAACCUUCACA      2830
Mouse       ACCAUGUCGUCAC-UGUGCACUGUGAAUGGACUUUGUAUUAUUUUU---AAA-CCUUACA      2745
              * ***  **** *************** *****************   *** * * ***

Human       UUACGUGUAGAUAUUAUUGCAACUUAUAUUUUGCCUGAGCUUGAUCAAAGGUCAUUUGUG      2890
Mouse       CUCGAUGUAAAUGUUACUACAACUUAUAUU-UGCCUGUGCUUGACCUAAGGUCAUUUGUG      2804
             *   **** ** *** * *********** ****** ****** * *************

Human       UAGAUGAGUAAUUAAAAAAUAUUUAAAUCACAUUAUAAUUCUAUUAUUGGAGAGCAUCUU      2950
Mouse       UAGAUGGGUAAUUAAAGGAUACUGAAGUGAUAUUAUGAUUCUAUUAUUGGAGAGUAUCUU      2864
            ****** *********  *** * ** * * ***** ***************** *****
```

Optic Atrophy 3 (OPA3)

Human: ENST00000263275.5

Mouse: ENSMUSU00000063976.9

```
Human       AAGCCAAGAAACAGGUUCUGAAACUUUUCUUUUCUUCUUUUCUCUUCUUUUUUCUUUUCU      3347
Mouse       AACC---------AAUACUGAAACUGUACCUCAGUUU----C--UU--------------      2100
            ** *           * ******** * * *   **     *  **

Human       UUUCUUUCGGAGACAGUCUAGCUCCGUCACCCUGACGGAGUGCAGUGGUGCAAUCUCGGC      3407
Mouse       -----CUAGAAGAAGCUGAAGU------------------UGGUGUCUUUAAAUUUAGGA      2137

                  * * ***   *  **                  **  **  *  *** * **
```

Parkin (PARK2)

Human Transcript: NM_013988.3

Mouse Transcript: NM_001403470.1

```
Human ACAUGGAUUGGAUUUCAGUUCAAUCAAACUUUCAGCUUUUUUUUUCAGCCAUUCACAACAC      1225
Mouse ACAUGCAUCACACUCAAGUG---UUAAUCUUUCAAGGUUUUCUUUUCUUUUUCC------      1046
      ***** **   * *  ***    * ** ******   **** **      ***
```

4.6 Materials & Methods

Mice

C57BL/6 *HuD*$^{-/-}$ mice (Akamatsu et al., 2005) were generated and gifted by Hideyuki Okano (Keio University, Tokyo). Experimental mice were bred by crossing HuD heterozygous mice to generate wild type, heterozygous, and knockout mice in the same litter. Note that the data were derived from the same cohort of mice used in the studies described in Chapter 2. Therefore, the mice were crossed onto the C57BL/6 (J) background used to generate Lrrk2 G2019S mice. Only mice wild type for Lrrk2 were represented in the data. Mice were fed the Envigo Teklad rodent 2018 standard chow throughout the studies.

MRI and Indirect Calorimetry

EchoMRI: The EchoMRI measures fat mass, lean mass, and total water in the body. Fat mass includes the mass of all fat molecules in the body. Lean mass includes muscle tissue and all organs. It excludes fat mass, bone minerals, and any other tissues that are not detected by the NMR signal. Each mouse was evaluated by EchoMRI for a 40 second scan. Mice were conscious during the procedure. Indirect calorimetry: The Comprehensive Lab Animal Monitoring System (CLAMS; Columbus Instruments) was used to measure oxygen consumption, energy expenditure, food intake, and physical activity in the same cohort of mice at 4 months of age, and again at 8 months. Mice were individually housed in CLAMS chambers at thermoneutrality (28-30°C). Gas exchange and motor activity were automatically measured every 26 min over the 72-hour test period. The mice were acclimated to the cages for the first 48 hours and data from the final 24 hours were plotted for analysis. WT and *HuD*$^{-/-}$ mice were randomized and an equal number of mice from each genotype were tested simultaneously for each CLAMS run.

Glucose Tolerance Test

Mice were individually housed in cages with cotton bedding and fasted for 6 hours (4-month-old mice) or 16 hours (8-month -old mice). Each mouse was administered 2mg/g body weight of 20% glucose solution by oral gavage. Saphenous vein bleeds were used for samples and measured using a glucometer at 0 min, 15 min, 30 min, 60 min, 90 min, and 120 min post-gavage.

Pulse Oximetry

The oxygen saturation measurements were conducted at 12 months of age. Mice were anesthetized with isoflurane and the Mouse Ox Plus® oximeter sensor (Starr Life Sciences Corp.) was placed over the shaved, right thigh of each mouse to detect blood oxygen saturation of the femoral artery. Arterial blood oxygen saturation, heart rate (beats per minute), and respiratory rate (breaths per minute) were recorded for a minimum of 30 seconds using the Mouse Ox Plus® Premium Application software.

RNA-immunoprecipitation

Tissue used for RNA-immunoprecipitation (R-IP) were lysed in R-IP buffer [50 mM Tris, (pH 7.4), 150 mM NaCl, 1% NP-40 and 1X cOmplete ™protease inhibitor cocktail (Catalogue # 4693159011)] tumbled for 20 min at 4°C and centrifuged at 10,000xg for 10 min. Supernatants were pre-cleared using 10 uL wet volume of Dynabeads ™Protein G magnetic beads (Catalog # 10004D, Thermo Fisher). RNA-protein complexes were immunoprecipitated using 750-1000 ug of pre-cleared supernatants incubated with 4ug HuD (sc-48421, Santa Cruz) antibody vs. mouse IgG control for 2 hours at 4°C. RNA-protein complexes were captured by adding 25 uL wet volume of beads and tumbled for 1 hour at 4°C. Complexes bound to beads were washed (3 min x

5) in wash buffer [50 mM Tris, (pH 7.4), 150 mM NaCl, 0.1% NP-40] and resuspended in wash buffer. Ten percent of IP was used for western blot detection and remaining beads were resuspended in TRIzol for RNA isolation following manufacturer's protocol.

RT-qPCR

Equal volumes of RNA from control and experimental immunoprecipitates were used to generate cDNA using the iScript cDNA synthesis kit (Catalogue 170-8891, BioRad). For total RNA, 500 ng of RNA was used in a mMulv RT cDNA synthesis reaction. qPCR was performed using GoTaq ® qPCR master mix (Catalogue A6002, Promega). The cycling conditions were as follows 95°C, 2min, [95°C for 15 sec, 60°C for 1 min,] x 40 cycles. RNA levels from experimental immunoprecipitates were normalized to IgG control and expressed as a fold change relative to IgG R-IP. RNA levels were normalized to band intensity of respective IP to control for the amount of immunoprecipitated proteins between control and experimental groups. Total RNA was normalized to housekeeping genes Gapdh and Actb. Fold change was calculated using the $2^{\wedge -\Delta\Delta Ct}$ method. Primer sequences are in Table 4.6.1.

Western Blot

Mice were euthanized at 12 months of age and tissues were harvested for western blot analysis. Tissue samples were lysed in RIPA buffer [50 mM Tris, pH 8.0, 150 mM NaCl, 0.5% sodium deoxycholate, 0.1% SDS, 1% Triton X-100, and 1X cOmplete ™protease inhibitor cocktail (Catalogue # 4693159011)], tumbled for 20 min at 4°C, and centrifuged at 10, 000xg for 10 min. Supernatant concentration was estimated using the RC DC ™ Protein Assay (Catalogue 500-0122, BioRad) and diluted in Laemmli sample buffer. Samples were run on 10% polyacrylamide gels

and transferred to PVDF membranes. Membranes were blocked in 5% milk for 1 hour at room temperature and incubated in primary antibody overnight followed by secondary antibody for 1 hour at room temperature. Images were obtained using the Image Quant LAS4010 Biomolecular Imager (GE Healthcare). Protein quantification was performed using Image J (Fiji) to calculate mean band intensity normalized to the mean intensity of a housekeeping gene. Antibodies used are found in Table 4.6.2.

Statistical Analyses

Statistical analysis was performed using GraphPad Prism 9. One sample t-tests were performed when comparing to a no-variance control group. Two-tailed t-test with Welch's correction was performed when comparing two independent groups. All other data were analyzed using a Two-way ANOVA (analysis of variance) with Holm-Sidak post-hoc test. All data were represented as mean ± SEM. Statistical significance was represented with the following notation: *$p<0.05$; **$p<0.01$, ***$p<0.001$, ****$p<0.001$.

Table 4.6.1 Primers

Gene	Assay	Primer Sequence (5'-3')	Citation
HuD	Genotyping	HuD3- CAC AGC CCA GTC TCT CTG CTC CAT C (both reactions)	(Akamatsu et al., 2005)
		RT3- TGA ATT CCT CTT GGG TCA TA (WT reaction)	
		PGK2- AAG GGC CAG CTC ATT CCT CCC ACT C (KO reaction)	
Actb	qPCR	F-ACTGCCGCATCCTCTTCCTC	
		R- GGATGCCACAGGATTCCATACC	
Gapdh	qPCR	F- ATGGCCTTCCGTGTTCCTACC	
		R- GTAGCCCAAGATGCCCTTCAG	
Mff	qPCR	F-GGCCCAGGGGATAAAAGTGG	
		R-CTGCCCCACTCACCAAATGT	
Mfn1	qPCR	F-CAGGGACGGAGTGAGTGTCC	

		R-GTTTCTGCCATTATGCACCTGG	
Mfn2	qPCR	F-GCTTGGACAGGTGGAGTCAA	
		R-GGACTCGAGGTCTCCTCTGT	
Opa1	qPCR	F-CAGGAGAAGTAGACTGTGTC	(Sarzi et al., 2018)
		R-TGTGACTTTATTTTGCACGG	
Opa3	qPCR	F-AGCTGTTCTACTTGGGCATCC	
		R-CAGTGGTACAGCTGGGCT	
Park2	qPCR	F-AAGAAGACCACCAAGCCTTGTC	(Palomo et al., 2018)
		R-CAAACCAGTGATCTCCCATGC	
Pink1	qPCR	F-AGACTCCCAGTTCTCGCCT	
		R-AGGGACAGCCATCTGAGTCC	

Table 4.6.2 Antibodies

Protein	**Dilution**	**Vendor**	**Catalogue#**
β-Actin	1:10,000	Sigma	A5441-.2ML
HuD/ELAVl4 (H-9)	1:5000	Santa Cruz	sc48421
MFN2	1:10000	Proteintech	12186-1-ap
OPA1	1:2000	Cell Signaling	D7C1A
PINK1	1:10,000	Novus Biologicals	NB600-973
Parkin	1:5000	Biolegend	870501

Chapter 5: General Discussion

5.1 Project Overview

Since the discovery of LRRK2, a threonine-serine kinase, as a causative gene for PD in 2004 (Paisán-Ruíz et al., 2004; Zimprich et al., 2004), large-scale efforts have been made to understand how it contributes to PD pathology. The most common mutation, *LRRK2 G2019S* has been the center of attention. A primary goal in the LRRK2 field has been identifying its phosphorylation substrates. Several studies have proposed substrates with roles in cytoskeleton remodelling, endocytosis, and gene expression control (Berwick et al., 2019), but to date it is still unclear how many of these proposed substrates are misregulated in PD patients, and if they contribute to hallmark characteristics of the disease.

From a genetic screen in *Drosophila*, homologues of the ELAVL family of RNA-binding proteins were found to be related to LRRK2-induced pathology (Marcogliese et al., 2017). One of these members, HuD, is primarily neuronally restricted and was found to modify the age-at-onset and susceptibility of PD (DeStefano et al., 2008; Noureddine et al., 2005). A mechanism for HuD in PD pathology has not yet been elucidated. The purpose of this thesis was to investigate the role of HuD, and its homologues, in LRRK2-dependent models of PD.

In Chapters 2 and 3 we described the roles for the nELAVL homologues HuB-C-D, and the ubiquitously expressed homologue HuR, in neuronal models and models of inflammation relevant to LRRK2 pathology, respectively. The overarching finding is that LRRK2 and the ELAVL proteins function in a feedback loop where loss of an ELAVL member increases LRRK2 protein levels, and LRRK2 phosphorylates the ELAVL proteins and controls their binding to target mRNA transcripts to modify phenotypes relevant to PD. Thus, we propose that the ELAVL family of

RNA-binding proteins are among LRRK2 kinase substrates that are misregulated in and contribute to PD pathogenesis.

5.2 Post-translational control of ELAVL proteins

A large body of literature has highlighted the role of post-translational modifications of the ELAVL proteins and their implications on subcellular localization and RNA-binding, however, the effects of PTMs on other functions like splicing, or translational control are less well defined (Bronicki & Jasmin, 2013; Grammatikakis et al., 2017). Furthermore, the effect of PTMs on ELAVL proteins are often not investigated in a genome-wide manner and are typically limited to their effects on pre-selected targets. To date, the only validated kinase shown to phosphorylate HuD is Protein Kinase C (PKC), but its effect on the transcriptome is incompletely characterized. It was shown, however, that HuD represses either the translation or localization of the *Bdnf* mRNA harboring the long 3'UTR, and this is inhibited by PKC activation, presumably through phosphorylation of HuD (Vanevski & Xu, 2015). Our study shows increased BDNF protein in the brains of *HuD*$^{-/-}$ mice, suggesting that HuD destabilizes or translationally represses *Bdnf* mRNA, consistent with previously published findings. Co-expression of mutant *Lrrk2* in *HuD*$^{-/-}$ mice results in rescue of this phenotype, possibly due to post-translational control of the remaining nELAVLs.

The fact that binding to the same targets can be controlled by multiple kinases, leads to a new question- what are the upstream signals driving nELAVL control by PKC vs. LRRK2, or other kinases? We found that LRRK2 exacerbates some phenotypes associated with loss of HuD, like loss of dopaminergic neurons or protein levels of nELAVL targets but has no impact on other

phenotypes like mouse energy metabolism. We initially performed CLAMS indirect calorimetry analysis including *Lrrk2 G2019S* and *Lrrk2 G2019S x HuD*$^{-/-}$ mice but found no significant effects of *Lrrk2 G2019S*. For that reason, LRRK2 was removed from further analyses, but these observations provide evidence that LRRK2 is not upstream of all ELAVL pathways.

In agreement, we observed little to no effect of LRRK2 on abundance of HuR mRNA targets in LPS-treated RAW cells, though it is possible that splicing or translation of these and other targets are misregulated in a LRRK2-dependent manner. It is well established that HuR is phosphorylated by many kinases like PKC and p38 including in the context of inflammation (Grammatikakis et al., 2017), therefore it is likely that LRRK2 is dispensable in certain contexts. Future work should focus on defining upstream signals for LRRK2 control of ELAVL proteins.

In Chapter 2, we expand on the knowledge of genome-wide effects of post-translational control of nELAVL proteins. We note that loss of *HuD* has three distinct pools of targets (i.e., upregulated, downregulated, and misspliced), as expected. The most striking finding in our study is that in the brains of *HuD*$^{-/-}$ mice, mutant hyperactive kinase LRRK2 exacerbates the effect on total transcript levels of mRNAs bound by nELAVL proteins, but almost completely rescues the effect on splicing (Fig. 2.4.8). The mechanism for this is still unclear but could be explained by hyperphosphorylation of the remaining ELAVL proteins, including HuR. Several studies on HuR have shown that its phosphorylation at a specific residue can impact RNA-binding affinity and nucleocytoplasmic shuttling (Schulz et al., 2013). It is possible that phosphorylation of T144, or homologous sites, mediated by LRRK2 controls both RNA-binding and shuttling of all the ELAVL proteins in the brain where it can have various effects on RNA metabolism.

Evidence from the literature supports a direct role for nELAVL in splicing control. Previously published CLIP data indicated that differentially spliced exon cassettes in human neuronal cells neighbor AREs bound by nELAVL within introns (Scheckel et al., 2016). HuD was also shown to directly interact with RNA polymerase II and histone deacetylase 2 (HDAC2) to control splicing (Bronicki & Jasmin, 2013). In contrast, the effects on splicing could also be indirect. DNA and RNA binding proteins were among the enriched GO terms from our microarray data. *Celf4*, a target that was significantly misspliced in *HuD*$^{-/-}$ brain tissue is itself an RNA-binding protein involved in splicing (Ladd et al., 2001). The effect on *Celf4* splicing in *HuD*-deficient mice was rescued by the G2019S mutant and provides an indirect mechanism for differentially spliced targets in these mice. The dominant narrative surrounding ELAVL function is that they bind and exclusively stabilize their target mRNAs which makes them unique compared to other ARE-binding proteins like TIAR, TTP, or AUF1 that strictly destabilize RNA or repress translation (Dolicka et al., 2020). The microarray dataset from this study challenges this model and is supported by published CLIP-seq datasets (Ince-Dunn et al., 2012; Scheckel et al., 2016), where upregulated and downregulated populations of RNA were identified in *HuC* or *HuD* knockout mice, though this aspect has often been neglected in published works.

The reasons for the two populations of HuD target mRNAs are unclear. The differentially regulated targets that we analyzed were directly bound by nELAVL in immunoprecipitates, suggesting that this is not due to indirect effects. We performed an analysis of the ARE motifs in the upregulated and downregulated genes of *HuD*$^{-/-}$ vs. *WT* and *Lrrk2 G2019S x HuD*$^{-/-}$ vs. *WT* using ARE site 2.0 predicter (Fallmann et al., 2016). The percent distribution of the ARE motif WUUUW where W

may be an A or a U varied subtly between populations (data not shown). This analysis should be performed using more rigorous methods but may provide clues into the mechanisms controlling up vs. downregulated genes. These findings could then be expanded to investigate how LRRK2 modifies this preference. Some evidence from *in vitro* gel shift studies with PKC isoforms and HuR indicate that phosphorylation at residues 158 or 318 decreases binding to Class I and II AREs but significantly increases affinity for Class III AREs (Schulz et al., 2013). We observed similar results in *in vitro* gel shift assays where LRRK2 had no effect on HuR affinity for a Class II ARE (TNF), but decreased affinity for Class III (polyU), although this was not reproduced *in vivo* (Fig.3.3.2-4). In mouse colon tissue, loss of LRRK2 diminished HuR binding to the *Tnfa* ARE, suggesting the presence of other contributing factors *in vivo* (Fig. 3.3.8). With respect to nELAVL, we found FLAG-HuD and nELAVL immunoprecipitates bound *BDNF*, *SNCA*, and *LRRK2* mRNA in SH-SY5Y cells and mouse midbrain tissue, respectively (Fig. 2.4.1 and Fig. 2.4.4). Both human and mouse *SNCA* 3'UTRs are more U-rich, whereas *LRRK2* human and mouse 3'UTRs are more AU-rich, and the experimentally defined binding site in *BDNF* is AU-rich (Allen et al., 2013). *In vitro* gel shift experiments with HuD and LRRK2 should be performed with Class I-III in parallel to define this mechanism.

The sites we identified to be phosphorylated in HuD *in vitro* and in mouse tissue are conserved in HuB and HuC. We showed that LRRK2 phosphorylates the other nELAVL members both *in vitro* and in mouse brain tissue. Therefore, we hypothesize that LRRK2 controls the ELAVL homologues similarly, but there are likely subtle differences. Given that the relative expression levels of each of the ELAVLs and LRRK2 differ between brain regions (Okano & Darnell, 1997; West et al., 2014), we could expect to see neuron subtype or brain region specific effects on each

ELAVL homologue and their shared or respective targets. In agreement, we note regional variations in the expression of the ELAVL targets we evaluated, namely LRRK2, BDNF, and α-synuclein.

A peculiar finding from GO analysis of all RNAs bound to nELAVL and differentially expressed in *HuD*$^{-/-}$ *vs*. *WT* and *Lrrk2 G2019S x HuD*$^{-/-}$ vs. *WT* is that the misregulated genes shifted from general cellular functions (e.g., DNA/RNA binding, endosome, and cytoplasmic granules) to neuron-specific pathways (e.g., neurogenesis, and (post)synapse). This shift in RNAs bound and differentially regulated by nELAVL in the presence of mutant LRRK2 towards primarily neuron-specific functions may provide clues into the reasons for the exacerbated phenotypes on motor function and dopaminergic neurons in *Lrrk2 G2019S x HuD*$^{-/-}$mice.

5.3 Post-transcriptional control of PD-linked genes

A major challenge in the PD field has been the paucity of animal models that faithfully recapitulate hallmark symptoms of PD. Numerous iterations of genetic rodent models have been produced to express wild type or mutant forms of human or endogenous PD associated genes (Lama et al., 2021), but an often-overlooked consideration in the development of these models has been the role of regulatory sequences controlling expression of the gene of interest. Understandably, the focus has been on the coding sequences of these PD-linked genes since disease causing mutations are typically found in these regions (Flagmeier et al., 2016; Thakur et al., 2022). However, accumulating data, including the findings in this study, highlight the importance of regulatory sequences in controlling PD-like phenotypes.

Notable differences in regional *LRRK2* expression have been described between mouse, rat, and human brain tissue (West et al., 2014), suggesting species-specific mechanisms of gene expression control. In contrast, rodents expressing LRRK2-BAC constructs bearing the human sequence resulted in expression patterns that more closely mimicked the human brain (West et al., 2014). In macrophages, where *LRRK2* is highly expressed, mouse *Lrrk2* expression equaled one-fifth of the levels detected in human macrophages under identical culture conditions (Xu et al., 2022). These findings suggest that untranslated regions and other regulatory sequences should be investigated in more detail.

In our datasets, we found that FLAG-HuD and nELAVL bind human and mouse *SNCA* transcripts, respectively and this is corroborated by CLIP-seq data (Fig. 2.4.1 and Fig. 2.4.4) (Scheckel et al., 2016), suggesting that the there is a degree of conservation in the regulation of α-synuclein between species. The trans-acting factors controlling *SNCA* expression have been described in greater detail than that of *LRRK2*, likely because *SNCA* gene dosage is associated with PD in patients (Chartier-Harlin et al., 2004; Singleton et al., 2003).

Interestingly, a longer 3'UTR isoform leads to the accumulation of α-synuclein protein in cells and in patient samples, where the ratio of long 3'UTR vs. short is increased (Rhinn et al., 2012). In cells this promoted the accumulation and cellular redistribution away from synaptic terminals towards mitochondria (Rhinn et al., 2012). These findings highlight the importance of understanding post-transcriptional regulation of risk genes. Furthermore, GWAS data indicate the presence of SNPs associated with PD in the *SNCA* 3'UTR (Blaželković et al., 2021; Simón-Sánchez

et al., 2009). Mutations within the 3'UTR might impact RBP or miRNA binding resulting in α-synuclein misregulation.

As stated above, LRRK2-PD is mostly associated with mutations in the coding sequences, particularly those encoding GTPase and kinase catalytic domains, but increased levels of LRRK2 have been identified in immune cells and cerebrospinal fluid of patients (Mabrouk et al., 2020; Wallings et al., 2020). This implies that gene expression control of *LRRK2* is altered in patients. Additionally, noncoding variants associated with idiopathic PD have been identified within the *LRRK2* gene (Lewis, 2022). Despite this, little is known about the post-transcriptional regulation of *LRRK2* mRNA.

In this study, we showed that loss of HuD in mouse brain, and the inhibition of HuR in LPS-treated macrophage-like cells resulted in significant increases in LRRK2 protein levels (Fig.2.4.3 and Fig. 3.3.7), suggesting that the ELAVL proteins typically suppress its expression. The general 3'UTR sequence of *SNCA* and *LRRK2* mRNA from mouse and human are poorly conserved. Specifically, the human 3'UTRs are longer than in mice, suggesting more complex post-transcriptional regulation, though predicted AU-rich elements were identified in both. Since both *SNCA* and *LRRK2* mRNA were enriched in immunoprecipitates from human SH-SY5Y cells and mouse brain tissue, it suggests a degree of evolutionary conservation in control of these mRNAs and justifies the use of these models in this context.

5.4 HuD binds and controls other PD-linked genes

An unexpected finding in this study was the misregulation of other PD associated genes besides *Lrrk2* and *Snca*. *PRKN/PARK2* (Parkin) and *PINK1* are both early-onset PD risk genes (Ge et al., 2020). Our microarray analysis indicated that *Pink1* and *Park2* were among the targets that were misregulated by loss of HuD in mouse brain tissue. No evidence in our study or the literature suggests that *Pink1* is a direct target of nELAVL, but it may be regulated by HuR or other RNA-binding proteins. In contrast, *PARK2* was among the top 1000 misregulated genes in a CLIP study in human brain tissue (Scheckel et al., 2016), and we confirmed that it co-immunoprecipitated with nELAVL from mouse tissue, indicating that it is directly bound by nELAVL proteins *in vivo* and is a shared target between mouse and human. We also found that the 3'UTR binding site was conserved between mouse and human by nucleotide alignment, but this should be experimentally validated. We did not investigate the relationship between mouse and human for the intronic binding sites, but our microarray study indicated that *Park2* is misspliced and differentially expressed in the brains of $HuD^{-/-}$ mice. Western blot analysis indicated variable expression of Parkin in $HuD^{-/-}$ mice, and the discrepancy between microarray data and western blot may be due to translational control or the age of the mice analyzed between the microarray study and the energy metabolism study. The significant splicing index in $HuD^{-/-}$ vs. *WT* brain tissue and the abundance of nELAVL binding sites in the introns of the human transcript suggest that splicing is impaired and should be experimentally validated. The Pink1/Parkin interaction is commonly discussed in the context of mitophagy, but the importance of this pathway in primary neurons and *in vivo* is unclear since recruitment of Pink1/Parkin to mitochondria in neurons or in mouse brain is not nearly as robust as in cell lines (Ge et al., 2020). Furthermore, basal mitophagy is unchanged in *Pink1* or *Park2*-deficient mice compared to controls (Ge et al., 2020). Nonetheless, the

regulation of mRNA encoding early onset risk alleles by HuD may provide an alternative mechanism for HuD as an age-of-onset modifier and risk gene for PD, independent of *LRRK2* and *SNCA* control.

5.5 HuD in mitochondrial control

In addition to *Pink1* and *Park2*, we found that HuD binds and regulates targets encoding other proteins involved in mitochondrial quality control (MQC). In our microarray study, we found that the mRNA encoding fusion proteins *Opa1/3*, *Mfn1/2*, and the fission-associated protein *Mff* were all among the misregulated targets in the brains of $HuD^{-/-}$ mice. Scheckel et al. 2016 also identified these targets among those bound and regulated by nELAVL proteins in human brain samples. To date, only *Mfn2* has been previously characterized as a HuD target in pancreatic β cells, where it was shown to bind its 3'UTR and increase MFN2 levels (Hong et al., 2020). Downregulation of HuD resulted in impaired mitochondrial potential and ATP output due to excessively fragmented mitochondria (Hong et al., 2020). In SH-SY5Y cells, HuR has been shown to regulate the fission protein Dynamin related protein 1 (*Drp1*). Overexpression of HuR results in increased mitochondrial fragmentation. These findings suggest that the ELAVL proteins regulate mitochondrial dynamics in both mice and humans (Bae et al., 2019).

Since nELAVL proteins appear to bind and control several genes involved in MQC, this suggests that they may exist in an mRNA regulon that has not been previously characterized. These regulons describe a system in which an RBP can regulate multiple transcripts involved in a pathway or response (Simone & Keene, 2013). In this case it is possible that nELAVL orchestrates pathways related to MQC. This parallels HuR function, which is a master regulator of inflammation and cell

cycle control through its binding and control of several functionally related transcripts (Srikantan & Gorospe, 2012).

A well characterized function of HuD is its role in neuronal development. Akamatsu et al., 2005, characterized the first *HuD*$^{-/-}$ mouse model that was used in this study. Neurosphere assays derived from cells lacking HuD, indicated enhanced self-renewal of neural stem/progenitor cells and fewer postmitotic neurons, where *HuD* mRNA is downregulated, suggesting that HuD plays a role in inhibiting neural stem cell self-renewal and promoting differentiation (Akamatsu et al., 2005). Many known targets of HuD are involved in various aspects of neuronal maturation including GAP-43, Tau, p21, p27, and cells lacking HuD show significantly shorter neurites (Silvestri et al., 2022), establishing it as a key regulator of neuronal function.

Interestingly, mitochondrial dynamics are associated with regulating neural stem cell fate decisions (Khacho et al., 2016). Given the role for HuD in neuronal development, it is possible that this is another pathway orchestrated by HuD or its homologues during development through splicing or translational control of MQC proteins. Impaired mitochondrial dynamics as well as other MQC mechanisms are associated with neurodegenerative diseases (Yang et al., 2021). If HuD has a more global role in mitochondrial function through coordinating expression of several mitochondrial genes, it is possible that this is one of the pathways governing neural stem cell fate decisions and leading to impaired neuronal maturation or neurodegeneration. This remains highly speculative at this time, but future studies should investigate the role of nELAVLs in neuron-specific mitochondrial function.

5.6 HuD in energy metabolism

In this study we found that loss of the neuronally enriched RNA-binding protein HuD controls energy metabolism in mice. It was previously shown that HuD inhibits the translation of the insulin mRNA in pancreatic β cells by binding the 5'UTR of preproinsulin (*Ins2*) mRNA, but its effects on energy metabolism were not evaluated by indirect calorimetry (Lee et al., 2012). The study by Lee et al., showed increased plasma glucose and lower insulin following a glucose tolerance test in HuD overexpressing mice compared to controls. As discussed in Chapter 4, we expected the opposite result in the *HuD*$^{-/-}$ mice but found no difference. This may be explained by experimental methods including intraperitoneal administration of glucose vs. oral administration and HuD-Tg mice vs. knockout.

The brain utilizes 20% of the body's oxygen (Watts et al., 2018), which makes it plausible that impairment of a neuronal protein could manifest as whole-body energy impairments. Interestingly, GWAS data identifying 56 novel BMI-associated loci in a European population found that *ELAVL4* was among the hits (Locke et al., 2015). Within the same population, *PARK2* encoding Parkin was also associated with obesity. Analysis of the tissues and cell types in which the hits were highly enriched revealed that 27 out of 31 of the significantly enriched tissues were within the CNS (Locke et al., 2015). A more granular evaluation of the tissues showed enrichment in known regulators of appetite, the hypothalamus and pituitary gland, but found a stronger association within the hippocampus and limbic system (Locke et al., 2015). A subsequent study found that *ELAVL4* was among the top 20 obesity associated genes in which specific epigenomic elements were enriched in the promoters (Dong et al., 2016). In the CLAMS indirect calorimetry study, we found that *HuD*$^{-/-}$ mice displayed altered body composition in the ECHO MRI, where

body fat percentage significantly decreased in 8-month-old male mice and trended lower in females (Fig. 4.3.1 and Supplementary Fig. 4.1). In the case of Parkin mouse models, several studies have indicated that Parkin-deficient mice are resistant to weight gain, even on a high fat diet and show improved insulin control (Costa et al., 2016; K.-Y. Kim et al., 2011; Moore et al., 2022). Together, these findings suggest that HuD and its targets could control energy metabolism and should be investigated further.

Alternative hypotheses to the effects we observed on mouse energy metabolism are alterations within the hypothalamus and pituitary gland. The hypothalamus controls many functions such as energy expenditure, glucose homeostasis, thermoregulation, sleep and circadian rhythm, respiratory control, and appetite (Bao & Swaab, 2019; Seoane-Collazo et al., 2015). We did not experimentally evaluate all these phenotypes; however, the CLAMS experiments suggest that at least some hypothalamic functions are intact. For example, we did not observe any effects on blood glucose in the OGTT, or food consumption, suggesting that glucose homeostasis and appetite were not altered in *HuD*$^{-/-}$ mice (Fig. 4.3.2). We also note differences between the dark and light cycle in activity levels and gas exchange (i.e., VO_2, VCO_2, RER) (Fig.4.3.2-3), suggesting that *HuD*$^{-/-}$ mice still respond to circadian cues. Furthermore, *HuD* was only weakly detected in the adult mouse hypothalamus (Okano & Darnell, 1997), therefore its contribution to hypothalamic function is unclear but should be experimentally tested.

Though we provide evidence for loss of HuD in the brain as a possible contributor to impaired energy metabolism, it is important to acknowledge that it is expressed at detectable levels in some non-neuronal tissues. While HuD levels are low enough that it cannot be identified by western blot

(Abdelmohsen et al., 2010, Supplementary Fig. 4.3), transcriptomics and immunohistochemistry showed that it is significantly enriched within the medulla of the adrenal gland where it was localized to the nuclei of norepinephrine producing cells (Bergman et al., 2017). The function of HuD in the adrenal gland has not been elucidated but its nuclear localization suggests that it could regulate splicing of its targets within these cells. Norpinephrine/epinephrine release during a fight-or-flight response has effects on cardiac and pulmonary function and glucose metabolism and may provide an alternative hypothesis for the metabolic phenotypes we observed in *HuD*$^{-/-}$ mice.

5.7 LRRK2 and HuR in inflammation

As discussed in Chapter 3, many studies have emerged investigating the role of LRRK2 in DSS colitis, with most studies concluding that expression of WT or mutant LRRK2 exacerbates colitis associated phenotypes (Cabezudo et al., 2023; Lin et al., 2022; Takagawa et al., 2018). The first LRRK2 DSS study by Liu et al., 2011 suggested that a lack of LRRK2 was associated with a worsened phenotype and this was due to translocation of NFAT to the nucleus, where transcription of proinflammatory cytokines is initiated. In wild-type mice, LRRK2 sequesters NFAT in the cytoplasm, and inflammation is attenuated. The next study by Takagawa et al., 2018, showed that LRRK2 overexpression induces a more severe phenotype in a kinase-dependent manner. In these mice, LRRK2 was expressed 8-fold more than in wild-type mice which likely results in greater activity than the 2-3-fold increase in kinase activity typically observed in LRRK2 hyperactive mutant models (West et al., 2005b). In a more physiologically relevant context, they showed that treatment of both wild-type and *LRRK2-Tg* with LRRK2 kinase inhibitors reduced colitis severity, suggesting that this phenotype is LRRK2 kinase-dependent. Interestingly, Takagawa et al., also tested *Lrrk2*$^{-/-}$mice and found no significant effect and suggested that the effect observed by Liu et

al., was due to the comparison of wild-type mice from the vendor vs. *Lrrk2*$^{-/-}$ mice bred within their own animal facility. In the same study, C57/BL6 mice housed in different facilities were tested in parallel, and the colitis severity varied between them by as much as ~15% in body weight at the study end point (Takagawa et al., 2018).

A recent study employing metagenomic analysis of >500 laboratory mice treated with DSS and housed in the same facility indicated significant differences in weight loss and intestinal pathology between lineages, despite being derived from a single breeding pair (Forster et al., 2022). The importance of these findings is directly relevant to LRRK2 biology and could help explain why in our study *Lrrk2*$^{-/-}$ mice produced a more severe phenotype compared to published studies. The mice used in our study were bred through heterozygous crosses and thus wild-type and *Lrrk2*$^{-/-}$ were littermates and randomly sorted into cages. Accumulating evidence suggests that the role for LRRK2 is protective in pathogen control, and this may be pathogen-specific and kinase independent (Härtlova et al., 2018; Shutinoski et al., 2019). For example, LRRK2 interacts with the bacterial sensor, NOD2, to control *Listeria monocytogenes* in the intestines of mice by promoting mucosal immunity (Zhang et al., 2015). It is also linked to *Salmonella typhimurium* infection, where *Lrrk2*-deficient mice are more susceptible to infection and death compared to wild-type controls (W. Liu et al., 2017). If LRRK2 does play a protective role, it is possible that its loss could cause a more severe phenotype in a DSS colitis model, depending on the profile of the microbiome of the experimental animals. Future experiments should compare knockout and mutant models simultaneously, along with microbiome profiling experiments to delineate how LRRK2 variants respond to colitis.

Several mechanisms have been described for LRRK2 in models of colitis or infections including through association with NFAT, NLRC4 inflammasome, NOD2, or NF-κB (W. Liu et al., 2017; Z. Liu et al., 2011; Takagawa et al., 2018; Zhang et al., 2015). In this study we proposed that LRRK2 contributes to the immune response via phosphorylation and control of the RNA-binding protein HuR. From the *in vitro* studies we found that LRRK2 phosphorylates and controls HuR binding to RNA (Fig. 3.3.1-4, Fig.3.3.8). As described in the nELAVL study, we observed differential effects and trends between targets when HuR was inhibited with CMLD-2(Allegri et al., 2019) in LPS-treated or control RAW cells. For example, inhibition of HuR had no effect on *Tnfa,* but trended towards increased *p21* and decreased *HuR* mRNA levels but LRRK2 appeared to only influence *HuR* mRNA (Fig. 3.3.7).

These discrepancies are likely related to upstream control by different post-translational modifications, the class and/or density of the AREs within the 3'UTR sequences, or other regulatory sequences bound by trans-acting factors in the cells. For example, *Tgfb* translation is suppressed by HuR, but does not have an ARE, though similar sequences have been identified (Katsanou et al., 2005; Yiakouvaki et al., 2012). In contrast, *Tnfa* contains a Class II ARE (Ripin et al., 2019). Also replicating our findings in the nELAVL study, we found that inhibition of an ELAVL homologue, in this case HuR, results in increased LRRK2 protein levels, specifically in LPS treated cells (Fig. 3.3.7). This potentially points to a role for HuR in controlling LRRK2 expression in early immune responses.

An outstanding question following this study is how do LRRK2 and HuR interact in models of chronic inflammation? There is evidence that both proteins are involved in acute and chronic

phases of inflammation. In the case of LRRK2, its activity is rapidly increased in response to pathogenic stimuli and remains consistently elevated in cells derived from PD and CD patients (Dzamko et al., 2016; Herrick & Tansey, 2021). Furthermore, its effects on phagocytosis in myeloid cells ranges from 2-16 hours in vitro (Ahmadi Rastegar et al., 2022; K. S. Kim et al., 2018). The role for HuR is equally as complex. Yiakouvaki et al., 2012 showed that HuR appears to control the balance between the initiation and resolution of an inflammatory response since loss of HuR in LPS stimulated primary macrophages was associated with elevated cytokine levels suggesting an M1 proinflammatory profile, while simultaneously expressing a cytokine profile associated with an M2 or resolving profile. In cells expressing HuR, it was noted that its interactions with cytokine mRNA increase at later time points, consistent with a role in cessation of the proinflammatory response (Katsanou et al., 2005; Yiakouvaki et al., 2012). In a chronic model of DSS-induced colitis, loss of HuR in the myeloid cell lineage resulted in an exacerbated colitis phenotype, followed by a comparatively rapid recovery, and more severe inflammation than WT mice in a subsequent round of DSS administration, suggesting that it is a negative regulator of inflammation in this context (Yiakouvaki et al., 2012).

Since HuR binding to *Tnfa* in colon tissues is significantly reduced in the absence of LRRK2 and TNF-α secretion is increased (Fig. 3.3.8), it suggests that loss of LRRK2 mimics HuR loss of function during acute inflammation. If HuR is required for attenuating the response, then this would suggest a model in which the decreased binding of HuR to *Tnfa* mRNA enables its increased translation thereby driving the exacerbated colitis phenotype in the *Lrrk2*$^{-/-}$ mice. Future studies should be aimed at defining the activating signals of the LRRK2-HuR interaction e.g., TLR signaling.

To ascertain the relevance of HuR in the context of LRRK2 colitis responses, additional experiments should be completed to inhibit HuR function in *Lrrk2*$^{-/-}$ or mutant mice through crosses with myeloid cell conditional HuR knockouts. Similarly, bone marrow transplants in LRRK2 mice using HuR myeloid knockout donor mice could be employed to restrict the analyses to immune cells. Alternatively, HuR could be inhibited pharmacologically using the *in vivo* validated MS-444 inhibitor, with the caveat that HuR is inhibited in all cell types (Blanco et al., 2016).

5.8 Relevance to Parkinson's Disease and Crohn's Disease

As discussed throughout the thesis, LRRK2 is related to Crohn's disease and Parkinson's disease through its links to inflammation (Alessi & Sammler, 2018). HuR differential expression was linked to Crohn's and Ulcerative colitis in patient samples (Burakoff et al., 2011; Li et al., 2020), but not PD. The findings from the DSS colitis model used in this study were extrapolated to gut pathology relevant to CD and PD. A limitation to this is that inflammation in these disorders is chronic, but the model employed here is acute inflammation. Future studies evaluating gut inflammation should be aimed at monitoring LRRK2 and HuR and their interaction in a chronic model of gut inflammation.

We also quantified markers of PD associated pathology in the brains of DSS treated mice. Interestingly, we found a subtle, but significant increase in α-synuclein protein levels in the cortex of DSS treated *Lrrk2*$^{-/-}$. It was unclear if the accumulation of α-synuclein was established within the brain or was induced systemically. Emerging evidence suggests that α-synuclein functions in

immunity as an anti-microbial peptide, including in the context of gastrointestinal infection or impaired gut permeability (Barbut et al., 2019). It is possible that the aggravated colitis phenotype in the *Lrrk2*-deficient mice triggered a protective accumulation of α-synuclein in the brain and should be explored further.

5.9 Conclusions

At the onset of this study, no ELAVL members were described as candidate LRRK2 phosphorylation substrates. The most well characterized of the nELAVL homologues, HuD, was identified as an age-at-onset modifier and susceptibility gene for PD in a 2005 GWAS (Noureddine et al., 2005). The identified SNPs were of unknown function, and a mechanism for HuD in pathogenesis had yet to be elucidated. In 2016, a landmark study by Steger et al., describing a phosphoproteomic screen in MEFs identified several proteins phosphorylated by LRRK2. Among the targets was the ubiquitously expressed RNA binding protein, HuR (ELAVL1), but this was not experimentally validated. Unpublished data from a screen in *Drosophila* from our collaborators showed that Rbp9, an ELAV homologue, was required for retinal degeneration induced by the human LRRK2-I2020T kinase mutant. Given the extensive body of literature implicating LRRK2 kinase mutations in PD pathology, we hypothesized that LRRK2 phosphorylates ELAVL homologues. Using *in vitro* systems like recombinant proteins, human neuroblastoma cell lines, and mouse models, we showed that LRRK2 phosphorylates the four mammalian homologues of the ELAVL family, HuB-D (ELAVL1-4). Phosphorylation by LRRK2 controls ELAVL binding to target mRNA encoding genes related to inflammation and neurodegeneration like *Tnfa*, *Snca*, and *Lrrk2* itself. Loss of function, or mutations in the ELAVL proteins and LRRK2 resulted in a range of PD-relevant phenotypes from altered protein production, dopaminergic neuron loss,

motor deficits, and peripheral inflammation. Together, the data presented in this thesis support a role for the ELAVL family of RNA-binding proteins in LRRK2-dependent models of disease.

References

Abbott, A. (2010). Levodopa: the story so far. *Nature*, *466*(7310), S6–S7. https://doi.org/10.1038/466S6a

Abdelmohsen, K., Hutchison, E. R., Lee, E. K., Kuwano, Y., Kim, M. M., Masuda, K., Srikantan, S., Subaran, S. S., Marasa, B. S., Mattson, M. P., & Gorospe, M. (2010). miR-375 Inhibits Differentiation of Neurites by Lowering HuD Levels. *Molecular and Cellular Biology*, *30*(17), 4197–4210. https://doi.org/10.1128/MCB.00316-10

Ahmadi Rastegar, D., Hughes, L. P., Perera, G., Keshiya, S., Zhong, S., Gao, J., Halliday, G. M., Schüle, B., & Dzamko, N. (2022). Effect of LRRK2 protein and activity on stimulated cytokines in human monocytes and macrophages. *Npj Parkinson's Disease*, *8*(1), 34. https://doi.org/10.1038/s41531-022-00297-9

Ait-Aissa, K., Blaszak, S. C., Beutner, G., Tsaih, S.-W., Morgan, G., Santos, J. H., Flister, M. J., Joyce, D. L., Camara, A. K. S., Gutterman, D. D., Donato, A. J., Porter, G. A., & Beyer, A. M. (2019). Mitochondrial Oxidative Phosphorylation defect in the Heart of Subjects with Coronary Artery Disease. *Scientific Reports*, *9*(1), 7623. https://doi.org/10.1038/s41598-019-43761-y

Akamatsu, W., Fujihara, H., Mitsuhashi, T., Yano, M., Shibata, S., Hayakawa, Y., Okano, H. J., Sakakibara, S., Takano, H., Takano, T., Takahashi, T., Noda, T., & Okano, H. (2005). The RNA-binding protein HuD regulates neuronal cell identity and maturation. *Proceedings of the National Academy of Sciences of the United States of America*, *102*(12), 4625–4630. http://www.ncbi.nlm.nih.gov/entrez/query.fcgi?cmd=Retrieve&db=PubMed&dopt=Citation&list_uids=15764704

Albers, J. A., Chand, P., & Anch, A. M. (2017). Multifactorial sleep disturbance in Parkinson's disease. *Sleep Medicine*, *35*, 41–48. https://doi.org/10.1016/j.sleep.2017.03.026

Alessi, D. R., & Sammler, E. (2018). LRRK2 kinase in Parkinson's disease. *Science*, *360*(6384), 36–37. https://doi.org/10.1126/science.aar5683

Aleyasin, H., Rousseaux, M. W. C., Marcogliese, P. C., Hewitt, S. J., Irrcher, I., Joselin, A. P., Parsanejad, M., Kim, R. H., Rizzu, P., Callaghan, S. M., Slack, R. S., Mak, T. W., & Park, D. S. (2010). DJ-1 protects the nigrostriatal axis from the neurotoxin MPTP by modulation of the AKT pathway. *Proceedings of the National Academy of Sciences*, *107*(7), 3186–3191. https://doi.org/10.1073/pnas.0914876107

Allegri, L., Baldan, F., Roy, S., Aubé, J., Russo, D., Filetti, S., & Damante, G. (2019). The HuR CMLD-2 inhibitor exhibits antitumor effects via MAD2 downregulation in thyroid cancer cells. *Scientific Reports*, *9*(1). https://doi.org/10.1038/s41598-019-43894-0

Allen, M., Bird, C., Feng, W., Liu, G., Li, W., Perrone-Bizzozero, N. I., & Feng, Y. (2013). HuD Promotes BDNF Expression in Brain Neurons via Selective Stabilization of the BDNF Long 3′UTR mRNA. *PLoS ONE*, *8*(1), e55718. https://doi.org/10.1371/journal.pone.0055718

Andersen, M. A., Wegener, K. M., Larsen, S., Badolo, L., Smith, G. P., Jeggo, R., Jensen, P. H., Sotty, F., Christensen, K. V., & Thougaard, A. (2018). PFE-360-induced LRRK2 inhibition induces reversible, non-adverse renal changes in rats. *Toxicology*, *395*, 15–22. https://doi.org/10.1016/j.tox.2018.01.003

Andrikopoulos, S., Blair, A. R., Deluca, N., Fam, B. C., & Proietto, J. (2008). Evaluating the glucose tolerance test in mice. *American Journal of Physiology-Endocrinology and Metabolism*, *295*(6), E1323–E1332. https://doi.org/10.1152/ajpendo.90617.2008

Anglin, R. E., Tarnopolsky, M. A., Mazurek, M. F., & Rosebush, P. I. (2012). The Psychiatric Presentation of Mitochondrial Disorders in Adults. *The Journal of Neuropsychiatry and Clinical Neurosciences*, *24*(4), 394–409. https://doi.org/10.1176/appi.neuropsych.11110345

Antonini, A., Tolosa, E., Mizuno, Y., Yamamoto, M., & Poewe, W. H. (2009). A reassessment of risks and benefits of dopamine agonists in Parkinson's disease. *The Lancet Neurology*, *8*(10), 929–937. https://doi.org/10.1016/S1474-4422(09)70225-X

Aranda-Abreu, G. E., Behar, L., Chung, S., Furneaux, H., & Ginzburg, I. (1999). Embryonic Lethal Abnormal Vision-Like RNA-Binding Proteins Regulate Neurite Outgrowth and Tau Expression in PC12 Cells. *The Journal of Neuroscience*, *19*(16), 6907–6917. https://doi.org/10.1523/JNEUROSCI.19-16-06907.1999

Ariga, H., Takahashi-Niki, K., Kato, I., Maita, H., Niki, T., & Iguchi-Ariga, S. M. M. (2013). Neuroprotective Function of DJ-1 in Parkinson's Disease. *Oxidative Medicine and Cellular Longevity*, *2013*, 1–9. https://doi.org/10.1155/2013/683920

Armstrong, M. J., & Okun, M. S. (2020). Diagnosis and Treatment of Parkinson Disease. *JAMA*, *323*(6), 548. https://doi.org/10.1001/jama.2019.22360

Arranz, A. M., Delbroek, L., Van Kolen, K., Guimarães, M. R., Mandemakers, W., Daneels, G., Matta, S., Calafate, S., Shaban, H., Baatsen, P., De Bock, P.-J., Gevaert, K., Vanden Berghe, P., Verstreken, P., De Strooper, B., & Moechars, D. (2014). LRRK2 functions in synaptic vesicle endocytosis through a kinase-dependent mechanism. *Journal of Cell Science*. https://doi.org/10.1242/jcs.158196

Atashrazm, F., Hammond, D., Perera, G., Bolliger, M. F., Matar, E., Halliday, G. M., Schüle, B., Lewis, S. J. G., Nichols, R. J., & Dzamko, N. (2019). LRRK2-mediated Rab10 phosphorylation in immune cells

from Parkinson's disease patients. *Movement Disorders*, *34*(3), 406–415. https://doi.org/10.1002/mds.27601

Atlas, R., Behar, L., Sapoznik, S., & Ginzburg, I. (2007). Dynamic association with polysomes during P19 neuronal differentiation and an untranslated-region-dependent translation regulation of the tau mRNA by the tau mRNA-associated proteins IMP1, HuD, and G3BP1. *Journal of Neuroscience Research*, *85*(1), 173–183. https://doi.org/10.1002/jnr.21099

Bae, J. E., Park, S. J., Hong, Y., Jo, D. S., Lee, H., Park, N. Y., Kim, J. B., Park, H. J., Bunch, H., Chang, J. H., Lee, E. K., & Cho, D.-H. (2019). Loss of RNA binding protein, human antigen R enhances mitochondrial elongation by regulating Drp1 expression in SH-SY5Y cells. *Biochemical and Biophysical Research Communications*, *516*(3). https://doi.org/10.1016/j.bbrc.2019.06.091

Bagli, E., Zikou, K. A., Agnantis, N., & Kitsos, G. (2017). Mitochondrial Membrane Dynamics and Inherited Optic Neuropathies. *In Vivo*, *31*(4), 511–525. https://doi.org/10.21873/invivo.11090

Bandres-Ciga, S., Diez-Fairen, M., Kim, J. J., & Singleton, A. B. (2020). Genetics of Parkinson's disease: An introspection of its journey towards precision medicine. *Neurobiology of Disease*, *137*, 104782. https://doi.org/10.1016/j.nbd.2020.104782

Baptista, M. A. S., Dave, K. D., Frasier, M. A., Sherer, T. B., Greeley, M., Beck, M. J., Varsho, J. S., Parker, G. A., Moore, C., Churchill, M. J., Meshul, C. K., & Fiske, B. K. (2013). Loss of Leucine-Rich Repeat Kinase 2 (LRRK2) in Rats Leads to Progressive Abnormal Phenotypes in Peripheral Organs. *PLoS ONE*, *8*(11), e80705. https://doi.org/10.1371/journal.pone.0080705

Baptista, M. A. S., Merchant, K., Barrett, T., Bhargava, S., Bryce, D. K., Ellis, J. M., Estrada, A. A., Fell, M. J., Fiske, B. K., Fuji, R. N., Galatsis, P., Henry, A. G., Hill, S., Hirst, W., Houle, C., Kennedy, M. E., Liu, X., Maddess, M. L., Markgraf, C., … Sherer, T. B. (2020). LRRK2 inhibitors induce reversible changes in nonhuman primate lungs without measurable pulmonary deficits. *Science Translational Medicine*, *12*(540). https://doi.org/10.1126/scitranslmed.aav0820

Barbosa, A. C., Kim, M.-S., Ertunc, M., Adachi, M., Nelson, E. D., McAnally, J., Richardson, J. A., Kavalali, E. T., Monteggia, L. M., Bassel-Duby, R., & Olson, E. N. (2008). MEF2C, a transcription factor that facilitates learning and memory by negative regulation of synapse numbers and function. *Proceedings of the National Academy of Sciences*, *105*(27), 9391–9396. https://doi.org/10.1073/pnas.0802679105

Barrett, M. J., Sargent, L., Nawaz, H., Weintraub, D., Price, E. T., & Willis, A. W. (2021). Antimuscarinic Anticholinergic Medications in Parkinson Disease: To Prescribe or Deprescribe? *Movement Disorders Clinical Practice*, *8*(8), 1181–1188. https://doi.org/10.1002/mdc3.13347

Behl, T., Kaur, G., Fratila, O., Buhas, C., Judea-Pusta, C. T., Negrut, N., Bustea, C., & Bungau, S. (2021). Cross-talks among GBA mutations, glucocerebrosidase, and α-synuclein in GBA-associated

Parkinson's disease and their targeted therapeutic approaches: a comprehensive review. *Translational Neurodegeneration*, *10*(1), 4. https://doi.org/10.1186/s40035-020-00226-x

Bell, L. R., Maine, E. M., Schedl, P., & Cline, T. W. (1988). Sex-lethal, a Drosophila sex determination switch gene, exhibits sex-specific RNA splicing and sequence similarity to RNA binding proteins. *Cell*, *55*(6). https://doi.org/10.1016/0092-8674(88)90248-6

Bergman, J., Botling, J., Fagerberg, L., Hallström, B. M., Djureinovic, D., Uhlén, M., & Pontén, F. (2017). The Human Adrenal Gland Proteome Defined by Transcriptomics and Antibody-Based Profiling. *Endocrinology*, *158*(2), 239–251. https://doi.org/10.1210/en.2016-1758

Berndsen, K., Lis, P., Yeshaw, W. M., Wawro, P. S., Nirujogi, R. S., Wightman, M., Macartney, T., Dorward, M., Knebel, A., Tonelli, F., Pfeffer, S. R., & Alessi, D. R. (2019). PPM1H phosphatase counteracts LRRK2 signaling by selectively dephosphorylating Rab proteins. *ELife*, *8*. https://doi.org/10.7554/eLife.50416

Bhatti, J. S., Bhatti, G. K., & Reddy, P. H. (2017). Mitochondrial dysfunction and oxidative stress in metabolic disorders — A step towards mitochondria based therapeutic strategies. *Biochimica et Biophysica Acta (BBA) - Molecular Basis of Disease*, *1863*(5), 1066–1077. https://doi.org/10.1016/j.bbadis.2016.11.010

Bieri, G., Brahic, M., Bousset, L., Couthouis, J., Kramer, N. J., Ma, R., Nakayama, L., Monbureau, M., Defensor, E., Schüle, B., Shamloo, M., Melki, R., & Gitler, A. D. (2019). LRRK2 modifies α-syn pathology and spread in mouse models and human neurons. *Acta Neuropathologica*, *137*(6), 961–980. https://doi.org/10.1007/s00401-019-01995-0

Biskup, S., Moore, D. J., Rea, A., Lorenz-Deperieux, B., Coombes, C. E., Dawson, V. L., Dawson, T. M., & West, A. B. (2007). Dynamic and redundant regulation of LRRK2 and LRRK1 expression. *BMC Neuroscience*, *8*(1), 102. https://doi.org/10.1186/1471-2202-8-102

Blanco, F. F., Preet, R., Aguado, A., Vishwakarma, V., Stevens, L. E., Vyas, A., Padhye, S., Xu, L., Weir, S. J., Anant, S., Meisner-Kober, N., Brody, J. R., & Dixon, D. A. (2016). Impact of HuR inhibition by the small molecule MS-444 on colorectal cancer cell tumorigenesis. *Oncotarget*, *7*(45), 74043–74058. https://doi.org/10.18632/oncotarget.12189

Blonder, L. X., & Slevin, J. T. (2011). Emotional dysfunction in Parkinson's disease. *Behavioural Neurology*, *24*(3), 201–217. https://doi.org/10.3233/BEN-2011-0329

Bolognani, F., Contente-Cuomo, T., & Perrone-Bizzozero, N. I. (2009). Novel recognition motifs and biological functions of the RNA-binding protein HuD revealed by genome-wide identification of its targets. *Nucleic Acids Research*, *38*(1), 117–130. https://doi.org/10.1093/nar/gkp863

Bonifati, V., Rizzu, P., van Baren, M. J., Schaap, O., Breedveld, G. J., Krieger, E., Dekker, M. C. J., Squitieri, F., Ibanez, P., Joosse, M., van Dongen, J. W., Vanacore, N., van Swieten, J. C., Brice, A.,

Meco, G., van Duijn, C. M., Oostra, B. A., & Heutink, P. (2003). Mutations in the *DJ-1* Gene Associated with Autosomal Recessive Early-Onset Parkinsonism. *Science*, *299*(5604), 256–259. https://doi.org/10.1126/science.1077209

Brocks, D. R. (1999). Anticholinergic drugs used in Parkinson's disease: An overlooked class of drugs from a pharmacokinetic perspective. *Journal of Pharmacy & Pharmaceutical Sciences : A Publication of the Canadian Society for Pharmaceutical Sciences, Societe Canadienne Des Sciences Pharmaceutiques*, *2*(2), 39–46.

Bronicki, L. M., & Jasmin, B. J. (2013). Emerging complexity of the HuD/ELAVl4 gene; implications for neuronal development, function, and dysfunction. *RNA (New York, N.Y.)*, *19*(8), 1019–1037. https://doi.org/10.1261/rna.039164.113

Bucur, M., & Papagno, C. (2023). Deep Brain Stimulation in Parkinson Disease: A Meta-analysis of the Long-term Neuropsychological Outcomes. *Neuropsychology Review*, *33*(2), 307–346. https://doi.org/10.1007/s11065-022-09540-9

Burakoff, R., Chao, S., Perencevich, M., Ying, J., Friedman, S., Makrauer, F., Odze, R., Khurana, H., & Liew, C.-C. (2011). Blood-based biomarkers can differentiate ulcerative colitis from crohn's disease and noninflammatory diarrhea. *Inflammatory Bowel Diseases*, *17*(8), 1719–1725. https://doi.org/10.1002/ibd.21574

Burré, J., Sharma, M., Tsetsenis, T., Buchman, V., Etherton, M. R., & Südhof, T. C. (2010). α-Synuclein Promotes SNARE-Complex Assembly in Vivo and in Vitro. *Science*, *329*(5999), 1663–1667. https://doi.org/10.1126/science.1195227

Carrascoso, I., Alcalde, J., Sánchez-Jiménez, C., González-Sánchez, P., & Izquierdo, J. M. (2017). T-Cell Intracellular Antigens and Hu Antigen R Antagonistically Modulate Mitochondrial Activity and Dynamics by Regulating Optic Atrophy 1 Gene Expression. *Molecular and Cellular Biology*, *37*(17). https://doi.org/10.1128/MCB.00174-17

Chartier-Harlin, M. C., Kachergus, J., Roumier, C., Mouroux, V., Douay, X., Lincoln, S., Levecque, C., Larvor, L., Andrieux, J., Hulihan, M., Waucquier, N., Defebvre, L., Amouyel, P., Farrer, M., & Destee, A. (2004). alpha-Synuclein locus duplication as a cause of familial Parkinson's disease. *Lancet*, *364*(9440), 1167–1169. https://doi.org/10.1016/S0140-6736(04)17103-1

Chen, J., Chen, Y., & Pu, J. (2018). Leucine-Rich Repeat Kinase 2 in Parkinson's Disease: Updated from Pathogenesis to Potential Therapeutic Target. *European Neurology*, *79*(5–6), 256–265. https://doi.org/10.1159/000488938

Chen, S.-J., & Lin, C.-H. (2022). Gut microenvironmental changes as a potential trigger in Parkinson's disease through the gut–brain axis. *Journal of Biomedical Science*, *29*(1), 54. https://doi.org/10.1186/s12929-022-00839-6

Chen, T., Yang, Y., Luo, P., Liu, W., Dai, S., Zheng, X., Fei, Z., & Jiang, X. (2013). Homer1 knockdown protects dopamine neurons through regulating calcium homeostasis in an in vitro model of Parkinson's disease. *Cellular Signalling*, *25*(12), 2863–2870. https://doi.org/10.1016/j.cellsig.2013.09.004

Cheng, H.-C., Ulane, C. M., & Burke, R. E. (2010). Clinical progression in Parkinson disease and the neurobiology of axons. *Annals of Neurology*, *67*(6), 715–725. https://doi.org/10.1002/ana.21995

Chiba-Falek, O. (2001). Effect of allelic variation at the NACP-Rep1 repeat upstream of the alpha-synuclein gene (SNCA) on transcription in a cell culture luciferase reporter system. *Human Molecular Genetics*, *10*(26), 3101–3109. https://doi.org/10.1093/hmg/10.26.3101

Chinnery, P. F. (1993). *Primary Mitochondrial Disorders Overview*.

Cho, H.-U., Kim, S., Sim, J., Yang, S., An, H., Nam, M.-H., Jang, D.-P., & Lee, C. J. (2021). Redefining differential roles of MAO-A in dopamine degradation and MAO-B in tonic GABA synthesis. *Experimental & Molecular Medicine*, *53*(7), 1148–1158. https://doi.org/10.1038/s12276-021-00646-3

Christodoulou-Vafeiadou, E., Ioakeimidis, F., Andreadou, M., Giagkas, G., Stamatakis, G., Reczko, M., Samiotaki, M., Papanastasiou, A. D., Karakasiliotis, I., & Kontoyiannis, D. L. (2018). Divergent Innate and Epithelial Functions of the RNA-Binding Protein HuR in Intestinal Inflammation. *Frontiers in Immunology*, *9*. https://doi.org/10.3389/fimmu.2018.02732

Chung, S., Jiang, L., Cheng, S., & Furneaux, H. (1996). Purification and Properties of HuD, a Neuronal RNA-binding Protein. *Journal of Biological Chemistry*, *271*(19), 11518–11524. https://doi.org/10.1074/jbc.271.19.11518

Connor-Robson, N., Booth, H., Martin, J. G., Gao, B., Li, K., Doig, N., Vowles, J., Browne, C., Klinger, L., Juhasz, P., Klein, C., Cowley, S. A., Bolam, P., Hirst, W., & Wade-Martins, R. (2019). An integrated transcriptomics and proteomics analysis reveals functional endocytic dysregulation caused by mutations in LRRK2. *Neurobiology of Disease*, *127*, 512–526. https://doi.org/10.1016/j.nbd.2019.04.005

Dalmau, J., Furneaux, H. M., Gralla, R. J., Kris, M. G., & Posner, J. B. (1990). Detection of the anti-Hu antibody in the serum of patients with small cell lung cancer?A quantitative western blot analysis. *Annals of Neurology*, *27*(5). https://doi.org/10.1002/ana.410270515

Danzer, K. M., Krebs, S. K., Wolff, M., Birk, G., & Hengerer, B. (2009). Seeding induced by α-synuclein oligomers provides evidence for spreading of α-synuclein pathology. *Journal of Neurochemistry*, *111*(1), 192–203. https://doi.org/10.1111/j.1471-4159.2009.06324.x

de Bie, R. M. A., Clarke, C. E., Espay, A. J., Fox, S. H., & Lang, A. E. (2020). Initiation of pharmacological therapy in Parkinson's disease: when, why, and how. *The Lancet Neurology*, *19*(5), 452–461. https://doi.org/10.1016/S1474-4422(20)30036-3

De Santis, R., Alfano, V., de Turris, V., Colantoni, A., Santini, L., Garone, M. G., Antonacci, G., Peruzzi, G., Sudria-Lopez, E., Wyler, E., Anink, J. J., Aronica, E., Landthaler, M., Pasterkamp, R. J., Bozzoni, I., & Rosa, A. (2019a). Mutant FUS and ELAVL4 (HuD) Aberrant Crosstalk in Amyotrophic Lateral Sclerosis. *Cell Reports*, *27*(13), 3818-3831.e5. https://doi.org/10.1016/j.celrep.2019.05.085

De Santis, R., Alfano, V., de Turris, V., Colantoni, A., Santini, L., Garone, M. G., Antonacci, G., Peruzzi, G., Sudria-Lopez, E., Wyler, E., Anink, J. J., Aronica, E., Landthaler, M., Pasterkamp, R. J., Bozzoni, I., & Rosa, A. (2019b). Mutant FUS and ELAVL4 (HuD) Aberrant Crosstalk in Amyotrophic Lateral Sclerosis. *Cell Reports*, *27*(13), 3818-3831.e5. https://doi.org/10.1016/j.celrep.2019.05.085

de Toeuf, B., Soin, R., Nazih, A., Dragojevic, M., Jurėnas, D., Delacourt, N., Vo Ngoc, L., Garcia-Pino, A., Kruys, V., & Gueydan, C. (2018). ARE-mediated decay controls gene expression and cellular metabolism upon oxygen variations. *Scientific Reports*, *8*(1), 5211. https://doi.org/10.1038/s41598-018-23551-8

DeBoer, E. M., Azevedo, R., Vega, T. A., Brodkin, J., Akamatsu, W., Okano, H., Wagner, G. C., & Rasin, M.-R. (2014). Prenatal deletion of the RNA-binding protein HuD disrupts postnatal cortical circuit maturation and behavior. *The Journal of Neuroscience*, *34*(10), 3674–3686. https://doi.org/10.1523/JNEUROSCI.3703-13.2014

DeStefano, A. L., Latourelle, J., Lew, M. F., Suchowersky, O., Klein, C., Golbe, L. I., Mark, M. H., Growdon, J. H., Wooten, G. F., Watts, R., Guttman, M., Racette, B. A., Perlmutter, J. S., Marlor, L., Shill, H. A., Singer, C., Goldwurm, S., Pezzoli, G., Saint-Hilaire, M. H., … Myers, R. H. (2008). Replication of association between ELAVL4 and Parkinson disease: the GenePD study. *Human Genetics*, *124*(1). https://doi.org/10.1007/s00439-008-0526-4

Di Fonzo, A., Tassorelli, C., De Mari, M., Chien, H. F., Ferreira, J., Rohé, C. F., Riboldazzi, G., Antonini, A., Albani, G., Mauro, A., Marconi, R., Abbruzzese, G., Lopiano, L., Fincati, E., Guidi, M., Marini, P., Stocchi, F., Onofrj, M., Toni, V., … Bonifati, V. (2006). Comprehensive analysis of the LRRK2 gene in sixty families with Parkinson's disease. *European Journal of Human Genetics*, *14*(3), 322–331. https://doi.org/10.1038/sj.ejhg.5201539

Di Maio, R., Hoffman, E. K., Rocha, E. M., Keeney, M. T., Sanders, L. H., De Miranda, B. R., Zharikov, A., Van Laar, A., Stepan, A. F., Lanz, T. A., Kofler, J. K., Burton, E. A., Alessi, D. R., Hastings, T. G., & Greenamyre, J. T. (2018). LRRK2 activation in idiopathic Parkinson's disease. *Science Translational Medicine*, *10*(451). https://doi.org/10.1126/scitranslmed.aar5429

Dierssen, M., Fructuoso, M., Martínez de Lagrán, M., Perluigi, M., & Barone, E. (2020). Down Syndrome Is a Metabolic Disease: Altered Insulin Signaling Mediates Peripheral and Brain Dysfunctions. *Frontiers in Neuroscience*, *14*. https://doi.org/10.3389/fnins.2020.00670

Dolicka, D., Sobolewski, C., Correia de Sousa, M., Gjorgjieva, M., & Foti, M. (2020). mRNA Post-Transcriptional Regulation by AU-Rich Element-Binding Proteins in Liver Inflammation and Cancer. *International Journal of Molecular Sciences*, *21*(18), 6648. https://doi.org/10.3390/ijms21186648

Doller, A., Winkler, C., Azrilian, I., Schulz, S., Hartmann, S., Pfeilschifter, J., & Eberhardt, W. (2011). High-constitutive HuR phosphorylation at Ser 318 by PKCδ propagates tumor relevant functions in colon carcinoma cells. *Carcinogenesis*, *32*(5), 676–685. https://doi.org/10.1093/carcin/bgr024

Doorduijn, A. S., de van der Schueren, M., van de Rest, O., de Leeuw, F. A., Hendriksen, H. M., Teunissen, C. E., Scheltens, P., van Der Flier, W., & Visser, M. (2020). Energy intake and expenditure in patients with Alzheimer's disease and mild cognitive impairment: The NUDAD project. *Alzheimer's & Dementia*, *16*(S10). https://doi.org/10.1002/alz.042429

Dorsey, E. R., Sherer, T., Okun, M. S., & Bloem, B. R. (2018). The Emerging Evidence of the Parkinson Pandemic. *Journal of Parkinson's Disease*, *8*(s1), S3–S8. https://doi.org/10.3233/JPD-181474

Du, X., Xie, X., & Liu, R. (2020). The Role of α-Synuclein Oligomers in Parkinson's Disease. *International Journal of Molecular Sciences*, *21*(22), 8645. https://doi.org/10.3390/ijms21228645

Durie, D., Lewis, S. M., Liwak, U., Kisilewicz, M., Gorospe, M., & Holcik, M. (2011). RNA-binding protein HuR mediates cytoprotection through stimulation of XIAP translation. *Oncogene*, *30*(12), 1460–1469. https://doi.org/10.1038/onc.2010.527

Dwyer, Z., Rudyk, C., Thompson, A., Farmer, K., Fenner, B., Fortin, T., Derksen, A., Sun, H., & Hayley, S. (2020). Leucine-rich repeat kinase-2 (LRRK2) modulates microglial phenotype and dopaminergic neurodegeneration. *Neurobiology of Aging*, *91*, 45–55. https://doi.org/10.1016/j.neurobiolaging.2020.02.017

El Kodsi, D. N., Tokarew, J. M., Sengupta, R., Lengacher, N. A., Chatterji, A., Nguyen, A. P., Boston, H., Jiang, Q., Palmberg, C., Pileggi, C., Holterman, C. E., Shutinoski, B., Li, J., Fehr, T. K., LaVoie, M. J., Ratan, R. R., Shaw, G. S., Takanashi, M., Hattori, N., … Schlossmacher, M. G. (2023). Parkin coregulates glutathione metabolism in adult mammalian brain. *Acta Neuropathologica Communications*, *11*(1), 19. https://doi.org/10.1186/s40478-022-01488-4

Farinatti, P., Castinheiras Neto, A. G., & Amorim, P. R. S. (2016). Oxygen Consumption and Substrate Utilization During and After Resistance Exercises Performed with Different Muscle Mass. *International Journal of Exercise Science*, *9*(1), 77–88.

Fava, V. M., Manry, J., Cobat, A., Orlova, M., Van Thuc, N., Ba, N. N., Thai, V. H., Abel, L., Alcaïs, A., & Schurr, E. (2016). A Missense LRRK2 Variant Is a Risk Factor for Excessive Inflammatory

Responses in Leprosy. *PLOS Neglected Tropical Diseases*, *10*(2), e0004412. https://doi.org/10.1371/journal.pntd.0004412

Fearnley, J. M., & Lees, A. J. (1991). AGEING AND PARKINSON'S DISEASE: SUBSTANTIA NIGRA REGIONAL SELECTIVITY. *Brain*, *114*(5), 2283–2301. https://doi.org/10.1093/brain/114.5.2283

Femat-Roldán, G., Gaitán Palau, M. A., Castilla-Cortázar, I., Elizondo Ochoa, G., Moreno, N. G., Martín-Estal, I., & Jiménez Yarza, M. (2020). Altered Body Composition and Increased Resting Metabolic Rate Associated with the Postural Instability/Gait Difficulty Parkinson's Disease Subtype. *Parkinson's Disease*, *2020*, 1–9. https://doi.org/10.1155/2020/8060259

Fernandes, H. J. R., Patikas, N., Foskolou, S., Field, S. F., Park, J.-E., Byrne, M. L., Bassett, A. R., & Metzakopian, E. (2020). Single-Cell Transcriptomics of Parkinson's Disease Human In Vitro Models Reveals Dopamine Neuron-Specific Stress Responses. *Cell Reports*, *33*(2). https://doi.org/10.1016/j.celrep.2020.108263

Finsterer, J. (2008). Leigh and Leigh-Like Syndrome in Children and Adults. *Pediatric Neurology*, *39*(4), 223–235. https://doi.org/10.1016/j.pediatrneurol.2008.07.013

Franssen, E. H., Somen, L. E. M., Torossian, C. L., & Reisberg, B. (1999). Equilibrium and Limb Coordination in Mild Cognitive Impairment and Mild Alzheimer's Disease. *Journal of the American Geriatrics Society*, *47*(4), 463–469. https://doi.org/10.1111/j.1532-5415.1999.tb07240.x

Fuchs, J., Tichopad, A., Golub, Y., Munz, M., Schweitzer, K. J., Wolf, B., Berg, D., Mueller, J. C., & Gasser, T. (2008). Genetic variability in the *SNCA* gene influences α-synuclein levels in the blood and brain. *The FASEB Journal*, *22*(5), 1327–1334. https://doi.org/10.1096/fj.07-9348com

Fukao, A., Sasano, Y., Imataka, H., Inoue, K., Sakamoto, H., Sonenberg, N., Thoma, C., & Fujiwara, T. (2009). The ELAV Protein HuD Stimulates Cap-Dependent Translation in a Poly(A)- and eIF4A-Dependent Manner. *Molecular Cell*, *36*(6), 1007–1017. https://doi.org/10.1016/j.molcel.2009.11.013

Fukao, A., Tomohiro, T., & Fujiwara, T. (2021a). Translation Initiation Regulated by RNA-Binding Protein in Mammals: The Modulation of Translation Initiation Complex by Trans-Acting Factors. *Cells*, *10*(7), 1711. https://doi.org/10.3390/cells10071711

Fukao, A., Tomohiro, T., & Fujiwara, T. (2021b). Translation Initiation Regulated by RNA-Binding Protein in Mammals: The Modulation of Translation Initiation Complex by Trans-Acting Factors. *Cells*, *10*(7), 1711. https://doi.org/10.3390/cells10071711

Funayama, M., Hasegawa, K., Kowa, H., Saito, M., Tsuji, S., & Obata, F. (2002). A new locus for Parkinson's disease (PARK8) maps to chromosome 12p11.2-q13.1. *Annals of Neurology*, *51*(3). https://doi.org/10.1002/ana.10113

Gan-Or, Z., Leblond, C. S., Mallett, V., Orr-Urtreger, A., Dion, P. A., & Rouleau, G. A. (2015). LRRK2 mutations in Parkinson disease; a sex effect or lack thereof? A meta-analysis. *Parkinsonism & Related Disorders*, *21*(7), 778–782. https://doi.org/10.1016/j.parkreldis.2015.05.002

Gardet, A., Benita, Y., Li, C., Sands, B. E., Ballester, I., Stevens, C., Korzenik, J. R., Rioux, J. D., Daly, M. J., Xavier, R. J., & Podolsky, D. K. (2010). LRRK2 Is Involved in the IFN-γ Response and Host Response to Pathogens. *The Journal of Immunology*, *185*(9), 5577–5585. https://doi.org/10.4049/jimmunol.1000548

Gasser, T. (2004). Genetics of Parkinson's disease. *Dialogues in Clinical Neuroscience*, *6*(3), 295–301. https://doi.org/10.31887/DCNS.2004.6.3/tgasser

Gasser, T. (2011). Genetic basis of Parkinson's disease: inheritance, penetrance, and expression. *The Application of Clinical Genetics*, 67. https://doi.org/10.2147/TACG.S11639

Gehrke, S., Imai, Y., Sokol, N., & Lu, B. (2010). Pathogenic LRRK2 negatively regulates microRNA-mediated translational repression. *Nature*, *466*(7306), 637–641. https://doi.org/10.1038/nature09191

Geraedts, V. J., Kuijf, M. L., van Hilten, J. J., Marinus, J., Oosterloo, M., & Contarino, M. F. (2019). Selecting candidates for Deep Brain Stimulation in Parkinson's disease: the role of patients' expectations. *Parkinsonism & Related Disorders*, *66*, 207–211. https://doi.org/10.1016/j.parkreldis.2019.07.011

Ghosh, M., Aguila, H. L., Michaud, J., Ai, Y., Wu, M.-T., Hemmes, A., Ristimaki, A., Guo, C., Furneaux, H., & Hla, T. (2009). Essential role of the RNA-binding protein HuR in progenitor cell survival in mice. *Journal of Clinical Investigation*, *119*(12). https://doi.org/10.1172/JCI38263

Giaime, E., Tong, Y., Wagner, L. K., Yuan, Y., Huang, G., & Shen, J. (2017). Age-Dependent Dopaminergic Neurodegeneration and Impairment of the Autophagy-Lysosomal Pathway in LRRK-Deficient Mice. *Neuron*, *96*(4), 796-807.e6. https://doi.org/10.1016/j.neuron.2017.09.036

Gialluisi, A., Reccia, M. G., Modugno, N., Nutile, T., Lombardi, A., Di Giovannantonio, L. G., Pietracupa, S., Ruggiero, D., Scala, S., Gambardella, S., Noyce, A. J., Kaiyrzhanov, R., Middlehurst, B., Kia, D. A., Tan, M., Houlden, H., Morris, H. R., Plun-Favreau, H., Holmans, P., … Esposito, T. (2021). Identification of sixteen novel candidate genes for late onset Parkinson's disease. *Molecular Neurodegeneration*, *16*(1), 35. https://doi.org/10.1186/s13024-021-00455-2

Gilsbach, B. K., & Kortholt, A. (2014). Structural biology of the LRRK2 GTPase and kinase domains: implications for regulation. *Frontiers in Molecular Neuroscience*, *7*. https://doi.org/10.3389/fnmol.2014.00032

Godena, V. K., Brookes-Hocking, N., Moller, A., Shaw, G., Oswald, M., Sancho, R. M., Miller, C. C. J., Whitworth, A. J., & De Vos, K. J. (2014). Increasing microtubule acetylation rescues axonal transport

and locomotor deficits caused by LRRK2 Roc-COR domain mutations. *Nature Communications*, *5*(1), 5245. https://doi.org/10.1038/ncomms6245

Goetz, C. G. (2011). The History of Parkinson's Disease: Early Clinical Descriptions and Neurological Therapies. *Cold Spring Harbor Perspectives in Medicine*, *1*(1), a008862–a008862. https://doi.org/10.1101/cshperspect.a008862

Gómez-Benito, M., Granado, N., García-Sanz, P., Michel, A., Dumoulin, M., & Moratalla, R. (2020). Modeling Parkinson's Disease With the Alpha-Synuclein Protein. *Frontiers in Pharmacology*, *11*. https://doi.org/10.3389/fphar.2020.00356

Gonçalves, F. B., & Morais, V. A. (2021). PINK1: A Bridge between Mitochondria and Parkinson's Disease. *Life*, *11*(5), 371. https://doi.org/10.3390/life11050371

Good, P. J. (1995). A conserved family of elav-like genes in vertebrates. *Proceedings of the National Academy of Sciences*, *92*(10), 4557–4561. https://doi.org/10.1073/pnas.92.10.4557

Gorman, G. S., Chinnery, P. F., DiMauro, S., Hirano, M., Koga, Y., McFarland, R., Suomalainen, A., Thorburn, D. R., Zeviani, M., & Turnbull, D. M. (2016). Mitochondrial diseases. *Nature Reviews Disease Primers*, *2*(1), 16080. https://doi.org/10.1038/nrdp.2016.80

Grammatikakis, I., Abdelmohsen, K., & Gorospe, M. (2017). Posttranslational control of <scp>HuR</scp> function. *WIREs RNA*, *8*(1). https://doi.org/10.1002/wrna.1372

Grassi, E., Santoro, R., Umbach, A., Grosso, A., Oliviero, S., Neri, F., Conti, L., Ala, U., Provero, P., DiCunto, F., & Merlo, G. R. (2019). Choice of Alternative Polyadenylation Sites, Mediated by the RNA-Binding Protein Elavl3, Plays a Role in Differentiation of Inhibitory Neuronal Progenitors. *Frontiers in Cellular Neuroscience*, *12*. https://doi.org/10.3389/fncel.2018.00518

Greffard, S., Verny, M., Bonnet, A.-M., Beinis, J.-Y., Gallinari, C., Meaume, S., Piette, F., Hauw, J.-J., & Duyckaerts, C. (2006). Motor Score of the Unified Parkinson Disease Rating Scale as a Good Predictor of Lewy Body–Associated Neuronal Loss in the Substantia Nigra. *Archives of Neurology*, *63*(4), 584. https://doi.org/10.1001/archneur.63.4.584

Greggio, E., & Cookson, M. R. (2009). Leucine-Rich Repeat Kinase 2 Mutations and Parkinson's Disease: Three Questions. *ASN Neuro*, *1*(1), AN20090007. https://doi.org/10.1042/AN20090007

Grosch, J., Winkler, J., & Kohl, Z. (2016). Early Degeneration of Both Dopaminergic and Serotonergic Axons – A Common Mechanism in Parkinson's Disease. *Frontiers in Cellular Neuroscience*, *10*. https://doi.org/10.3389/fncel.2016.00293

Guaitoli, G., Raimondi, F., Gilsbach, B. K., Gómez-Llorente, Y., Deyaert, E., Renzi, F., Li, X., Schaffner, A., Jagtap, P. K. A., Boldt, K., von Zweydorf, F., Gotthardt, K., Lorimer, D. D., Yue, Z., Burgin, A., Janjic, N., Sattler, M., Versées, W., Ueffing, M., … Gloeckner, C. J. (2016). Structural model of the dimeric Parkinson's protein LRRK2 reveals a compact architecture involving distant interdomain

contacts. *Proceedings of the National Academy of Sciences*, *113*(30). https://doi.org/10.1073/pnas.1523708113

Häbig, K., Walter, M., Poths, S., Riess, O., & Bonin, M. (2008). RNA interference of LRRK2–microarray expression analysis of a Parkinson's disease key player. *Neurogenetics*, *9*(2), 83–94. https://doi.org/10.1007/s10048-007-0114-0

Hafen, B. B., & Sharma, S. (2023). *Oxygen Saturation*.

Hakimi, M., Selvanantham, T., Swinton, E., Padmore, R. F., Tong, Y., Kabbach, G., Venderova, K., Girardin, S. E., Bulman, D. E., Scherzer, C. R., Lavoie, M. J., Gris, D., Park, D. S., Angel, J. B., Shen, J., Philpott, D. J., & Schlossmacher, M. G. (2011). Parkinson's disease-linked LRRK2 is expressed in circulating and tissue immune cells and upregulated following recognition of microbial structures. *Journal of Neural Transmission*, *118*(5), 795–808. https://doi.org/10.1007/s00702-011-0653-2

Han, R., Liu, Y., Li, S., Li, X.-J., & Yang, W. (2023). PINK1-PRKN mediated mitophagy: differences between *in vitro* and *in vivo* models. *Autophagy*, *19*(5), 1396–1405. https://doi.org/10.1080/15548627.2022.2139080

Haugarvoll, K., Toft, M., Ross, O. A., Stone, J. T., Heckman, M. G., White, L. R., Lynch, T., Gibson, J. M., Wszolek, Z. K., Uitti, R. J., Aasly, J. O., & Farrer, M. J. (2007). ELAVL4, PARK10, and the Celts. *Movement Disorders*, *22*(4). https://doi.org/10.1002/mds.21336

Healy, D. G., Falchi, M., O'Sullivan, S. S., Bonifati, V., Durr, A., Bressman, S., Brice, A., Aasly, J., Zabetian, C. P., Goldwurm, S., Ferreira, J. J., Tolosa, E., Kay, D. M., Klein, C., Williams, D. R., Marras, C., Lang, A. E., Wszolek, Z. K., Berciano, J., … Wood, N. W. (2008a). Phenotype, genotype, and worldwide genetic penetrance of LRRK2-associated Parkinson's disease: a case-control study. *The Lancet Neurology*, *7*(7), 583–590. https://doi.org/10.1016/S1474-4422(08)70117-0

Healy, D. G., Falchi, M., O'Sullivan, S. S., Bonifati, V., Durr, A., Bressman, S., Brice, A., Aasly, J., Zabetian, C. P., Goldwurm, S., Ferreira, J. J., Tolosa, E., Kay, D. M., Klein, C., Williams, D. R., Marras, C., Lang, A. E., Wszolek, Z. K., Berciano, J., … Wood, N. W. (2008b). Phenotype, genotype, and worldwide genetic penetrance of LRRK2-associated Parkinson's disease: a case-control study. *The Lancet Neurology*, *7*(7), 583–590. https://doi.org/10.1016/S1474-4422(08)70117-0

Hentze, M. W., Castello, A., Schwarzl, T., & Preiss, T. (2018). A brave new world of RNA-binding proteins. *Nature Reviews Molecular Cell Biology*, *19*(5), 327–341. https://doi.org/10.1038/nrm.2017.130

Herrick, M. K., & Tansey, M. G. (2021). Is LRRK2 the missing link between inflammatory bowel disease and Parkinson's disease? *Npj Parkinson's Disease*, *7*(1), 26. https://doi.org/10.1038/s41531-021-00170-1

Herzig, M. C., Kolly, C., Persohn, E., Theil, D., Schweizer, T., Hafner, T., Stemmelen, C., Troxler, T. J., Schmid, P., Danner, S., Schnell, C. R., Mueller, M., Kinzel, B., Grevot, A., Bolognani, F., Stirn, M., Kuhn, R. R., Kaupmann, K., van der Putten, P. H., … Shimshek, D. R. (2011). LRRK2 protein levels are determined by kinase function and are crucial for kidney and lung homeostasis in mice. *Human Molecular Genetics*, *20*(21), 4209–4223. https://doi.org/10.1093/hmg/ddr348

Hicks, A. A., Pétursson, H., Jónsson, T., Stefánsson, H., Jóhannsdóttir, H. S., Sainz, J., Frigge, M. L., Kong, A., Gulcher, J. R., Stefánsson, K., & Sveinbjörnsdóttir, S. (2002). A susceptibility gene for late-onset idiopathic Parkinson's disease. *Annals of Neurology*, *52*(5), 549–555. https://doi.org/10.1002/ana.10324

Ho, D.-H., Nam, D., Seo, M., Park, S.-W., Seol, W., & Son, I. (2022). LRRK2 Inhibition Mitigates the Neuroinflammation Caused by TLR2-Specific α-Synuclein and Alleviates Neuroinflammation-Derived Dopaminergic Neuronal Loss. *Cells*, *11*(5), 861. https://doi.org/10.3390/cells11050861

Hong, Y., Tak, H., Kim, C., Kang, H., Ji, E., Ahn, S., Jung, M., Kim, H. L., Lee, J.-H., Kim, W., & Lee, E. K. (2020). RNA binding protein HuD contributes to β-cell dysfunction by impairing mitochondria dynamics. *Cell Death & Differentiation*, *27*(5), 1633–1643. https://doi.org/10.1038/s41418-019-0447-x

Horn, T., Gosliga, A., Li, C., Enculescu, M., & Legewie, S. (2023). Position-dependent effects of RNA-binding proteins in the context of co-transcriptional splicing. *Npj Systems Biology and Applications*, *9*(1), 1. https://doi.org/10.1038/s41540-022-00264-3

Hotamisligil, G. S. (2006). Inflammation and metabolic disorders. *Nature*, *444*(7121), 860–867. https://doi.org/10.1038/nature05485

Hubers, L., Valderrama-Carvajal, H., Laframboise, J., Timbers, J., Sanchez, G., & Côté, J. (2011). HuD interacts with survival motor neuron protein and can rescue spinal muscular atrophy-like neuronal defects. *Human Molecular Genetics*, *20*(3), 553–579. https://doi.org/10.1093/hmg/ddq500

Hui, K. Y., Fernandez-Hernandez, H., Hu, J., Schaffner, A., Pankratz, N., Hsu, N.-Y., Chuang, L.-S., Carmi, S., Villaverde, N., Li, X., Rivas, M., Levine, A. P., Bao, X., Labrias, P. R., Haritunians, T., Ruane, D., Gettler, K., Chen, E., Li, D., … Peter, I. (2018). Functional variants in the *LRRK2* gene confer shared effects on risk for Crohn's disease and Parkinson's disease. *Science Translational Medicine*, *10*(423). https://doi.org/10.1126/scitranslmed.aai7795

Ibáñez, P., Bonnet, A.-M., Débarges, B., Lohmann, E., Tison, F., Agid, Y., Dürr, A., Brice, A., & Pollak, P. (2004). Causal relation between α-synuclein locus duplication as a cause of familial Parkinson's disease. *The Lancet*, *364*(9440), 1169–1171. https://doi.org/10.1016/S0140-6736(04)17104-3

Imai, Y., Gehrke, S., Wang, H.-Q., Takahashi, R., Hasegawa, K., Oota, E., & Lu, B. (2008). Phosphorylation of 4E-BP by LRRK2 affects the maintenance of dopaminergic neurons in Drosophila. *The EMBO Journal*, *27*(18), 2432–2443. https://doi.org/10.1038/emboj.2008.163

Ince-Dunn, G., Okano, H. J., Jensen, K. B., Park, W.-Y., Zhong, R., Ule, J., Mele, A., Fak, J. J., Yang, C., Zhang, C., Yoo, J., Herre, M., Okano, H., Noebels, J. L., & Darnell, R. B. (2012). Neuronal Elav-like (Hu) Proteins Regulate RNA Splicing and Abundance to Control Glutamate Levels and Neuronal Excitability. *Neuron*, *75*(6), 1067–1080. https://doi.org/10.1016/j.neuron.2012.07.009

Irving, C. A., & Chaudhari, M. P. (2012). Cardiovascular abnormalities in Down's syndrome: spectrum, management and survival over 22 years. *Archives of Disease in Childhood*, *97*(4), 326–330. https://doi.org/10.1136/adc.2010.210534

Jaleel, M., Nichols, R. J., Deak, M., Campbell, D. G., Gillardon, F., Knebel, A., & Alessi, D. R. (2007). LRRK2 phosphorylates moesin at threonine-558: characterization of how Parkinson's disease mutants affect kinase activity. *Biochemical Journal*, *405*(2), 307–317. https://doi.org/10.1042/BJ20070209

Jennings, D., Huntwork-Rodriguez, S., Henry, A. G., Sasaki, J. C., Meisner, R., Diaz, D., Solanoy, H., Wang, X., Negrou, E., Bondar, V. V., Ghosh, R., Maloney, M. T., Propson, N. E., Zhu, Y., Maciuca, R. D., Harris, L., Kay, A., LeWitt, P., King, T. A., … Troyer, M. D. (2022). Preclinical and clinical evaluation of the LRRK2 inhibitor DNL201 for Parkinson's disease. *Science Translational Medicine*, *14*(648). https://doi.org/10.1126/scitranslmed.abj2658

Jeong, G. R., Jang, E.-H., Bae, J. R., Jun, S., Kang, H. C., Park, C.-H., Shin, J.-H., Yamamoto, Y., Tanaka-Yamamoto, K., Dawson, V. L., Dawson, T. M., Hur, E.-M., & Lee, B. D. (2018). Dysregulated phosphorylation of Rab GTPases by LRRK2 induces neurodegeneration. *Molecular Neurodegeneration*, *13*(1), 8. https://doi.org/10.1186/s13024-018-0240-1

Joseph, B., Orlian, M., & Furneaux, H. (1998). p21waf1 mRNA Contains a Conserved Element in Its 3′-Untranslated Region That Is Bound by the Elav-like mRNA-stabilizing Proteins. *Journal of Biological Chemistry*, *273*(32), 20511–20516. https://doi.org/10.1074/jbc.273.32.20511

Jung, M., & Lee, E. K. (2021). RNA–Binding Protein HuD as a Versatile Factor in Neuronal and Non–Neuronal Systems. *Biology*, *10*(5), 361. https://doi.org/10.3390/biology10050361

Kalogeropulou, A. F., Purlyte, E., Tonelli, F., Lange, S. M., Wightman, M., Prescott, A. R., Padmanabhan, S., Sammler, E., & Alessi, D. R. (2022). Impact of 100 LRRK2 variants linked to Parkinson's disease on kinase activity and microtubule binding. *Biochemical Journal*, *479*(17), 1759–1783. https://doi.org/10.1042/BCJ20220161

Kamath, T., Abdulraouf, A., Burris, S. J., Langlieb, J., Gazestani, V., Nadaf, N. M., Balderrama, K., Vanderburg, C., & Macosko, E. Z. (2022). Single-cell genomic profiling of human dopamine neurons

identifies a population that selectively degenerates in Parkinson's disease. *Nature Neuroscience*, *25*(5). https://doi.org/10.1038/s41593-022-01061-1

Kang, M.-J., Abdelmohsen, K., Hutchison, E. R., Mitchell, S. J., Grammatikakis, I., Guo, R., Noh, J. H., Martindale, J. L., Yang, X., Lee, E. K., Faghihi, M. A., Wahlestedt, C., Troncoso, J. C., Pletnikova, O., Perrone-Bizzozero, N., Resnick, S. M., de Cabo, R., Mattson, M. P., & Gorospe, M. (2014a). HuD Regulates Coding and Noncoding RNA to Induce APP→Aβ Processing. *Cell Reports*, *7*(5), 1401–1409. https://doi.org/10.1016/j.celrep.2014.04.050

Kang, M.-J., Abdelmohsen, K., Hutchison, E. R., Mitchell, S. J., Grammatikakis, I., Guo, R., Noh, J. H., Martindale, J. L., Yang, X., Lee, E. K., Faghihi, M. A., Wahlestedt, C., Troncoso, J. C., Pletnikova, O., Perrone-Bizzozero, N., Resnick, S. M., de Cabo, R., Mattson, M. P., & Gorospe, M. (2014b). HuD Regulates Coding and Noncoding RNA to Induce APP→Aβ Processing. *Cell Reports*, *7*(5), 1401–1409. https://doi.org/10.1016/j.celrep.2014.04.050

Karayel, Ö., Tonelli, F., Virreira Winter, S., Geyer, P. E., Fan, Y., Sammler, E. M., Alessi, D. R., Steger, M., & Mann, M. (2020). Accurate MS-based Rab10 Phosphorylation Stoichiometry Determination as Readout for LRRK2 Activity in Parkinson's Disease. *Molecular & Cellular Proteomics*, *19*(9), 1546–1560. https://doi.org/10.1074/mcp.RA120.002055

Katsanou, V., Milatos, S., Yiakouvaki, A., Sgantzis, N., Kotsoni, A., Alexiou, M., Harokopos, V., Aidinis, V., Hemberger, M., & Kontoyiannis, D. L. (2009). The RNA-Binding Protein Elavl1/HuR Is Essential for Placental Branching Morphogenesis and Embryonic Development. *Molecular and Cellular Biology*, *29*(10), 2762–2776. https://doi.org/10.1128/MCB.01393-08

Katsanou, V., Papadaki, O., Milatos, S., Blackshear, P. J., Anderson, P., Kollias, G., & Kontoyiannis, D. L. (2005). HuR as a negative posttranscriptional modulator in inflammation. *Molecular Cell*, *19*(6), 777–789. https://doi.org/10.1016/j.molcel.2005.08.007

Ke, Y., Lv, X., Fu, X., Zhang, J., Bohio, A. A., Zeng, X., Hao, W., Wang, R., Boldogh, I., & Ba, X. (2021). Poly(ADP-ribosyl)ation enhances HuR oligomerization and contributes to pro-inflammatory gene mRNA stabilization. *Cellular and Molecular Life Sciences*, *78*(4). https://doi.org/10.1007/s00018-020-03618-4

Killinger, B. A., Madaj, Z., Sikora, J. W., Rey, N., Haas, A. J., Vepa, Y., Lindqvist, D., Chen, H., Thomas, P. M., Brundin, P., Brundin, L., & Labrie, V. (2018). The vermiform appendix impacts the risk of developing Parkinson's disease. *Science Translational Medicine*, *10*(465). https://doi.org/10.1126/scitranslmed.aar5280

Kim, B., Yang, M.-S., Choi, D., Kim, J.-H., Kim, H.-S., Seol, W., Choi, S., Jou, I., Kim, E.-Y., & Joe, E. (2012). Impaired Inflammatory Responses in Murine Lrrk2-Knockdown Brain Microglia. *PLoS ONE*, *7*(4), e34693. https://doi.org/10.1371/journal.pone.0034693

Kim, C., Beilina, A., Smith, N., Li, Y., Kim, M., Kumaran, R., Kaganovich, A., Mamais, A., Adame, A., Iba, M., Kwon, S., Lee, W.-J., Shin, S.-J., Rissman, R. A., You, S., Lee, S.-J., Singleton, A. B., Cookson, M. R., & Masliah, E. (2020). LRRK2 mediates microglial neurotoxicity via NFATc2 in rodent models of synucleinopathies. *Science Translational Medicine*, *12*(565). https://doi.org/10.1126/scitranslmed.aay0399

Kim, C., Kim, W., Lee, H., Ji, E., Choe, Y.-J., Martindale, J. L., Akamatsu, W., Okano, H., Kim, H.-S., Nam, S. W., Gorospe, M., & Lee, E. K. (2014). The RNA-binding Protein HuD Regulates Autophagosome Formation in Pancreatic β Cells by Promoting Autophagy-related Gene 5 Expression. *Journal of Biological Chemistry*, *289*(1), 112–121. https://doi.org/10.1074/jbc.M113.474700

Kim, C., Lee, H., Kang, H., Shin, J. J., Tak, H., Kim, W., Gorospe, M., & Lee, E. K. (2016). RNA-binding protein HuD reduces triglyceride production in pancreatic β cells by enhancing the expression of insulin-induced gene 1. *Biochimica et Biophysica Acta (BBA) - Gene Regulatory Mechanisms*, *1859*(4), 675–685. https://doi.org/10.1016/j.bbagrm.2016.02.017

Kim, H. H., Abdelmohsen, K., Lal, A., Pullmann, R., Yang, X., Galban, S., Srikantan, S., Martindale, J. L., Blethrow, J., Shokat, K. M., & Gorospe, M. (2008). Nuclear HuR accumulation through phosphorylation by Cdk1. *Genes & Development*, *22*(13), 1804–1815. https://doi.org/10.1101/gad.1645808

Kim, H. H., Kuwano, Y., Srikantan, S., Lee, E. K., Martindale, J. L., & Gorospe, M. (2009). HuR recruits let-7/RISC to repress c-Myc expression. *Genes & Development*, *23*(15), 1743–1748. https://doi.org/10.1101/gad.1812509

Kim, K. S., Marcogliese, P. C., Yang, J., Callaghan, S. M., Resende, V., Abdel-Messih, E., Marras, C., Visanji, N. P., Huang, J., Schlossmacher, M. G., Trinkle-Mulcahy, L., Slack, R. S., Lang, A. E., Park, D. S., Brown, E., Gibbings, D., Hayley, S., Park, D., Philpott, D. C., … Schurr, E. (2018a). Regulation of myeloid cell phagocytosis by LRRK2 via WAVE2 complex stabilization is altered in Parkinson's disease. *Proceedings of the National Academy of Sciences*, *115*(22). https://doi.org/10.1073/pnas.1718946115

Kim, K. S., Marcogliese, P. C., Yang, J., Callaghan, S. M., Resende, V., Abdel-Messih, E., Marras, C., Visanji, N. P., Huang, J., Schlossmacher, M. G., Trinkle-Mulcahy, L., Slack, R. S., Lang, A. E., Park, D. S., Brown, E., Gibbings, D., Hayley, S., Park, D., Philpott, D. C., … Schurr, E. (2018b). Regulation of myeloid cell phagocytosis by LRRK2 via WAVE2 complex stabilization is altered in Parkinson's disease. *Proceedings of the National Academy of Sciences*, *115*(22). https://doi.org/10.1073/pnas.1718946115

Kim, Y., & Baker, B. (1993). The Drosophila gene rbp9 encodes a protein that is a member of a conserved group of putative RNA binding proteins that are nervous system-specific in both flies and humans. *The Journal of Neuroscience*, *13*(3). https://doi.org/10.1523/JNEUROSCI.13-03-01045.1993

Kitada, T., Asakawa, S., Hattori, N., Matsumine, H., Yamamura, Y., Minoshima, S., Yokochi, M., Mizuno, Y., & Shimizu, N. (1998). Mutations in the parkin gene cause autosomal recessive juvenile parkinsonism. *Nature*, *392*(6676), 605–608. https://doi.org/10.1038/33416

Klein, C., & Westenberger, A. (2012). *Genetics of Parkinson ' s Disease*. https://doi.org/10.1016/j.cell.2015.01.019

Koene, S., Wortmann, S. B., de Vries, M. C., Jonckheere, A. I., Morava, E., de Groot, I. J. M., & Smeitink, J. A. M. (2013). Developing outcome measures for pediatric mitochondrial disorders: Which complaints and limitations are most burdensome to patients and their parents? *Mitochondrion*, *13*(1), 15–24. https://doi.org/10.1016/j.mito.2012.11.002

Koenig, M. K. (2008). Presentation and Diagnosis of Mitochondrial Disorders in Children. *Pediatric Neurology*, *38*(5), 305–313. https://doi.org/10.1016/j.pediatrneurol.2007.12.001

Korkmaz Eryılmaz, S., Polat, M., Soyal, M., & Aydoğan, S. (2018). The Relationship between the Isocapnic Buffering Phase and Ventilatory Threshold in Endurance Athletes and Team Sport Athletes during an Incremental Exercise Test. *Annals of Applied Sport Science*, *6*(1), 1–9. https://doi.org/10.29252/aassjournal.6.1.1

Kühlbrandt, W. (2015). Structure and function of mitochondrial membrane protein complexes. *BMC Biology*, *13*(1), 89. https://doi.org/10.1186/s12915-015-0201-x

Kullmann, M., Göpfert, U., Siewe, B., & Hengst, L. (2002). ELAV/Hu proteins inhibit p27 translation via an IRES element in the p27 5′UTR. *Genes and Development*, *16*(23), 3087–3099. https://doi.org/10.1101/gad.248902

Kumar, A., Greggio, E., Beilina, A., Kaganovich, A., Chan, D., Taymans, J.-M., Wolozin, B., & Cookson, M. R. (2010). The Parkinson's Disease Associated LRRK2 Exhibits Weaker In Vitro Phosphorylation of 4E-BP Compared to Autophosphorylation. *PLoS ONE*, *5*(1), e8730. https://doi.org/10.1371/journal.pone.0008730

Kumari, U., & Tan, E.-K. (2010). Leucine-Rich Repeat Kinase 2-Linked Parkinson's Disease: Clinical and Molecular Findings. *Journal of Movement Disorders*, *3*(2), 25–31. https://doi.org/10.14802/jmd.10008

Kundu, P., Fabian, M. R., Sonenberg, N., Bhattacharyya, S. N., & Filipowicz, W. (2012). HuR protein attenuates miRNA-mediated repression by promoting miRISC dissociation from the target RNA. *Nucleic Acids Research*, *40*(11), 5088–5100. https://doi.org/10.1093/nar/gks148

Kuwahara, T., & Iwatsubo, T. (2020). The Emerging Functions of LRRK2 and Rab GTPases in the Endolysosomal System. *Frontiers in Neuroscience*, *14*. https://doi.org/10.3389/fnins.2020.00227

Lal, A., Kawai, T., Yang, X., Mazan-Mamczarz, K., & Gorospe, M. (2005). Antiapoptotic function of RNA-binding protein HuR effected through prothymosin α. *The EMBO Journal*, *24*(10), 1852–1862. https://doi.org/10.1038/sj.emboj.7600661

Lang, M., Berry, D., Passecker, K., Mesteri, I., Bhuju, S., Ebner, F., Sedlyarov, V., Evstatiev, R., Dammann, K., Loy, A., Kuzyk, O., Kovarik, P., Khare, V., Beibel, M., Roma, G., Meisner-Kober, N., & Gasche, C. (2017). HuR small-molecule inhibitor elicits differential effects in adenomatosis polyposis and colorectal carcinogenesis. *Cancer Research*, *77*(9), 2424–2438. https://doi.org/10.1158/0008-5472.CAN-15-1726

Lavalley, N. J., Slone, S. R., Ding, H., West, A. B., & Yacoubian, T. A. (2016). 14-3-3 Proteins regulate mutant LRRK2 kinase activity and neurite shortening. *Human Molecular Genetics*, *25*(1), 109–122. https://doi.org/10.1093/hmg/ddv453

Lee, A. J., Wang, Y., Alcalay, R. N., Mejia-Santana, H., Saunders-Pullman, R., Bressman, S., Corvol, J.-C., Brice, A., Lesage, S., Mangone, G., Tolosa, E., Pont-Sunyer, C., Vilas, D., Schüle, B., Kausar, F., Foroud, T., Berg, D., Brockmann, K., Goldwurm, S., … Marder, K. (2017). Penetrance estimate of *LRRK2* p.G2019S mutation in individuals of non-Ashkenazi Jewish ancestry. *Movement Disorders*, *32*(10), 1432–1438. https://doi.org/10.1002/mds.27059

Lee, C.-H., Olson, P., Hevener, A., Mehl, I., Chong, L.-W., Olefsky, J. M., Gonzalez, F. J., Ham, J., Kang, H., Peters, J. M., & Evans, R. M. (2006). PPARdelta regulates glucose metabolism and insulin sensitivity. *Proceedings of the National Academy of Sciences of the United States of America*, *103*(9), 3444–3449. https://doi.org/10.1073/pnas.0511253103

Lee, E. K., Kim, W., Tominaga, K., Martindale, J. L., Yang, X., Subaran, S. S., Carlson, O. D., Mercken, E. M., Kulkarni, R. N., Akamatsu, W., Okano, H., Perrone-Bizzozero, N. I., de Cabo, R., Egan, J. M., & Gorospe, M. (2012). RNA-Binding Protein HuD Controls Insulin Translation. *Molecular Cell*, *45*(6). https://doi.org/10.1016/j.molcel.2012.01.016

Levine, A. P., Pontikos, N., Schiff, E. R., Jostins, L., Speed, D., Lovat, L. B., Barrett, J. C., Grasberger, H., Plagnol, V., & Segal, A. W. (2016). Genetic Complexity of Crohn's Disease in Two Large Ashkenazi Jewish Families. *Gastroenterology*, *151*(4), 698–709. https://doi.org/10.1053/j.gastro.2016.06.040

Levy, D. R., Udgata, A., Tourlomousis, P., Symmons, M. F., Hopkins, L. J., Bryant, C. E., & Gay, N. J. (2020). The Parkinson's disease–associated kinase LRRK2 regulates genes required for cell adhesion, polarization, and chemotaxis in activated murine macrophages. *Journal of Biological Chemistry*, *295*(31), 10857–10867. https://doi.org/10.1074/jbc.RA119.011842

Li, H., Li, Q., Sun, S., Lei, P., Cai, X., & Shen, G. (2020). Integrated Bioinformatics Analysis Identifies ELAVL1 and APP as Candidate Crucial Genes for Crohn's Disease. *Journal of Immunology Research*, *2020*, 1–20. https://doi.org/10.1155/2020/3067273

Li, J.-Q., Tan, L., & Yu, J.-T. (2014). The role of the LRRK2 gene in Parkinsonism. *Molecular Neurodegeneration*, *9*(1), 47. https://doi.org/10.1186/1750-1326-9-47

Li, Y., Liu, W., Oo, T. F., Wang, L., Tang, Y., Jackson-Lewis, V., Zhou, C., Geghman, K., Bogdanov, M., Przedborski, S., Beal, M. F., Burke, R. E., & Li, C. (2009). Mutant LRRK2R1441G BAC transgenic mice recapitulate cardinal features of Parkinson's disease. *Nature Neuroscience*, *12*(7), 826–828. https://doi.org/10.1038/nn.2349

Li, Y.-J., Scott, W. K., Hedges, D. J., Zhang, F., Gaskell, P. C., Nance, M. A., Watts, R. L., Hubble, J. P., Koller, W. C., Pahwa, R., Stern, M. B., Hiner, B. C., Jankovic, J., Allen, F. H., Goetz, C. G., Mastaglia, F., Stajich, J. M., Gibson, R. A., Middleton, L. T., … Pericak-Vance, M. A. (2002). Age at Onset in Two Common Neurodegenerative Diseases Is Genetically Controlled. *The American Journal of Human Genetics*, *70*(4), 985–993. https://doi.org/10.1086/339815

Liao, W.-L., Wang, W.-C., Chang, W.-C., & Tseng, J. T. (2011). The RNA-binding Protein HuR Stabilizes Cytosolic Phospholipase A2α mRNA under Interleukin-1β Treatment in Non-small Cell Lung Cancer A549 Cells. *Journal of Biological Chemistry*, *286*(41), 35499–35508. https://doi.org/10.1074/jbc.M111.263582

Lim, J., Bang, Y., Choi, J.-H., Han, A., Kwon, M.-S., Liu, K. H., & Choi, H. J. (2018). LRRK2 G2019S Induces Anxiety/Depression-like Behavior before the Onset of Motor Dysfunction with 5-HT $_{1A}$ Receptor Upregulation in Mice. *The Journal of Neuroscience*, *38*(7), 1611–1621. https://doi.org/10.1523/JNEUROSCI.4051-15.2017

Lindenschot, M., de Groot, I. J. M., Koene, S., Satink, T., Steultjens, E. M. J., & Nijhuis-van der Sanden, M. W. G. (2018). Everyday Activities for Children with Mitochondrial Disorder: A Retrospective Chart Review. *Occupational Therapy International*, *2018*, 1–8. https://doi.org/10.1155/2018/5716947

Litteljohn, D., Rudyk, C., Dwyer, Z., Farmer, K., Fortin, T., & Hayley, S. (2018). The impact of murine LRRK2 G2019S transgene overexpression on acute responses to inflammatory challenge. *Brain, Behavior, and Immunity*, *67*, 246–256. https://doi.org/10.1016/j.bbi.2017.09.002

Liu, G.-H., Qu, J., Suzuki, K., Nivet, E., Li, M., Montserrat, N., Yi, F., Xu, X., Ruiz, S., Zhang, W., Wagner, U., Kim, A., Ren, B., Li, Y., Goebl, A., Kim, J., Soligalla, R. D., Dubova, I., Thompson, J., … Belmonte, J. C. I. (2012). Progressive degeneration of human neural stem cells caused by pathogenic LRRK2. *Nature*, *491*(7425), 603–607. https://doi.org/10.1038/nature11557

Liu, W., Liu, X., Li, Y., Zhao, J., Liu, Z., Hu, Z., Wang, Y., Yao, Y., Miller, A. W., Su, B., Cookson, M. R., Li, X., & Kang, Z. (2017). LRRK2 promotes the activation of NLRC4 inflammasome during *Salmonella* Typhimurium infection. *Journal of Experimental Medicine*, *214*(10), 3051–3066. https://doi.org/10.1084/jem.20170014

Liu, X., & Le, W. (2020). Profiling Non-motor Symptoms in Monogenic Parkinson's Disease. *Frontiers in Aging Neuroscience*, *12*. https://doi.org/10.3389/fnagi.2020.591183

Liu, Z., Lee, J., Krummey, S., Lu, W., Cai, H., & Lenardo, M. J. (2011). The kinase LRRK2 is a regulator of the transcription factor NFAT that modulates the severity of inflammatory bowel disease. *Nature Immunology*, *12*(11). https://doi.org/10.1038/ni.2113

Locke, A. E., Kahali, B., Berndt, S. I., Justice, A. E., Pers, T. H., Day, F. R., Powell, C., Vedantam, S., Buchkovich, M. L., Yang, J., Croteau-Chonka, D. C., Esko, T., Fall, T., Ferreira, T., Gustafsson, S., Kutalik, Z., Luan, J., Mägi, R., Randall, J. C., … Speliotes, E. K. (2015). Genetic studies of body mass index yield new insights for obesity biology. *Nature*, *518*(7538), 197–206. https://doi.org/10.1038/nature14177

Ma, W.-J., Cheng, S., Campbell, C., Wright, A., & Furneaux, H. (1996). Cloning and Characterization of HuR, a Ubiquitously Expressed Elav-like Protein. *Journal of Biological Chemistry*, *271*(14), 8144–8151. https://doi.org/10.1074/jbc.271.14.8144

MacLeod, D., Dowman, J., Hammond, R., Leete, T., Inoue, K., & Abeliovich, A. (2006). The Familial Parkinsonism Gene LRRK2 Regulates Neurite Process Morphology. *Neuron*, *52*(4), 587–593. https://doi.org/10.1016/j.neuron.2006.10.008

Maekawa, T., Mori, S., Sasaki, Y., Miyajima, T., Azuma, S., Ohta, E., & Obata, F. (2012). The I2020T Leucine-rich repeat kinase 2 transgenic mouse exhibits impaired locomotive ability accompanied by dopaminergic neuron abnormalities. *Molecular Neurodegeneration*, *7*(1), 15. https://doi.org/10.1186/1750-1326-7-15

Manyam, B. V. (1990). Paralysis agitans and levodopa in ?Ayurveda?: Ancient Indian medical treatise. *Movement Disorders*, *5*(1), 47–48. https://doi.org/10.1002/mds.870050112

Marchese, D., Botta-Orfila, T., Cirillo, D., Rodriguez, J. A., Livi, C. M., Fernández-Santiago, R., Ezquerra, M., Martí, M. J., Bechara, E., Tartaglia, G. G., Ávila, A., Bayés, À., Botta-Orfila, T., Caballol, N., Calopa, M., Campdelacreu, J., Compta, Y., Ezquerra, M., de Fàbregues, O., … Valldeoriola, F. (2017). Discovering the 3′ UTR-mediated regulation of alpha-synuclein. *Nucleic Acids Research*, *45*(22). https://doi.org/10.1093/nar/gkx1048

Marcogliese, P. C., Abuaish, S., Kabbach, G., Abdel-Messih, E., Seang, S., Li, G., Slack, R. S., Haque, M. E., Venderova, K., & Park, D. S. (2017). LRRK2(I2020T) functional genetic interactors that modify

eye degeneration and dopaminergic cell loss in Drosophila. *Human Molecular Genetics*, *26*(7), 1247–1257. https://doi.org/10.1093/hmg/ddx030

Mariani, E., Frabetti, F., Tarozzi, A., Pelleri, M. C., Pizzetti, F., & Casadei, R. (2016). Meta-Analysis of Parkinson's Disease Transcriptome Data Using TRAM Software: Whole Substantia Nigra Tissue and Single Dopamine Neuron Differential Gene Expression. *PLOS ONE*, *11*(9), e0161567. https://doi.org/10.1371/journal.pone.0161567

Martin, I., Kim, J. W., Lee, B. D., Kang, H. C., Xu, J.-C., Jia, H., Stankowski, J., Kim, M.-S., Zhong, J., Kumar, M., Andrabi, S. A., Xiong, Y., Dickson, D. W., Wszolek, Z. K., Pandey, A., Dawson, T. M., & Dawson, V. L. (2014). Ribosomal Protein s15 Phosphorylation Mediates LRRK2 Neurodegeneration in Parkinson's Disease. *Cell*, *157*(2), 472–485. https://doi.org/10.1016/j.cell.2014.01.064

Masliah, E., Rockenstein, E., Veinbergs, I., Mallory, M., Hashimoto, M., Takeda, A., Sagara, Y., Sisk, A., & Mucke, L. (2000). Dopaminergic Loss and Inclusion Body Formation in α-Synuclein Mice: Implications for Neurodegenerative Disorders. *Science*, *287*(5456), 1265–1269. https://doi.org/10.1126/science.287.5456.1265

Mazan-Mamczarz, K., Galbán, S., de Silanes, I. L., Martindale, J. L., Atasoy, U., Keene, J. D., & Gorospe, M. (2003). RNA-binding protein HuR enhances p53 translation in response to ultraviolet light irradiation. *Proceedings of the National Academy of Sciences*, *100*(14), 8354–8359. https://doi.org/10.1073/pnas.1432104100

McGrath, E., Waschbüsch, D., Baker, B. M., & Khan, A. R. (2021). LRRK2 binds to the Rab32 subfamily in a GTP-dependent manner *via* its armadillo domain. *Small GTPases*, *12*(2), 133–146. https://doi.org/10.1080/21541248.2019.1666623

Menzies, C., Naz, S., Patten, D., Alquier, T., Bennett, B. M., & Lacoste, B. (2021). Distinct Basal Metabolism in Three Mouse Models of Neurodevelopmental Disorders. *Eneuro*, *8*(2), ENEURO.0292-20.2021. https://doi.org/10.1523/ENEURO.0292-20.2021

Miraglia, F., Ricci, A., Rota, L., & Colla, E. (2018). Subcellular localization of alpha-synuclein aggregates and their interaction with membranes. *Neural Regeneration Research*, *13*(7), 1136. https://doi.org/10.4103/1673-5374.235013

Moehle, M. S., Daher, J. P. L., Hull, T. D., Boddu, R., Abdelmotilib, H. A., Mobley, J., Kannarkat, G. T., Tansey, M. G., & West, A. B. (2015). The G2019S LRRK2 mutation increases myeloid cell chemotactic responses and enhances LRRK2 binding to actin-regulatory proteins. *Human Molecular Genetics*, *24*(15), 4250–4267. https://doi.org/10.1093/hmg/ddv157

Moehle, M. S., Webber, P. J., Tse, T., Sukar, N., Standaert, D. G., DeSilva, T. M., Cowell, R. M., & West, A. B. (2012). LRRK2 Inhibition Attenuates Microglial Inflammatory Responses. *The Journal of Neuroscience*, *32*(5), 1602–1611. https://doi.org/10.1523/JNEUROSCI.5601-11.2012

Monlleo-Neila, L., Toro, M. del, Bornstein, B., Garcia-Arumi, E., Sarrias, A., Roig-Quilis, M., & Munell, F. (2013). Leigh Syndrome and the Mitochondrial m.13513G>A Mutation. *Journal of Child Neurology*, *28*(11), 1531–1534. https://doi.org/10.1177/0883073812460580

Muddapu, V. R., Dharshini, S. A. P., Chakravarthy, V. S., & Gromiha, M. M. (2020). Neurodegenerative Diseases – Is Metabolic Deficiency the Root Cause? *Frontiers in Neuroscience*, *14*. https://doi.org/10.3389/fnins.2020.00213

Mulligan, M. R., & Bicknell, L. S. (2023). The molecular genetics of nELAVL in brain development and disease. *European Journal of Human Genetics*. https://doi.org/10.1038/s41431-023-01456-z

Ng, C.-H., Mok, S. Z. S., Koh, C., Ouyang, X., Fivaz, M. L., Tan, E.-K., Dawson, V. L., Dawson, T. M., Yu, F., & Lim, K.-L. (2009). Parkin Protects against LRRK2 G2019S Mutant-Induced Dopaminergic Neurodegeneration in Drosophila. *The Journal of Neuroscience*, *29*(36), 11257–11262. https://doi.org/10.1523/JNEUROSCI.2375-09.2009

Nguyen, A. P. T., & Moore, D. J. (2017). *Understanding the GTPase Activity of LRRK2: Regulation, Function, and Neurotoxicity* (pp. 71–88). https://doi.org/10.1007/978-3-319-49969-7_4

Nguyen, H. N., Byers, B., Cord, B., Shcheglovitov, A., Byrne, J., Gujar, P., Kee, K., Schüle, B., Dolmetsch, R. E., Langston, W., Palmer, T. D., & Pera, R. R. (2011). LRRK2 Mutant iPSC-Derived DA Neurons Demonstrate Increased Susceptibility to Oxidative Stress. *Cell Stem Cell*, *8*(3), 267–280. https://doi.org/10.1016/j.stem.2011.01.013

Nichols, R. J., Dzamko, N., Morrice, N. A., Campbell, D. G., Deak, M., Ordureau, A., Macartney, T., Tong, Y., Shen, J., Prescott, A. R., & Alessi, D. R. (2010). 14-3-3 binding to LRRK2 is disrupted by multiple Parkinson's disease-associated mutations and regulates cytoplasmic localization. *Biochemical Journal*, *430*(3), 393–404. https://doi.org/10.1042/BJ20100483

Nikonova, E. V., Xiong, Y., Tanis, K. Q., Dawson, V. L., Vogel, R. L., Finney, E. M., Stone, D. J., Reynolds, I. J., Kern, J. T., & Dawson, T. M. (2012). Transcriptional responses to loss or gain of function of the leucine-rich repeat kinase 2 (LRRK2) gene uncover biological processes modulated by LRRK2 activity. *Human Molecular Genetics*, *21*(1), 163–174. https://doi.org/10.1093/hmg/ddr451

Nirujogi, R. S., Tonelli, F., Taylor, M., Lis, P., Zimprich, A., Sammler, E., & Alessi, D. R. (2021). Development of a multiplexed targeted mass spectrometry assay for LRRK2-phosphorylated Rabs and Ser910/Ser935 biomarker sites. *Biochemical Journal*, *478*(2), 299–326. https://doi.org/10.1042/BCJ20200930

Noda, S., Sato, S., Fukuda, T., Tada, N., Uchiyama, Y., Tanaka, K., & Hattori, N. (2020). Loss of Parkin contributes to mitochondrial turnover and dopaminergic neuronal loss in aged mice. *Neurobiology of Disease*, *136*, 104717. https://doi.org/10.1016/j.nbd.2019.104717

Noureddine, M. A., Qin, X. J., Oliveira, S. A., Skelly, T. J., van der Walt, J., Hauser, M. A., Pericak-Vance, M. A., Vance, J. M., & Li, Y. J. (2005). Association between the neuron-specific RNA-binding protein ELAVL4 and Parkinson disease. *Human Genetics*, *117*(1), 27–33. https://doi.org/10.1007/s00439-005-1259-2

Ogawa, Y., Kakumoto, K., Yoshida, T., Kuwako, K., Miyazaki, T., Yamaguchi, J., Konno, A., Hata, J., Uchiyama, Y., Hirai, H., Watanabe, M., Darnell, R. B., Okano, H., & Okano, H. J. (2018). Elavl3 is essential for the maintenance of Purkinje neuron axons. *Scientific Reports*, *8*(1), 2722. https://doi.org/10.1038/s41598-018-21130-5

O'Hara, D. M., Pawar, G., Kalia, S. K., & Kalia, L. V. (2020). LRRK2 and α-Synuclein: Distinct or Synergistic Players in Parkinson's Disease? *Frontiers in Neuroscience*, *14*. https://doi.org/10.3389/fnins.2020.00577

Okano, H. J., & Darnell, R. B. (1997). A Hierarchy of Hu RNA Binding Proteins in Developing and Adult Neurons. *The Journal of Neuroscience*, *17*(9), 3024–3037. https://doi.org/10.1523/JNEUROSCI.17-09-03024.1997

Orenstein, S. J., Kuo, S.-H., Tasset, I., Arias, E., Koga, H., Fernandez-Carasa, I., Cortes, E., Honig, L. S., Dauer, W., Consiglio, A., Raya, A., Sulzer, D., & Cuervo, A. M. (2013). Interplay of LRRK2 with chaperone-mediated autophagy. *Nature Neuroscience*, *16*(4), 394–406. https://doi.org/10.1038/nn.3350

Otsuka, H., Fukao, A., Funakami, Y., Duncan, K. E., & Fujiwara, T. (2019). Emerging Evidence of Translational Control by AU-Rich Element-Binding Proteins. *Frontiers in Genetics*, *10*. https://doi.org/10.3389/fgene.2019.00332

Paisán-Ruíz, C., Jain, S., Evans, E. W., Gilks, W. P., Simón, J., van der Brug, M., de Munain, A. L., Aparicio, S., Gil, A. M., Khan, N., Johnson, J., Martinez, J. R., Nicholl, D., Carrera, I. M., Peňa, A. S., de Silva, R., Lees, A., Martí-Massó, J. F., Pérez-Tur, J., … Singleton, A. B. (2004). Cloning of the Gene Containing Mutations that Cause PARK8-Linked Parkinson's Disease. *Neuron*, *44*(4). https://doi.org/10.1016/j.neuron.2004.10.023

Palomo, G. M., Granatiero, V., Kawamata, H., Konrad, C., Kim, M., Arreguin, A. J., Zhao, D., Milner, T. A., & Manfredi, G. (2018). Parkin is a disease modifier in the mutant <scp>SOD</scp> 1 mouse model of <scp>ALS</scp>. *EMBO Molecular Medicine*, *10*(10). https://doi.org/10.15252/emmm.201808888

Parisiadou, L., Xie, C., Cho, H. J., Lin, X., Gu, X.-L., Long, C.-X., Lobbestael, E., Baekelandt, V., Taymans, J.-M., Sun, L., & Cai, H. (2009). Phosphorylation of Ezrin/Radixin/Moesin Proteins by LRRK2 Promotes the Rearrangement of Actin Cytoskeleton in Neuronal Morphogenesis. *The Journal of Neuroscience*, *29*(44), 13971–13980. https://doi.org/10.1523/JNEUROSCI.3799-09.2009

Park, S., Myszka, D. G., Yu, M., Littler, S. J., & Laird-Offringa, I. a. (2000). HuD RNA recognition motifs play distinct roles in the formation of a stable complex with AU-rich RNA. *Molecular and Cellular Biology*, *20*(13), 4765–4772. https://doi.org/10.1128/MCB.24.15.6888.2004

Parkash, O. (2009). Classification of leprosy into multibacillary and paucibacillary groups: an analysis. *FEMS Immunology & Medical Microbiology*, *55*(1), 1–5. https://doi.org/10.1111/j.1574-695X.2008.00491.x

Pascale, A., Amadio, M., Scapagnini, G., Lanni, C., Racchi, M., Provenzani, A., Govoni, S., Alkon, D. L., & Quattrone, A. (2005). Neuronal ELAV proteins enhance mRNA stability by a PKCalpha-dependent pathway. *Proceedings of the National Academy of Sciences of the United States of America*, *102*(34), 12065–12070. https://doi.org/10.1073/pnas.0504702102

Pastic, A., Negeri, O., Ravel-Chapuis, A., Savard, A., Trung, M. T., Palidwor, G., Guo, H., Marcogliese, P., Taylor, J. A., Okano, H., Trinkle-Mulcahy, L., Jasmin, B. J., Park, D., & Gibbings, D. (2022). LRRK2 Phosphorylates Neuronal Elav RNA-Binding Proteins to Regulate Phenotypes Relevant to Parkinson's Disease. *BioRxiv*, 2022.04.24.489327. https://doi.org/10.1101/2022.04.24.489327

Paul, S., & Pickrell, A. M. (2021). Hidden phenotypes of PINK1/Parkin knockout mice. *Biochimica et Biophysica Acta (BBA) - General Subjects*, *1865*(6), 129871. https://doi.org/10.1016/j.bbagen.2021.129871

Paumier, K. L., Luk, K. C., Manfredsson, F. P., Kanaan, N. M., Lipton, J. W., Collier, T. J., Steece-Collier, K., Kemp, C. J., Celano, S., Schulz, E., Sandoval, I. M., Fleming, S., Dirr, E., Polinski, N. K., Trojanowski, J. Q., Lee, V. M., & Sortwell, C. E. (2015). Intrastriatal injection of pre-formed mouse α-synuclein fibrils into rats triggers α-synuclein pathology and bilateral nigrostriatal degeneration. *Neurobiology of Disease*, *82*, 185–199. https://doi.org/10.1016/j.nbd.2015.06.003

PD MED Collaborative Group. (2014). Long-term effectiveness of dopamine agonists and monoamine oxidase B inhibitors compared with levodopa as initial treatment for Parkinson's disease (PD MED): a large, open-label, pragmatic randomised trial. *The Lancet*, *384*(9949), 1196–1205. https://doi.org/10.1016/S0140-6736(14)60683-8

Perez Carrion, M., Pischedda, F., Biosa, A., Russo, I., Straniero, L., Civiero, L., Guida, M., Gloeckner, C. J., Ticozzi, N., Tiloca, C., Mariani, C., Pezzoli, G., Duga, S., Pichler, I., Pan, L., Landers, J. E., Greggio, E., Hess, M. W., Goldwurm, S., & Piccoli, G. (2018). The LRRK2 Variant E193K Prevents

Mitochondrial Fission Upon MPP+ Treatment by Altering LRRK2 Binding to DRP1. *Frontiers in Molecular Neuroscience*, *11*. https://doi.org/10.3389/fnmol.2018.00064

Peter, I., Dubinsky, M., Bressman, S., Park, A., Lu, C., Chen, N., & Wang, A. (2018). Anti–Tumor Necrosis Factor Therapy and Incidence of Parkinson Disease Among Patients With Inflammatory Bowel Disease. *JAMA Neurology*, *75*(8). https://doi.org/10.1001/jamaneurol.2018.0605

Pfeiffer, R. F. (2016). Non-motor symptoms in Parkinson's disease. *Parkinsonism & Related Disorders*, *22*, S119–S122. https://doi.org/10.1016/j.parkreldis.2015.09.004

Poehlman, E. T., & Dvorak, R. V. (2000). Energy expenditure, energy intake, and weight loss in Alzheimer disease,,,. *The American Journal of Clinical Nutrition*, *71*(2), 650S-655S. https://doi.org/10.1093/ajcn/71.2.650s

Polychronis, S., Niccolini, F., Pagano, G., Yousaf, T., & Politis, M. (2019). Speech difficulties in early de novo patients with Parkinson's disease. *Parkinsonism & Related Disorders*, *64*, 256–261. https://doi.org/10.1016/j.parkreldis.2019.04.026

Polymeropoulos, M. H., Lavedan, C., Leroy, E., Ide, S. E., Dehejia, A., Dutra, A., Pike, B., Root, H., Rubenstein, J., Boyer, R., Stenroos, E. S., Chandrasekharappa, S., Athanassiadou, A., Papapetropoulos, T., Johnson, W. G., Lazzarini, A. M., Duvoisin, R. C., Di Iorio, G., Golbe, L. I., & Nussbaum, R. L. (1997). Mutation in the α-Synuclein Gene Identified in Families with Parkinson's Disease. *Science*, *276*(5321). https://doi.org/10.1126/science.276.5321.2045

Pycroft, L., Stein, J., & Aziz, T. (2018). Deep brain stimulation: An overview of history, methods, and future developments. *Brain and Neuroscience Advances*, *2*, 239821281881601. https://doi.org/10.1177/2398212818816017

Quinn, P. M. J., Moreira, P. I., Ambrósio, A. F., & Alves, C. H. (2020). PINK1/PARKIN signalling in neurodegeneration and neuroinflammation. *Acta Neuropathologica Communications*, *8*(1), 189. https://doi.org/10.1186/s40478-020-01062-w

Ramonet, D., Daher, J. P. L., Lin, B. M., Stafa, K., Kim, J., Banerjee, R., Westerlund, M., Pletnikova, O., Glauser, L., Yang, L., Liu, Y., Swing, D. A., Beal, M. F., Troncoso, J. C., McCaffery, J. M., Jenkins, N. A., Copeland, N. G., Galter, D., Thomas, B., … Moore, D. J. (2011). Dopaminergic Neuronal loss, Reduced Neurite Complexity and Autophagic Abnormalities in Transgenic Mice Expressing G2019S Mutant LRRK2. *PLoS ONE*, *6*(4). https://doi.org/10.1371/journal.pone.0018568

Ramos-Jiménez, A., Hernández-Torres, R. P., Torres-Durán, P. V, Romero-Gonzalez, J., Mascher, D., Posadas-Romero, C., & Juárez-Oropeza, M. A. (2008). The Respiratory Exchange Ratio is Associated with Fitness Indicators Both in Trained and Untrained Men: A Possible Application for People with Reduced Exercise Tolerance. *Clinical Medicine. Circulatory, Respiratory and Pulmonary Medicine*, *2*, 1–9. https://doi.org/10.4137/ccrpm.s449

Reimand, J., Arak, T., Adler, P., Kolberg, L., Reisberg, S., Peterson, H., & Vilo, J. (2016). g:Profiler—a web server for functional interpretation of gene lists (2016 update). *Nucleic Acids Research*, *44*(W1), W83–W89. https://doi.org/10.1093/nar/gkw199

Rektorova, I. (2019). Current treatment of behavioral and cognitive symptoms of Parkinson's disease. *Parkinsonism & Related Disorders*, *59*, 65–73. https://doi.org/10.1016/j.parkreldis.2019.02.042

Repici, M., & Giorgini, F. (2019). DJ-1 in Parkinson's Disease: Clinical Insights and Therapeutic Perspectives. *Journal of Clinical Medicine*, *8*(9), 1377. https://doi.org/10.3390/jcm8091377

Rhinn, H., Qiang, L., Yamashita, T., Rhee, D., Zolin, A., Vanti, W., & Abeliovich, A. (2012). Alternative α-synuclein transcript usage as a convergent mechanism in Parkinson's disease pathology. *Nature Communications*, *3*, 1084. https://doi.org/10.1038/ncomms2032

Riboldi, G. M., & Di Fonzo, A. B. (2019). GBA, Gaucher Disease, and Parkinson's Disease: From Genetic to Clinic to New Therapeutic Approaches. *Cells*, *8*(4), 364. https://doi.org/10.3390/cells8040364

Ripin, N., Boudet, J., Duszczyk, M. M., Hinniger, A., Faller, M., Krepl, M., Gadi, A., Schneider, R. J., Šponer, J., Meisner-Kober, N. C., & Allain, F. H.-T. (2019). Molecular basis for AU-rich element recognition and dimerization by the HuR C-terminal RRM. *Proceedings of the National Academy of Sciences*, *116*(8), 2935–2944. https://doi.org/10.1073/pnas.1808696116

Robinow, S., Campos, A. R., Yao, K.-M., & White, K. (1988). The *elav* Gene Product of *Drosophila* , Required in Neurons, Has Three RNP Consensus Motifs. *Science*, *242*(4885). https://doi.org/10.1126/science.3144044

Rocha, E. M., Keeney, M. T., Di Maio, R., De Miranda, B. R., & Greenamyre, J. T. (2022). LRRK2 and idiopathic Parkinson's disease. *Trends in Neurosciences*, *45*(3), 224–236. https://doi.org/10.1016/j.tins.2021.12.002

Roos, D. S., Klein, M., Deeg, D. J. H., Doty, R. L., & Berendse, H. W. (2022). Prevalence of Prodromal Symptoms of Parkinson's Disease in the Late Middle-Aged Population. *Journal of Parkinson's Disease*, *12*(3), 967–974. https://doi.org/10.3233/JPD-213007

Russo, I., Berti, G., Plotegher, N., Bernardo, G., Filograna, R., Bubacco, L., & Greggio, E. (2015). Leucine-rich repeat kinase 2 positively regulates inflammation and down-regulates NF-κB p50 signaling in cultured microglia cells. *Journal of Neuroinflammation*, *12*(1), 230. https://doi.org/10.1186/s12974-015-0449-7

Russo, I., Kaganovich, A., Ding, J., Landeck, N., Mamais, A., Varanita, T., Biosa, A., Tessari, I., Bubacco, L., Greggio, E., & Cookson, M. R. (2019). Transcriptome analysis of LRRK2 knock-out microglia cells reveals alterations of inflammatory- and oxidative stress-related pathways upon treatment with α-synuclein fibrils. *Neurobiology of Disease*, *129*, 67–78. https://doi.org/10.1016/j.nbd.2019.05.012

Sandor, C., Robertson, P., Lang, C., Heger, A., Booth, H., Vowles, J., Witty, L., Bowden, R., Hu, M., Cowley, S. A., Wade-Martins, R., & Webber, C. (2017). Transcriptomic profiling of purified patient-derived dopamine neurons identifies convergent perturbations and therapeutics for Parkinson's disease. *Human Molecular Genetics*, ddw412. https://doi.org/10.1093/hmg/ddw412

Santacroce, L., Del Prete, R., Charitos, I. A., & Bottalico, L. (2021). Mycobacterium leprae: A historical study on the origins of leprosy and its social stigma. *Infezioni in Medicina*, *29*(4). https://doi.org/10.53854/liim-2904-18

Santiago, J. A., Bottero, V., & Potashkin, J. A. (2017). Biological and Clinical Implications of Comorbidities in Parkinson's Disease. *Frontiers in Aging Neuroscience*, *9*. https://doi.org/10.3389/fnagi.2017.00394

Santiago, J. A., & Potashkin, J. A. (2021). The Impact of Disease Comorbidities in Alzheimer's Disease. *Frontiers in Aging Neuroscience*, *13*. https://doi.org/10.3389/fnagi.2021.631770

Sarzi, E., Seveno, M., Piro-Mégy, C., Elzière, L., Quilès, M., Péquignot, M., Müller, A., Hamel, C. P., Lenaers, G., & Delettre, C. (2018). OPA1 gene therapy prevents retinal ganglion cell loss in a Dominant Optic Atrophy mouse model. *Scientific Reports*, *8*(1), 2468. https://doi.org/10.1038/s41598-018-20838-8

Sassone, J., Reale, C., Dati, G., Regoni, M., Pellecchia, M. T., & Garavaglia, B. (2021). The Role of VPS35 in the Pathobiology of Parkinson's Disease. *Cellular and Molecular Neurobiology*, *41*(2), 199–227. https://doi.org/10.1007/s10571-020-00849-8

Schapansky, J., Nardozzi, J. D., Felizia, F., & LaVoie, M. J. (2014). Membrane recruitment of endogenous LRRK2 precedes its potent regulation of autophagy. *Human Molecular Genetics*, *23*(16), 4201–4214. https://doi.org/10.1093/hmg/ddu138

Scheckel, C., Drapeau, E., Frias, M. A., Park, C. Y., Fak, J., Zucker-Scharff, I., Kou, Y., Haroutunian, V., Ma'ayan, A., Buxbaum, J. D., & Darnell, R. B. (2016). Regulatory consequences of neuronal ELAV-like protein binding to coding and non-coding RNAs in human brain. *ELife*. https://doi.org/10.7554/eLife.10421

Schmidt, S., Vogt Weisenhorn, D. M., & Wurst, W. (2022). Chapter 5 – "Parkinson's disease – A role of non-enzymatic posttranslational modifications in disease onset and progression?" *Molecular Aspects of Medicine*, *86*, 101096. https://doi.org/10.1016/j.mam.2022.101096

Schulz, C., Paus, M., Frey, K., Schmid, R., Kohl, Z., Mennerich, D., Winkler, J., & Gillardon, F. (2011). Leucine-Rich Repeat Kinase 2 Modulates Retinoic Acid-Induced Neuronal Differentiation of Murine Embryonic Stem Cells. *PLoS ONE*, *6*(6), e20820. https://doi.org/10.1371/journal.pone.0020820

Seaman, M. N. J., Michael McCaffery, J., & Emr, S. D. (1998). A Membrane Coat Complex Essential for Endosome-to-Golgi Retrograde Transport in Yeast. *The Journal of Cell Biology*, *142*(3), 665–681. https://doi.org/10.1083/jcb.142.3.665

Seegobin, S. P., Heaton, G. R., Liang, D., Choi, I., Blanca Ramirez, M., Tang, B., & Yue, Z. (2020). Progress in LRRK2-Associated Parkinson's Disease Animal Models. *Frontiers in Neuroscience*, *14*. https://doi.org/10.3389/fnins.2020.00674

Seirafi, M., Kozlov, G., & Gehring, K. (2015). Parkin structure and function. *The FEBS Journal*, *282*(11), 2076–2088. https://doi.org/10.1111/febs.13249

Selbach, M., Schwanhäusser, B., Thierfelder, N., Fang, Z., Khanin, R., & Rajewsky, N. (2008). Widespread changes in protein synthesis induced by microRNAs. *Nature*, *455*(7209), 58–63. https://doi.org/10.1038/nature07228

Sena, R. M., Twiss, J. L., Gardiner, A. S., Dell'Orco, M., Linsenbardt, D. N., & Perrone-Bizzozero, N. I. (2021). The RNA-Binding Protein HuD Regulates Alternative Splicing and Alternative Polyadenylation in the Mouse Neocortex. *Molecules*, *26*(10), 2836. https://doi.org/10.3390/molecules26102836

Shah, I. (2017). Lactic Acidosis in Children – A Varied Presentation. *Journal of Pediatric Intensive Care*, *06*(03), 206–208. https://doi.org/10.1055/s-0036-1596065

Shahmoradian, S. H., Lewis, A. J., Genoud, C., Hench, J., Moors, T. E., Navarro, P. P., Castaño-Díez, D., Schweighauser, G., Graff-Meyer, A., Goldie, K. N., Sütterlin, R., Huisman, E., Ingrassia, A., Gier, Y. de, Rozemuller, A. J. M., Wang, J., Paepe, A. De, Erny, J., Staempfli, A., … Lauer, M. E. (2019). Lewy pathology in Parkinson's disease consists of crowded organelles and lipid membranes. *Nature Neuroscience*, *22*(7), 1099–1109. https://doi.org/10.1038/s41593-019-0423-2

Shatsky, I. N., Terenin, I. M., Smirnova, V. V., & Andreev, D. E. (2018). Cap-Independent Translation: What's in a Name? *Trends in Biochemical Sciences*, *43*(11), 882–895. https://doi.org/10.1016/j.tibs.2018.04.011

Shimozawa, A., Ono, M., Takahara, D., Tarutani, A., Imura, S., Masuda-Suzukake, M., Higuchi, M., Yanai, K., Hisanaga, S., & Hasegawa, M. (2017). Propagation of pathological α-synuclein in marmoset brain. *Acta Neuropathologica Communications*, *5*(1), 12. https://doi.org/10.1186/s40478-017-0413-0

Shutinoski, B., Hakimi, M., Harmsen, I. E., Lunn, M., Rocha, J., Lengacher, N., Zhou, Y. Y., Khan, J., Nguyen, A., Hake-Volling, Q., El-Kodsi, D., Li, J., Alikashani, A., Beauchamp, C., Majithia, J., Coombs, K., Shimshek, D., Marcogliese, P. C., Park, D. S., … Schlossmacher, M. G. (2019). *Lrrk2* alleles modulate inflammation during microbial infection of mice in a sex-dependent manner. *Science Translational Medicine*, *11*(511). https://doi.org/10.1126/scitranslmed.aas9292

Silvestri, B., Mochi, M., Garone, M. G., & Rosa, A. (2022). Emerging Roles for the RNA-Binding Protein HuD (ELAVL4) in Nervous System Diseases. *International Journal of Molecular Sciences*, *23*(23), 14606. https://doi.org/10.3390/ijms232314606

Simone, L. E., & Keene, J. D. (2013). Mechanisms coordinating ELAV/Hu mRNA regulons. *Current Opinion in Genetics & Development*, *23*(1), 35–43. https://doi.org/10.1016/j.gde.2012.12.006

Simón-Sánchez, J., Schulte, C., Bras, J. M., Sharma, M., Gibbs, J. R., Berg, D., Paisan-Ruiz, C., Lichtner, P., Scholz, S. W., Hernandez, D. G., Krüger, R., Federoff, M., Klein, C., Goate, A., Perlmutter, J., Bonin, M., Nalls, M. A., Illig, T., Gieger, C., … Gasser, T. (2009). Genome-wide association study reveals genetic risk underlying Parkinson's disease. *Nature Genetics*, *41*(12), 1308–1312. https://doi.org/10.1038/ng.487

Singh, A., Zhi, L., & Zhang, H. (2019). LRRK2 and mitochondria: Recent advances and current views. *Brain Research*, *1702*, 96–104. https://doi.org/10.1016/j.brainres.2018.06.010

Singleton, B., Farrer, M., Johnson, J., Singleton, A., Hague, S., Kachergus, J., Hulihan, M., Peuralinna, T., Dutra, A., Nussbaum, R., Lincoln, S., Crawley, A., Hanson, M., Maraganore, D., Adler, C., Cookson, M. R., Muenter, M., Baptista, M., Miller, D., … Gwinn-Hardy, K. (2003). alpha-Synuclein locus triplication causes Parkinson's disease. *Science (New York, N.Y.)*, *302*(5646), 841. https://doi.org/10.1126/science.1090278

Small, L., Ehrlich, A., Iversen, J., Ashcroft, S. P., Trošt, K., Moritz, T., Hartmann, B., Holst, J. J., Treebak, J. T., Zierath, J. R., & Barrès, R. (2022). Comparative analysis of oral and intraperitoneal glucose tolerance tests in mice. *Molecular Metabolism*, *57*, 101440. https://doi.org/10.1016/j.molmet.2022.101440

Smith, L., & Schapira, A. H. V. (2022). GBA Variants and Parkinson Disease: Mechanisms and Treatments. *Cells*, *11*(8), 1261. https://doi.org/10.3390/cells11081261

Speakman, J. R. (2013). Measuring Energy Metabolism in the Mouse – Theoretical, Practical, and Analytical Considerations. *Frontiers in Physiology*, *4*. https://doi.org/10.3389/fphys.2013.00034

Spillantini, M. G., Schmidt, M. L., Lee, V. M.-Y., Trojanowski, J. Q., Jakes, R., & Goedert, M. (1997). α-Synuclein in Lewy bodies. *Nature*, *388*(6645). https://doi.org/10.1038/42166

Srikantan, S., & Gorospe, M. (2012). HuR function in disease. *Frontiers in Bioscience*, *17*(1), 189–205. https://doi.org/10.2741/3921

Stafa, K., Tsika, E., Moser, R., Musso, A., Glauser, L., Jones, A., Biskup, S., Xiong, Y., Bandopadhyay, R., Dawson, V. L., Dawson, T. M., & Moore, D. J. (2014). Functional interaction of Parkinson's disease-associated LRRK2 with members of the dynamin GTPase superfamily. *Human Molecular Genetics*, *23*(8), 2055–2077. https://doi.org/10.1093/hmg/ddt600

Stefanis, L. (2012). -Synuclein in Parkinson's Disease. *Cold Spring Harbor Perspectives in Medicine*, *2*(2), a009399–a009399. https://doi.org/10.1101/cshperspect.a009399

Steger, M., Diez, F., Dhekne, H. S., Lis, P., Nirujogi, R. S., Karayel, O., Tonelli, F., Martinez, T. N., Lorentzen, E., Pfeffer, S. R., Alessi, D. R., & Mann, M. (2017). Systematic proteomic analysis of LRRK2-mediated Rab GTPase phosphorylation establishes a connection to ciliogenesis. *ELife*, *6*. https://doi.org/10.7554/eLife.31012

Steger, M., Tonelli, F., Ito, G., Davies, P., Trost, M., Vetter, M., Wachter, S., Lorentzen, E., Duddy, G., Wilson, S., Baptista, M. A., Fiske, B. K., Fell, M. J., Morrow, J. A., Reith, A. D., Alessi, D. R., & Mann, M. (2016). Phosphoproteomics reveals that Parkinson's disease kinase LRRK2 regulates a subset of Rab GTPases. *ELife*, *5*. https://doi.org/10.7554/eLife.12813

Steiner, A. A., Flatow, E. A., Brito, C. F., Fonseca, M. T., & Komegae, E. N. (2017). Respiratory gas exchange as a new aid to monitor acidosis in endotoxemic rats: relationship to metabolic fuel substrates and thermometabolic responses. *Physiological Reports*, *5*(1). https://doi.org/10.14814/phy2.13100

Szabo, A., Dalmau, J., Manley, G., Rosenfeld, M., Wong, E., Henson, J., Posner, J. B., & Furneaux, H. M. (1991). HuD, a paraneoplastic encephalomyelitis antigen, contains RNA-binding domains and is homologous to Elav and sex-lethal. *Cell*, *67*(2), 325–333. https://doi.org/10.1016/0092-8674(91)90184-Z

Szumlinski, K. K., Dehoff, M. H., Kang, S. H., Frys, K. A., Lominac, K. D., Klugmann, M., Rohrer, J., Griffin, W., Toda, S., Champtiaux, N. P., Berry, T., Tu, J. C., Shealy, S. E., During, M. J., Middaugh, L. D., Worley, P. F., & Kalivas, P. W. (2004). Homer Proteins Regulate Sensitivity to Cocaine. *Neuron*, *43*(3), 401–413. https://doi.org/10.1016/j.neuron.2004.07.019

Tagliaferro, P., Kareva, T., Oo, T. F., Yarygina, O., Kholodilov, N., & Burke, R. E. (2015). An early axonopathy in a hLRRK2(R1441G) transgenic model of Parkinson disease. *Neurobiology of Disease*, *82*, 359–371. https://doi.org/10.1016/j.nbd.2015.07.009

Takagawa, T., Kitani, A., Fuss, I., Levine, B., Brant, S. R., Peter, I., Tajima, M., Nakamura, S., & Strober, W. (2018). An increase in LRRK2 suppresses autophagy and enhances dectin-1–induced immunity in a mouse model of colitis. *Science Translational Medicine*. https://doi.org/10.1126/scitranslmed.aan8162

Tan, Y.-Y., Jenner, P., & Chen, S.-D. (2022). Monoamine Oxidase-B Inhibitors for the Treatment of Parkinson's Disease: Past, Present, and Future. *Journal of Parkinson's Disease*, *12*(2), 477–493. https://doi.org/10.3233/JPD-212976

Taneera, J., Lang, S., Sharma, A., Fadista, J., Zhou, Y., Ahlqvist, E., Jonsson, A., Lyssenko, V., Vikman, P., Hansson, O., Parikh, H., Korsgren, O., Soni, A., Krus, U., Zhang, E., Jing, X.-J., Esguerra, J. L.

S., Wollheim, C. B., Salehi, A., … Groop, L. (2012). A Systems Genetics Approach Identifies Genes and Pathways for Type 2 Diabetes in Human Islets. *Cell Metabolism*, *16*(1), 122–134. https://doi.org/10.1016/j.cmet.2012.06.006

Taylor, M., & Alessi, D. R. (2020). Advances in elucidating the function of leucine-rich repeat protein kinase-2 in normal cells and Parkinson's disease. *Current Opinion in Cell Biology*, *63*, 102–113. https://doi.org/10.1016/j.ceb.2020.01.001

Taymans, J.-M., Fell, M., Greenamyre, T., Hirst, W. D., Mamais, A., Padmanabhan, S., Peter, I., Rideout, H., & Thaler, A. (2023). Perspective on the current state of the LRRK2 field. *Npj Parkinson's Disease*, *9*(1), 104. https://doi.org/10.1038/s41531-023-00544-7

Tebaldi, T., Zuccotti, P., Peroni, D., Köhn, M., Gasperini, L., Potrich, V., Bonazza, V., Dudnakova, T., Rossi, A., Sanguinetti, G., Conti, L., Macchi, P., D'Agostino, V., Viero, G., Tollervey, D., Hüttelmaier, S., & Quattrone, A. (2018). HuD Is a Neural Translation Enhancer Acting on mTORC1-Responsive Genes and Counteracted by the Y3 Small Non-coding RNA. *Molecular Cell*, *71*(2), 256-270.e10. https://doi.org/10.1016/j.molcel.2018.06.032

Thakur, G., Kumar, V., Lee, K. W., & Won, C. (2022). Structural Insights and Development of LRRK2 Inhibitors for Parkinson's Disease in the Last Decade. *Genes*, *13*(8), 1426. https://doi.org/10.3390/genes13081426

Thomas, T., Craigen, W. J., Moore, R., Czosek, R., & Jefferies, J. L. (2015). Arrhythmia as a cardiac manifestation in MELAS syndrome. *Molecular Genetics and Metabolism Reports*, *4*, 9–10. https://doi.org/10.1016/j.ymgmr.2015.05.002

Tilokani, L., Nagashima, S., Paupe, V., & Prudent, J. (2018). Mitochondrial dynamics: overview of molecular mechanisms. *Essays in Biochemistry*, *62*(3), 341–360. https://doi.org/10.1042/EBC20170104

Tiruchinapalli, D. M., Caron, M. G., & Keene, J. D. (2008). Activity-dependent expression of ELAV/Hu RBPs and neuronal mRNAs in seizure and cocaine brain. *Journal of Neurochemistry*, *107*(6), 1529–1543. https://doi.org/10.1111/j.1471-4159.2008.05718.x

Tokarew, J. M., El-Kodsi, D. N., Lengacher, N. A., Fehr, T. K., Nguyen, A. P., Shutinoski, B., O'Nuallain, B., Jin, M., Khan, J. M., Ng, A. C. H., Li, J., Jiang, Q., Zhang, M., Wang, L., Sengupta, R., Barber, K. R., Tran, A., Im, D. S., Callaghan, S., … Schlossmacher, M. G. (2021). Age-associated insolubility of parkin in human midbrain is linked to redox balance and sequestration of reactive dopamine metabolites. *Acta Neuropathologica*, *141*(5), 725–754. https://doi.org/10.1007/s00401-021-02285-4

Tolosa, E., Vila, M., Klein, C., & Rascol, O. (2020). LRRK2 in Parkinson disease: challenges of clinical trials. *Nature Reviews Neurology*, *16*(2), 97–107. https://doi.org/10.1038/s41582-019-0301-2

Tong, Y., Pisani, A., Martella, G., Karouani, M., Yamaguchi, H., Pothos, E. N., & Shen, J. (2009). R1441C mutation in LRRK2 impairs dopaminergic neurotransmission in mice. *Proceedings of the National Academy of Sciences*, *106*(34), 14622–14627. https://doi.org/10.1073/pnas.0906334106

Tong, Y., Yamaguchi, H., Giaime, E., Boyle, S., Kopan, R., Kelleher, R. J., & Shen, J. (2010). Loss of leucine-rich repeat kinase 2 causes impairment of protein degradation pathways, accumulation of α-synuclein, and apoptotic cell death in aged mice. *Proceedings of the National Academy of Sciences*, *107*(21), 9879–9884. https://doi.org/10.1073/pnas.1004676107

Trancikova, A., Mamais, A., Webber, P. J., Stafa, K., Tsika, E., Glauser, L., West, A. B., Bandopadhyay, R., & Moore, D. J. (2012). Phosphorylation of 4E-BP1 in the Mammalian Brain Is Not Altered by LRRK2 Expression or Pathogenic Mutations. *PLoS ONE*, *7*(10), e47784. https://doi.org/10.1371/journal.pone.0047784

Trinh, J., Schymanski, E. L., Smajic, S., Kasten, M., Sammler, E., & Grünewald, A. (2022). Molecular mechanisms defining penetrance of *LRRK2* -associated Parkinson's disease. *Medizinische Genetik*, *34*(2), 103–116. https://doi.org/10.1515/medgen-2022-2127

Tsika, E., Kannan, M., Foo, C. S.-Y., Dikeman, D., Glauser, L., Gellhaar, S., Galter, D., Knott, G. W., Dawson, T. M., Dawson, V. L., & Moore, D. J. (2014). Conditional expression of Parkinson's disease-related R1441C LRRK2 in midbrain dopaminergic neurons of mice causes nuclear abnormalities without neurodegeneration. *Neurobiology of Disease*, *71*, 345–358. https://doi.org/10.1016/j.nbd.2014.08.027

Turrens, J. F. (2003). Mitochondrial formation of reactive oxygen species. *The Journal of Physiology*, *552*(2), 335–344. https://doi.org/10.1113/jphysiol.2003.049478

Uhlén, M., Fagerberg, L., Hallström, B. M., Lindskog, C., Oksvold, P., Mardinoglu, A., Sivertsson, Å., Kampf, C., Sjöstedt, E., Asplund, A., Olsson, I., Edlund, K., Lundberg, E., Navani, S., Szigyarto, C. A.-K., Odeberg, J., Djureinovic, D., Takanen, J. O., Hober, S., … Pontén, F. (2015). Tissue-based map of the human proteome. *Science*, *347*(6220). https://doi.org/10.1126/science.1260419

Utari, A., Adams, E., Berry-Kravis, E., Chavez, A., Scaggs, F., Ngotran, L., Boyd, A., Hessl, D., Gane, L. W., Tassone, F., Tartaglia, N., Leehey, M. A., & Hagerman, R. J. (2010). Aging in fragile X syndrome. *Journal of Neurodevelopmental Disorders*, *2*(2), 70–76. https://doi.org/10.1007/s11689-010-9047-2

Valente, E. M., Abou-Sleiman, P. M., Caputo, V., Muqit, M. M. K., Harvey, K., Gispert, S., Ali, Z., Del Turco, D., Bentivoglio, A. R., Healy, D. G., Albanese, A., Nussbaum, R., González-Maldonado, R., Deller, T., Salvi, S., Cortelli, P., Gilks, W. P., Latchman, D. S., Harvey, R. J., … Wood, N. W. (2004). Hereditary Early-Onset Parkinson's Disease Caused by Mutations in *PINK1*. *Science*, *304*(5674), 1158–1160. https://doi.org/10.1126/science.1096284

van der Vlag, M., Havekes, R., & Heckman, P. R. A. (2020). The contribution of Parkin, PINK1 and DJ-1 genes to selective neuronal degeneration in Parkinson's disease. *European Journal of Neuroscience*, *52*(4), 3256–3268. https://doi.org/10.1111/ejn.14689

Vanevski, F., & Xu, B. (2015). HuD Interacts with Bdnf mRNA and Is Essential for Activity-Induced BDNF Synthesis in Dendrites. *PLOS ONE*, *10*(2), e0117264. https://doi.org/10.1371/journal.pone.0117264

Váradi, C. (2020). Clinical Features of Parkinson's Disease: The Evolution of Critical Symptoms. *Biology*, *9*(5), 103. https://doi.org/10.3390/biology9050103

Velázquez-Cruz, A., Baños-Jaime, B., Díaz-Quintana, A., De la Rosa, M. A., & Díaz-Moreno, I. (2021). Post-translational Control of RNA-Binding Proteins and Disease-Related Dysregulation. *Frontiers in Molecular Biosciences*, *8*. https://doi.org/10.3389/fmolb.2021.658852

Verschuur, C. V. M., Suwijn, S. R., Boel, J. A., Post, B., Bloem, B. R., van Hilten, J. J., van Laar, T., Tissingh, G., Munts, A. G., Deuschl, G., Lang, A. E., Dijkgraaf, M. G. W., de Haan, R. J., & de Bie, R. M. A. (2019). Randomized Delayed-Start Trial of Levodopa in Parkinson's Disease. *New England Journal of Medicine*, *380*(4), 315–324. https://doi.org/10.1056/NEJMoa1809983

Vizziello, M., Borellini, L., Franco, G., & Ardolino, G. (2021). Disruption of Mitochondrial Homeostasis: The Role of PINK1 in Parkinson's Disease. *Cells*, *10*(11), 3022. https://doi.org/10.3390/cells10113022

Wang, J., Guo, Y., Chu, H., Guan, Y., Bi, J., & Wang, B. (2013). Multiple Functions of the RNA-Binding Protein HuR in Cancer Progression, Treatment Responses and Prognosis. *International Journal of Molecular Sciences*, *14*(5), 10015–10041. https://doi.org/10.3390/ijms140510015

Wang, X., Yan, M. H., Fujioka, H., Liu, J., Wilson-Delfosse, A., Chen, S. G., Perry, G., Casadesus, G., & Zhu, X. (2012). LRRK2 regulates mitochondrial dynamics and function through direct interaction with DLP1. *Human Molecular Genetics*, *21*(9), 1931–1944. https://doi.org/10.1093/hmg/dds003

Watts, M. E., Pocock, R., & Claudianos, C. (2018). Brain Energy and Oxygen Metabolism: Emerging Role in Normal Function and Disease. *Frontiers in Molecular Neuroscience*, *11*. https://doi.org/10.3389/fnmol.2018.00216

West, A. B., Moore, D. J., Biskup, S., Bugayenko, A., Smith, W. W., Ross, C. A., Dawson, V. L., & Dawson, T. M. (2005a). Parkinson's disease-associated mutations in leucine-rich repeat kinase 2 augment kinase activity. *Proceedings of the National Academy of Sciences*, *102*(46), 16842–16847. https://doi.org/10.1073/pnas.0507360102

West, A. B., Moore, D. J., Biskup, S., Bugayenko, A., Smith, W. W., Ross, C. A., Dawson, V. L., & Dawson, T. M. (2005b). Parkinson's disease-associated mutations in leucine-rich repeat kinase 2

augment kinase activity. *Proceedings of the National Academy of Sciences*, *102*(46), 16842–16847. https://doi.org/10.1073/pnas.0507360102

West, A. B., Moore, D. J., Choi, C., Andrabi, S. A., Li, X., Dikeman, D., Biskup, S., Zhang, Z., Lim, K.-L., Dawson, V. L., & Dawson, T. M. (2007). Parkinson's disease-associated mutations in LRRK2 link enhanced GTP-binding and kinase activities to neuronal toxicity. *Human Molecular Genetics*, *16*(2), 223–232. https://doi.org/10.1093/hmg/ddl471

Westerlund, M., Belin, A. C., Anvret, A., Bickford, P., Olson, L., & Galter, D. (2008). Developmental regulation of leucine-rich repeat kinase 1 and 2 expression in the brain and other rodent and human organs: Implications for Parkinson's disease. *Neuroscience*, *152*(2), 429–436. https://doi.org/10.1016/j.neuroscience.2007.10.062

Xian, H., & Liou, Y.-C. (2021). Functions of outer mitochondrial membrane proteins: mediating the crosstalk between mitochondrial dynamics and mitophagy. *Cell Death & Differentiation*, *28*(3), 827–842. https://doi.org/10.1038/s41418-020-00657-z

Xiong, Y., Neifert, S., Karuppagounder, S. S., Liu, Q., Stankowski, J. N., Lee, B. D., Ko, H. S., Lee, Y., Grima, J. C., Mao, X., Jiang, H., Kang, S.-U., Swing, D. A., Iacovitti, L., Tessarollo, L., Dawson, T. M., & Dawson, V. L. (2018). Robust kinase- and age-dependent dopaminergic and norepinephrine neurodegeneration in LRRK2 G2019S transgenic mice. *Proceedings of the National Academy of Sciences*, *115*(7), 1635–1640. https://doi.org/10.1073/pnas.1712648115

Xu, E., Boddu, R., Abdelmotilib, H. A., Sokratian, A., Kelly, K., Liu, Z., Bryant, N., Chandra, S., Carlisle, S. M., Lefkowitz, E. J., Harms, A. S., Benveniste, E. N., Yacoubian, T. A., Volpicelli-Daley, L. A., Standaert, D. G., & West, A. B. (2022). Pathological α-synuclein recruits LRRK2 expressing pro-inflammatory monocytes to the brain. *Molecular Neurodegeneration*, *17*(1), 7. https://doi.org/10.1186/s13024-021-00509-5

Yellen, G. (2018). Fueling thought: Management of glycolysis and oxidative phosphorylation in neuronal metabolism. *Journal of Cell Biology*, *217*(7), 2235–2246. https://doi.org/10.1083/jcb.201803152

Yiakouvaki, A., Dimitriou, M., Karakasiliotis, I., Eftychi, C., Theocharis, S., & Kontoyiannis, D. L. (2012). Myeloid cell expression of the RNA-binding protein HuR protects mice from pathologic inflammation and colorectal carcinogenesis. *Journal of Clinical Investigation*, *122*(1). https://doi.org/10.1172/JCI45021

Zhang, C., Hastings, M. L., Krainer, A. R., & Zhang, M. Q. (2007). Dual-specificity splice sites function alternatively as 5′ and 3′ splice sites. *Proceedings of the National Academy of Sciences*, *104*(38), 15028–15033. https://doi.org/10.1073/pnas.0703773104

Zhang, F.-R., Huang, W., Chen, S.-M., Sun, L.-D., Liu, H., Li, Y., Cui, Y., Yan, X.-X., Yang, H.-T., Rong-De Yang, Chu, T.-S., Zhang, C., Zhang, L., Han, J.-W., Yu, G.-Q., Quan, C., Yu, Y.-X., Zhang, Z.,

Shi, B.-Q., … Liu, J.-J. (2009). Genomewide Association Study of Leprosy. *New England Journal of Medicine*, *361*(27), 2609–2618. https://doi.org/10.1056/NEJMoa0903753

Zhang, P., Fan, Y., Ru, H., Wang, L., Magupalli, V. G., Taylor, S. S., Alessi, D. R., & Wu, H. (2019). Crystal structure of the WD40 domain dimer of LRRK2. *Proceedings of the National Academy of Sciences*, *116*(5), 1579–1584. https://doi.org/10.1073/pnas.1817889116

Zhang, Q., Pan, Y., Yan, R., Zeng, B., Wang, H., Zhang, X., Li, W., Wei, H., & Liu, Z. (2015). Commensal bacteria direct selective cargo sorting to promote symbiosis. *Nature Immunology*, *16*(9), 918–926. https://doi.org/10.1038/ni.3233

Zhang, Z.-X., Dong, Z.-H., & Román, G. C. (2006). Early Descriptions of Parkinson Disease in Ancient China. *Archives of Neurology*, *63*(5), 782. https://doi.org/10.1001/archneur.63.5.782

Zheng, X., Boyer, L., Jin, M., Mertens, J., Kim, Y., Ma, L., Ma, L., Hamm, M., Gage, F. H., & Hunter, T. (2016). Metabolic reprogramming during neuronal differentiation from aerobic glycolysis to neuronal oxidative phosphorylation. *ELife*, *5*. https://doi.org/10.7554/eLife.13374

Zhou, H.-L., Hinman, M. N., Barron, V. A., Geng, C., Zhou, G., Luo, G., Siegel, R. E., & Lou, H. (2011). Hu proteins regulate alternative splicing by inducing localized histone hyperacetylation in an RNA-dependent manner. *Proceedings of the National Academy of Sciences*, *108*(36). https://doi.org/10.1073/pnas.1103344108

Zilberter, Y., & Zilberter, M. (2017). The vicious circle of hypometabolism in neurodegenerative diseases: Ways and mechanisms of metabolic correction. *Journal of Neuroscience Research*, *95*(11), 2217–2235. https://doi.org/10.1002/jnr.24064

Zimprich, A., Biskup, S., Leitner, P., Lichtner, P., Farrer, M., Lincoln, S., Kachergus, J., Hulihan, M., Uitti, R. J., Calne, D. B., Stoessl, A. J., Pfeiffer, R. F., Patenge, N., Carbajal, I. C., Vieregge, P., Asmus, F., Müller-Myhsok, B., Dickson, D. W., Meitinger, T., … Gasser, T. (2004). Mutations in LRRK2 Cause Autosomal-Dominant Parkinsonism with Pleomorphic Pathology. *Neuron*, *44*(4). https://doi.org/10.1016/j.neuron.2004.11.005

Zweier, M., Gregor, A., Zweier, C., Engels, H., Sticht, H., Wohlleber, E., Bijlsma, E. K., Holder, S. E., Zenker, M., Rossier, E., Grasshoff, U., Johnson, D. S., Robertson, L., Firth, H. V., Cornelia Kraus, Ekici, A. B., Reis, A., & Rauch, A. (2010). Mutations in MEF2C from the 5q14.3q15 microdeletion syndrome region are a frequent cause of severe mental retardation and diminish MECP2 and CDKL5 expression. *Human Mutation*, *31*(6), 722–733. https://doi.org/10.1002/humu.21253